Functionalization of cellulose nanofibrils for the development of biobased medical devices

Hippolyte Durand

Communauté
UNIVERSITÉ Grenoble Alpes

THÈSE

Pour obtenir le grade de

DOCTEUR DE LA COMMUNAUTE UNIVERSITE GRENOBLE ALPES

Spécialité : **Matériaux, Mécanique, Génie Civil, Électrochimie**

Arrêté ministériel : 25 mai 2016

Présentée par

Hippolyte DURAND

Thèse dirigée par
Julien BRAS, Maître de Conférences, Grenoble INP

et codirigée par
Naceur BELGACEM, Professeur, Grenoble INP

préparée au sein du **Laboratoire de Génie des Procédés Papetiers**

dans **l'École Doctorale IMEP-2 – Ingénierie, Matériaux, Mécanique, Environnement, Énergétique, Procédés, Production**

FUNCTIONALIZATION OF CELLULOSE NANOFIBRILS FOR THE DEVELOPMENT OF BIOBASED MEDICAL DEVICES

Thèse soutenue publiquement le **08 Février 2019**,
devant le jury composé de :

Pr. Roberta BONGIOVANNI
Professeur à l'Université Polytechnique de Turin, Présidente
Pr. Eva MALMSTRÖM JONSSON
Professeur à KTH – Institut Royal de Technologie, Rapporteur
Dr. Timo LAAKSONEN
Maître de Conférences à l'Université d'Helsinki, Rapporteur
Dr. Julien BRAS
Maître de Conférences à Grenoble INP, Directeur de thèse
Pr. Naceur BELGACEM
Professeur à Grenoble INP, Co-directeur de thèse
Dr. Elisa ZENO
Ingénieure au Centre Technique du Papier, Co-encadrante
Dr. Yves BAYON
Responsable R&D Senior chez Medtronic, Membre invité

“God made the bulk; surfaces were invented by the devil.”

Wolfgang Pauli

“A pessimist sees the difficulty in every opportunity;

An optimist sees the opportunity in every difficulty.”

Winston Churchill

Remerciements (*Acknowledgements)*

Allons droit au but. Je n'ai jamais cherché à faire une thèse. Merci donc à Karim Missoum (InoFib) de m'avoir permis d'évoluer au sein du LGP2 avec lui pendant une année. C'est cette expérience qui m'a conduit à cette opportunité de thèse. J'avais dix jours pour décider des trois prochaines années de ma vie !! (merci Julien Bras). Le fait est que je ne vois pas comment j'aurais pu aussi facilement apprendre à me connaître professionnellement et personnellement aussi vite, sans avoir choisi cette thèse. Cette expérience unique m'a marqué profondément. Et c'est avant tout une aventure humaine. J'ai donc quelques personnes à remercier.

Commençons par les plus proches, et ceux avec qui on partage le plus : les collègues doctorants, plus particulièrement ceux de l'équipe MATBIO. Dans le bureau le B120 (*B120 for life*), avec Charlène, Megan et Erwan, j'ai pu atterrir tout en douceur et découvrir progressivement le monde de la recherche académique au LGP2. Vous avoir pour partager cette première moitié de thèse était du pur BONHEUR. Merci à tous les trois. Merci aussi à Flavien pour les nombreuses discussions et confidences sur la vie. Relation toute particulière avec toi, qui est naît, et perdurera, dans la fumée et l'ethanol. Fleur et Johanna, deux inspirations en termes d'investissement et de persévérance, merci. Mais les meilleures choses ont une fin, et cette team s'est peu à peu morcelée pour faire place à de nouveaux visages ! J'avais parfois pour eux le rôle que le B120 avait eu pour moi au début. Merci donc à Gabriel, Estelle, Lili, Matthieu et Bastien. Spéciale dédicace à Hugo Spieser pour ces moments microbio, un petit bébé dont on avait la charge juste tous les deux. J'espère que la DAS sera indulgente.

Autour de ces personnes formidables gravitent d'autres êtres humains. Ils sont tous soudés pour faire marcher la locomotive du LGP2. Ils entretiennent le matériel, s'occupe du secrétariat, des finances et m'ont toujours accueilli à bras ouverts dès que j'avais envie de les embêter (et j'adore ça). Vous faites du LGP2 un établissement où il fait bon vivre et bon travailler. Merci à Stéphane D., le service technique (dédicace à Chu et Olivier pour mes aventures cycliste de selle), le secrétariat (Isabelle et Nathalie) et les finances (Stéphane, Anne Marie et Laurence). Au cœur de ce petit nuage, un merci tout spécial à Cécile, partenaire CELLICAL de premier choix et longtemps gardienne de la bonne pratique en labo de chimie. Merci pour tout ton soutien, tes conseils et ton aide !

En parlant de CELLICAL. Belle équipe. La pluridisciplinarité était la clé de ce projet. Et grâce à chacun des partenaires j'ai pu monter en compétence sur tous les sujets abordés pendant ces trois dernières années. Un immense merci à Sébastien, Martine et Isabelle, Valérie, Youness et Juergen pour le côté académique. Un immense merci également à Yves, Kevin et Sophie pour le côté industriel. Au sein de

ce projet collaboratif, de nombreux non-permanents ont apporté leur pierre à l'édifice : merci à ceux que j'ai encadré, Paul, Marion et Elsa. Mais aussi Heloïse, Jennifer, David, Cyril, Bastien et Nourhene.

Et un jour arrive le moment de la soutenance. Et même si ils ne liront probablement jamais ces mots, j'aimerais remercier chaleureusement tous les membres de mon jury. Roberta Bongiovanni, Eva Malmström, Timo Laaksonen et Yves Bayon. C'était un honneur de sentir mon travail passer au crible de vos expertises, et un plaisir d'échanger et discuter lors de la soutenance.

Mais dans toutes ces relations professionnelles, il en est quelques une qui méritent encore plus d'attention. L'équipe encadrante. Julien, Elisa et Naceur. Privilège de l'âge, commençons avec Naceur. Il faut savoir que je fréquente cette personne depuis bien avant la thèse. Sur les bancs de PAGORA déjà je buvais ses paroles. On est même parti en voyage scolaire. Et revenus sain et sauf. Au-delà de ces *private jokes* reste un véritable pilier de mon passage à PAGORA-LGP2. D'une humanité incroyable et toujours pourfendeur de la manière franco-française de parler trop souvent négativement-positivement des choses. Tu as compté énormément pour moi. Tes enseignements, et surtout ceux au-delà de la science, sont gravés dans le marbre.

Un papa, une maman. Les deux se reconnaîtront. On a mis du temps à s'entendre tous les trois, et j'ai dû faire le médiateur régulièrement le temps qu'on trouve le rythme de réunion parfait. Elisa. Je me rappelle bien ce tout premier rendez-vous dans ton bureau où tu voulais évaluer un peu le candidat que Julien avait choisi… J'étais incapable de parler de soxlhet, imaginez la pauvre. S'en est suivi trois ans d'apprentissage. C'est avec plaisir que je venais chercher conseils et réconfort au CTP. Ta droiture, ta rigueur et ta persévérance sont aujourd'hui également mes armes. Encore plus présente pendant la rédaction, tu m'as transmis énormément sur cette période *which* was finally amazing. Grazzie mille.

Julien : "Hippo, tu regarderas l'offre de thèse que j'ai publié?!" lança-t-il à travers le bureau d'InoFib comme une suggestion. J'ai répondu "Bah tu sais Julien, ça ne m'intéresse pas trop la thèse". Voilà. Ma première erreur. Vite corrigée. Dix jours plus tard et après quelques enquêtes, j'étais décidé ! Alors merci pour cette opportunité, pour la confiance qui s'est rapidement établie, pour les idées, les débats, pour le partage, les coups de pied au cul, et par-dessus tout cette capacité à me faire voir le verre à moitié plein, plutôt qu'à moitié vide. Tu es le centre de cet apprentissage professionnel et personnel que la thèse est si unique à proposer. Merci pour cette belle relation qu'on a pu construire. Si j'ai pu soutenir ma thèse dans un tel esprit de confiance et de plaisir c'est grâce à ton investissement jusqu'au dernier moment. MERCI.

Table of Content

Scientific contributions (2016 – 2019)

Publications in scientific journals

1. **H. Durand**, C. Darpentigny, E. Zeno, N. Belgacem, J. Bras – *Single step immobilization of ciprofloxacin on cellulose nanofibers for antimicrobial membrane development,* submitted in October 2018 to *Material Science Engineering: C*
2. **H. Durand**, E. Zeno, M. Demeunynck, I. Baussanne, M.-C. Brochier Salon, M. Bardet, J. Vigier-Gravel, L. Emsley, N. Belgacem, J. Bras – *Two-steps immobilization of metronidazole on TEMPO-oxidized cellulose nanofibrils from wood through thiol-yne click chemistry*, submitted in November 2018 to *Chemical Communication*
3. **H. Durand**, C. Balsollier, S. Fort, M. Demeunynck, I. Baussanne, D. Lee, G. de Paepe, A. Kumar, E. Zeno, N. Belgacem, J. Bras – *Investigation of active principle ingredient grafting on cellulose nanofibrils through Diels Alder reaction with DNP-enhanced ssNMR,* submitted in November 2018 to *ACS Applied Nano Materials*
4. **H. Durand**, P. Jaouen, E. Faure, C. Sillard, E. Zeno, N. Belgacem, J. Bras – *Cellulose nanofiber films as medical device with drug release abilities for topical applications,* submitted in November 2018 to *Cellulose*

In preparation:

5. **H. Durand**, N. Esseghir, Y. Karrout, J. Siepmann, E. Zeno, N. Belgacem, J. Bras – *Drug release from cellulose nanofibrils collagen composites and influence of gamma radiation sterilization*

Author's contributions:

1. Hippolyte Durand, Elisa Zeno, Julien Bras and Naceur Belgacem were responsible for the experimental design and planning of the work. Hippolyte Durand performed most of the experiments, analyzed the results and wrote the manuscript as principal author under the supervision of Dr. Julien Bras and Dr. Elisa Zeno. Clémentine Darpentigny performed the successive zone of inhibition tests.
2. Hippolyte Durand, Elisa Zeno, Julien Bras and Naceur Belgacem were responsible for the experimental design and planning of the work. Hippolyte Durand performed most of the

experiments, analyzed the results and wrote the manuscript as principal author under the supervision of Dr. Julien Bras and Dr. Elisa Zeno. Martine Demeunynck and Isabelle Baussanne were responsible for the synthesis of the prodrug. Marie Christine Brochier-Salon performed the ssNMR experiments. Jasmine Vigier Gravel, Pr. Lyndon Emsley and Michel Bardet performed the DNP-NMR measurements and analyzed the results.

3. Hippolyte Durand, Elisa Zeno, Julien Bras and Naceur Belgacem were responsible for the experimental design and planning of the work. Hippolyte Durand performed most of the experiments, analyzed the results and wrote the manuscript as principal author under the supervision of Dr. Julien Bras and Dr. Elisa Zeno. Martine Demeunynck, Isabelle Baussanne Cyril Balsollier and Sébastien Fort were responsible for the synthesis of the prodrug and provided their expertise on Diels Alder reaction. Akshay Kumar, Daniel Lee and Gael De Paepe performed the DNP-NMR measurements and analyzed the results.
4. Hippolyte Durand, Elisa Zeno, Julien Bras and Naceur Belgacem were responsible for the experimental design and planning of the work. Hippolyte Durand supervised Paul Jaouen during his 6 months master thesis and performed some of the experiments, analyzed the results and wrote the manuscript as principal author under the supervision of Dr. Julien Bras and Dr. Elisa Zeno. Cécile Sillard supervised Elsa Faure during her 3 months bachelor thesis and performed AFM imaging.
5. Hippolyte Durand, Elisa Zeno, Julien Bras and Naceur Belgacem were responsible for the experimental design and planning of the work. Hippolyte Durand prepared the composites and performed part of the experiments. Nourhene Esseghir was supervised by Dr. Youness Karrout and Pr. Juergen Siepmann during her 6 months master thesis and performed the release study experiments.

Oral presentations in international conferences

H. Durand, E. Zeno, H. Le Drezen, M. Demeunynck, I. Baussane, S. Fort, N. Belgacem, Julien Bras – *Functionalization of cellulose nanofibrils from wood for immobilization of pro-drug molecule by click chemistry,* in the 5th **EPNOE** – International Polysaccharide Conference, Jenna (Germany), August 20-24, **2017**

H. Durand, E. Zeno, M. Demeunynck, I. Baussanne, S. Fort, N. Belgacem, J. Bras – *Cellulose nanofibrils from wood as a new substrate for covalent immobilization of pro-drug molecule by click chemistry,* in 255th American Chemical Society **ACS**, New Orleans (U.S.), March 18-22, **2018**

H. Durand, E. Zeno, M. Demeunynck, I. Baussanne, S. Fort, N. Belgacem, J. Bras – *Cellulose nanofibrils from wood as a new substrate for covalent immobilization of pro-drug molecule by click chemistry,* in Glyco@ALps Days, Col du Lautaret (France), April 23-24, **2018**

Posters in scientific conferences

H. Durand, E. Zeno, H. Le Drezen, , I. Baussane, N. Belgacem, J. Bras – *Cellulose nanofiber surface functionalization for functional medical membrane applications,* in 253th American Chemical Society **ACS**, San Francisco (U.S.), April 2-6, **2017**

H. Durand, S. Saini, D. Quinot, E. Zeno, N. Belgacem, J. Bras – *Cellulose nanofibrils as a new substrate for beta-cyclodextrin immobilization in medical devices,* in 17ième Journées des Cyclodextrines, October 6-7, **2016**

Non-scientific communications:

Ma Thèse en 180 secondes (MT180), french version of the **Tree Minute Thesis (3MT)** worldwide competition, ranked 2nd of Grenoble regional education authority

Abbreviations

Materials and Chemicals

AMUpol	15-{[(7-oxyl-3,11-dioxa-7-azadispiro[5.1.5.3]hexadec-15-yl)carbamoyl][2-(2,5,8,11-tetraoxatridecan-13-ylamino)}-[3,11-dioxa-7-azadispiro[5.1.5.3]hexadec-7-yl])oxidanyl
CNC	Cellulose nanocrystals
CNF	Cellulose nanofibrils
CNF-e	Cellulose nanofibrils produced by enzymatic pretreatment
CNF-t	Cellulose nanofibrils produced by TEMPO mediated oxidation pretreatment
DCC	N,N-Dicyclohexylcarbodiimide
digCHX	Chlorhexidine digluconate
DMAP	4-(Dimethylamino)pyridine
EDC	N-(3-Dimethylaminopropyl)-N'-ethylcarbodiimide
Gly	Glycerol
HCl	Hydrochloric acid
KBr	Potassium bromide
LAP	Lithium Phenyl(2,4,6-trimethylbenzoyl)phosphinate
NaOH	Sodium hydroxide
NHS	N-Hydroxysuccinimide
PBS	Phosphate Buffer Saline
PEG	Polyethylene Glycol
TCEP	Tris(2-carboxyethyl)phosphine hydrochloride
TEMPO	2,2,6,6-Tetramethylpiperidine 1-oxyl
TFA	Trifluoroacetic acid
TiPS	Triisopropylsilane
TRIS	Tris(hydroxymethyl) aminomethane

Methods

AFM	Atomic Force Microscopy
DNP-NMR	Dynamic Nuclear Polarization enhanced Nuclear Magnetic Resonance
EA	Elemental Analysis
FTIR	Fourier Transformed InfraRed spectroscopy
HPLC	High Performance Liquid Chromatography
MIC	Minimum Inhibitory Concentration
NMR	Nuclear Magnetic Resonance
SEM	Scanning electron microscopy
ssNMR	Solid State Nuclear Magnetic Resonance
ZOI	Zone Of Inhibition

General Introduction

General introduction

Life expectancy has been significantly increased over the last century, thanks to highly innovative and scientifically supported treatments. However, remaining clinical needs such as infection, pain and recurrence are still major concerns. In particular, from the medical devices that heal chronic wounds to the complex implants designed to remain in the human body, infections can arise and prevent proper healing. This post-operative complication and consequent re-do surgeries involve impairment of quality life and high medico-social costs. Thus, smart and bioactive medical devices remain to be developed in order to better cope with infections. For such a purpose, there is a need for developing relevant biomaterials with enhanced functionalities.

Biomaterials encompass ceramics, metals and polymers that are exploited in contact with living tissues, organisms or microorganisms, as stated in the definition from IUPAC in 2012 [1]. Metals and ceramics were traditionally used for bone or dental repair and replacement, since they exhibit good biocompatibility and net-shape parts [2]. Nevertheless, they are presently replaced with petroleum-derived polymers in an increasing number of biomedical applications. Actually, polymers present high flexibility and low melt temperature that enable easy processing and complex structures design [3]. Their main drawback is the possible emission of by-products and plasticizer residues that can lead to undesired inflammatory response. An alternative solution relies on the use of biobased polymers that present inherent biocompatibility. The depletion of fossil resources and growing environmental concerns are additional strong drivers for their adoption instead of petroleum-based products. Thus, chitin, cellulose or collagen as new biomaterials are more and more exploited, as highlighted by several reviews in the recent literature [4]–[6].

Within this framework, an excellent candidate for new biobased materials is nanocellulose. This term refers to cellulose particles with at least one dimension in the nanometric range of 1-100 nm. Two different types of nanocellulose are usually described: cellulose nanofibrils (CNF) and cellulose nanocrystals (CNC, whiskers), as depicted in Figure 1. Nowadays, they are mainly obtained from wood at the pilot/industrial scale and supplied as suspensions in water or re-dispersible powders, even if other renewable sources could be available: annual plants, animals and micro-organisms, for which processing and industrialization are still limited.

Cellulose nanocrystals
Length 150-500 nm
Width 5-10 nm

Cellulose nanofibrils
Length several µm
Width 5-50 nm

Figure 1: Schematic representation of cellulose nanocrystals and cellulose nanofibrils

A tremendous enthusiasm is shown by the scientific community on nanocellulose. Owing to its renewability, biodegradability, widespread availability, low density and excellent mechanical properties, an exponential growth of the number of scientific papers and patents is detected over the last decades (Figure 2).

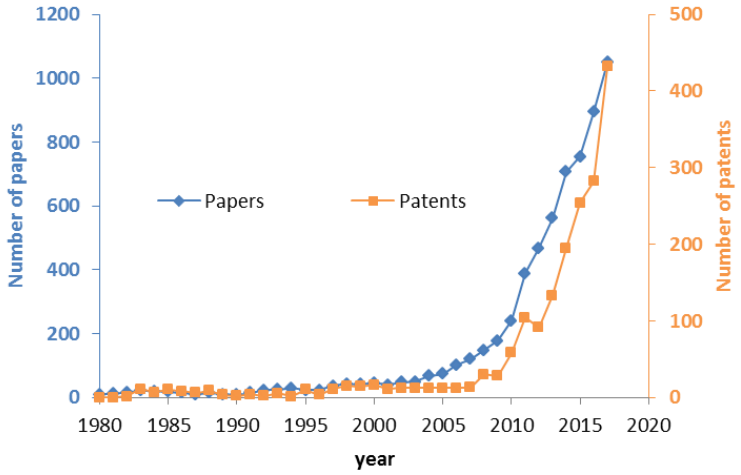

Figure 2: Number of papers and patents released each year dealing with CNF and CNC until 2017 (extracted from SciFinder in July 2018, descriptors are cellulose nanofibrils / cellulose microfibril / microfibrillated cellulose / nanofibrillated cellulose / cellulose nanocrystals / cellulose nanowhiskers / nanocrystalline cellulose / cellulose whiskers)

Since their first isolation in the 1980s [7], [8], the industrial production of cellulose nanofibrils has been extensively studied and optimized. TEMPO mediated oxidation and enzymatic pre-treatments drastically decreased the energy required to produce CNF suspensions, allowing for cheaper and easily implemented processes, compared to CNC. Research efforts are now switching towards potential applications, especially in the biomedical field. Actually, CNF present inexistent or very low biological response and are considered as biocompatible. Moreover, good cell proliferation and migration upon their contact have been confirmed [9], [10]. In addition, their tunable surface chemistry and high specific surface area open wide range of chemical surface modification through adsorption or covalent binding of molecules, potentially including bioactive compounds. For instance, penicillin was covalently immobilized onto CNF resulting in contact-active antibacterial

systems [11]. CNFs are thus considered as an outstanding candidate for new biomaterials. Furthermore, 2D and 3D CNF nanostructures can be easily obtained by various methods such as filtration, solvent casting or freeze-drying. Accordingly, different CNF based materials can be specifically tailored for biomedical applications [12]–[14]. As an example, CNF films, under the form of highly entangled networks, can entrap active principle ingredients (APIs) and sustain the drug release over months [15]. Another possibility is the API loading of CNF aerogels obtained by freeze drying, after CNF modification by poly-(ethylene imine) (PEI) that enabled the drug release upon specific pH and temperature conditions [16]. Otherwise, the combination of CNF with other biobased polymers such as alginate recently allowed the preparation of hydrogels with better mechanical properties and enhanced stability in physiological conditions [17]. Still, the covalent immobilization of API onto the surface of CNF appears to be under investigated. This strategy is believed to bring innovative drug release systems that exploit both the entrapment by CNF entangled network and its tunable surface chemistry.

Consequently, a consortium of several academic and industrial partners was gathered to investigate the development and use of CNF and active molecules, specifically designed for biomedical purposes. Such collaboration led to a project, CELLICAL, supported by the French National Research Agency (ANR-15-CE08-0033) and started in January 2016. This Ph.D. has been carried out in the frame work of the CELLICAL project and addressed the following objectives:

i. Functionalization of cellulose nanofibrils surface with active molecules
ii. Preparation of 100% CNF and CNF composite structures
iii. Investigation of the drug release abilities and antibacterial properties of CNF based structures

In order to achieve these objectives, an active collaboration was developed during the three years with almost all the consortium members, from the academic laboratories / technical research center up to the industry. In particular, strong interactions occurred with experts for nanocellulose production and functionalization (LGP2[1], CTP[2], TEMBEC Rayonier group), glycol-conjugates (CERMAV[3]), drug and prodrug design (DPM[4]), and active molecule release and modeling (INSERM[5]). An important contribution was also given by the know-how of the global leader of medical devices (Medtronic). Finally, a start-up, InoFib, was also involved for nanocellulose functionalization.

[1] LGP2 : Laboratory of Pulp and Paper Science and Graphic Arts
[2] CTP : The Pulp and Paper Research & Technical Centre
[3] CERMAV : Centre de Recherches sur les Macromolecules Vegetales
[4] DPM: Département de Pharmacochimie Moléculaire
[5] INSERM: Institut National de la Santé et de la Recherche Médical

Thus, this Ph.D. took place in a very dynamic context. Experiments/characterization could be performed in various partner's facilities, by taking profit of the variety of tools and knowledge in a very broad field, from the molecules up to the final medical application. This variety also translated in a multiplicity of technical languages, scientific areas and experimental uses (i.e. from the micro-milligrams traditionally synthetized in organic chemistry labs, up to the hundreds of grams required for characterization in pulp and paper science) that made this Ph.D. a really challenging and learning experience.

Finally, the Ph.D. involved also extra-consortium international collaborations to access highly innovative characterization techniques such as ionic liquid assisted NMR and especially Dynamic Nuclear Polarization enhanced NMR. The latter allowed for unique characterization of modified CNF.

This manuscript endeavors to describe the most promising strategies developed and the results obtained, for preparing bioactive grades of CNF and designing CNF based materials for medical devices. Three chapters will provide the reader with an extensive description of the thesis approach and the most relevant results.

In c***hapter I***, the literature review covers biomedical science and currently used biomaterials. A focus on biobased polymers of importance for this project (cellulose and collagen) is exposed. The nanocellulose isolation processes, emerging market, health and toxicity aspects and upcoming biomedical applications are presented. Moreover, surface functionalization of CNF through potentially water based reactions, of interest for fully exploiting the "green" character of such materials, is reviewed. Thus, an insight on the techniques selected for the experimental part is given (namely on esterification, amidation and click chemistry).

Then, the ***chapter II*** presents the results obtained with these functionalization strategies applied to CNFs in order to immobilize active principle ingredients (API). In *chapter II-1*, a single step water based procedure is used to covalently immobilize ciprofloxacin on CNF films. Such films present advantages in the development of active membranes with prolonged antimicrobial properties for topical application (*scientific paper n°1*). The *chapter II-2* presents a two-step immobilization of metronidazole onto CNF suspension, while still being water-based. The first step uses amidation to provide the CNF with pending alkynes functions, which bind with thiol modified metronidazole through thiol-yne click chemistry in the second step (*scientific paper n°2*). Likewise, *chapter II-3* describes a similar approach where CNF are provided with pending furan functions, available for subsequent Diels Alder click chemistry with maleimide modified metronidazole (*scientific paper n°3*).

Finally, ***chapter III*** focuses on the use of these tailored CNF films and suspensions to prepare 100% CNF and collagen-CNF composite materials with antibacterial properties, to be used in different model medical devices. The characterization of such materials is mainly done by water uptake measurements, drug release experiments and antibacterial activity assessments. *Chapter III-1* illustrates the drug release of CNF films that only physically entrap ciprofloxacin. Subsequently, the antibacterial activity of such CNF films is compared with that of films containing immobilized ciprofloxacin (likely by covalent bonding) and the advantages of the latter approach are pointed out (*scientific paper n°4*). Collagen-CNF composites preparation with metronidazole modified CNF suspensions is then detailed in *chapter III-2*. The esterase enzyme-triggered release is discussed, together with antibacterial activity against anaerobic bacteria, confirming the interest of such a strategy. To conclude, another application is targeted in *chapter III-3,* by developing collagen-CNF composites with adsorbed chlorhexidine digluconate that are characterized with a focus on the drug release and antibacterial activity. The influence of gamma radiation on composite structure and antibacterial activity of these samples is finally presented.

The organization of these chapters is graphically described on Figure 3. The reader should keep in mind that most of the sub-chapters are structured as scientific publications, but further comments that are suitable for a more complete Ph.D. discussion are added in the text in grey italic font.

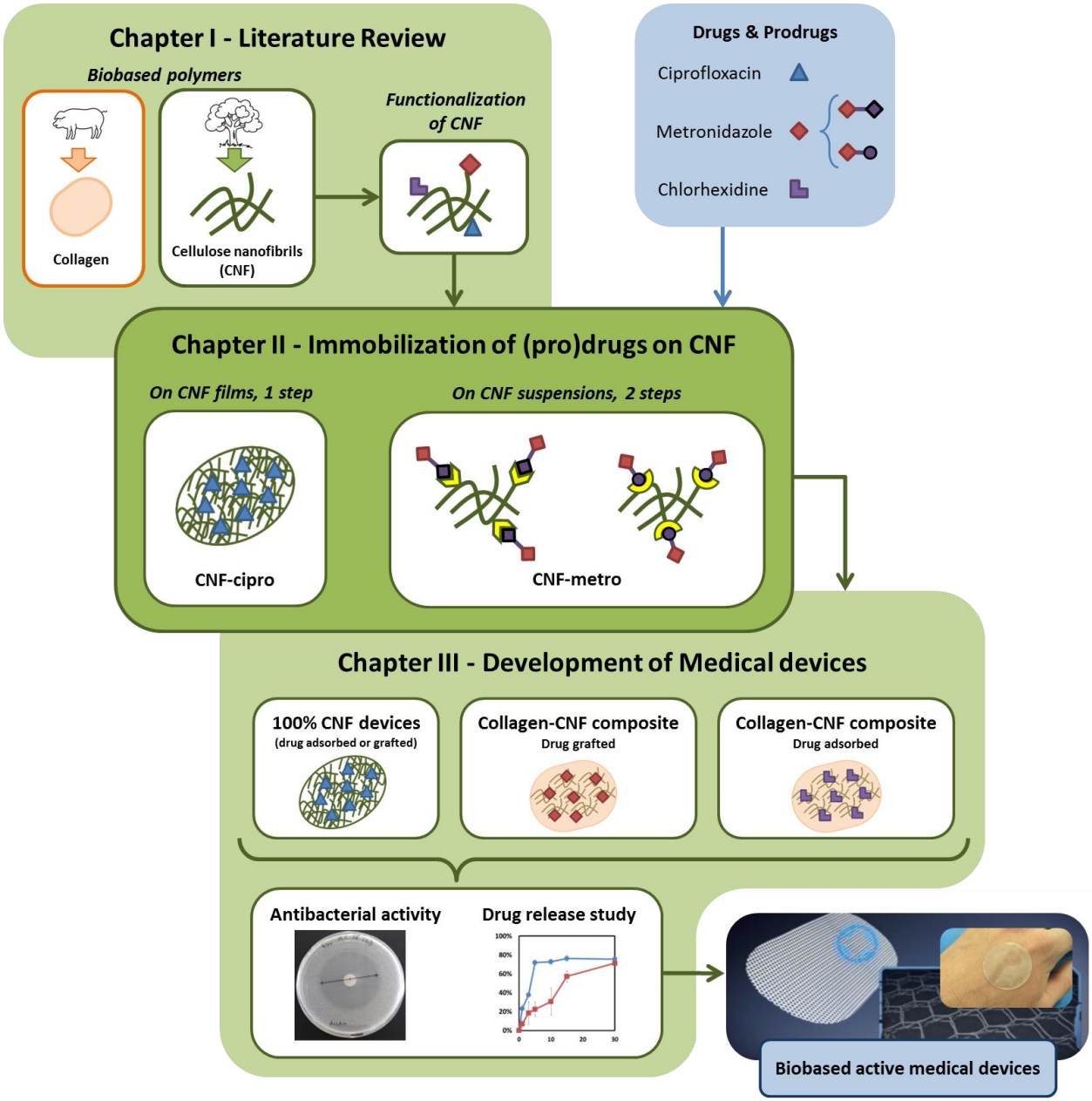

Figure 3: Graphical representation of the Ph.D. manuscript content

This Ph.D. work provides the scientific community with innovative API immobilization routes, water based and likely easy to up-scale. Moreover, it shows the possibility to further investigate nanocellulose with emerging high technology characterization tools such as DNP-enhanced NMR. The Ph.D. outcomes can be useful also for the medical device industry, which gains new insights on nanocellulose potential for healthcare.

Bibliography

[1] H. Pun, "Terminology for biorelated polymers and applications (IUPAC Recommendations 2012," Jul. 2018.

[2] B. J. Love, *Biomaterials : A Systems Approach to Engineering Concepts*. Elsevier Science, 2017.

[3] T. Srichana and A. J. Domb, "Polymeric Biomaterials," in *Biomedical Materials*, Springer, Boston, MA, 2009, pp. 83–119.

[4] R. P. Babu, K. O'connor, and R. Seeram, "Current progress on bio-based polymers and their future trends," *Progress in Biomaterials*, vol. 2, no. 1, p. 8, 2013.

[5] L. S. Nair and C. T. Laurencin, "Biodegradable polymers as biomaterials," *Progress in Polymer Science*, vol. 32, no. 8–9, pp. 762–798, Aug. 2007.

[6] L. Bedian, A. M. Villalba-Rodríguez, G. Hernández-Vargas, R. Parra-Saldivar, and H. M. N. Iqbal, "Bio-based materials with novel characteristics for tissue engineering applications – A review," *International Journal of Biological Macromolecules*, vol. 98, pp. 837–846, May 2017.

[7] A. F. Turbak, F. W. Snyder, and K. R. Sandberg, "Microfibrillated cellulose, a new cellulose product: properties, uses, and commercial potential," *J. Appl. Polym. Sci.: Appl. Polym. Symp.; (United States)*, vol. 37, Jan. 1982.

[8] F. W. Herrick, R. L. Casebier, J. K. Hamilton, and K. R. Sandberg, "Microfibrillated cellulose: morphology and accessibility," *J. Appl. Polym. Sci.: Appl. Polym. Symp.; (United States)*, vol. 37, Jan. 1982.

[9] C. Endes *et al.*, "A critical review of the current knowledge regarding the biological impact of nanocellulose," *Journal of Nanobiotechnology*, vol. 14, no. 1, p. 78, Dec. 2016.

[10] A. Rashad, K. Mustafa, E. B. Heggset, and K. Syverud, "Cytocompatibility of Wood-Derived Cellulose Nanofibril Hydrogels with Different Surface Chemistry," *Biomacromolecules*, vol. 18, no. 4, pp. 1238–1248, Apr. 2017.

[11] S. Saini, N. Belgacem, J. Mendes, G. Elegir, and J. Bras, "Contact Antimicrobial Surface Obtained by Chemical Grafting of Microfibrillated Cellulose in Aqueous Solution Limiting Antibiotic Release," *ACS Applied Materials & Interfaces*, vol. 7, no. 32, pp. 18076–18085, Aug. 2015.

[12] M. Jorfi and E. J. Foster, "Recent advances in nanocellulose for biomedical applications," *J. Appl. Polym. Sci.*, vol. 132, no. 14, p. n/a-n/a, 2014.

[13] N. Lin and A. Dufresne, "Nanocellulose in biomedicine: Current status and future prospect," *European Polymer Journal*, vol. 59, pp. 302–325, Oct. 2014.

[14] N. Halib *et al.*, "Potential Applications of Nanocellulose-Containing Materials in the Biomedical Field," *Materials*, vol. 10, no. 8, p. 977, Aug. 2017.

[15] R. Kolakovic, L. Peltonen, A. Laukkanen, J. Hirvonen, and T. Laaksonen, "Nanofibrillar cellulose films for controlled drug delivery," *European Journal of Pharmaceutics and Biopharmaceutics*, vol. 82, no. 2, pp. 308–315, Oct. 2012.

[16] J. Zhao, C. Lu, X. He, X. Zhang, W. Zhang, and X. Zhang, "Polyethylenimine-Grafted Cellulose Nanofibril Aerogels as Versatile Vehicles for Drug Delivery," *ACS Appl. Mater. Interfaces*, vol. 7, no. 4, pp. 2607–2615, Feb. 2015.

[17] O. Aarstad, E. B. Heggset, I. S. Pedersen, S. H. Bjørnøy, K. Syverud, and B. L. Strand, "Mechanical Properties of Composite Hydrogels of Alginate and Cellulose Nanofibrils," *Polymers*, vol. 9, no. 8, p. 378, Aug. 2017.

Chapter I

Literature review

Table of content

I. Literature Review

Introduction to chapter I

The overall context of this Ph.D. project will be described through this literature review, based on more than 200 references, mostly no more than 5 years old, confirming that the topic is emerging. The objective is to introduce the concepts related to the project to "non-expert" scientists by providing them with general knowledge on every topic, but also to experienced scientists by presenting relevant data through tables and schematic representations. The transitions in between each section will include comments in grey italic font on how the project is related to the cited literature.

The first part of the literature review offers an overview of the standard biomaterials currently available. Biobased polymers that present potential use as biomaterial are introduced: collagen and cellulose origin, chemical structure and existing biomedical applications are exposed.

The second part focuses on nanocellulose. Its peculiar characteristics arising from its diverse isolation processes are described. The topics of its industrialization together with health and toxicology are detailed and an emphasis on the biomedical applications of cellulose nanofibrils (CNF) is proposed.

Finally, the last part covers the functionalization strategies of CNF and how it can further extend its potential for being used in medical devices. The Figure I.1 summarizes the graphical structure of this chapter.

This literature review is believed to provide the reader with insight on CNF in order to easily go over the next chapters.

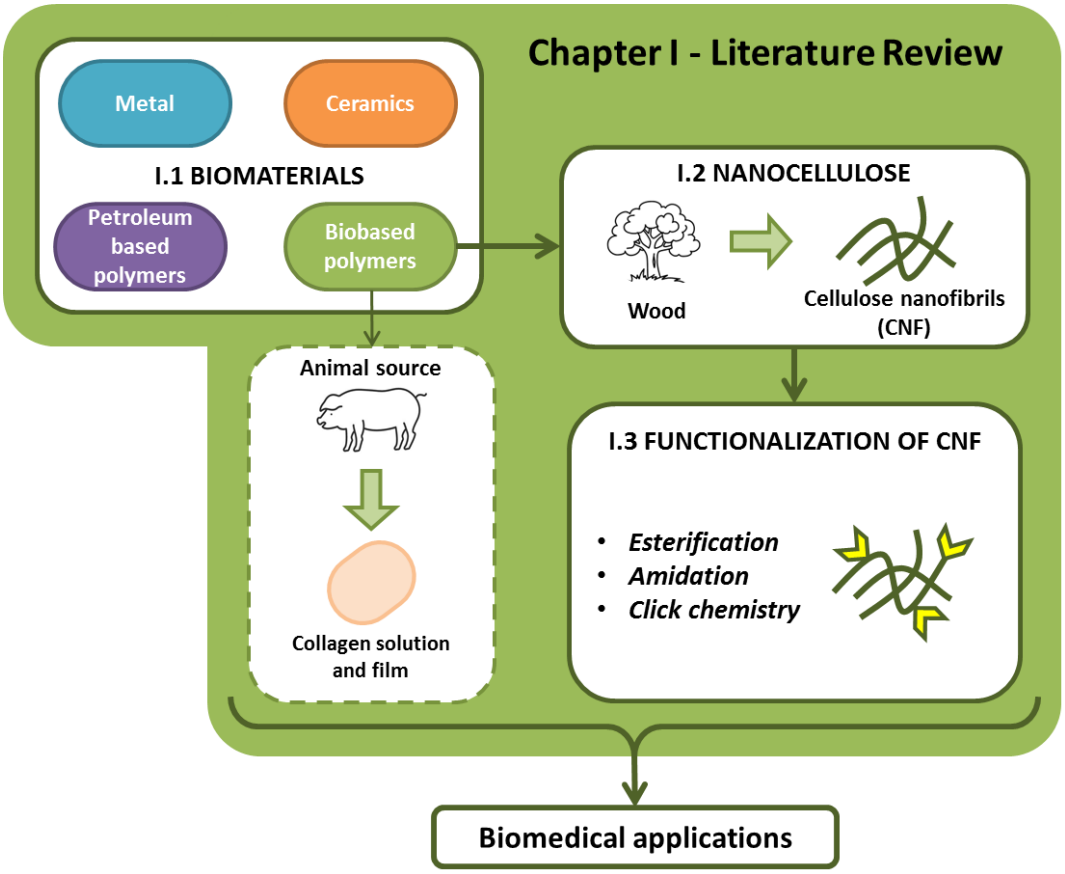

Figure I.1: Graphical representation of chapter I structure

1. Trends of biobased polymers in biomedical application

Biobased polymers are produced from renewable resources in nature. They can be biodegradable but a clear difference lies in the fact that biodegradable polymers can also be synthesized from fossil resources. Likewise, biobased polymers are not all biodegradable as in the case of green polyethylene for instance [1]. The global production of biobased polymers is constantly rising and reached more than 2 million tons in 2017, which is still less than 1% of the 320 million tons of plastics produced annually [2].

However, the growing concern about the depletion of fossil resources drives the population and the research community towards more sustainable material resources and processes. In 2011, the European innovation policy, called Lead Market Initiative (LMI), identified biobased products as one of six important sectors that are supported by actions to bring new products or services to the market [3]. Similarly, in North-America, the *Biopreferred®* program is implemented by the United States Department of Agriculture (USDA) and aim at increasing the purchase and use of bio-based products. The program was recently extended by the 2014 Farm Bill [4].

The first generation of bio-based polymers was mainly extracted from agricultural feedstocks such as corn and potatoes, but an important shift was recently made in order to move away from food resources. Nowadays, three principal ways are identified for the production of bio-based polymers, i) extracting natural polymers from plant and animal resources (cellulose, collagen or chitin for instance) and apply partial modification, ii) using bio-based monomers produced by fermentation or conventional process and carry out classic polymerization processes (PLA, PBS, etc.) or iii) producing bio-based polymers directly from bacteria (PHAs) [5].

Tendencies of the past few decades regarding population aging and increased incidence of chronic diseases or disabilities, call for the development of novel medical grade materials [6]. The need for highly functional systems that are able to reproduce the biological conditions of living organisms is one of the key points in order to address the 21st century human health diseases. Nowadays, nature derived therapeutic constructs are of great relevance in the current biomedical sector. Most of biobased materials present several complementary properties such as unique chemical structure, bioactivity, nontoxicity and biocompatibility which make them good candidates for the use in medical applications. Some polymers from natural sources are known to mimic the extracellular matrix and promote cell adhesion, interaction and differentiation. Such functionalities match with the requirements of tissue engineering materials [7].

This first section aims at describing the landscape of existing biobased materials that are used in the biomedical field, and will focus on collagen and cellulose since these biobased materials are used in this Ph.D. work.

1.1 Introduction to biomedical engineering

Biomedical engineering has emerged in modern hospitals over the last fifty years and encompasses interdisciplinary scientific fields. It aims at applying engineering principles and methods to the understanding of living tissues and the design and development of products that maintain, restore or improve tissue functions. It includes a wide range of discipline such as diagnostics and physiologic instrumentation, medical imaging, biological system analysis (modeling, simulation, control), materials for medical devices, artificial organs and rehabilitation, controlled drug delivery and tissue engineering [8]. Biomedical engineering implements solutions to a variety of medical fields as depicted on Figure I.2.

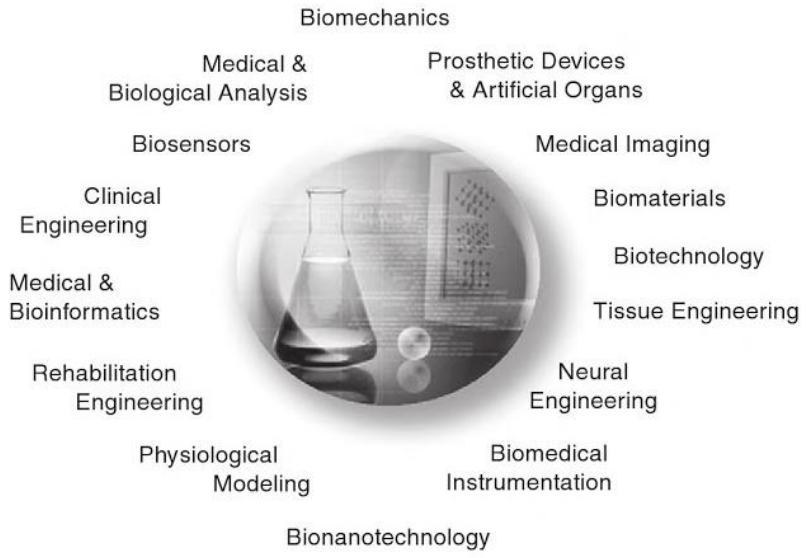

Figure I.2: The world of biomedical engineering, adapted from [9]

Tissue engineering and drug delivery are key biomedical applications these days. They are among the most investigated fields regarding emerging uses of biobased polymers.

Tissue engineering has a very wide scope. The IUPAC describe tissue engineering as “Use of a combination of cells, engineering and materials methods, and suitable biochemical and physico-chemical factors to improve or replace biological functions” [10]. In other words, it aims at building up new functional living tissues by using cells that are grown in combination with a matrix or scaffolds to guide their development. The new cell structure is grown in vivo or in vitro and then implanted in the human body. Tissue engineering thus also encompasses wound healing field in

which implants are used. The main challenges associated with tissue engineering are i) cells handling for in-vitro or in-vivo growth of the new tissue and its blood supply, ii) materials used for scaffolding that can be permanent or biodegradable, natural, synthetic or hybrid and tuned according the targeted application, iii) cell type combination for complex structure, iv) stem cell use, v) integration of digital information and computer-assisted design, vi) time dimension of the implantation (acceptation, degradation of scaffold), vii) social and regulatory challenges [11]. To sum up tissue engineering challenges, three pillars can be identified, as depicted in Figure I.3: cells, scaffolds (biomaterials) and regulatory signals.

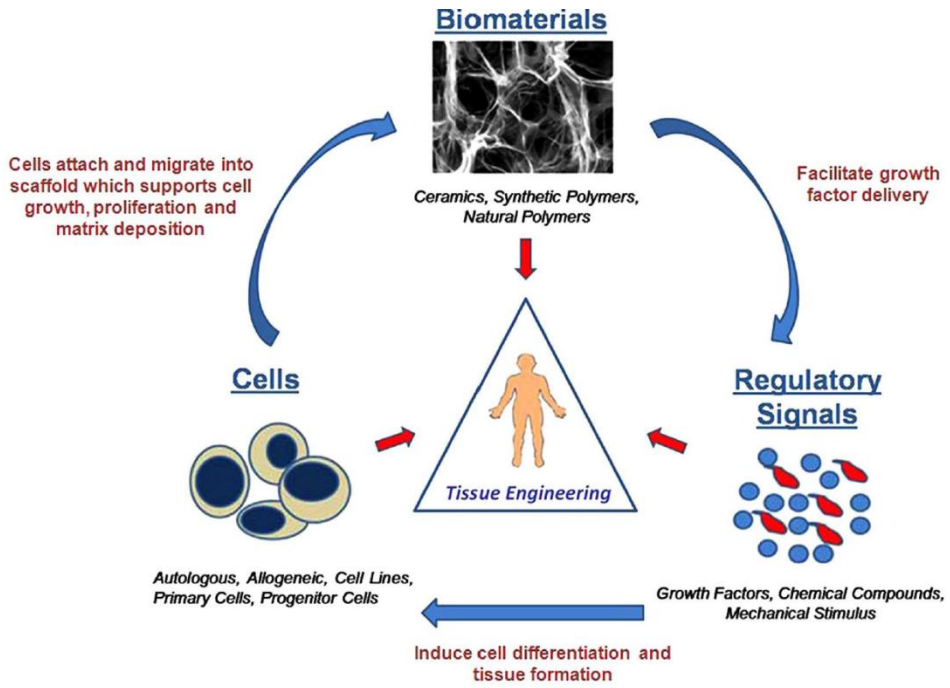

Figure I.3: Illustration of tissue engineering principle triad composed of the biomaterial used for scaffolding, the cells and the biological signals [12]

The requirements for a material to be a good scaffold candidate for tissue engineering applications are a highly porous 3D structure that provides good cell attachment, guide the production of extra cellular matrix (ECM) by the cells, ensure the mechanical strength before the new tissue has grown enough to support itself, and sometimes to deliver bioactive molecules [13]. This induces proliferation and differentiation of cell and finally neo-tissue genesis. Keys physical properties for the scaffold candidates are: pore size, water content, mechanical strength, cell adhesion, biocompatibility and degradability. Also, it should be noted that tissue engineering application does not require the same cell proliferation process as for natural development. An accelerated regeneration process is targeted and naturally occurring ECM or derivatives may actually be detrimental for the success of the tissue engineering procedure. For instance, natural tissue matrices

often show a lack of macro/micro pores structure, which is necessary for uniform cell proliferation [14].

This Ph.D. focuses on the development of substrates intended for the design of wound healing devices for external (topical) or internal use (like in soft tissue repair).

Drug delivery is defined as *a process of administration of a bioactive substance of pharmacological interest* by the IUPAC. The report also indicates that a drug delivery system can be a stationary implant or an active or passive moving system (inside the body), with or without targeting abilities. A slight difference is also identified between controlled and sustained drug delivery in IUPAC. A drug delivery system is described as *sustained* if it shows slow release abilities for therapeutics effects. If the system also achieves the pharmacokinetic requirements, it can be described as *controlled* drug delivery system [10]. Typical drug concentration profiles are illustrated in Figure I.4, which compares conventional release profiles with sustained and controlled release. The minimum and maximum therapeutic concentrations form the therapeutic window in which the drug is supposed have the most suitable therapeutic effect. Conventional dosage forms usually show peaks and drops out of the therapeutic window. These fluctuations of the drug level can lead to undesirable side effects. Sustained release dosage forms offer a slower drug release with a drug concentration that remains for a certain period of time inside the therapeutic window before losing its potency. Only controlled drug release profiles provide both slow and prolonged levels inside the therapeutic window. A zero-order kinetic release rate is the first key to achieve controlled drug release. The second objective is to maintain the drug concentration stable by the use of intelligent carriers that cope with the unpredictable depletion rates of the drug in-vivo [15].

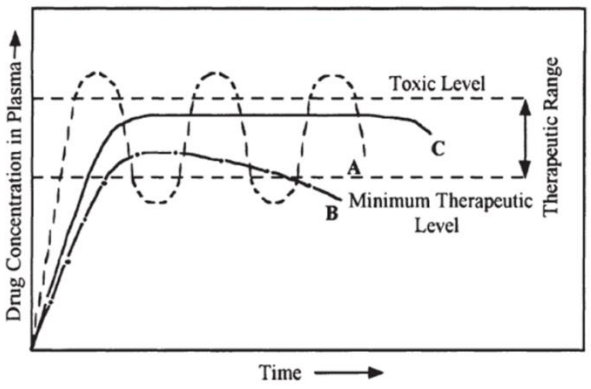

Figure I.4: Typical plasma drug concentration profiles: conventional dosage forms (A), sustained (B), and (C) controlled release dosage forms, extracted from [15]

Biomedical field and associated topics are described more in detail in afore-mentioned books and reviews. Many materials are available for building scaffolds for tissue engineering or designing

controlled drug release systems. In this Ph.D. project, the focus will be on biobased materials which are currently of high interest for this research area.

1.2 Overview of biobased materials for biomedical applications

1.2.1. Biomaterials, a definition

In the context of scientific research the consistency of terminology is crucial, especially for fast growing fields of investigation. For instance, patenting process can be affected by the different uses of inaccurate words, often leading to litigious war [16]. The use of words with the prefix bio- can imply different meaning. For instance, *biomaterial* is a word that can have two meanings. It can refer to a material that helps "life", as in the field of biomedical engineering where it is supposed to be in contact with living tissues, or it can refer to a material that is extracted from biomass (plants and animals), which is different. One could misuse *biomaterial* to describe these two topics. When it comes to build up synergies in between biomedical world and nature-extracted material experts, a clear definition is required. According to the IUPAC definition of 2012, a biomaterial is a material that is exploited in contact with living tissues, organisms or microorganisms. The notion of exploitation includes utility for applications and fundamental research. The use of *polymeric biomaterial* is recommended when one wants to deal with polymer for medical purpose [10]. The definition by IUPAC is chosen for this entire manuscript.

Biomaterials encompass various types of materials ranging from metals to ceramics, synthetic and biobased polymers as depicted on Figure I.5.

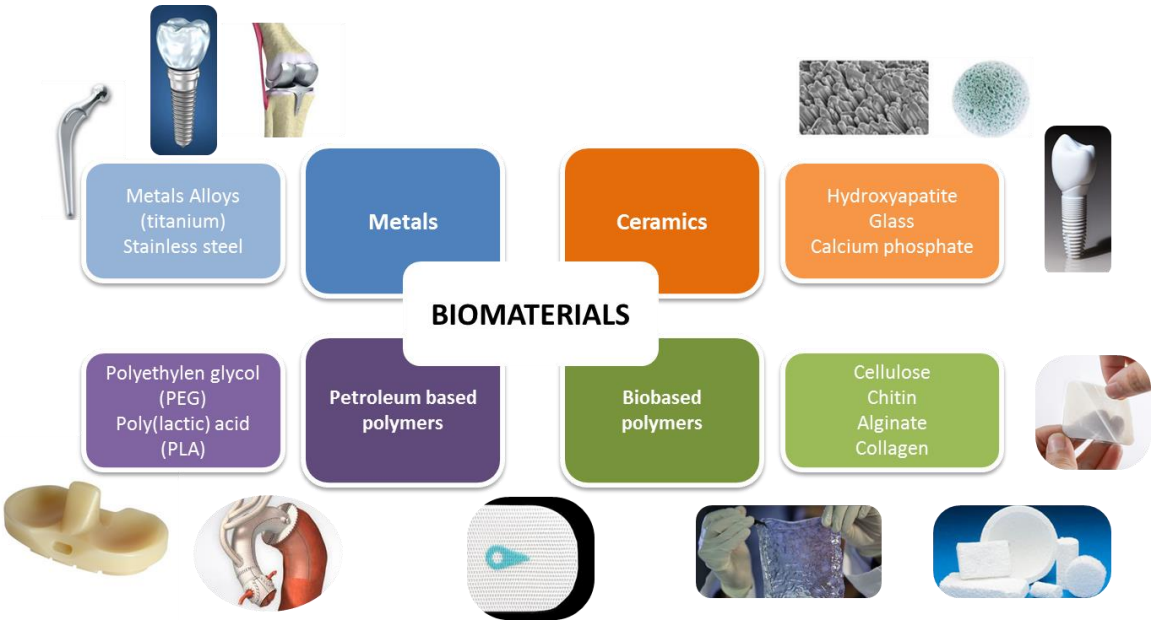

Figure I.5: Commonly used biomaterials, inspired from [17]

Metals and metal alloy biomaterials have been used for temporary or permanent medical implant, prosthetics and instrumentation for many decades thanks to their biocompatibility. Metallic biomaterials have a good in-vivo mechanical, ionic and electrical response and they allow for the design of net-shape parts. Alloy such as stainless steel, cobalt-chromium, titanium alloys and other precious metal alloy are now developed for such applications. Nowadays, the main areas where metal biomaterials are used are hard tissue applications such as bone and dental repair and replacement [18].

Ceramics are produced by the combination of groups of ions and cations to form crystals with regular repeating structure and unit cell shape and dimensions. Calcium Hydroxyapatite (CaHAP), Aluminum Oxide Al_2O_3, Zirconia ZrO_2 and Porcelains (combination of SiO_2 and Al_2O_3) are examples of widely used ceramics biomaterials. They can be used as consolidated monoliths, coatings or fillers in matrices. In the form of monoliths they are mechanically comparable to metal so that their use in hard tissue is seen. Coating of reactive metal structures is another field of application since they are highly biocompatible [18].

Petroleum derived polymer can also be used as biomaterials. This category encompasses polyolefins (mainly polyethylene PE and polypropylene PP), methacrylates like poly(methyl metacrylate) PMMA, bis glycidyl methacrylate BisGMA), polyamides (Nylon 6,6, polyamide 6.10), polyesters (PET, PLA, PGA, PCL), polyethers (PEO and PPO) and silicones. Compared to metals and ceramics, the principal advantage of synthetic polymers is their really high flexibility and low melt temperature that allow for easy melt processing and complex structure design. Therefore, numerous biomedical applications can be addressed with synthetic polymers that are summarized on Table I.1. Vascular grafts prostheses design is one example, among many other, where melt processing is a key feature.

Table I.1: Medical uses of synthetic petroleum derived polymers, extracted from [19]

Polymer	Applications
Polyvinyl chloride	Extracorporeal devices; hemodialysis or hemoperfusion, blood tubing, cardiac catheters, blood bag and IV infusion set, endotracheal tubes surgical tapes, sheet oxygenator, artificial heart, blood pump, artificial limb
Ultrahigh MW polyethylene	Acetabulum in total hip prostheses, artificial knee prostheses
Polypropylene	Membrane oxygenator, finger joint prostheses, IV cannulae, unabsorbable sutures
Silicone rubber	Hydrocephalus shunts, catheters, membrane for oxygenator, artificial skin for burn dressing, plastic surgery implant, artificial heart, heart assisted pump, drug release system, atrioventricular shunts, ear prostheses, facial prostheses, artificial heart valve, tendon, finger joint repair, tracheal prostheses, bladder prostheses, bladder patch, intestine patch, dura-mater prostheses, retinal detachment, impressing materials, heart pacemaker leads
Polycarbonates	Membrane for oxygenator, hemodialyzer, plasmapheresis membrane
Polyester	Vascular graft prostheses, fixation device for tissue, hernia repair, patches for heart, bladder, arteries, suture
Polytetrafluoroethylene	Vascular graft prostheses, heart patch, retinal detachment, femoral stems
Polyurethane	Artificial heart pump material, balloon, heart valve prostheses, vascular graft prostheses, coating for blood compatibility
Polymethyl methacrylates	Bone cement, artificial teeth, denture material, bone prostheses, cranial bone replacement, intraocular lenses, membrane for dialysis

However, the drawback of synthetic polymer is by-products or plasticizers release (initiators, unreacted monomers…), upon degradation in physiological conditions, that can trigger inflammatory response [18].

Nature derived polymers (biobased polymers) have attracted increasing attention since petroleum resources are finite. Moreover, many biobased polymers present inherent biocompatibility properties. Biomimetic approaches are used to harvest the technological advances made by nature over millions years of development in order to design new innovative materials. Recent biomimetic approaches are strongly related to biobased polymers, such as cellulose [20], [21]. Consequently, biobased polymers are of particular interest in these approaches. The next part will thus deal with the novel use of biobased polymer in the field of biomedical engineering. The objective is to show how they can replace existing biomaterials and especially how they can allow for the development of new combinations of properties for innovative applications [1].

1.2.2. Biobased polymers

Biobased polymers can be of two sorts: synthetic or naturally occurring. Synthetic biobased polymers are chemically equivalent to synthetic petroleum-derived polymers such as bioPE. Biomass is exploited, sometimes de-structured (mainly by bacterial fermentation) and re-used through traditional processing routes to end up with biobased polymers. The second sort of biobased

polymers is directly harvested from biomass such as starch or cellulose, which are renewable and biodegradable. These polymers are naturally occurring polymers. Both synthetic biobased and naturally occurring polymers have already been used as biomaterials.

1.2.2.a. Synthetic biobased polymers

PLA

The thermoplastic polyester polylactic acid (PLA, Figure I.6) was first synthetized in 1845 by Theophile-Jules Pelouze through the poly-condensation of lactic acid (LA) into low molecular weight (800-5000 g/mol). The production process was improved over the 20th century, especially by DuPont chemists in the 1950s, to reach 100,000 g/mol. The mechanical properties of PLA were suitable for competing with other commercial polymers even if its high cost narrowed its use to mainly biomedical applications. A less expensive commercial process was invented in the late 1980s by Dr. P. R. Gruber, expanding the use of the polymer to low added value products such as disposable bags. PLA is now the first mostly traded biobased polymer worldwide.

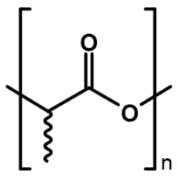

Figure I.6: PLA chemical structure

Lactic acid can be obtained from petrochemical feedstock but it is mainly produced (>90%) by fermentation of rice, corn, beets and other crops, for the production of PLA in large quantities [22]. PLA is thus derived from renewable resources and is also biodegradable under compost conditions. It has been thus considered as a good alternative to reduce petroleum-based plastics since it can also be successfully processed through a wide range of industrial setups: extrusion, injection molding, stretch blow molding, cast film, fiber spinning and compounding [23].

Interesting properties of PLA for biomedical applications are related to its good biocompatibility and its biodegradability into well-tolerated and safe degradation products [11]. It is also moldable which allow for a numerous shapes design like scaffolds, sutures, rods films, nanoparticles and micelles. According to a recent review [25], PLA is used in many medical fields such as orthopedic, dentistry, surgery as depicted in Figure I.7.

Plastic surgery
- Suture
- Reconstructive surgery
- Dermal fillers
- Skin graft

General surgery
- Hernia mesh

Gynecology
- Stress incontinence mesh

Radiology
- Theranostic imaging

Oncology
- Drug delivery
- Intracranial delivery
- Nanoparticles
  - Intranasal delivery
  - Micelles
  - Thermoresponsive hydrogels
  - Vaccines
  - Transdermal delivery

Orthopedic
- Peripheral nerve and spinal cord injury regeneration
- Bioabsorbable screws
- Meniscus repair
- Guided bone regeneration

Cardiac
- Chest wall reconstruction
- Stent
  - Synergy DES
  - Biolimus-eluting stent
  - Hybrid stents

Dentistry
- Guided tissue regeneration
- Biocompatible space fillers

Figure I.7: Overview of biomedical use of PLA, extracted from [25]

PHA

Polyhydroxyalkanoates (PHAs) comprise biodegradable polyesters that are synthesized by a large amount of microorganisms as an intracellular storage of carbon and energy [26]. An unbalanced nutritional supply leads the microorganisms to produce extensive amounts of PHAs in the form of granules. PHAs can then be recovered by fermentation, isolation and purification of the fermentation broth [1].

The first and simple PHA was discovered in 1926 by Maurice Lemoigne: polydroxybutyrate (PHB) was found in *Bacillus megaterium* [1]. The general chemical structure of this polyester family is depicted on Figure I.8. More than 150 monomers are identified for the PHAs family, which gives a broad range of properties to develop new structures and products.

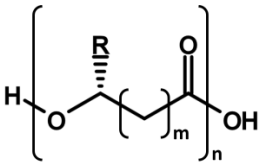

Figure I.8: General chemical structure of PHAs (m>1, R=H or C1 to C16 chains)

Some drawbacks remain in these polymers such as brittleness, tendency to acquire a high degree of crystallinity, poor stiffness, slow degradation rate, and hydrophobic character. However, PHAs are also biocompatible, biodegradable and have piezoelectric properties that make them suitable for tissue engineering applications. They support cell adhesion, cell growth and communication and cell organization to design the intended tissue scaffolds [7].

PBS

Poly(butylene succinate) (PBS) is a family of biodegradable thermoplastic polymers which are synthetized via poly-condensation of succinic acid or dimethyl succinate and 1,4 butanediol (BDO). Pioneer work on PBS synthesis is attributed to Carothers in 1931. Its chemical structure is exposed on Figure I.9.

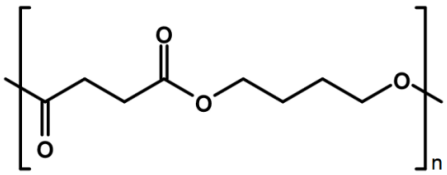

Figure I.9: Chemical structure of PBS

Succinic acid can be derived from fossil source, but can also be isolated from the fermentation of renewable feedstocks or by harvesting bacterial productions. BDO is also usually derived from petrochemical sources but direct fermentation of sugar or even catalytic reduction of succinic acid are relevant alternative routes [27]. PBS exists in the form of various copolymers that allow for the tuning of its physical properties [28].

PBS was originally studied for biodegradable packaging development, but recently its use for medical industry was reconsidered by researchers. Its excellent biodegradability is well known and its biocompatibility toward animal and human cells was demonstrated. PBS thus found applications in bone repair, scaffolding, composites, tissue engineering and drug delivery [29].

1.2.2.b. Naturally occurring polymers

Starch

Starch is the principal food reserve polysaccharide in plants. It is found in all staple foods like wheat, maize, rice, etc. Chemically speaking it is a mixture of two homopolymers composed of D-gluco-pyranose units: amylose and amylopectine. Amylose is a linear polymer of α(1→4) linked units while amylopectin is a branched polymer of α(1→4) linked units and α(1→6) branched units as depicted on Figure I.10.

Starch can be broken down by controlled enzymatic hydrolysis to give maltodextrins, mannitol or fructose, which are of importance in the food industry. Enzymatic hydrolysis of starch by D-glucotransferase allow for the production of cyclodextrins which are cage-like molecule widely used in the pharmaceutical industry to better solubilize hydrophobic active princi ple ingredients (API) and stabilize tablet systems [30].

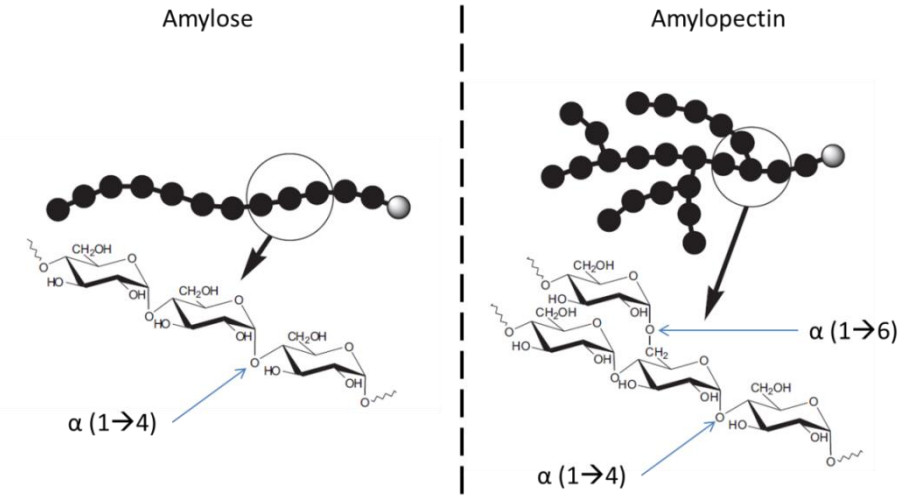

Figure I.10: Structure of Amylose and Amylopectin that compose Starch (adapted from [30])

Starch can also be used in biomedical. The feature of these polymers being their biodegradability, they were used as a temporary scaffolds composites for several medical applications such as orthopedic implants [31], bone cements or drug delivery carriers [32] and tissue engineering [33]. These works show that starch is a functional biomaterial.

Alginate

Alginate is a naturally occurring anionic polysaccharide obtained from brown seaweed (*Phaephyceae*) by chemical treatment with alkali solutions, mostly NaOH, before filtration and precipitation with sodium or calcium chloride addition. The powder obtained is water soluble. Chemically speaking, alginate is a linear copolymer containing blocks of (1,4)-linked β-D-mannuronate (M) and α-L-guluronate (G) residues in various ratios as described on Figure I.11.

Alginate is biocompatible, has low toxicity, relative low cost and form gels with the aid of divalent cations such as Ca^{2+} as shown on Figure I.11. This ability of alginate to form solid hydrogels is at the origin of its particular interest for medical application because such hydrogels closely resemble extra-cellular matrices (ECM). Area such as wound healing, drug delivery, in vitro cell culture and tissue engineering benefits from alginate hydrogels and their tunable crosslinking strategies as indicated in the extensive review by Lee & Money in 2012 [34]. Alginates have been used for over more than 40 years for raft-forming formulations in order to treat heartburn and esophagitis: gastric acid is converted to carbon dioxide by the bicarbonate containing alginate formulation which turns into a foam that floats on the gastric content, like a raft on water, and acts like a neutral-pH barrier. The commercial brand Gaviscon have been on the market for several decades for the treatment of reflux symptoms in infants and children and the management of heartburn and reflux during pregnancy [35].

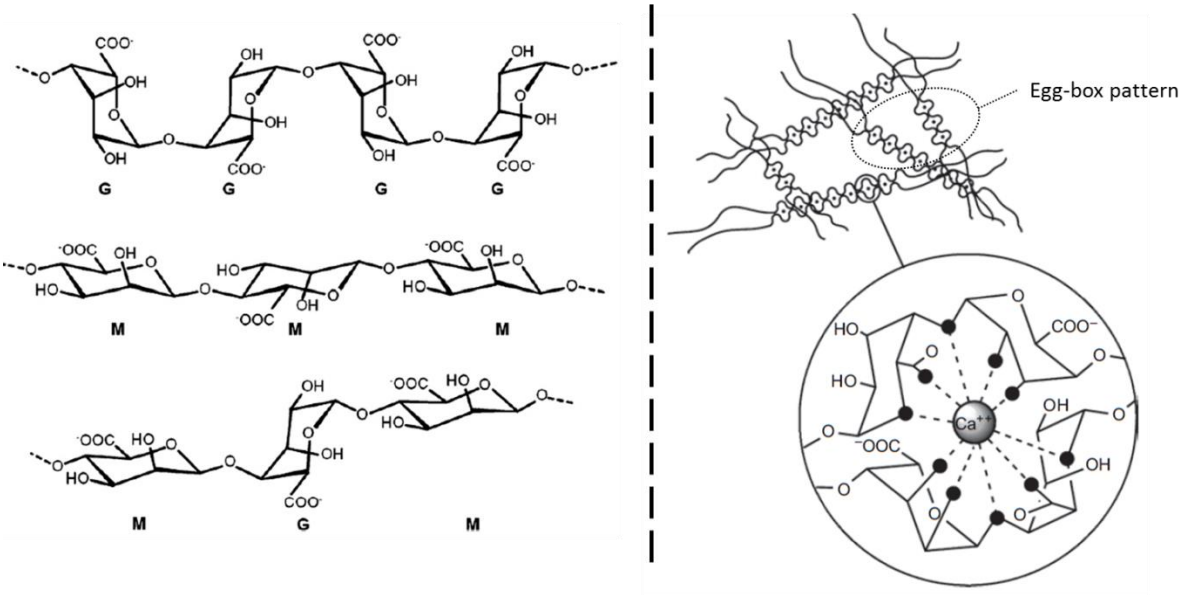

Figure I.11: LEFT , chemical structure of alginate polymer composed of (1,4)-linked β-D-mannuronate (M) and α-L-guluronate (G) residues [34] and RIGHT, eggbox structure of alginate cross-linking with divalent ions (Ca^{2+}) [36]

Epidermal and dermal wounds can also benefit from calcium-alginate dressings in the context of diabetic foot lesions or post-surgical wounds where immunological properties of alginate itself, in combination with Ca^{2+} that heals promotion, contribut to better treatment results in comparison to conventional products [37].

Calcium-alginate gels have also great potential in the immobilization of living cells. Calcium-alginate gel spheres can be designed as a vessel for cells and find application in cell transplantation for instance. Alginate solution is mixed with cells and the mixture is then added drop wise in a Ca^{2+} solution in order to cross-link the surface of the drops (through egg-box system) and immobilize the sphere structure. Cells can be released from the spheres by exposure to a calcium ion scavenger like phosphate or citrate. Low G content alginate quickly release the cells while high G contents alginate need hours [38].

Chitin/Chitosan

Chitin is the second most occurring polymer on earth after cellulose. It is found in shell of crustaceans, mainly crabs, shrimps and lobsters. Shell can be ground and treated with HCl for demineralization and chitin can be transformed into chitosan through deacetylation with concentrated NaOH [19]. Chitosan is a linear polymer composed of α(1→4) linked N-acetyl-D-glucosamine residues (Figure I.12). A common molecular weight of chitosan is in the range of 50,000-1,000,000 g/mol. Chitosan is normally insoluble in aqueous solution above pH 7 but is readily soluble in dilute acid (pH<5) where free amino groups are protonated. At pH above 5 amino groups start to

be deprotonated and become available for hydrogen bonding which will establish the gel structure of chitosan at some critical pH which depends on the degree of deacetylation and average molecular weight. Crystallinity also depends on the degree of deacetylation and is at the maximum when the polymer is fully acetylated which eventually influence also the biodegradation rate [7], [19].

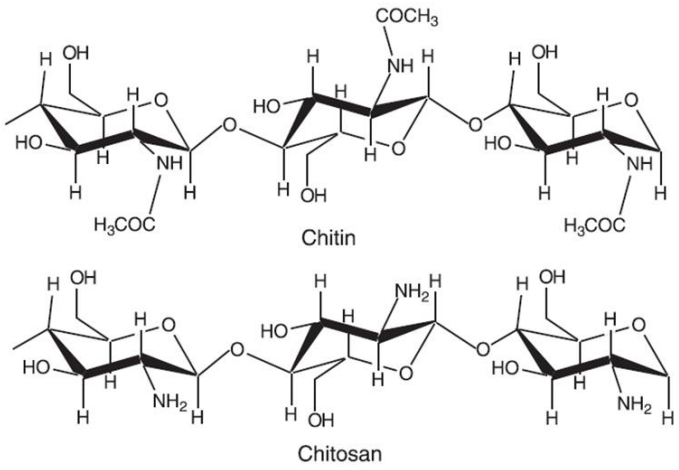

Figure I.12: Chitin and chitosan chemical structures [39]

The adhesive nature of chitin and chitosan, together with their permeability to oxygen and their antifungal and bactericidal character are very relevant properties for the treatment of wounds and burns. Hydrogels, fibers, membranes, scaffolds and sponges based on chitin and chitosan have been successfully prepared for such biomedical applications [39].

Tissue engineering and regenerative medicine is also a wide field of application for chitin and chitosan. For instance, electrospun nanofibers based on chitosan, collagen and hydroxyapatite can mimic the extracellular matrix and promote bone regeneration [40]. Liver tissue engineering was investigated with chitosan-gelatin 3D scaffolds crosslinked with genepin, which demonstrated suitable porosity and best biocompatibility [41].

The two next sub-chapters are dedicated to collagen and cellulose that are both naturally occurring polymers of importance for this Ph.D. work. A more detailed review of their physicochemical properties and medical applications is thus presented.

1.3 A focus on Collagen/gelatin in biomedical field

Collagen structure

Collagen is one of the most abundant proteins in all animals. Human collagen represents one -third of the total protein and around three quarters of the dry weight of skin, which is the largest organ in human body [42]. This means about 3.5 to 5 kg for average human beings. It is the main tensile element of tissues such as tendon, cartilage, and skin [43]. Figure I.13 shows an example of collagen organization in tendon.

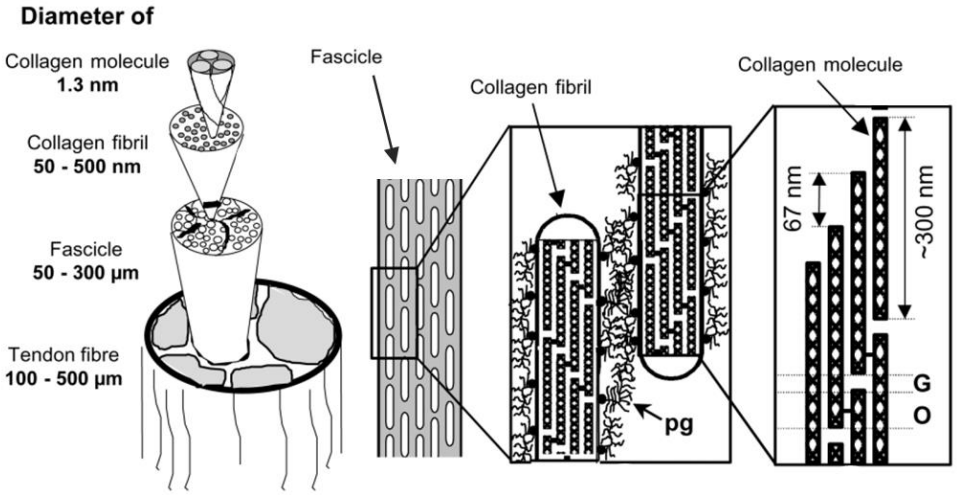

Figure I.13: Simplified tendon structure: a composite of collagen fibrils embedded in a proteoglycan-rich matrix (pg). Triple helical collagen molecules of about 300 nm are organized in fibrils with a regular axial spacing of 67 nm (without mechanical solicitation). Gaps (G) and overlap (O) zones thus appears (adapted from [44])

Collagen has a fibrous structure composed of three polypeptide chains (alpha-helix structure) wrap around each other in a supercoil triple helical structure as depicted in Figure I.14a. The collagen polypeptide chains have the general repeating sequence Gly-X-Y where Gly, X and Y are amino-acids. Gly stands for glycine and X and Y are most of the time proline and hydroxyproline amino acids as depicted on Figure I.14b [45]. X and Y amino-acids residue are located at the external surface of the triple helix providing the collagen molecule with a wide range of lateral interactions within the extracellular matrix, giving rise to a high number of potential supramolecular structures [46]. Hydrogen bonding is governing the interactions between the three strands involved in the triple helix [47], which is also shown in Figure I.14c.

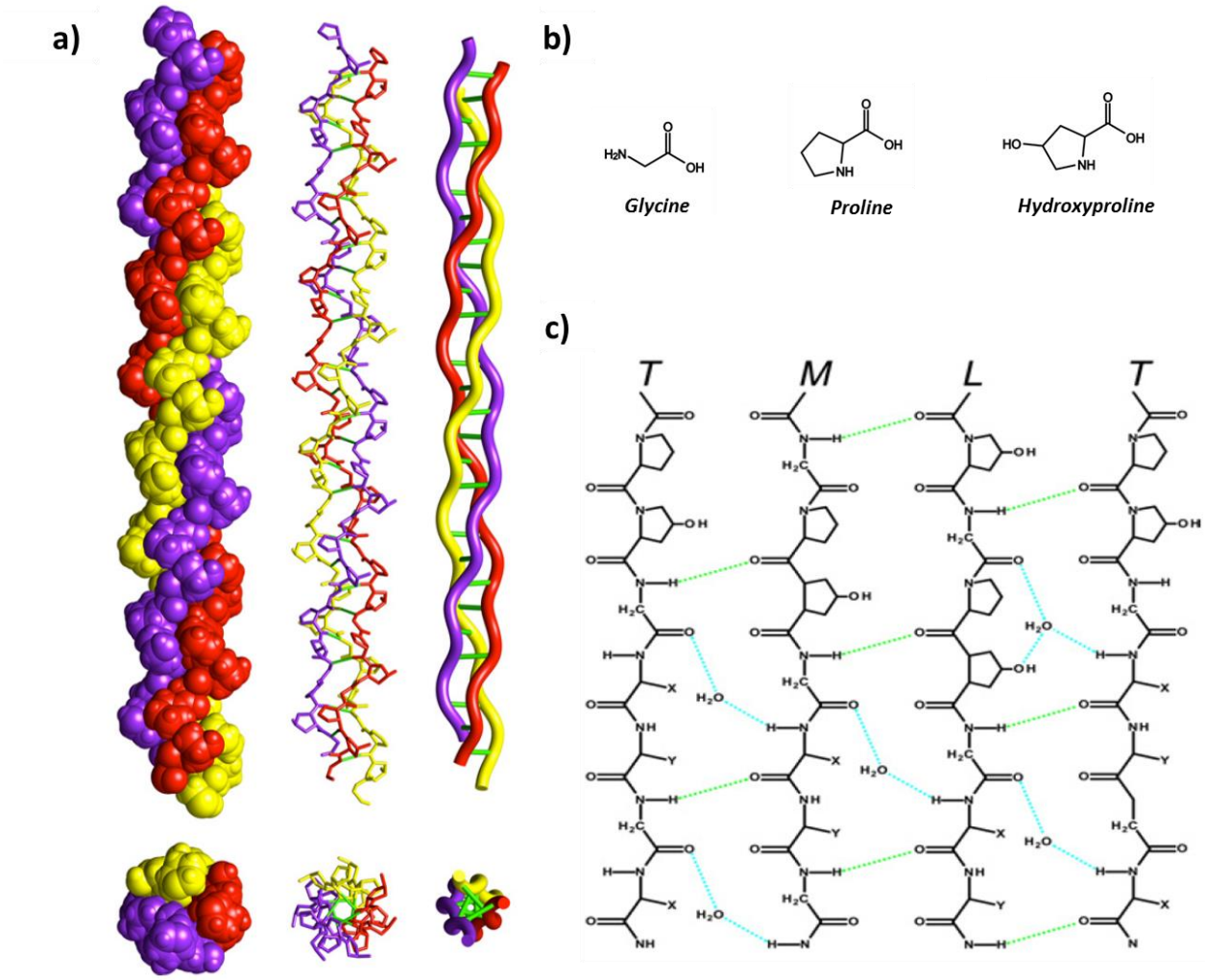

Figure I.14: From the molecular structure to triple helix organization of collagen, a) Side and Top views of the structure of a collagen triple helix in space-filling diagram (left), stick diagram (middle), and ribbon diagram (right), adpated from [48], b) structure of the main amino acids involved in collagen polypeptide chain formation, c) hydrogen-bonding topology of water bonded collagen model (polypeptide chains are labelled as trailing (T), middle (M), and leading (L), the T chain is repeated to better visualize the interaction

Until now the nomenclature describes 28 different types of vertebrate collagens that are designated with roman numbers (I – XXVIII) corresponding to the chronologic order of their identification. The three polypeptide chains are composed of one, two or three different genetic products [49]. The letter α was chosen to distinguish the polypeptide chains genetic origin. For example, the most common collagen type found in cartilage is collagen II which is composed of three α_1(II) chains, while the predominant collagen that is found in bones is collagen I and is composed of two α_1(I) and one α_2(I) chain [48].

Collagen types are naturally found in different superstructural organizations, the fibril organization being the most represented as indicated in Table I.2. The approximate size of the rod-like fibril forming collagens is 300 nm and ca. 1000 amino acids compose each of the three polypeptide chains. They are mainly present in connective tissues. Some collagens also self-organize as networks that act

like a supporting structure for cells and tissues or like selective molecular filters or barriers. Collagen VII is an anchoring collagen types which is involved in the connection of epidermis to the dermis. Transmembrane collagens play a role in cell adhesion, neuromuscular signaling and host defense against microbial agents. Multiplexin collagens are composed of multiple triple helices with interruptions and are found in the basement membrane zones of several tissues [50].

Table I.2: Collagen superstructures [49]

Suprastructure	Collagen types
Fibril	I, II, III, V, XI, XXIV, XXVII
Fibril-associated (FACIT[a])	IX, XII, XIV, XVI, XIX, XX, XXI, XXII
Network	IV, VI, VIII, X
Anchoring fibrils	VII
Transmembrane collagens	XIII, XVII, XXIII, XXV
Multiplexin	XV, XVIII

[a] Fibril-associated collagens with interrupted triple helices.

Collagen sources and production

Industrially speaking, collagen can be extracted from natural resources such as animals and plants. Another strategy is to produce collagen strands *in-vitro* thanks to genetic engineering that makes possible to produce recombinant human collagen by host cells, such as yeast, bacteria, transgenic animals and plants [51]. However, only unstable triple helices are produced and further development are required to obtain the same collagen quality level as in natural resources. Among the animal sources, the most common are bovine and porcine sources (mainly skin and bones), and scale fish and fish skin derived from the fish industry [52]. However, terrestrial animals are associated with a number of diseases that limit the use of their collagen for our daily applications. A sadly famous example is the bovine spongiform encephalopathy (BSE), commonly known as mad cow disease. An alternative source of collagen is thus required and the unexploited by-products of fish industry are under investigation for several years now. It is believed to be the safest source for the extraction of collagen, with the additional advantage of not interfering ethical or religious principles, contrary to terrestrial animal sources. However, extraction yields are still very low compared to land animal sources [53].

Due to the variety of sources available for collagen extraction, there is no standard method of extraction. An example of collagen isolation from bovine tendon is described on Figure I.15. The first steps are the conditioning of the raw material in cold solutions and removal of non-collagen proteins. The raw material is crushed and then subjected to 3 to 4 successive steps of gradual dissolution in acidic medium in the presence of enzyme (pepsine). The collagen is then obtained by precipitating

the supernatant after centrifugation of the previous mixture and further purification by dialysis [54]. Characterization tools for collagen analysis are amino-acid quantification by UV-visible spectra, denaturation temperature analysis and X-ray diffraction to name a few.

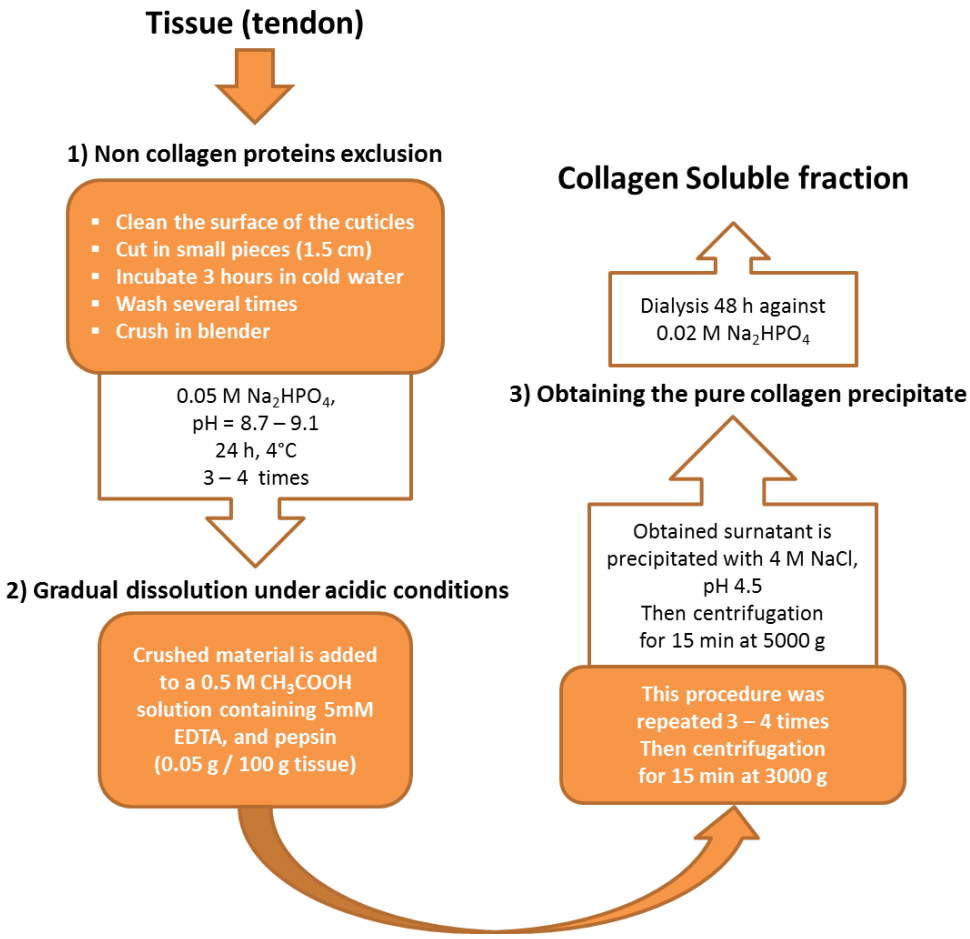

Figure I.15: An example of isolation procedure of collagen from bovine tendon [54]

Collagen is sometimes referred as Gelatin. Although chemically equivalent to collagen, macro-molecular arrangement of gelatin is different and is often described as denatured collagen. Gelatin can be isolated from collagen by thermal treatment that disrupts non covalent bonds of the collagen triple helix organization in order to recover partially isolated polypeptide chains [55], [56]. The process is also influenced by the pre-treatments performed to obtain the collagen [57]. The following global collagen market description includes both collagen and gelatin.

The worldwide production of collagen is difficult to assess because many companies extract and process themselves the collagen they are using in their products. It is also a way to tune the produced collagen and favor its integration into the end-product. The global collagen market revenue was 2.2 billion $US in 2016 and is forecasted to reach 5.4 billion $US in 2025 with an estimated 10,4% compound annual growth rate between 2017 and 2025 [58].

It is also relevant to take a closer look at the market share by applications that are depicted on Figure I.16. Healthcare holds 50% of the market but we can also keep in mind that food and beverages account for almost one third of the collagen market share. Aside from the biomedical applications, the cosmetic industry also implements collagen based systems but it is hard to collect data in this sector because of specific patenting strategies [59].

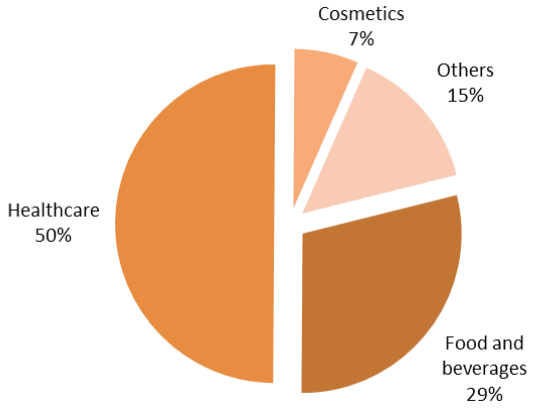

Figure I.16: Global collagen market share by application in 2016 [60]

However, the widespread application of collagen brings a problem about its excessive consumption. Collagen extracted from animals is limited in amount, thus, recombinant collagen plays an important role in the mass production of collagen.

Collagen applications in biomedical field

Collagen-based systems have been proven to possess excellent biocompatibility and sufficient mechanical properties and have gained great achievements in various biomedical applications. It can be used as a thin film, as 3D structure or even injectable solutions. Tissue engineering is one of the most relevant fields of biomedical application for collagen since it mimics well the extracellular matrices (ECM) where cells naturally grow and multiply. ECM also involves collagen in their natural composition [61]. Pure collagen scaffolds have been confirmed to be good scaffolds for tissue engineering under the form of electro spun fibers or freeze-dried solutions where the concentration allows for the tuning of the aerogel microstructure [63]. An extensive review on the use of collagen for tissue engineering have been recently published where authors detailed the design of collagen based scaffolds for nerve and cartilage tissues, bone, tendons and ligaments and also vascular grafts and skin [63].

However, many challenges are still to be overcome regarding the variety of possible end uses of collagen. It should be noted that even if pure collagen structures have excellent biological properties,

they often offer poor mechanical properties and structural stability. The use of chemical agents to increase cross-linking of collagen chains or fillers to re-inforce the collagen matrices are common strategies to further improve collagen-based systems. Industrial sterilization of collagen based medical devices is also known to trigger the crosslinking of collagen strands, thus improving its mechanical properties and its stability in wet physiological conditions [64], [65]. To conclude, collagen scaffold working well in one specific tissue may have a poor effect on another one, as tissue or organ in vivo has its own unique microenvironment.

Providing scaffolds with more functionality such as drug release is also a challenge for the coming years, and is investigated in this this Ph.D. project.

1.4 A focus on Cellulose and its derivatives for the biomedical field

Nature produces an estimated quantity of $300x10^9$ tons of biomass each year through photosynthesis, which about 90% of it is wood. Cellulose roughly correspond to 50% of wood components, i.e. an annual natural production of cellulose of 135 $x10^9$ tons each year [66]. In comparison, mankind extracted 4 to 5 $x10^9$ tons of oil in 2017 (including crude oil, shale oil, oil sands and NGLs: natural gas liquids, excluding liquid fuels from other sources such as biomass and derivatives of coal and natural gas) according to British Petroleum statistical review on world energy released on June 2018, almost thirty times less. In the current global concerns about environment and raw materials extraction, cellulose appears like a potential alternative to oil-based materials. It is the most abundant natural polymer on Earth. It is also renewable, biodegradable and biocompatible.

Cellulose is mainly found in the plant cell wall but also in a wide range of other sources. Wood is the most common source of cellulose but biomass encompasses numerous materials other than wood: annual plants such as cotton or flax, agricultural wastes, marine biomass like algae but also animals like tunicates or even bacteria and fungi are all used as cellulose sources [67].

The establishment of cellulose's chemical and physical structures was conducted over almost a century long period [68]. Its chemical identification is attributed to the French chemist Anselme Payen in 1838. In the beginning of the 20^{th} century, many scientists still doubted that it was a polymer but the molecular structure was revealed by Haworth et al. in 1930 [69]. This work confirmed that cellulose was a linear polymer composed of D-glucopyranose units linked by $\beta(1 \rightarrow 4)$ glycosidic bonds, resulting in anhydroglucose units ($C_6H_{10}O_5$). The repeating unit is the cellobiose that comprises two anhydroglucose units. Nevertheless, the degree of polymerization is commonly expressed as the number of anhydroglucose units. The degree of polymerization varies with the cellulose source, ranging from 10,000 in wood-derived cellulose up to 20,000 in cotton. A ten-fold

decrease is usually observed after industrial isolation. The pyranose rings have been found to be in the chair conformation with hydroxyl groups in equatorial position. All along the polymer chain, from one glucopyranose unit to the next, a rotation of 180° of the ring around the β link is observed. Figure I.17a describes the three types of anhydroglucose units (AGU): (i) the internal AGUs, (ii) a reducing end with a free hemi-acetal or aldehyde group in equilibrium and (iii) the non-reducing end with a free alcohol group.

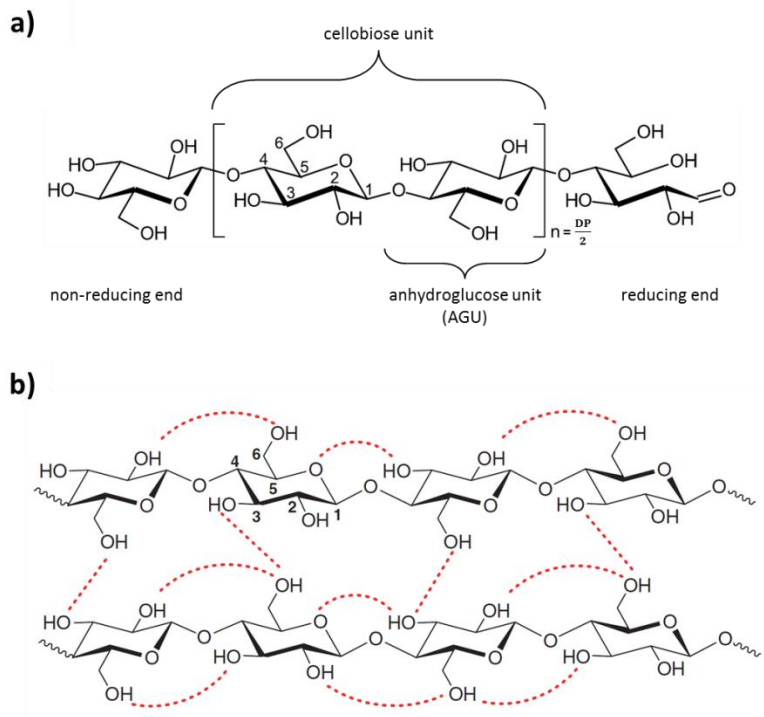

Figure I.17: Cellulose polymer chemical structure, a) molecular structure of cellulose polymer chain and b) hydrogen bonding in cellulose [70]

The hydroxyl side-groups of the polymer chain provide cellulose with intra and inter chain hydrogen bonding (see Figure I.17b). Hydrogen bonding is of quite weak energy in comparison with a covalent bond: about 20 kJ/mol for O-H--O systems are found in cellulose versus 400 kJ/mol for covalent bonds in cellulose. But the repetition of these weak energy hydrogen bonds plays a key role in cellulose structure and its physical organization. Indeed, they allow for the arrangement of cellulose polymeric chains into parallel arrays to form fibrils on the nano and micro scale, which will be described in the next sub-chapter. These nano and microfibers further assemble to form macroscopic wood fibers for instance, as described on Figure I.18.

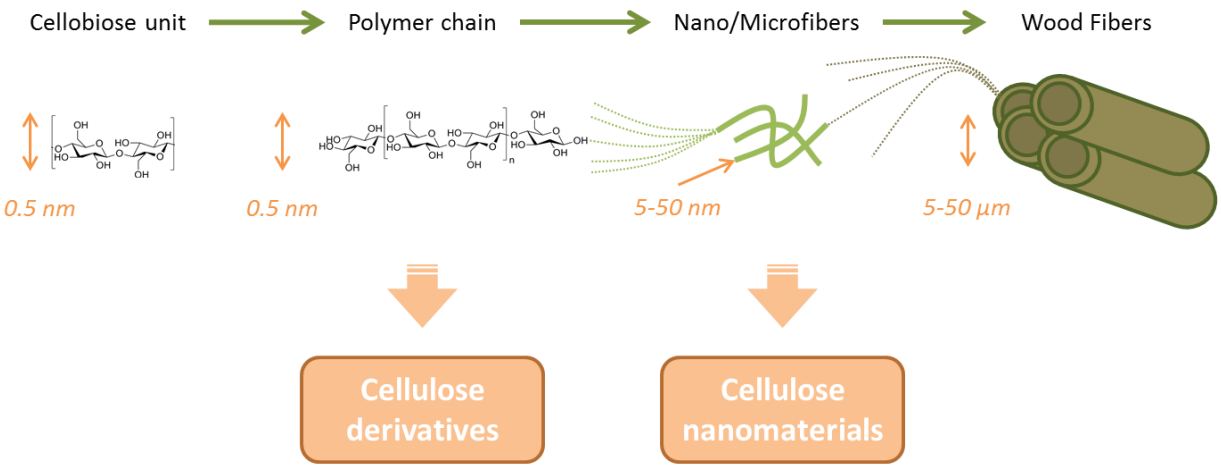

Figure I.18: Hierarchical organization of cellulose polymer chain into microfibers and wood fibers

Cellulose has been the subject of intensive research because of its sustainability, biodegradability, widespread availability and biosafety, and has been used extensively in recent years in the biomedical field [71]. One of the first large scale uses of cellulose in the medical industry appeared with the development of cellulose membranes for the treatment of renal failure in the beginning of the 20th century. Cellulose membranes were used for the hemodialysis that purifies patient's blood and act as artificial kidney [72], [73] . Nowadays, the trend for hemodialysis membranes is moving to synthetic polymers with a better controlled molecular cut-off.

Micro Crystalline Cellulose (MCC) is derived from high purity cellulose by hydrochloric acid treatment until a very low degree of polymerization is reached (a few hundred compared to starting cellulose of at least 1000). Avicel© is one of the most known brands of MCC. It is white, fine and odorless crystalline non-fibrous powder with particle size in the range of 20 µm to 200 µm depending on the production process [74]. In the pharmaceutical industry MCC is mainly used as an excipient for tablet production. It provides good interactions with the active principle ingredients (API) and allow for the preparation of stable pharmaceutical ingredients. MCC also gives a better disintegration in the stomach [75].

Moreover, the chemical modification of cellulose gave rise to new polymers that are also used in the medical field, the so-called cellulosics or cellulose derivatives. It mostly comprises oxidized cellulose, ether and ester of cellulose. The hydroxyl groups of C_2 and C_3 (secondary) and C_6 (primary) are available for numerous chemical modifications as described on Figure I.19, and more detailed later in chapter I-3 that is dedicated to nanocellulose functionalization. The hydroxyls groups of the amorphous regions of cellulose are more accessible for chemical modification whereas those of crystalline are very difficult to reach due to the close packing of cellulose chains and strong interchain

hydrogen bonding [76]. Cellulosics are known to be strong, of low cost, reproducible, recyclable and biocompatible, making some of them suitable for medical applications [77].

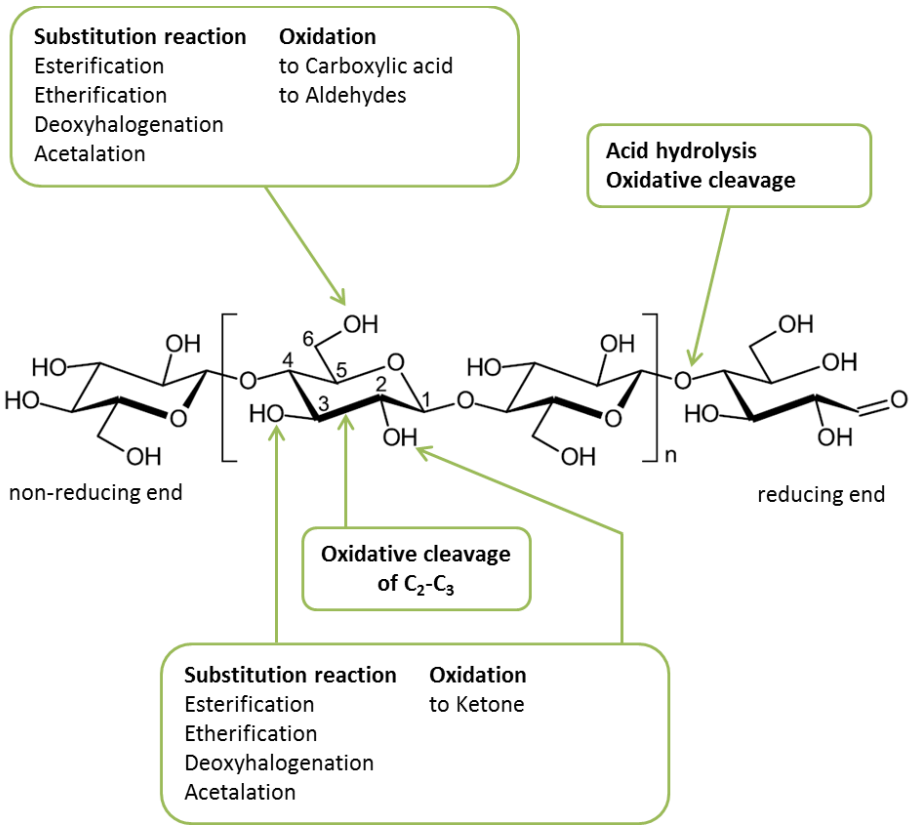

Figure I.19: Possible positions for cellulose chemical modifications, adapted from [77]

For instance, the cellulose ethers used in drug tableting industry, like hydroxymethylpropylcellulose (HPMC), form matrices that swell in aqueous media and create a tunable diffusion barrier to further control drug delivery, with the advantage of eventually solubilizing in the medium. This diffusional barrier was observed by colorimetric techniques and fitted to mathematical models that successfully described the drug release [78]–[80]. Cellulose esters such as cellulose acetate phthalate (CAP), were used to prepare enteric-coated granules. The microencapsulation of the granules with CAP significantly prolonged the release of the embedded drug and enhanced the effectiveness of the enteric coating. These formulations are able to go through the stomach and only dissolve and release the drug in gastric environment [81]. Table I.3 summarizes the cellulosics used in pharmaceutical preparations.

Table I.3: Cellulosics used as excipient and auxiliary for pharmaceutical preparations (MCC, microcrystalline cellulose; MC, methyl cellulose; HPC, hydroxypropyl cellulose; L-HPC, water insoluble HPC with a low DS; HPMC, hydroxypropylmethylcellulose; HEMC, hydroxyethylmethylcellulose; Na-CMC, Ca-CMC, H-CMC, sodium, calcium and acid form of carboxymethylcellulose; HEC, hydroxyethylcellulose; CMEC, carboxymethylethylcellulose), extracted and adapted from [73]

Function	*Cellulosic*
Filler or binder	MCC, MC, HPC, HPMC HEMC, Na-CMC,
Disintegrant	Ca-CMC, H-CMC, L-HPC
Binder for wet tableting	Na-CMC, MC, HPC (for organic solvent) HPMC
Binder for sugar coating	Na-CMC, MCC
Film coating	HEC, HPC
Enteric (film) coating	CMEC, HPC succinate, CA succinate, CA phthalate
Thickener, dispersion stabilizer, emulsifier for liquid preparations	MC, Na-CMC, MCC, HPC, HEC
Poultice plaster	Na CMC
Ointment base	HPMC

Likewise, thanks to their water-solubility, hydrogels of cellulose derivatives can also be formed for medical application, like hemostat and drug release [82]. Silylated hydroxypropylmethyl-cellulose hydrogels were successfully prepared in neutral pH conditions. Such conditions are suitable for their subsequent use for cell culture, bone defect treatment or model cartilage development [83]. Chemically crosslinked sodium-carboxymethylcellulose (Na-CMC) and hydroxyethylcellulose (HEC) hydrogels were also produced with non-toxic coupling agents such as citric acid resulting in super-absorbent material with possible hemostat applications [84]. Chemical crosslinking of cellulose derivatives hydrogels can also be achieved by irradiation techniques. Both degradation and cross-linking of polymers occurs upon such high-energy treatments, but concentrated polymer solutions (above 50 wt% for carboxymethylcellulose) seem to favor cross-linking [85]. Indeed, hydrogels were produced from carboxymethylcellulose (CMC) and acrylamide monomer (AM) through gamma radiation treatment, resulting in materials with greater swelling capacities than pure AM gels. Drug release from such material was also investigated and revealed a pH-dependent release behavior, with slower release in acidic conditions [86].

The widespread medical uses of cellulosics originate from their availability, physical properties and physiological inertness, which gave rise to numerous commercial products in the 20th century. Endless possibilities of cellulose derivatives polymers and derived materials (tablets, coating,

membranes and hydrogels) provide cellulose with a consistent and promising future in the medical field.

Many different conventional and biobased biomaterials have been introduced and their properties and applications have been described. Among cellulosic materials, a new class of high potential derivatives was unveiled in the 80's: the nanocellulose. It is a new tremendous field of research and it will find applications in many different areas, from papermaking to composites but also in medical industry. The next chapter will focus on nanocellulose material as it is the main raw material used in this Ph.D. project.

2. Nanocellulose: production, characterization, application and commercial aspects

Two main families of nanocellulose are identified, cellulose nanofibrils (CNF) and cellulose nanocrystals (CNC). Nanocellulose can be extracted from trees, plants and cellulose-containing micro-organisms and animal species. Although commercial applications are still limited, the exponentially growing interest from researchers and companies for these materials (see Figure I.20) make nanocellulose one of the most attractive natural and renewable polymers for advanced applications [87]. Even if we correlate these figures to the growing number of scientific journals and the increasing number of researchers that work with nanocellulose, the tendency remains the same. Nanocellulose really differs from traditional cellulose-derived products (paper industry and cellulose based polymers) and give rise to new fields of application. The main characteristics of nanocellulose are related to its widespread availability, biodegradability, biocompatibility, low density, excellent mechanical properties and tunable surface chemistry [88].

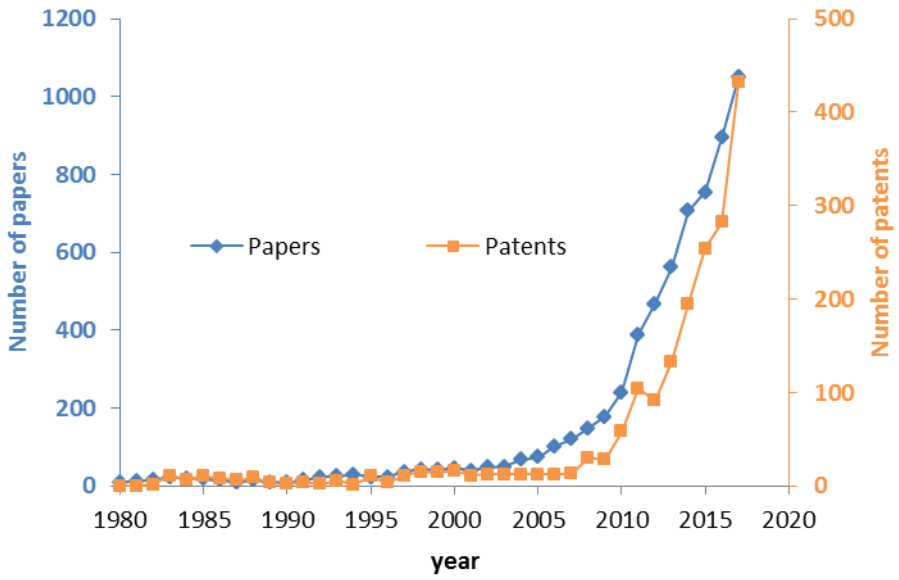

Figure I.20: Number of papers and patents released each year dealing with CNFs and CNCs until 2017 (extracted from SciFinder in July 2018, descriptors are cellulose nanofibrils / cellulose microfibril / microfibrillated cellulose / nanofibrillated cellulose / cellulose nanocrystals / cellulose nanowhiskers / nanocrystalline cellulose / cellulose whiskers)

The isolation techniques of different cellulose nanomaterial will be exposed. The nanocellulose type utilized in this Ph.D. project is the cellulose nanofibrils (CNF). Industrial aspects will be discussed in terms of health and safety, as it is related to the topic of this thesis, upcoming and first commercial products will be presented, especially those related to the biomedical field.

2.1 Isolation and characterization of nanocellulose materials

Nanocellulosic materials are mainly extracted from wood even if other sources are available such as annual plants wastes, animals and micro-organisms. Compared to structures previously shown in Figure I.18, a more detailed description of the hierarchical structure from the wood trunk to the cellulose polymeric chain, and where cellulose nanomaterials are embedded, is provided on Figure I.21. In order to isolate cellulose nanomaterials, purified cellulose fibers must be first obtained. Traditional cooking processes used in the paper industry produce high purity cellulose fibers from softwood or hardwood by removing hemicelluloses and lignin, resulting in material suitable for cellulosic nanomaterials isolation. Quite harsh chemical and mechanical treatments are used on purified cellulosic fibers, sometimes both combined to decrease mechanical energy consumption, which was the main drawback of the last decades for nanocellulose to reach the commercial production level.

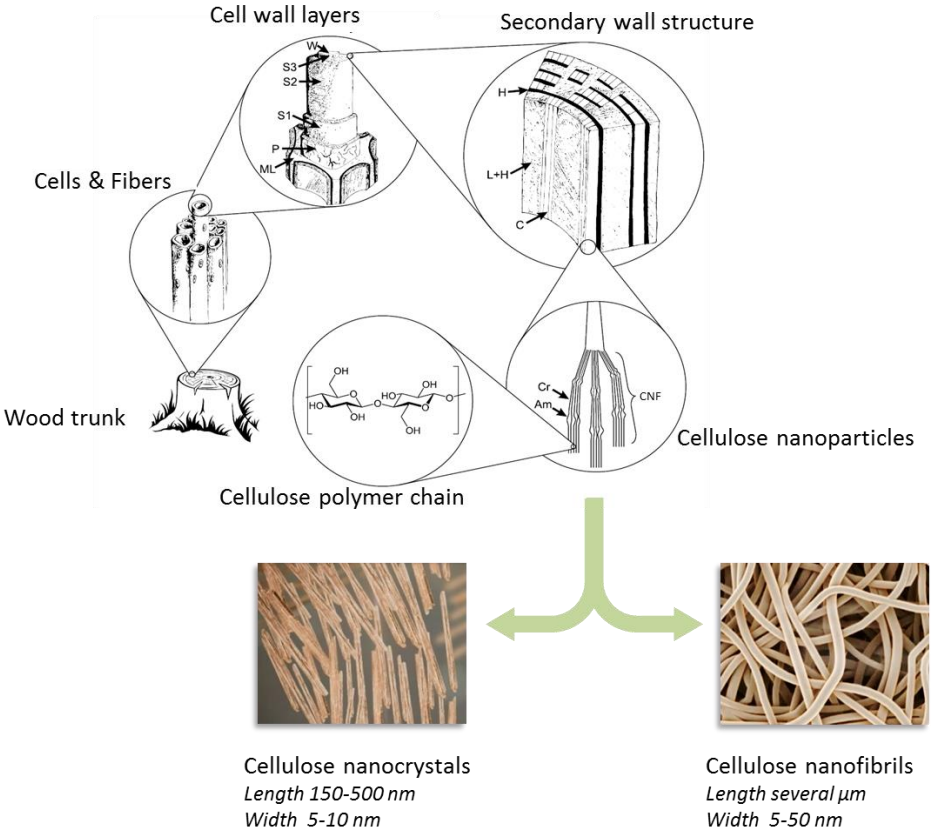

Figure I.21: From wood trunk to cellulose nanomaterials, the cell wall layer is composed of middle lamella (ML), the primary wall (P), the outer (S1), middle (S2) and inner (S3) layers of secondary wall and the warty layer (W). Cellulose (C), lignin (L) and hemicellulose (H) compose the secondary wall structure. On cellulose nanoparticles, crystalline (Cr) and amorphous (Am) domain are shown. Adapted from [89] and [90].

2.1.1. Cellulose Nanocrystals

Cellulose nanocrystals, sometimes referred as cellulose whiskers or nanowhiskers or even nanocrystalline cellulose, are composed of the crystalline part of cellulose nanoparticles. It is a rod-like nano-object with dimensions ranging from 150 to 500 nm in length and 5 to 10 nm in width resulting in high aspect ratio values (see representation in Figure I.22). The discovery of CNC is attributed to Rånby et al. in 1950 [91], [92]. Researchers were inspired by the work of Nickersson and Harble in the 1940's who observed the limited degradation of cellulose fibers by boiling in acidic conditions [93].

Isolation of CNC is thus currently done by strong acid hydrolysis of purified cellulosic material under controlled temperature and time conditions followed by sonication. The amorphous regions of the cellulose fibers have a lower density than the crystalline regions and thus are much more sensitive to the acidic treatment. Acidic ions can more easily penetrate the amorphous regions while crystalline regions remain untouched, and eventually result in cellulose nanocrystals [94]. Figure I.22 describes the general procedure to obtain CNC from wood. We can note that very similar procedures can be used on cotton or also industrial crops wastes.

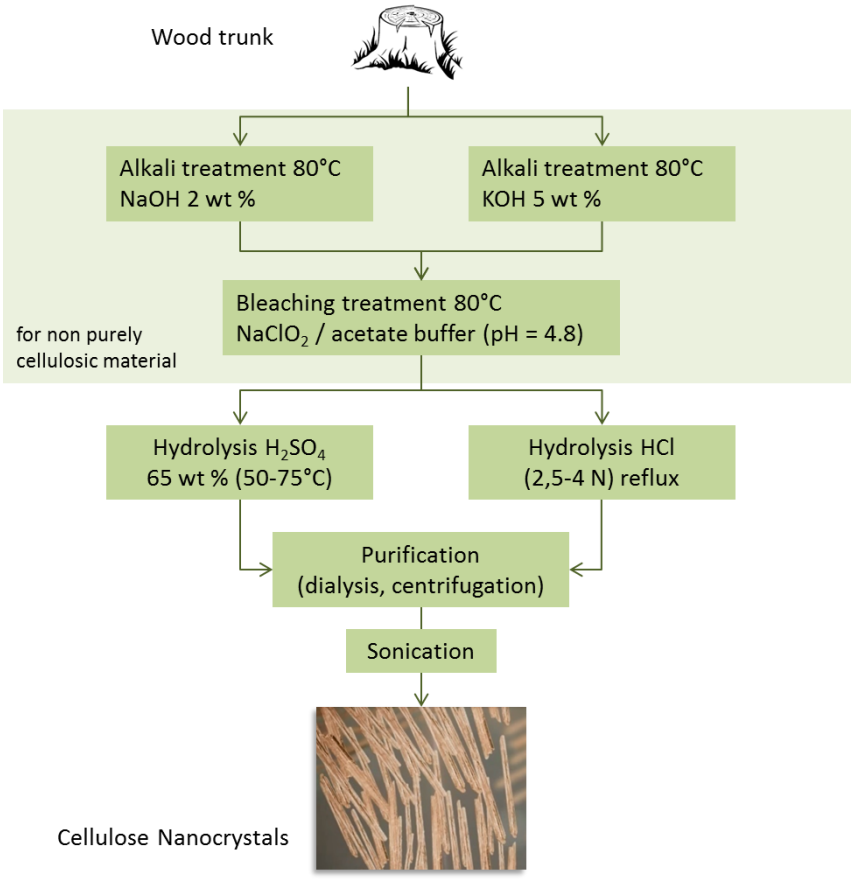

Figure I.22: General procedure to obtain cellulose nanocrystals [95])

2.1.2. Cellulose Nanofibrils

Meanwhile cellulose nanofibrils (CNF) can also be extracted from cellulosic fiber, they really differ from cellulose nanocrystals. Composed of both crystalline and amorphous regions of cellulose, CNF are long and flexible nanofibrils with dimensions of 5 to 50 nm in width and several micrometers in length, resulting in a higher aspect ratio than CNC. The terminology evolved over the time and terms like cellulose microfibrils, microfibrillated cellulose (MFC), nanofibrillated cellulose (NFC) all refer to CNF that has been selected by the scientific community as a standard terminology in 2012 [96].

In the 1980s, pioneer works of Turbak et al. and Herrick et al. unveiled a new component of cellulose fibers with lateral dimensions in the nanometer range, thanks to mechanical treatment. Softwood pulp was subjected to high pressure homogenizer (at least 3000 psi and several passes) so that the entangled networks of nanofibrils inside the cellulose fiber were isolated from each other under the high shearing forces. The treatment resulted in a gel-like dispersion composed of interconnected microfibrils and nanofibrils of 10-100 nm diameter at only 2 wt% in water with shear thining behavior [97]. Cellulose nanofibrils can be isolated from wood and annual plants like cotton by mechanical disintegration treatment. The high shear forces produce a longitudinal cleavage of the cellulose fibers and isolate to some extent the nanofibrils.

High energy consumption is often associated with pioneer work on isolation of CNF [97], [98]. In order to obtain viable commercial grades of CNF and upscale production facilities, researchers investigated many ways to decrease the energy needs of CNF isolation by proposing specific pre-treatments or development of new mechanical treatments. Mostly used processes to induce high shear forces to cellulose fibers suspensions were originally grinding, microfluidization and homogenization as depicted on Figure I.23 [99].

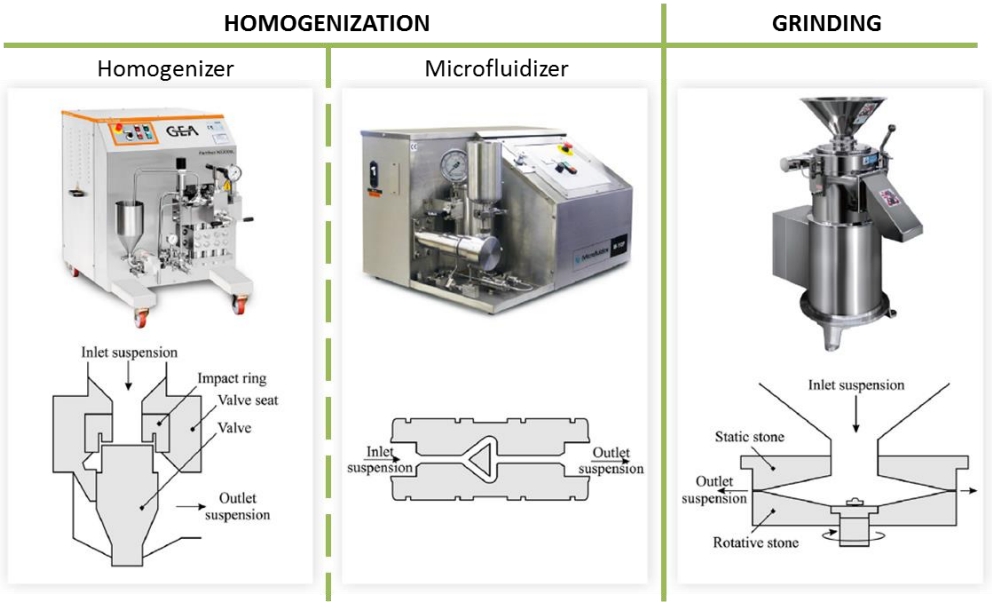

Figure I.23: Main mechanical treatment device for production of CNF suspension [89]

These techniques are efficient to delaminate the cellulose fiber and are also suitable for upscaling. They are used nowadays for first industrial production of CNF [89]. However, it is the use of a combination of mechanical and chemical or biochemical pre-treatments that really helps to decrease energy consumption from 100 kWh/kg for un-pretreated cellulosic materials to as little as 1-2 kWh/kg [100]. Worth-mentioning works proposed successive refining, enzymatic hydrolysis, refining again and finally homogenization [101], TEMPO-mediated oxidation in combination with blending [102], or in combination with homogenization [103], carboxymethylation or quaternization followed by homogenization [104]. Thus, a very wide number of procedures lead to a very wide range of CNF grades. The recent review of Nechyporchuk et al. extensively covered conventional and less conventional CNF production methods. Figure I.24 summarizes the general procedures to obtain cellulose nanofibrils suspension. As for the CNC, the first step deals with the purification of the starting raw material in order to retrieve the maximum amount of cellulose and get rid of lignin and hemicellulose. Second and third steps are mechanical or (bio)chemical pre-treatments that come before the fourth step of principal mechanical treatment. The final step aims at purifying the obtained CNF and further expands their properties. It clearly shows how a unique raw material such as cellulosic fibers extracted from biomass can lead to the isolation of more than 50 types of cellulose nanofibrils. A very recent review extensively describes all the possibilities used these days or under development for cellulose functionalization as a pre-treatment for CNF production [105].

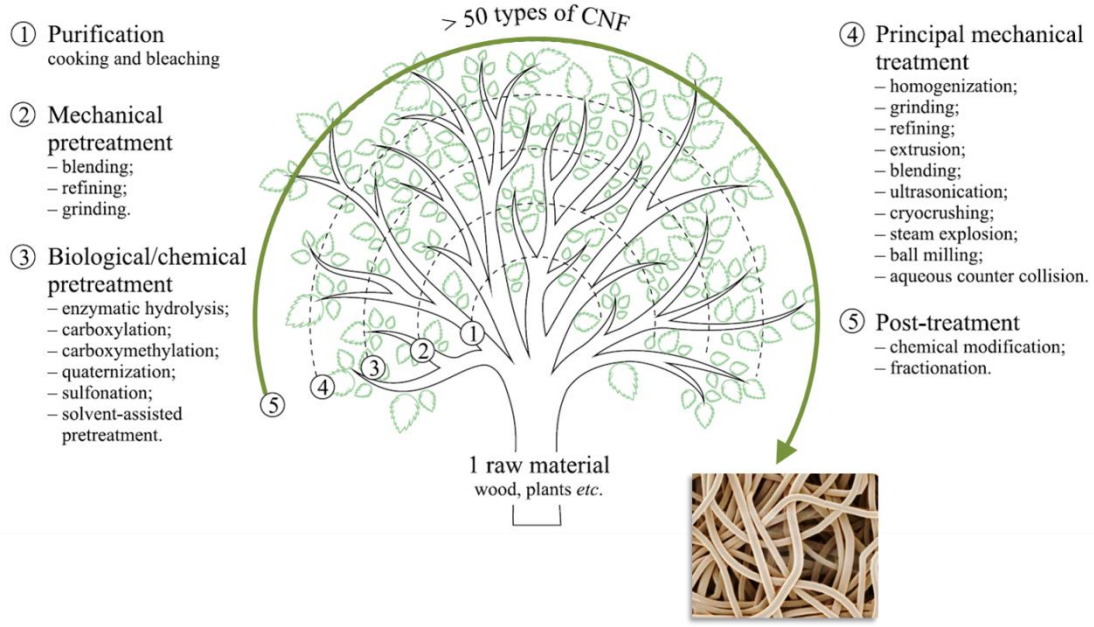

Figure I.24 : General procedures to obtain cellulose nanofibrils, adapted from [89]

Among all these procedures, enzymatic hydrolysis and the TEMPO-mediated oxidation pre-treatments deserve a particular consideration since they are the most studied procedures of this last decade. Moreover, these two types of CNF are the starting raw materials of this Ph.D. project. A comprehensive description of the state of the art associated with their production procedures is necessary to be able to understand the materials used in Chapter II.

2.1.2.a. Cellulose nanofibrils production through enzymatic pre-treatment

The purpose of enzymatic pre-treatment is to catalyze the hydrolysis of cellulose in order to favor the defibrillation process upon subsequent mechanical shearing. This process was patented in the paper industry in the 1960s to decrease the energy consumption of refining. Researchers also investigated enzymatic hydrolysis for the production of bioethanol through the conversion of cellulose to glucose and ethanol. But the pioneer results of CNF production assisted by enzymatic pre-treatments are attributed to Pääkkö et al. and Henriksson et al. in 2007 [101], [106]. Pääkkö et al. proposed a combination of refining, which increase cellulose swelling and accessibility of the enzyme, followed by the enzymatic treatment and washing plus a second step of refining before the actual homogenization process in a microfluidizer (Figure I.23) for 8 passes. Henriksson et al. used a very close procedure and compared enzymatic concentrations. The fibrillation process was performed with a homogenizer for 20 passes.

The enzymatic process comes with a decreasing DP and an increase of the crystallinity index [107]. Cellulose degrading enzymes are referred as cellulase and can be divided into three sub-families, a) endoglucanases (or endocellulases) that hydrolyze amorphous regions of cellulose; b)

cellobiohydrolases (exoglucanases) that degrade the ends of cellulose structures releasing cellobiose or cellobiose dimer; c) β-glucosidases (cellobiases) that hydrolyze the later small molecules into glucose. Figure I.25 shows the mode of action of each of the above mentioned cellulases on cellulose. In the end, these enzymatic isolated CNF have the same surface chemistry compared with cellulose fiber, with hydroxyl groups on their surface.

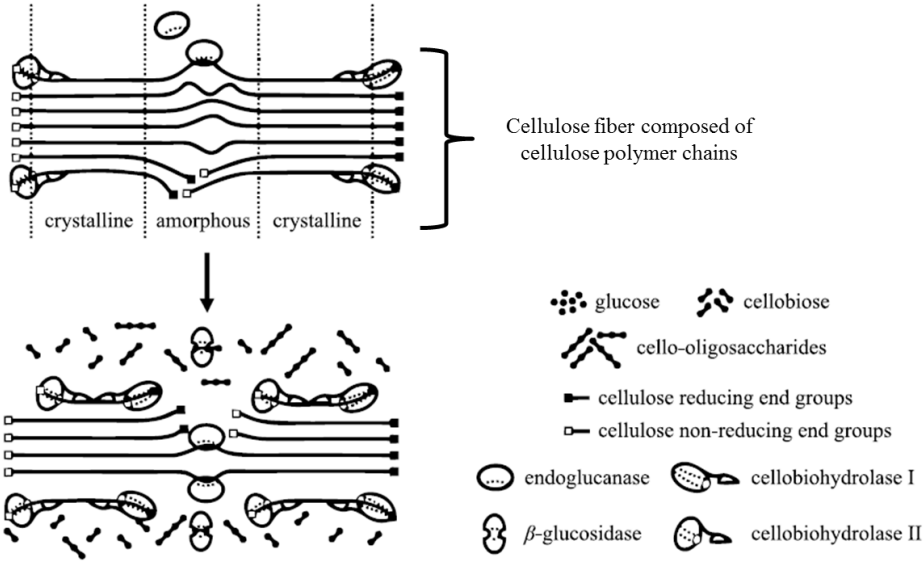

Figure I.25: Schematic representation of mode of action of cellulases on cellulose polymer chain. Adpated from [108]

2.1.2.b. Cellulose nanofibrils production through TEMPO-mediated oxidation pre-treatment

TEMPO mediated oxidation of cellulose fibers allows the introduction of negatively charged groups (carboxylate groups) at the surface of cellulose chains, which promotes ionic repulsion between cellulose chains and eventually help the defibrillation process under high shear mechanical treatment. It has become one of the most investigated pre-treatment strategy for cellulose oxidation and cellulose nanomaterials production. The pioneer work on the TEMPO mediated oxidation of sugar molecules was published by Davis and Flitsch in 1993 [109]. They presented a method to selectively oxidize the primary hydroxyl group of monosaccharides using sodium hypochlorite in the presence of catalytic amount of 2,2,6,6-tetramethylpiperidine-N-oxyl (TEMPO) radical. The research group of Pr. Akira Isogai further studied this reaction and came up with CNF isolated with a blending apparatus from ever dried cellulose from sulfite wood pulp, cotton, tunicate and bacterial cellulose. They achieved a carboxyl content of 1.5 mmol/g [102] and obtained highly individualized nanofibrils while the blending apparatus was of much lower energy input than conventional mechanical treatment. This research group also investigated many different reaction conditions in order to determine the most energy-efficient procedure to obtain CNF through TEMPO mediated oxidation

pre-treatments of cellulosic raw materials. Different amounts of NaClO and reaction times were tested and compared against each other by following carboxyl and aldehydes groups content and the DP evolution [110]. Figure I.26 exposes the proposed mechanisms for the TEMPO mediated oxidation using TEMPO/NaBr/NaClO in basic conditions or TEMPO/NaClO/$NaClO_2$ in neutral or slightly acidic pH. The later system has be proved to limit the depolymerisation of cellulose and the amount of aldehyde groups formation [111].

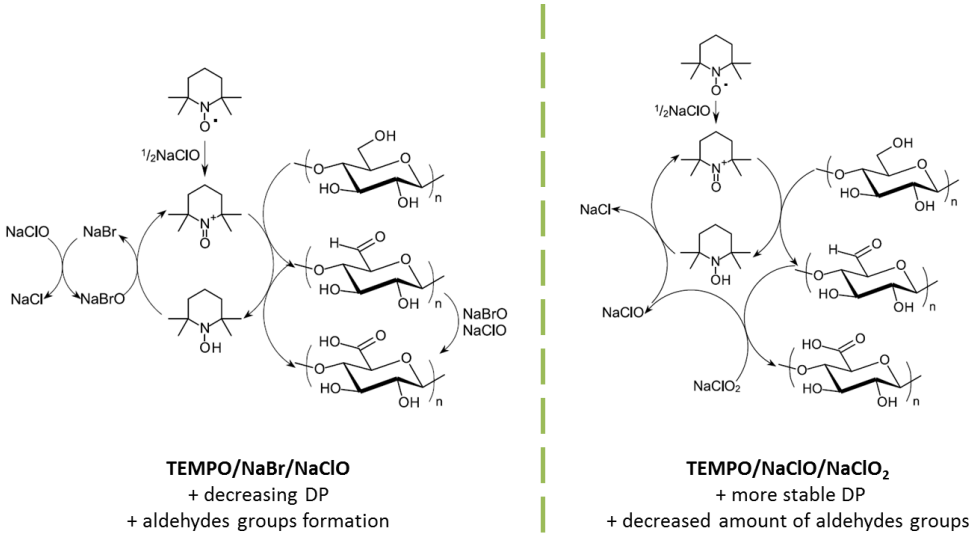

Figure I.26: Schematic mechanisms of regioselective oxidation of primary hydroxyl groups of cellulose by TEMPO/NaBr/NaClO in water in basic pH conditions on the left and TEMPO/NaClO/$NaClO_2$ in water at neutral or slightly acidic pH on the right. Adapted from [110].

Such TEMPO-oxidized CNF bring new opportunities of functionalization with the presence of carboxylic acid groups, together with aldehydes groups (not fully converted hydroxyls) and the remaining non-oxidized hydroxyls groups, on its surface.

This Ph.D. project aims at using only wood-derived nanocellulose. Bacterial nanocellulose is in competition with wood-derived nanocellulose for medical applications and thus deserves a short introduction and comparison. Bacterial nanocellulose is synthetized by bacteria in a high purity form. In comparison with wood, no hemicellulose or lignin removal is necessary. This material has been used for medical application based on its high purity.

2.1.3. Bacterial nanocellulose (BNC)

Populations of bacteria are generally divided into two types: planktonic, which refers to freely dispersed bacteria in bulk solution, and sessile, which refers to a united colony of bacteria embedded in a *biofilm*. Many different micro-organisms produce this so-called *biofilm* upon their development on every kind of surface [112]. It is acting as a matrix which contains the micro-organisms and provides them with a safe environment, preventing them from drying out, it also gives protection

from enemies, irradiation and lack of food or oxygen [113]. The biofilm is usually composed of extracellular polymeric substances.

In parallel to plant cellulose production, it appears that some bacteria strains are capable of producing biofilms that contains high amounts of cellulose in the form of nanofibers: *Acetobacter, Agrobacterium, Alcaligenes, Pseudonmonas, Rhizobium, Aerobacter, Achromobacter, Azotobacter, Salmonella* and *Sarcina* [114]. The most efficient and also the most studied strain appear to be *Acetobacter xylinum*, recently reclassified as *Gluconacetobacter xylinus*. It is part of the acetic acid bacteria (AAB) group which are known to perform specific oxidation reactions exploited for the production of numerous compounds including cellulose [115]. Figure I.27 shows *acetobacter xylinum* bacteria producing cellulose nanostructured architecture (black arrow).

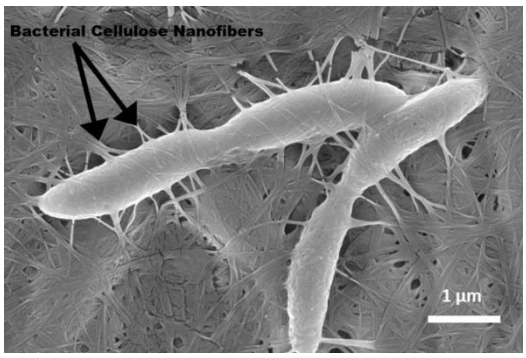

Figure I.27: Acetobacter xylinum producing bacterial cellulose nanofibers (black arrow) [116]

The efficiency of bacterial nanocellulose production is highly dependent on the strain but also on the culture medium: temperature, pH and more importantly oxygen supply during the process (since AAB are aerobic bacteria) and carbon source (such as D-glucose) [113], [114]. The bacteria synthesize the cellulose polymer at the air-liquid interface of the culture medium and always as a membrane. Two major systems are mentioned: static and agitated culture media and both show specific advantages and disadvantages. The main difference is the oxygen supply and diffusion in the culture medium.

The most important feature of bacterial nanocellulose is its inherent purity in comparison with wood derived nanocellulose. The latter contains hemicelluloses and lignin that requires complex chemical treatment to be removed. The nanostructure of BNC makes it a very good candidate for various biomedical applications such as tissue engineering. Its *in vivo* biocompatibility and potential use in biomedical field have been proven many times [117]–[119].

However, their industrialization is still limited and expensive compared to the development of wood derived nanocellulose pilot plants. Moreover, BNC seems quite difficult to obtain as a suspension or as a re-dispersible powder, which can be useful in formulation.

These three types of cellulose nanomaterials (CNC, CNF and BNC) can be subdivided in different grades in terms of nano-material proportion, morphology or even surface chemistry. Even if they are all cellulose on the molecular level, these different forms of nanocellulose can present specific features, thus becoming suitable for different application. Consequently, the next paragraph focuses on the characterization techniques of such materials.

2.2 Characterization of cellulosic nanomaterials (CNMs)

The development of reliable and accurate characterization methods for CNMs is driven by both the need for deeper scientific understanding of these materials by research communities, and the growing industrial commercialization. The available grades of CNMs on the market are really different. Industrial partners should be provided with clear guidelines for the choice of the most relevant CNMs according to the intended application.

Recently, a wide conglomerate of expert researchers from all around the world was gathered up to establish best practices, methods and techniques for characterizing CNM particles. It covers morphology, surface chemistry, surface charge, purity, crystallinity, rheological properties, mechanical properties and toxicity. Cellulose nanocrystals and cellulose nanofibrils were chosen to be the CNMs at the heart of this work [120]. Numerous decision-tree schemes were proposed to answer every potential needs a researcher from academic or industrial community would have. Figure I.28 describes the pathway one should follow when working with CNMs and associated characterization tools and techniques.

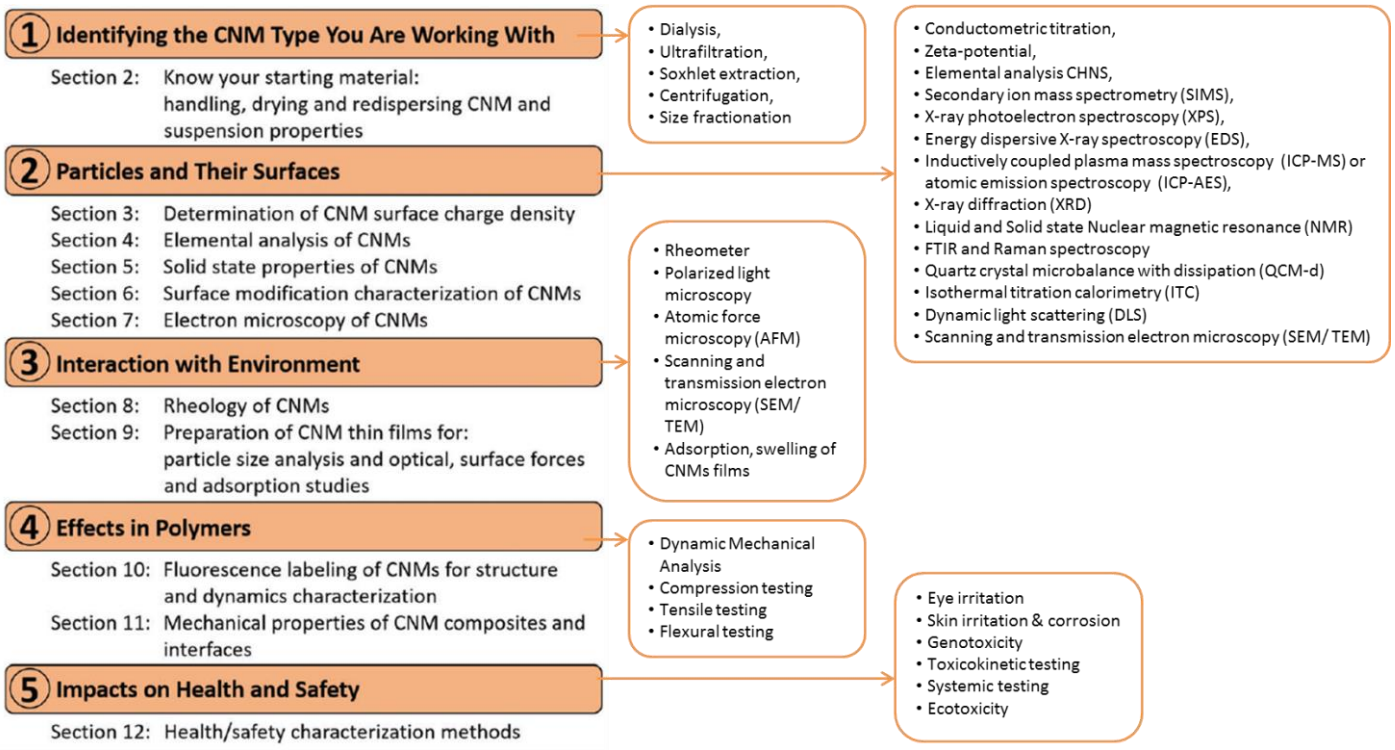

Figure I.28: Five topics for the characterization of CNMs and associated characterization tools, adapted from [120]

The first point emphasizes the critical importance of knowing the starting material. As already mentioned, hundreds of CNMs grades are available and differ regarding the wet or dry state (and respectively concentration and ability to be redispersed), presence of impurities and proportion of nano and microsized material. The second topic deals with the shape and surface of CNMs. Surface charge, morphology, elemental analysis study, crystallinity, surface chemical structure measurement methods are described. Topic three focuses on rheology of CNMs suspensions and adsorption mechanisms of CNMs particles. The topic four is dedicated to the development of CNMs composites and characterization of CNMs dispersions. Finally, health and safety aspects of CNMs are discussed in the fifth and last topic.

Other works especially focused on CNF quality characterization. For example, a review of different techniques used to characterize CNF was done by Kangas et al. while a quality index was developed based on 8 different characterization techniques to assess the homogeneity of CNF dispersion by Desmaisons et al [121], [122].

CNMs should obviously be characterized before and after any modification. Thus, their functionalization through chemical grafting can extend the choice of characterization techniques, depending on the grafted moieties, as it will be shown in Chapter II.

2.3 Industrialization of nanocellulose: first and upcoming applications

The global enthusiasm for nanocellulose was introduced by the Figure I.20 that shows the number of publication and patents dealing with nanocellulose. To deepen this overview, it could be interesting to consider the number of patents published by countries (Figure I.29, left). These data clearly indicate that the strong industrial interest for nanocellulose have spread worldwide. Furthermore, when these data are sorted according to the field of application, the multiple end uses of nanocellulose improved products is exposed, with composites being the field that holds most patents.

However, the first years of industrialization progress were limited by several factors concerning nanocellulose such as (i) a high production energy cost, (ii) the lack of high added value and/or cutting-edge applications, (iii) the competition with the existing renewable and non-renewable materials and (iv) the precaution about the "nano" aspect regarding health and safety. This explains why a relatively low number of patents were published before 2008.

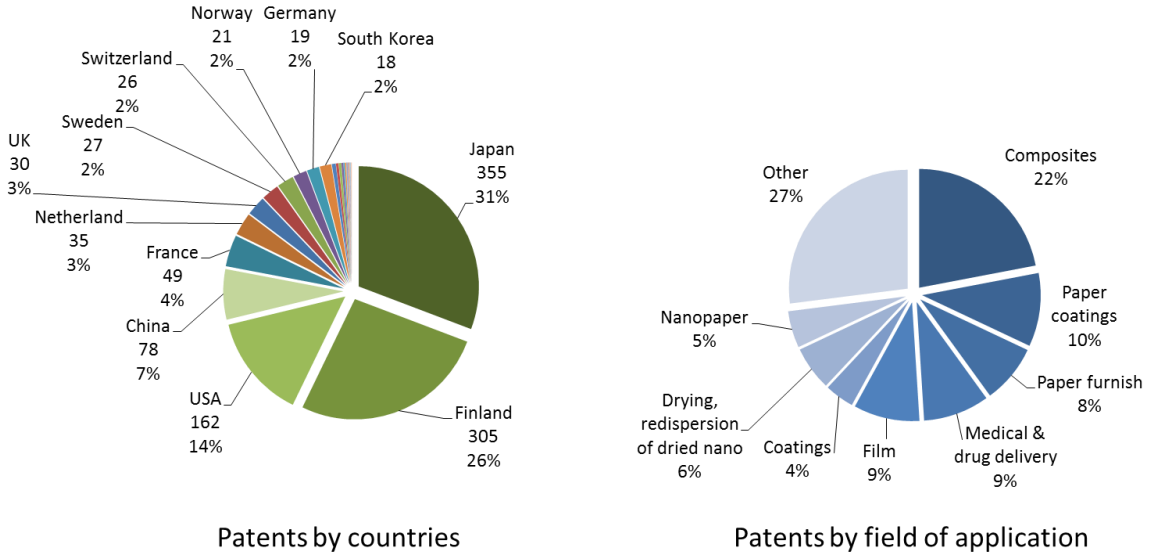

Figure I.29: LEFT, Number of patents dealing with CNF materials. Extracted from SciFinder in October 2018 with the following descriptors: cellulose nanofibrils / cellulose microfibrils / microfibrillated cellulose / nanofibrillated cellulose, RIGHT, nanocellulose (CNF, CNC and BNC) patents repartition in field of application, adapted from [123]

In the last decade, these challenges were intensively addressed by the scientific community in order to unlock the industrialization of nanocellulose. The development and optimization of cellulosic sources pre-treatments allow for the decrease of the energy consumption of nanocellulose production. The current identified producers of CNF and CNC are exposed on Table I.4.

Table I.4: Current industrial producers of CNF and CNC, including country of origin, yearly production and starting year

Company	Country	Capacity (/y)	Product type	Approximately since
Cellulose nanofibrils production				
FiberLean	France/Switzerland	10,000 t	CNF with fillers	2013
Performance Biofilament	Canada	2,000 t	Nanofilament	2014
Kruger/FPInnovation	Canada	1,000 t	Nanofilament	2015
Borregaard	Norway	1,000 t	CNF	2016
Paperlogic	USA	730 t	CNF	-
Nippon Paper	Japan	300 t	CNF Tempo	2017
American Process Inc.	USA	180 t	CNF	2015
University of Maine	USA	110 t	CNF	2014
Chuetsu Pulp & Paper	Japan	50 t	CNF	2016
DKS	Japan	50 t	CNF Tempo	2016
Sugino Machine	Japan	50 t	CNF	2017
Oji Holdings	Japan	40 t	phosphorylated CNF	2016
Suzano	Brazil	36 t	CNF	2018
Innventia	Sweden	35 t	CNF	2011
CTP	France	35 t	CNF	2011
PFI	Norway	35 t	CNF	2013
Seiko PMC	Japan	30 t	CNF	2018
Tokushu Tokai Paper	Japan	30 t	CNF	2018
VTT	Finland	15 t	CNF	2010
Inofib	France	0.5 t	CNF	2013
Icar-Circo	India	11 t	NA	2016
EMPA	Switzerland	5 t	CNF	2011
SAPPI	Netherlands	8 t	CNF	2016
Daio Paper Corporation	Japan	NA	CNF	2016
DIC corporation	Japan	NA	CNF	2017
Daicel Corporation	Japan	NA	CNF	2000
Stora Enso	Finland	NA	CNF	2013
UPM	Finland	NA	CNF	2011
Bettulium	Finland	NA	CNF Tempo	2013
Norske Skog	Sweden	NA	CNF	-
Weidmann	Switzerland	NA	MFC	2016
Cellucomp	UK	NA	CNF	2015
BioNC	Spain	NA	CNF	2018
Company	**Country**	**Yearly capacity**	**Production type**	**Starting year**
Cellulose Nanocrystals plant				
Celluforce	Canada	365 t	Sulfated CNC	-
American Process Inc.	USA	200 t	NA	-
Holmen/Melodea	Sweden	35 t	Sulfated CNC	-
Icar-Circo	India	10 t	NA	-
Alberta Innovates	Canada	7 t	Sulfated CNC	-
Blue Goose Biorefineries	Canada	4 t	Sulfated CNC	-
FPInnovations	Canada	4 t	Sulfated CNC	-
University of Maine	USA	4 t	Sulfated CNC	-
Melodea	Israel	NA/ Pilot	Sulfated CNC	-

2.4 Health and Toxicology: a concern for CNM development in biomedical field

As any emerging material, nanocellulose must undergo health and toxicology assessments in order to facilitate the development of industrial processes and ensure the safety of nanocellulose based products. When it comes to use nanocellulose as a biomaterial that is supposed to be in contact with living tissues and micro-organisms, biocompatibility evaluation is of first importance. Also, the "nano" aspect of these materials raises concerns since it is sometimes associated with more risks than traditional materials in the mind of the population. Moreover, it is well known that the human body does not possess cellulose degrading enzymes. Consequently, toxicological study has been carried out starting from the manufacturing processes that are used to produce CNMs, through the ways CNMs are handled and integrated or combined with other materials, until the fate of the CNMs in the product's end-of-life.

Cellulose in the form of cellulosic fibers used in papermaking or in the form of micro crystalline cellulose (MCC) is known to be safe [124]–[128]. But CNMs differ in terms of particle size and shape, surface charge and specific surface area, chemical properties and degree of agglomeration, so that health and toxicology risks must be assessed once again.

Attempts to evaluate CNMs toxicity are fairly recent. The review by Lin and Dufresne published in 2014 listed the preliminary works for the toxicological evaluations of nanocellulose [129]. The initial work for CNC was conducted by Kovacs et al. in 2010 [130]. The group of Canadian researchers assessed the ecotoxicology of CNC on aquatic species. Low toxicity potential and environmental risk were confirmed. Among Lin and Dufresne reviewed evaluations, only the potential respiratory toxicity was pointed out. Aerosolized CNCs were compared to carbon nanotubes and asbestos fibers on a model human lung cell structure. CNC revealed to be dose-dependent pro-inflammatory but of significantly lower impact than the two other materials. Stiffness, length and aspect ratio clearly influence the nano-object/cell interactions [131]. Slight pulmonary inflammation of mice was also noted for CNF in the European Sunpap project which ended in 2012 [132]. However, for the dozens of other works collected by Lin and Dufresne, no evidence of cytotoxicity were detected *in-vitro* nor *in-vivo*, especially on human cells (osteoblast, fibroblast and endothelial cells).

One of the preliminary health and environmental safety study about CNF was published in 2011 by Vartiainen and coworkers [133]. They assessed the exposures of workers to particles in air during production process of CNF through grinding and subsequent use by spray drying. Exposure to particles was very low or non-existent.

More recently a life cycle risk assessment testing guide focused on CNMs (nanoLCRA) was proposed by J.A. Shatkin, K.J. Ong and colleagues from American Process and can help the community to better assess the toxicity of CNMs [134]. The guide is divided into three endpoints: (i) physicochemical characterization, (ii) human health effects testing and (iii) environmental effects testing. The physicochemical characterization is necessary because various grades of CNMs are now available and their impact on the two second endpoints may vary with the particle size, aspect ratio, surface chemistry, etc. The details of the guide are exposed on Table I.5.

Table I.5: Testing plan to characterize safety of CNMs, extracted from [134]

Endpoint	Protocol
1. Physicochemical characterization	
Particle size distribution, shape and aspect ratio	Transmission electron microscopy Scanning electron microscopy
Composition	Infrared spectroscopy Inductively coupled plasma optical emission spectroscopy
Crystal structure	X-ray powder diffraction
Explosibility	Explosion severity test (ASTM E1226) Minimum explosible concentration test (ASTM E1515) Minimum ignition energy test (ASTM E2019)
Biodegradability	Aerobic biodegradation (OPPTS 835.3140) Anaerobic biodegradation (OECD 311)
2. Human health effects testing	
Acute oral toxicity	Up and down procedure in rats (OPPTS 870.1100)
Skin irritation	MatTek Epiderm skin irritation test (OECD 439)
Eye irritation	Hen's egg test chorioallantoic membrane test Bovine corneal opacity and permeability test (OECD 437)
3. Environmental effects testing	
Microbial bioassay	Kinetic luminescent bacteria test (ISO 11348–3)
Algal bioassay	Freshwater alga growth inhibition test (OECD 201)
Aquatic invertebrate bioassay	*Daphnia* sp. acute immobilization test (OECD 202)
Aquatic vertebrate bioassay	Acute toxicity to embryonic zebrafish

The study of Shatkin and Ong evaluated the toxicity of lignin-coated CNF and CNC. Neither of the two material caused acute oral, eye or dermal inflammation or irritation. Moreover, environmental testing, using high concentration (>1000 times of maximum predicted emission values), demonstrated a very low potential toxicity [134].

However, for biomedical purposes further characterizations and testing are necessary. Medical use of cellulose nanomaterials goes beyond the eye or skin irritations. Indeed, nanocellulose based medical devices could be used to treat wounds or even be implanted inside the human body, where physiological responses greatly differ from external contact. Even ingestion of materials and their

way through the human digestion system can still be considered as external in comparison with implants. New aspects ranging from the simple cytotoxicity testing to the more complex genotoxicity, inflammatory response, reproductive and carcinogenic and toxicokinetic effects must be addressed to better evaluate the biocompatibility of CNMs [71], [120].

From now on, the discussion will only focus on CNF since it will be used in the following chapters of this Ph.D. thesis. A few comparisons will be established again with BNC owing to its previously mentioned particular properties for biomedical use.

The genotoxicity of CNF was assessed by Hannukainen et al., using enzymatically pre-treated CNF and TEMPO oxidized CNF were used with human bronchial epithelial cells (BEAS 2B). Both types of CNF exhibited DNA damage, but authors indicated that the testing procedure (enzyme comet assay) might have been incorrectly adapted to these new types of fibrous nanomaterials confirming the need for further analysis [135].

Another study has been carried out by the group of G. C. Carrasco and K. Syverud in 2013. Dense films and 3D porous structures of oxidized CNF (high amount of anionic charge) and neat CNF were evaluated in terms of cytotoxicity against 3T3 human fibroblast cells. Cell membrane, cell mitochondrial activity (indication of cell fuel source) and DNA replication were not affected by direct and indirect contact with CNF materials [136].

Also, researchers from Sweden investigated the relation between structure, surface charge and biological response of CNF. Anionic and cationic CNF were obtained through chemical modifications: carboxymethylation or condensation of glycidyltrimethylammonium chloride (EPTMAC) respectively. Films were then produced by vacuum filtration. Indirect contact cytotoxicity test were performed with human fibroblast. No cytotoxic effect was detected and cell adhesion was promoted due to CNF alignment [137].

An extensive overview of recent papers on the toxicological assessment of CNFs is exposed on Table I.6. This table gathers up studies that were mentioned in relevant reviews such as Lin and Dufresne in 2014 [129], Endes et al. published in 2016 [138] and Kangas et al. published in 2016 also [139]. The objective is to summarize the different types and forms of CNF that were already investigated in terms of biological response over five endpoints: cytotoxicity, inflammatory response (or immunotoxicity), oxidative stress, genotoxicity and ecotoxicity. In the literature, many publications combine different types of cells with CNF without studying its potential toxicity as a principal objective, as the publications that are gathered in Table I.6 do. Yet, those works also indirectly give information on CNF toxicity.

Table I.6: Extensive overview of toxicological assessment of cellulose nanofibrils over time

CNF type and form	CNF Source	Testing procedure	Biological impact				Comments	Authors	Year	Ref
			Cytotoxicity	Inflammatory response	Genotoxicity	Ecotoxicity				
Unmodified CNF	bleached birch kraft pulp, fir/beech woods	Cytotoxicity on mouse hepatonoma et human keratinocyte and cervix carcinoma	**no**	n/a	**no**	n/a	-	Pitkanën et al.	2010	[140]
CNF suspension and powder	never dried ECF bleached birch kraf pulp	Air particle concentration, Cytoxicity on mouse and human macrophages, Ecotoxicity test	**no**	**no**	n/a	mild	testing procedure not really adapted to CNF	Vartiainen et al.	2011	[133]
Commercial CNF (Booregard) suspension	n/a	Cytotoxicity assay on macrophage-like THP-1 cells [illegible] luminometric assay),	**no**	n/a	n/a	n/a	-	Kollar et al.	2011	[141]
Enz. and TEMPO CNF suspension	n/a	*In vitro* genotoxicity in human bronchial epithelial BEAS 2B cells	**no**	n/a	**yes**	n/a	unclear success of genotoxicity assay	Hannukainen et al.	2012	[135]
Various grades of enz. and TEMPO CNF	n/a	Cytotoxicity on human cervical HeLa cells Genotoxicity on human bronchial BEAS 2B cells Immunotoxicity, TNF-α and IL 1β detection *In-vivo* against Nematode model Pharyngeal aspiration exposure of mice	low	no	**no**	mild	pulmonary inflammation detected	Norppa et al.	2012	[132]
Neat and TEMPO CNF films and aerogels	*Eucalyptus* and *P. radiata*	Cytotoxicity on 3T3 fibroblast cells	**no**	n/a	n/a	n/a	-	Alexandrescu et al.	2013	[136]
Unmodified, anionic and cationic CNF films	*Cladophora* green algae and softwood dissolving pulp	Cytotoxicity on human dermal fibroblasts Cell adhesion and viability	**no**	n/a	n/a	n/a	surface properties influence to be noted	Hua et al.	2014	[137]

Neat CNF suspension	bleached hardwood kraft pulp	Cytotoxicity with HTD, TPC and RNA synthesis inhibition, Genotoxicity with Ames test *in vitro*, Ecotoxicity on nematodes	mild	n/a	**no**	**no**	effect of biocide to clarify	Pitkanën et al.	2014	[142]
Commercial CNF (USDA) suspension	n/a	Biodurability on in vitro cell-free and RAW 264.7 cell line models	n/a	n/a	n/a	mild	CNf are biodurable in human lung	Stefaniak et al.	2014	[143]
Neat CNF suspension	Norway spruce *Picea abies*	Cytotoxicity on L929 cells, rat thymocytes or human peripheral blood mononuclear cells Inflammatory by cytokines detection	**no**	**no**	n/a	n/a	-	Čolić et al.	2015	[144]
Unmodified, anionic and cationic CNF films	never dried bleached sulfite softwood dissolving pulp	Macrophage/monocyte behavior Immunotoxicity, TNF-α, IL 10 and IL 1ra detection	n/a	**no**	n/a	n/a	-	Hua et al.	2015a	[145]
CNF suspension and films, CNF in paper	never-dried bleached birch kraft pulp	Ecotoxicity, bioluminescence test with *Vibrio fischeri*	n/a	n/a	n/a	no	-	Vikman et al.	2015	[146]
Unmodified, anionic and cationic CNF films	Cladophora green algae	Inflammatory response of THP-1 cells (monocytes, macrophages) w/ or w/o lipopolysaccharide	n/a	**no**	n/a	n/a	-	Hua et al.	2015b	[147]
TEMPO CNF suspension and aerogels	never dried bleached *Pinus radiata* pulp	Cytotoxicity on Normal Human Dermal Fibroblasts and Human Epidermal Keratinocytes Inflammatory by 27 cytokines detection	**no**	**no**	n/a	n/a	-	Nordli et al.	2016	[148]
Unmodified and TEMPO commercial CNFsuspensions (USDA & Maine)	n/a	Ecotoxicology on embryonic zebrafish	**no**	n/a	n/a	**no**	no influence of aspect ratio	Harper et al.	2016	[149]
CNF suspension	bleached dissolving pulp from the Norway spruce (*Picea abies*)	Cytotoxicity on human monocyte derived Dendritic cells	**no**	**no**	n/a	n/a	-	Tomić et al.	2016	[150]
TEMPO CNF suspension	spruce sulphite dissolving pulp	Comet assay in bronchoalveolar lavage (BAL) and lung cells Bone marrow erythrocyte micronucleus assay	no	yes	**yes**	**yes**	Toxicity on lung cells	Catalán et al.	2017	[151]

Commercial Neat CNF gels and powder (USDA)	n/a	Cytotxicity, inflammatory and oxidative stress on human lung epithelial cells (A549)	mild	**no**	n/a	n/a	CNf are not taken up by cells, like CNC	Menas et al.	2017	[152]
Unmodified, anionic and cationic CNF suspensions	never dried bleached sulfite softwood dissolving pulp	Cytotoxicity on human dermal fibroblasts, human MRC-5 lung fibroblast cell line and human THP-1 monocytic cell line, Alamar Blue assay, ROS production, Inflammatory TNF-α and IL1-β detection	**no**	mild	n/a	n/a	surface charge influence	Lopes et al.	2017	[153]
Lignin coated CNF (Bioplus)	n/a	Acute oral toxicity, Skin and eye irritation, Ecotoxicology with algal, microbial and aquatic assay	**no**	**no**	n/a	no	-	Ong et al.	2017	[134]
TEMPO and carboxymethylated CNF hydrogels	n/a	Cytotoxicity on mouse fibroblasts L929 cells utilizing crystal violet, MTT, and LDH assays Cell-hydrogel interaction	no	n/a	n/a	n/a	Good cell proliferation and migration	Rashad et al.	2017	[154]
Commercial neat and carboxymethylated CNF (Innventia)	softwood sulphite dissolving pulp	(1,3)-β-D-glucan/ endotoxin-specific Limulus Amebocyte Lysate (LAL) end point test	n/a	**no**	n/a	n/a	No immunogenic contaminants detected	Liu et al.	2018	[155]
TEMPO CNF	bleached *Eucalyptus globulus* kraft pulp	cytotoxic, immunotoxic and genotoxic effects on a co-culture of lung epithelial alveolar (A549) cells and monocyte derived macrophages (THP-1 cells)	mild	**no**	mild	n/a	concentration-dependent effects	Ventura et al.	2018	[156]
Neat and fluorophore grafted CNF suspension	bleached never-dried softwood sulfite dissolving pulp	Ecotoxicity on feeding and life-history traits of *Daphnia magna*	mild	n/a	n/a	**no**	concentration-dependent effects	Ogonowski et al.	2018	[157]
Neat, carboxymethylated and carboxylated CNF	n/a	Cytotoxicity by actate dehydrogenase (LDH) release assay, Inflammatory cytokines detection in THP-1 cells, Pulmonary effects and biopersistence of the materials in mice	mild	mild	n/a	n/a	CNf still present after one months in lung	Ilves et al.	2018	[158]
Neat CNF suspension	softwood bleached kraft fiber	Sterility/biological assessment Endotoxin assessment	n/a	n/a	n/a	n/a	free of endotoxins and bacteria	Pyrgiotakis et al.	2018	[159]
Neat CNF suspension	Curauá leaf fibers *Ananas erectifolius*	Cytoxicity on fibroblast Vero cells Adhesion test	**no**	n/a	n/a	n/a	high affinity of cells to CNF	Souza et al.	2018	[160]

The overall toxicity of CNF towards cells from various lines appears to be very limited. However, the following endpoints should be kept in mind when trying to characterize the toxicity of CNF.

One should note the importance of careful sample characterization and exclusion of interfering factors like endotoxins or toxic chemical impurities that were used to prepare the samples (chemical agents or biocides). The objective is to avoid inaccurate conclusions from toxicity assessment [161]. Moreover, the biodurability of CNF in *in-vivo* conditions grants extended period of time for such contaminants to leach out. Regarding this endpoints, the case of bacterial nanocellulose (BNC) is of particular interest. Synthetized by bacteria, no contaminants are to be removed, thanks to this high purity, a very good biocompatibility was confirmed several times by in-vivo testing since the end of the 1990s. Commercial product based on BNC such as Biofill® were implanted in animals [162], artificial blood vessel made out of BNC were also successfully implanted in rats [163]. Reconstructive microsurgery of rat carotid artery was performed during 1 year with BNC model vascular system proving the high biocompatibility of BNC [164].

Secondly, even if CNFs mostly do not reveal any strong hazardous effect on human derived cells and the environment or when it is used as a biomaterial, one should keep in mind that the surface modification of these materials could give different results. In the publication of G. C. Carasco and K. Syverud groups that was mentioned before, the introduction of polyethylenimine (PEI) as a crosslinker or cetyl trimethylammonium bromide (CTAB) as debonding agent on the CNF revealed toxic behavior with detrimental effects on survival, viability and proliferation of cells [136]. In comparison, more recent work by Harper et al. revealed that various surface chemistries implemented on CNFs appeared to be of low toxicity to the development of zebrafish [149]. This indicates that careful biocompatibility studies must be undertaken when CNF surface is modified, either by covalent bonding or just adsorption.

To conclude on health and toxicology concerns, sporadic toxic response can be detected depending on the morphology, the presence of contaminants from the raw materials or the isolation process, and the surface chemistry of CNF. However, the inexistent or low biological response demonstrated in every above mentioned studies are relevant proofs that CNF are cytocompatible and mostly not hazardous to human health. Moreover, good cell proliferation and migration was also observed. Nonetheless, precautionary principle must be respected and the best way to clarify the potential toxicity of CNF is to implement testing conditions that are as close as possible to the intended end application.

2.5 Cellulose nanofibrils and medical applications

Since bacterial nanocellulose is synthetized by bacteria with near-perfect purity, it led to the development of the first commercial clinical applications of nanocellulose. Namely Bioprocess®, XCell® and BioFill® used for topical applications such as burn treatment as depicted on Figure I.30. The remarkable conformability and the ability to maintain a moist environment allow for the reduction of patient pain and contributed to the success of these products.

Figure I.30: Bacterial nanocellulose for topical wound dressing. Shape conformability and moist environment for reduction of pain [165], [166]

Although bacterial nanocellulose is wrapped in an enthusiastic trend for medical application, large scale production facilities are still missing and improvements has to be made regarding the time required for the production which is commonly up to two weeks as pointed out in several reviews and papers [113], [167], [168].

Wood derived nanocellulose is produced in a larger scale and quicker time so its use in the biomedical would be preferable. Many examples of the use of CNF for biomedical application in several fields are available in the literature [129], [169].

As an introduction to the wide following overview of the strong academic research that involves CNF for medical application, it should be noted that a first industrial grade of CNF designed for biomedical appeared recently. It is produced by the Finnish company UPM under the commercial name of GrowDex® and is extracted from birch hardwood. It is said to be biocompatible and to mimic the extracellular matrix (ECM) that support the growth and differentiation of cells. Moreover, the suspension is dispersed in ultra-pure water and is then easily mixed with culture media. Specifically designed to be used in 2D and 3D cell culture, GrowDex® CNF hydrogels can also be used in combination with microfluidics devices to mimic organs. At high concentrations the thick gel acts as a barrier system preventing cell migration without hindering the migration of smaller compounds like nutrients and drugs. Drug delivery systems also benefits from this barrier effect. This commercial product is for research use only, but increasing investigation might soon end up with diagnostic and therapeutic products. For instance, GrowDex® CNF have been proven to better promote the

maturation of hepatocyte like cells [170]. Finally, GrowDex® CNF based medical prototypes were developed such as wound healing, antimicrobial film and hydrogel, scaffold, injectable hydrogels and bone tissue engineering as described by P. Laurén in a recently released Ph.D. thesis and from which Table I.7 is extracted [171].

Table I.7: Plant derived CNF based materials for biomedical applications [171]

Polymer composition	Formulation	Application
NFC	Aerogel and film	Wound healing
NFC-hemicellulose	Composite hydrogel	Wound healing
NFC*	Surface modified film	Antimicrobial film
NFC	Cross-linked hydrogel	Antimicrobial hydrogel
NFC**	Hydrogel bioink	Tailor-made wound dressings
NFC	NFC wound dressing	Wound healing (clinical study)
NFC-alginate	Composite hydrogel bioink	Cell-laden ear cartilage scaffold
NFC-carbon nanotube	Conductive hydrogel bioink	Neural tissue engineering
NFC-polyvinyl acetate	Composite polymer film	Self-softening *in situ* implantation
Plant cellulose tissue	De-cellularized scaffold	Subcutaneous implantation (*in vivo*-study)
NFC	Hydrogel	Injectable *in situ* implantation (*in vivo*-study)
ANFC-chitosan	Hydrogel	Injectable *in situ* implantation (*in vivo*-study)
NFC	Hydrogel	Injectable hydrogel for localized chemotherapy
NFC-alginate	Composite hydrogel	Suture coating for cell therapy (*ex vivo*-study)
NFC***	Cross-linked thread	Stem cell delivery (*ex vivo*-study)
NFC	Hydrogel	3D organoid development
NFC	Hydrogel	3D cell culture scaffold
NFC	Hydrogel	3D culturing of pluripotent stem cells
NFC-RS/P	Composite film	Bioadhesive film
NFC-PEG	Composite hydrogel	Mucoadhesion
NFC	Aerogel	Gastroretentive drug delivery system
(A)NFC-polymer†	Composite film	Bioadhesive film
NFC-chitin	Composite scaffold	Bone tissue engineering
NFC-gelatin	Composite scaffold	Bone tissue engineering
NFC-hydroxyapatite	Composite scaffold	Bone tissue engineering
CNC-GIC††	Composite dental cement	Restorative dentistry

*Octadecyldimethyl(3-trimethoxysilylpropyl)ammonium chloride modified
**Carboxymethylated and periodate oxidated
***Glutaraldehyde cross-linked
†ANFC- and NFC-Pectin, -mucin and -chitosan composites
††CNC acquired from NFC and reinforced with glass ionomer cement (GIC)

Two main applications are classically concerned: (i) drug delivery and (ii) wound healing/tissue engineering. These two applications will be considered for the medical devices development during this Ph.D. project. Therefore, the following overview will focus first on 100% CNF formulations before the description of more complex structures that involve CNF together with other polymers or compounds, for drug delivery and wound healing/tissue engineering.

One of the pioneer works that involved CNF for drug delivery application used 2D structures: a matrix carrier in the form of films was produced by filtration and showed drugs loadings of 20% to 40%. The mechanical properties of the films were suitable for easy handling and shape tailoring. The release was sustained for up to three months with a close to zero order kinetic thanks to the tight nanofiber network in which the drug compound was entrapped. This result indicates how efficient CNF are to extend release period [172]. Figure I.31 shows SEM pictures of the drug loaded CNF film before and after the release experiment and the cumulative amount of drug released over time that demonstrates the sustained release. An even further characterization of the interaction of different types of drug (size and charge) with CNF was conducted. Permeation through CNF films, binding abilities and thermodynamics of the binding process to CNF were monitored with HPLC and ITC. The results suggested a size dependence for the permeation study and that pH and electrostatic forces governed the binding abilities and thermodynamics [173].

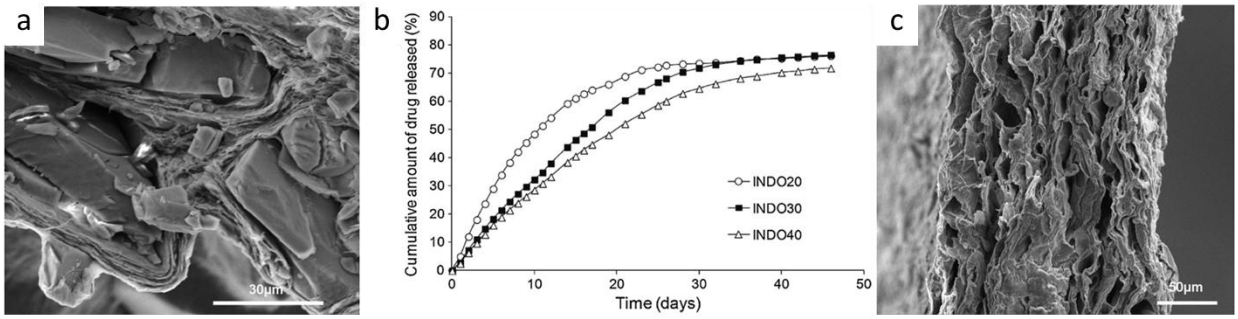

Figure I.31: Release study of indomethacin from CNF films produced by filtration, a) SEM pictures of the drug loaded film before the release showing the drug crystals, b) cumulative amount of drug released over time for three drug loadings and c) SEM pictures of the CNF film after the release, extracted from [172]

CNF 3D structures such as drug loaded aerogels were also designed for oral drug delivery applications. Four types of CNF were compared to microcrystalline cellulose (MCC). Hydrophobic drugs were successfully included in these highly porous reservoirs thanks to amphipilic hydrophobin proteins. Sustained drug release was obtained for TEMPO CNF and explained by the nanostructure and interactions with the protein coated drug [174]. Similarly, pH-responsive 3D micro-porous hydrogel structures were produced from periodate oxidized and carbomethylated CNF. The ionisable functional groups available at the surface of the material explained the pH-dependent swelling

degree (higher at neutral and alkaline pH than in acidic conditions). These hydrogels can achieve controlled and intelligent release of active principle ingredients (API) when exposed to specific pH conditions [175].

When combined to currently used polymers, CNF can improve the properties of existing controlled drug release systems. For instance, CNF has been used to enhance conventional MCC tablets loaded with paracetamol. CNF allow for a better flowability of powders and lower porosity upon packing even if high compacting forces were required since CNF are more ductile than MCC. Release was also quicker with CNF enhanced CMC tablets. Depending on the target of the delivery this might be an advantage [176]. Very recently, CNF were also used with other biobased polymers like chitosan to prepare a CNF/chitosan transdermal film for the delivery of ketorolac tromethamine (KT, antipain). The KT CNF/chitosan films exploited the CNF nanobarrier to help to sustain the release of the KT compound as proven by drug release profile and kinetics [177].

In order to combine CNF with other compounds, chemical surface modification can be explored. Poly ethylene imine polymeric chains were covalently bound to CNF surface before freeze drying and production of PEI/CNF aerogels. Those were successfully loaded with a model drug. The release study indicated a pH and temperature dependence of the release profiles. This work resulted in pH and temperature responsive release systems based on CNF offering a new innovative alternative to conventional release systems of the pharmaceutical industry [178]. Another interesting publication derived from P. Laurèn work used technetium-99m-labeled CNF (^{99m}Tc-CNF) injectable hydrogel for *in vivo* drug release application. The ^{99m}Tc-CNF were able to be traced after subcutaneous injection in the pelvic region of mice. The CNF did not migrate or disintegrate during the study whereas the animal was awake and free to move as illustrated on Figure I.32.

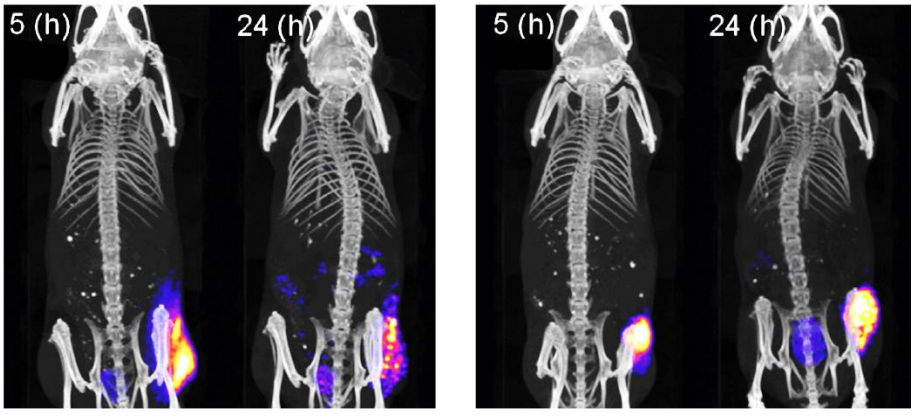

Figure I.32: SPECT/CT images of ^{99m}Tc labelled human serum albumin injected in mice with (right) or without (left) CNF hydrogel. Over 24 hours, the human serum albumin was maintained around the injection site when CNF were used, extracted from [179]

Such CNF hydrogels also allowed for a better controlled release of compounds compared to CNF-free injections [179].

Wound healing is a second topic where CNF could bring innovative formulations. As a 100% CNF structures, films and aerogels were used to develop chronic wounds dressings and evaluate their response to the Pseudomonas Aeruginosa strain growth. A dose-dependent inhibition of the bacterial growth was observed and the biofilm formation was hindered by the decreasing porosity and surface roughness of aerogels. These results demonstrate the potential of CNF in the design of novel wound dressings [180]. Similar growth prevention was observed for calcium and copper ions crosslinked TEMPO oxidized wood derived CNF aerogels exposed to *Staphylococcus epidermidis* and *Pseudomonas aeruginosa* bacterial strains. A bacterial barrier effect was also detected with SEM pictures as shown on Figure I.33.

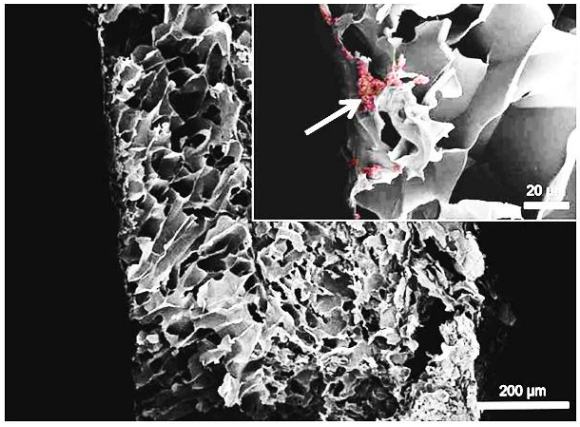

Figure I.33: SEM pictures of calcium crosslinked TEMPO CNF aerogels exposed to Staphylococcus epidermidis and visualization of bacterial barrier effect on the insert where bacteria grow on the surface of the aerogel but do not penetrate

Researchers also evaluated recently the elastic modulus of CNF hydrogels scaffolds for application in tissue engineering. TEMPO oxidized CNF that are known to bear carboxyl groups but also a few amount of aldehydes groups were crosslinked with primary diamines compounds of different chain length through Schiff base reaction (aldehydes-primary amine). Reversible gels were though converted to tunable irreversible gels. CNF gel structure can thus be controlled adding one relevant endpoints for the use of CNF based systems for tissue engineering applications [181].

Similarly to drug release topic, combining CNF with other biobased materials is of importance to beneficiate from the peculiar properties of both materials. CNF hydrogels were reinforce with alginate and were assessed in terms of mechanical properties such as rupture strength, compressibility and gel rigidity. The best combination used oxidized CNF with alginates hydrogels ending up with mechanically tunable systems and more stable in physiological conditions. Such

combination of two biobased polymers is of high interest in the scaffolding technology for tissue engineering and bio-printing [182].

Latest research proposes the use of CNF based inks to produce 3D scaffolds by bio-printing for neural tissue engineering applications. CNF and carbon nanotubes (CNT) as ink constituents allow for the printing of guidelines of less than 1 mm with conductive properties. The results showed that neural cells attached, proliferated and differentiated on the 3D printed guidelines. An overview of this work is provided by Figure I.34. Promising application in brain mimicking environment are expected [183].

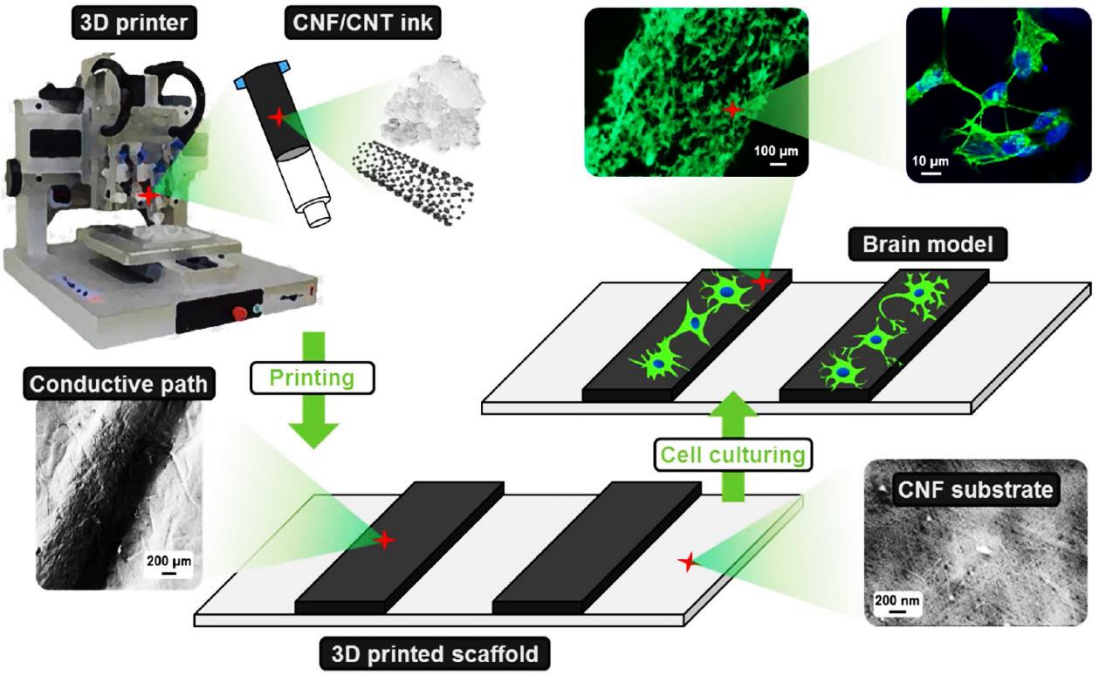

Figure I.34: Overview of the fabrication of the cellulose-derived nanofibrous scaffolds for neural network development based on CNF loaded inks, extracted from [183]

As a conclusion, cellulose nanofibrils are very promising materials for medical applications. The numerous and diverse research works about its use to improve existing medical formulation or to help designing new healing strategies show the wide potential of such material. Moreover, many researchers try to go further by providing cellulose nanofibrils with new functions thanks to surface chemical modification. Such strategy is the key part of this Ph.D. project and different surface modification of CNF will be described in Chapter II. Consequently, the last part of this first chapter is dedicated to CNF functionalization.

3. Functionalization of CNF surface

Nanocellulose functionalization started to be explored because of increasing attempts to use it in nanocomposite material. Actually, due to their nanosize, high specific surface area and strong mechanical properties, cellulose derived nanomaterials have a great potential as reinforcement. Nevertheless, the dispersion of such nanofillers in the conventional matrices is critical for the improvement of mechanical properties. The inherent hydrophilicity of nanocellulose and its inability to dissolve in most organic solvents make it difficult to achieve appropriate dispersion level in water-insoluble or non-water dispersible matrices [95]. Hydrogen bonding network that govern most of cellulose and nanocellulose properties tends to form aggregates which prevent good dispersion. Turning the surface hydrophilicity of nanocellulose into surface hydrophobicity appeared like the first strategy to reach a suitable compatibility between nanofillers and matrices. Surface modification of nanocellulose thus became an intensive research field.

The potential of surface modification do not only concerns polymer and new nanocomposites design since a wide variety of compounds can now be immobilized on nanocellulose surface. In addition to matrix compatibility increase, nanocellulose surface functionalization also brings a wide range of new functionalities depending on the type of chemical compounds that is immobilized. This gives interesting results in the sensor technology, environment protection, papermaking industry or even automotive applications [184]. Few reviews summarize the current trends of nanocellulose chemical modifications [185], [186].

Nanocellulose surface functionalization can be done by covalent or non-covalent binding of chemical compounds. In the case of covalent binding, also referred as grafting, small molecule or even polymers are suitable for functionalization. Polymers can be grafted by two processes: either “grafting onto” or “grafting from”. In the “grafting onto” approach, the terminal group of the polymer chain is exploited for the covalent binding, while in the “grafting from” approach, the monomer and initiator are mixed with nanocellulose, before the polymerization takes place at the surface of nanocellulose. Non-covalent functionalization relies on adsorption mechanisms that are governed by electrostatic attractions, hydrogen bonds or van der Waals forces [185]. The Figure I.35 gives a wide overview of the different approaches used to modify CNF surface.

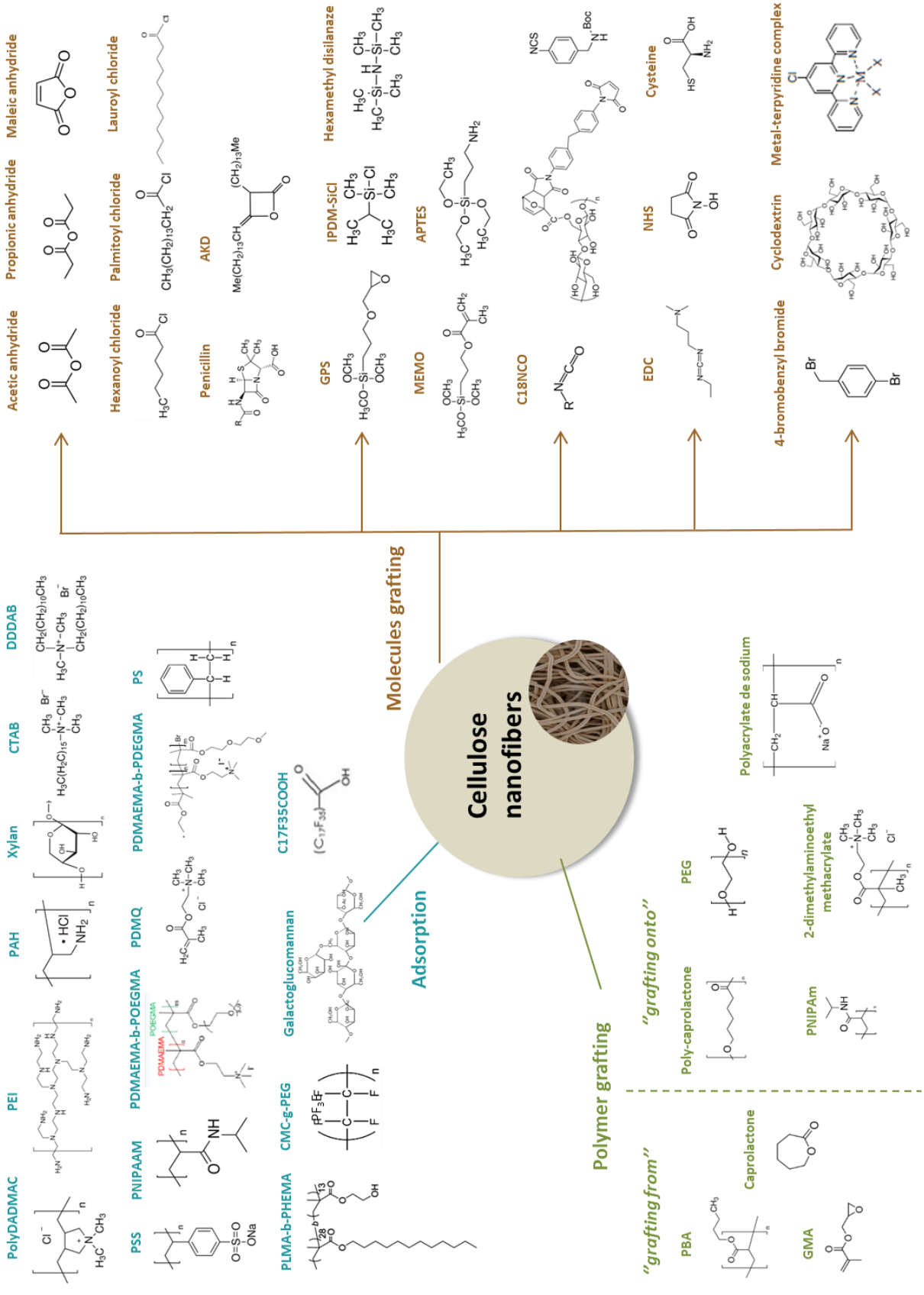

Figure I.35: Different approaches to modify cellulose nanofibrils surface, adapted from [105]

One of the most common ways to quantitatively characterize the grafting of molecules or polymers on CNMs is to calculate a degree of substitution (DS). When considering a single sugar unit of the cellulose polymer, three hydroxyls groups are available for the covalent bonding of a compound. The degree of substitution is a value in between 0 and 3 that describes the amount of hydroxyl groups that are substituted during the reaction of modification. It is always an average value due to the heterogeneity of grafting success related to CNMs. The DS is a characteristic of the bulk material, and can thus be measured through elemental analysis techniques. For an alternative analysis of the grafting success, another value has been introduced by researchers in the late 2000s. The degree of substitution of the surface (DSS) describes the amount of substituted hydroxyls of the cellulose polymers chain at the very first layers of cellulose nanofibrils or cellulose nanocrystals. This value can be determined through surface elemental analysis tools like X-ray Photoelectron Spectroscopy [187].

The current trend in CNMs surface modification goes toward more green procedures. The use of toxic solvents or reactants often hinders the upscaling of CNMs modification that will be required to reach industrial level processes. Moreover, sustainable process development is in accordance with the use of CNMs in our everyday life since they are renewable and biodegradable natural materials believed to be an alternative to petroleum based conventional polymers. In this context, water based chemical procedure that limit the use of toxic solvents or chemicals are of high interest and will be at the heart of Chapter II. Also, the discussion will be focused on CNF surface modification as it is the CNM used in this Ph.D., but other cellulose products will be mentioned for a few context descriptions and comparison of chemical reactions.

3.1 Esterification of nanocellulosic materials

Esterification introduces ester functional group (O-C=O) through the condensation of carboxylic acid, acid anhydrides or acyl chlorides with hydroxyl groups. It is one of the most versatile reactions for the modification of polysaccharides owing to the huge quantity of available hydroxyls groups. This provides access to a wide range of functionalized materials [188]. Cellulose acetate is one of the most known esterified natural polymers, cellulose triacetate and di acetate are mainly used for textile fibers, filter tow and thermoplastic mass [189]. Cellulose acetates are produced through the esterification of cellulose hydroxyl groups with acetic anhydride in the presence of sulfuric acid catalyst to give the fully acetylated cellulose (triacetate). A partial hydrolysis is applied to reach the intended polymer with proper DS and remove the catalyst [190].

As for cellulose itself, the esterification of CNF is widely used. Two kinds of conditions can be used for chemical reaction on CNF, either under swelling or non-swelling conditions. In the non-swelling conditions, the reaction only occurs at the surface of CNF and the limitations of the esterification lies

in the accessibility of the surface. The morphology of the nanofibers will remain the same upon the reaction. In the swelling conditions, esterified cellulose chains tend to be solubilized in the esterified medium. This has been observed already on CNC [191].

The esterification of CNF is fairly recent. One of the pioneering works of esterification of CNF was done by Herrick et al in 1983. They tried to produce CNF by mechanical shearing with the simultaneous acetylation of the material by using a mixture of acetic acid and acetic anhydride as a medium instead of water. Sulfuric acid was used as a catalyst.

During the last decades, many techniques were used to perform esterification on cellulose nanofibers. Heterogeneous versus homogeneous conditions were often discussed. Organic solvent allowed for significant DS achievements. For instance, CNF suspensions have been solvent exchanged to DMF in order to perform surface esterification. Several quantity of acetylated groups were obtained and allow for the production of nanocomposites by solvent casting with poly(lactic) acid (PLA) thanks to the enhanced interface adhesion. The acetylated CNF were proven to be better dispersed in the PLA matrix and the ensuing nanocomposites had a better transparency and an increased glass transition temperature which indicated a better fiber-matrix interaction [192]. Ionic liquids were used in 2012 to modify CNF in suspension again with anhydrides (acetic, butyric, iso-butyric and hexanoic). The ionic liquid used was [bmin][PF_6]. Successful grafting was proven by FTIR, elemental analysis and ToF-SIMS. DS and DSS were possible to calculate and reached 0,3 and 0,85-1,12 respectively [193].

In a solvent free method, researchers tried to esterify CNF in a dry form of aerogels, in gas phase with palmitoyl chloride at temperatures comprised between 100 and 200°C for 0,5 to 2 hours. This resulted in cellulose palmitates with DS ranging from 0 to 2.36. High DSs did not maintained the structure of CNF but low DSs (0,1 to 0,4) kept the intact structure of CNF [194].

All these examples are of high scientific interest and challenges but they lack upscaling perspectives. Moreover, many solvents and reactants are not really environmentally friendly. Alternative routes have also been proposed to cope with these two endpoints.

Contact active surfaces based on CNF modification with the antibiotic penicillin were produced. CNF films were produced by filtration and then immersed in the active principle ingredient solution. In a parallel strategy, penicillin was also introduced directly in the CNF suspension before the production of CNF film through solvent casting. Esterification was triggered by thermal treatment applied on both types of CNF films at 150°C for 2 hours. Grafting was confirmed by FTIR, elemental analysis and X-ray photoelectron spectroscopy. Antimicrobial properties were thus provided to CNF although the

reached DS were fairly low (<0,1) [195]. Such greener approaches are keys for the development of upscaling and environmentally friendly processes for esterification of CNF.

An improved version of this last mild solvent-free approach will used in the Chapter II to covalently bind active principle ingredient to CNF films. Indeed, the thermal treatment should be limited when working with sensitive molecule that is intended to grant active properties to CNF based devices.

3.2 Peptide linkage: amidation of oxidized nanocellulosic materials

Amidation is another example of reaction that readily operates in water and represents one of the most occurring reactions in Nature. Amidation reaction produces an amide bond (O=C-N) from the attachment of amine derivatives on carboxylic acid groups. Methodologies to form an amide bond are described since the very beginning of organic chemistry. Since the 1980's researchers focused their investigation on the use of coupling reagents such as the predominant carbodiimide and active ester strategy. Figure I.36 introduces the general principle of activation process for the formation of amide bond.

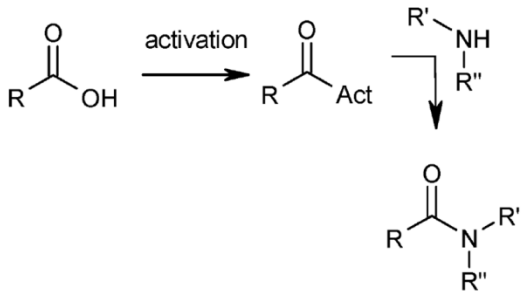

Figure I.36: Principle of the activation reaction in amide bond formation [196]

Other reagents appeared and scientists now have a wide panel of different conditions and strategies and can adapt to their research the most suitable ones [197]. Parameters of choice for coupling reagents can be the price, the homogeneous or heterogeneous aspect of the reaction, the use in excess or deficit of coupling reagents and the presence of other functional groups in the system that might interfere [198]. Pioneer work on nanocellulosic materials dealing with the formation of an amide bond are attributed to Araki et al. in 2001. The purpose of this work was to increase the colloidal stability of oxidized cellulose nanocrystals suspensions by grafting amine terminated poly(ethylene glycol) at their surface [199]. They used the water soluble 1-ethyl-3-(3-dimethyl aminopropyl) carbodiimide hydrochloride (EDC) and N-hydrosuccinimide sulfonate (NHS) coupling reagents. EDC/NHS coupling was also used more recently for the surface modification of cellulose nanofibrils but many different conditions were used as depicted on Table I.8.

The accepted mechanism of EDC/NHS coupling seems to follow the general formation of peptide bond. The carboxylic acid hydroxyl group must be replaced by an electron-withdrawing substituent in order to increase the electrophilicity of its carbon. A nucleophilic attack by an amino group is thus favored [200]. The EDC is a good electron-withdrawing substituent, and lead to the formation of the O-acyl-iso-urea compound. A publication from 1995 suggests that the best pH range for the activation by EDC is between 3,5 and 4, 5 [201]. Once the EDC is added on the carboxylic moiety, hydrolysis of the O-acyl-iso-urea by water is much more likely to happen than the direct attack by the amine molecule. The O-acyl-iso-urea can also undergo a (O→N) displacement that gives the more stable N-acyl-urea that is not reactive toward amines. The amide is very unlikely to be formed without the use of the complementary coupling reagent, N-hydrosuccinimide sulfonate (NHS). The role of this compound is to prevent the formation of N-acyl-urea, but also to turn the O-acyl-iso-urea into a less water hydrolysis-sensitive molecule by the formation of an ester bond. The hydroxyl group of NHS makes a nucleophilic attack on the O-acyl-iso-urea and gives the corresponding succinimidyl ester. The non-dissociated primary amine can then attack and produce the amide and regenerate the NHS as detailed on Figure I.37 [202].

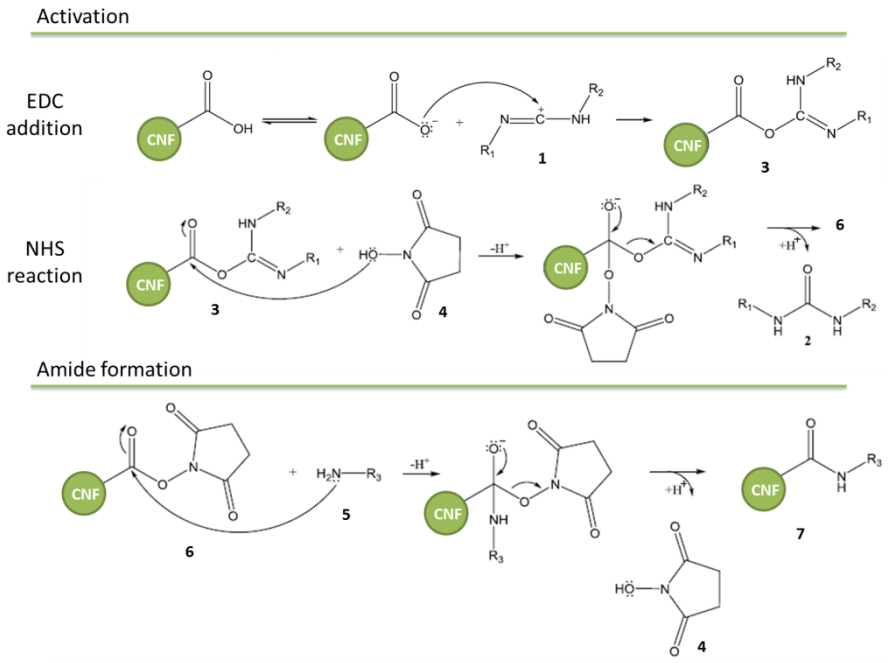

Figure I.37: Commonly accepted mechanism for amide bond formation with EDC/NHS coupling reagents. EDC (1) reacts with the carboxyl groups of oxidized CNF to give the O-acyl-iso-urea (3) which further reacts with NHS (4) to give the succinimidyl ester (6). The non-dissociated amine can attack and form the amide functionalized CNF (6) and regenerate NHS (4) (adapted from [202])

The EDC/NHS coupling reagents are mainly used for the formation of amide bond onto CNF aqueous suspensions. Only a few publications deal with the EDC/NHS coupling reaction on CNF only. They are all listed in the Table I.8. The order in which the coupling agents and the amine molecule are added

to the CNF suspensions differ and the three compounds can also be added simultaneously. The pH conditions are also different, researchers mostly use slightly acidic conditions but when coupling agents are added first, the pH is increased to neutral or low alkaline values when the amine is introduced. The pKa of the amine function plays a role here, the non-protonated -NH_2 form is necessary according to the above mentioned mechanism. However, stability and solubility of amine containing molecules that are intended to be grafted on CNF could be more important to ensure, even if the non-protonated form of the amine will be less available.

Table I.8: Cellulose nanofibrils modified with carbodiimide (EDC) mediated amidation in the literature

CNF type and form	Amine compound	Reaction medium	Order of chemicals adding	Activation		Amine coupling		Washing		Characterization	Ref.
				Time	pH	Time	pH	Temp.			
CNF-tempo suspension	Jeffamines	water	Amine first, then EDC/NHS	-	-	overnight	pH 7,5-8	RT	centrifugation or filtration and dialysis	conductometric titration	[203]
CNF-tempo suspension	Alkaline phosphatase	water	EDC/NHS first, then amine	15 min	pH 5	3h	pH 8 (borate buffer)	22°C	-	conductometric titration	[204]
Carboxymethylated CNF suspension	Dopamine	water	EDC/NHS/Amine at the same time	-	-	6h	pH 5	RT	dialyzed for 24 h in PBS buffer and then for five days in Milli-Q water	FTIR, UV	[205]
CNF tempo film on QCM-d sensor	Neutravidin or Avidin	water	EDC/NHS first, then amine	Tens of minute (QCM-d flow)	pH 5 (NaOAc buffer)	Tens of minute (QCM-d flow)	pH 5 (NaOAc buffer)	25°C	0.1 M ethanol amine at pH 8.5, 100 mM Glycine-HCl solution in Milli-Q-water (pH adjusted to 2.5 with HCl and NaOH)	QCM-d, XPS	[206]
CNF tempo film	Human antibodies	water	EDC/NHS first, then amine	20 min	pH 5	20 min	pH 7,4 (phosphate buffer)	NA	rinsing with 10 mM phosphate buffer (pH 7.4), and 10 mM NaCl (pH 10)	conductometric titration, XPS	[207]
CNF-tempo suspension	Propargyl amine	water	EDC/NHS/Amine at the same time	-	-	24h	pH 4 (MES buffer)	RT	dialysis (cutoff = 12 kDa) against a saturated NaCl for 1 day and then against distilled water for 3 days	FTIR (KBr disc), XPS, 13C NMR	[208]
CNF-tempo suspension	Amine groups covered carbon dots	water	EDC/NHS/Amine at the same time	-	-	overnight	pH 4,5 (NaAc/HAc buffer)	RT	dialysis against distilled water for 8 days (12–14 kDa)	SPR, polyelectrolytes titration	[209]

CNF-tempo suspension	Small peptides and enzymes	water	Amine first, then EDC for crosslinking	-	-	16h	pH 4,5 or 5,2 (MES buffer or NA)	4°C	performed twice in an equal volume of desorption buffer (pH 5.2 and ionic strength of 1000 mM for 1 h)	Amidolytic Activity	[210]
Tempo oxidized wood fiber for CNF production	Aminobenzophenone	DMSO/ water	EDC/NHS first, then amine	15 min	pH 5	overnight	pH 5	RT	washed first with 50/50 mix of DMSO/water and then with deionized water	Conductometric titration and FTIR	[211]
Gelatin / CNF-tempo mixture gels	Gelatin	water	Amine first, then EDC/NHS	-	-	24h	pH 5,5 (MES Buffer)	4°C	dialysis against water and stored at 4–8 °C	TNBS spectrophotometric assay	[212]
Carboxymethylated CNF	Dopamine	water	EDC (no NHS), then amine	1 min	pH 5	6h	pH 5	RT	dialysis for 6 days (2 days in Milli-Q water at pH 5 and 4 days in Milli-Q water at pH 7)	Polyelectrolytes titration, nitrogen analysis	[213]
CNF-tempo film on QCM-d sensors	Protein	water	EDC/NHS first, then amine	20 min	pH 5 (Hac buffer)	25 min	pH 5	25°C	sensors were rinsed with HAc buffer and washed with ethanolamine aqueous solution (1 M, pH 8.5) for 10 min	C-reactive protein binding with QCM-d	[214]
CNF-tempo	Amine terminated PEG	water	EDC, then NHS, then amine	15 min *2 (for EDC, then for NHS)	NA	overnight	pH 5	NA	dilution with MilliQ-water, pH was adjusted to 3.5, unbound reagents and excess polymer were removed by ultra-flow filtration against MilliQ-water	Elemental analysis, polyelectrolytes titration	[215]

Likewise, washing procedures are supposed to be adapted to each amine compounds. The removal of undesired molecules (coupling agents unreacted amine compounds) remains a challenging issue since strong adsorption is at stake with CNF. Consequently, characterization tools are not always able to distinguish the only adsorbed from the covalently bound molecules. Both duration and temperature of the amidation reactions are mostly identical: several hours at room temperature. Overall, amide bond formation is an environmentally friendly reaction since is occurs mainly in water under mild temperature conditions and in a relative short time.

In this work, amide bond formation will be used as a first step to modify CNF surface in suspension. Coupling agents EDC/NHS will be used in the most appropriate conditions for the amine molecule that will be grafted on CNF. CNF will be further modified with an environmentally friendly and easily scalable reaction family: click chemistry reactions.

3.3 Click Chemistry and nanocellulose

The click-chemistry principles were first described by Sharpless and co-workers in 2001. The vision behind the work of these researchers is to follow Nature's preferred methods of synthesis to address the development of powerful highly reliable and selective reactions. Click chemistry is sometimes referred to as a reaction that "clicks" compounds as molecular LEGO© bricks to produce complex architectures [216]. More precisely, a reaction earns the click chemistry status when it is modular, wide in scope and proceeds in simple synthetic conditions (atmospheric conditions) and results quickly in very high yields. Raw materials and reagents must be readily available. No solvents are allowed except benign ones such as water. Potential by-products must be inoffensive and easily removable. The reaction must be stereospecific (but not necessarily enantio-selective) and the product must be simple to isolate and stable under physiological conditions [217].

Click chemistry revolutionized many fields of chemistry. But one needs to keep in mind that the reasons behind this tremendous impact do not lay into the innovation of these coupling strategies. They were known for decades. However, contemporary methods and tools allowed researchers to improve and better characterize the kinetics and products of this type of reaction [218].

The copper(I)-catalysed azide-alkyne cycloaddition (CuAAC or Huisgen reaction) was considered as the "cream of the crop" click chemistry reaction, leading even to misunderstanding the general principles of click concept with this reaction. Therefore, it has evolved in a widely used coupling procedure in all chemical disciplines. The cycloaddition rate is strongly increased in the presence of transition-metal ions that also provide stereospecificity. Copper (I) ions are traditionally used with nitrogen-based ligand. But considering the growing concerns of cytotoxicity of copper, other types of

catalyst and even metal free procedure were developed, as depicted on Figure I.38. Meanwhile, in the last 15 years, metal-free [3+2] cycloaddition reactions, Diels Alder reactions, thiol-alkene and thiol-alkyne reactions also appeared to be classified as click reactions, mainly thanks to their simple synthetic procedures and high yields. [219]

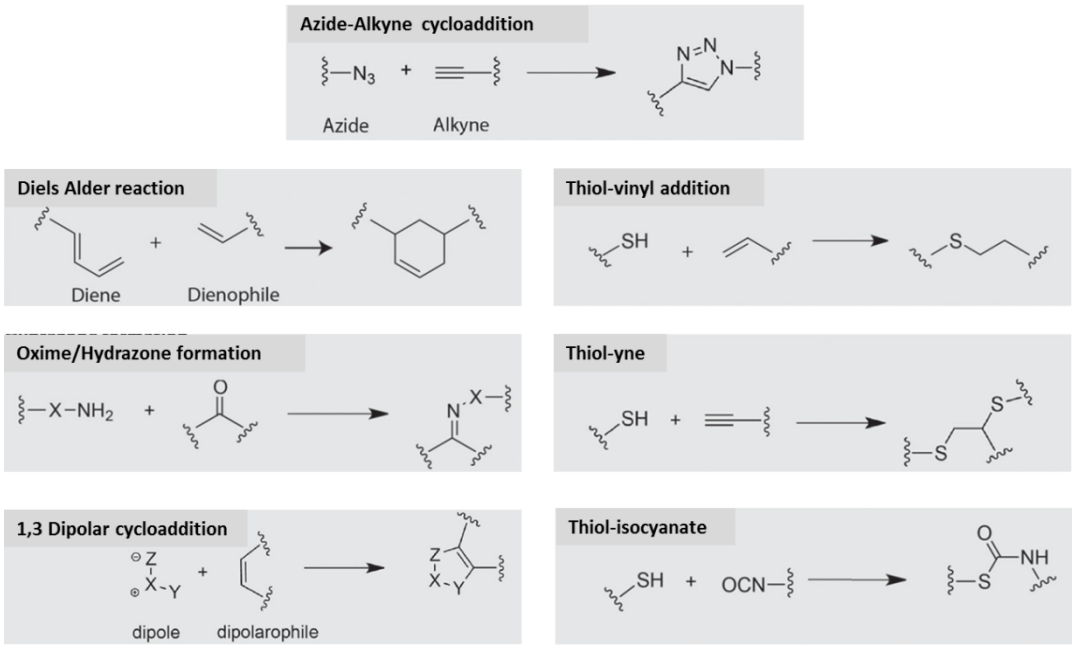

Figure I.38: Overview of main click chemistry reactions (adapted from [220])

The literature offers almost 18,000 publications on click chemistry but only about 200 deals with cellulose substrates as illustrated on Figure I.39. It also shows the proportion of cellulose nanomaterials (CNF, CNC, BNC) that are connected with click chemistry in the literature. A focus is also exposed on main click chemistry types used for chemical modification of CNF. Half of the publication deal with azide-alkyne cyclo-addition since it is the most widely used reaction. Consequently, only a very few publications are available on other types of click reaction for CNF modification. It confirms the room for improvement and innovation on the topic of metal free click chemistry applied to CNFs, especially thiol-yne click chemistry on which only one publication was found. Plus, this only work deals with microfluidic channels for biosensing and do not uses thiol yne click chemistry to bind active principles to CNFs [221].

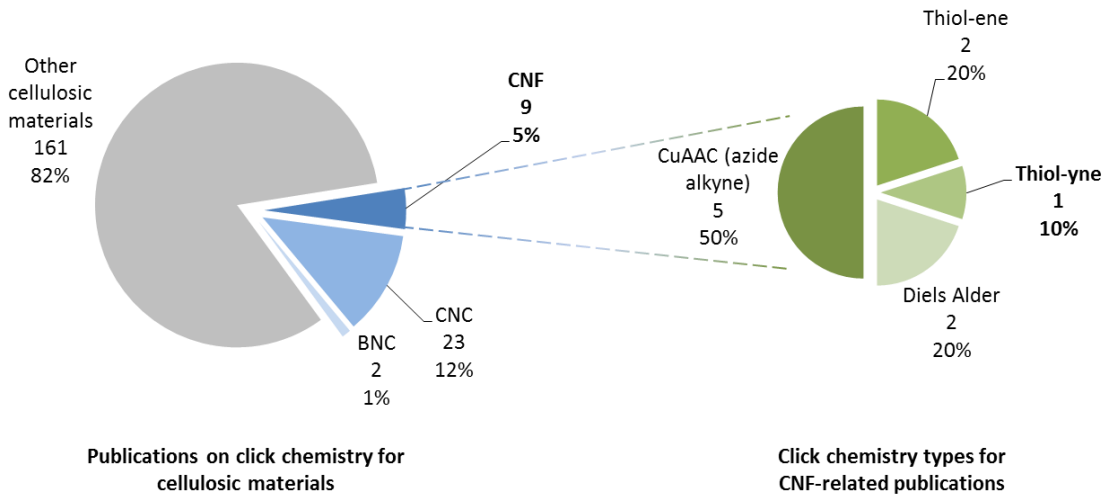

Figure I.39: Publications on click chemistry and cellulosic materials and zoom in click chemistry types and cellulose nanofibrils (Extracted from Scifinder, January 2019, "cellulose" topic result (limited with book/journal/review and English language) was refined with "click OR clicking" topic and further intersected with CNF, CNC and BNC descriptors mentioned earlier in the text in Figure I.20)

A quick overview of the three low-exploited click chemistry reactions will be presented along with a few example of these reactions conducted on cellulose and especially CNFs since they will be used in this Ph.D. project for covalent immobilization of active principle ingredients.

3.3.1. Thiol-ene

Despite considerations like odor, storage and stability, thiols have been used in many chemical reactions for more than a century. Improved methods of synthesis and development of efficient stabilizers now makes thiols good candidates for click chemistry reactions [219].

Thiol-ene chemistry can rely on two different mechanisms: thiol-Michael addition reaction [222] or radical addition reaction [223] between thiols and alkenes. Michael addition is traditionally performed under base catalysis and is extremely rapid and regioselective, proceed under bulk conditions in presence of air and water and give high yields. Radical addition also show rapid reaction rates since single thiol radical triggers hundreds to tens of thousands of chemical reaction events [222]. The radical mechanism is exposed on Figure I.40. But the reaction is usually performed under an inert atmosphere and by exposure to UV light for about 20 minutes up to several hours in presence of a photo-initiator [219].

The thiol-ene click chemistry was used to modify cellulose substrate. Thiol or alkene groups were bound to cellulose nanofibrils films through alkoxysilane chemistry and subsequent photo-chemical thiol-ene reaction was performed respectively with alkene or thiol groups-containing molecules [224].

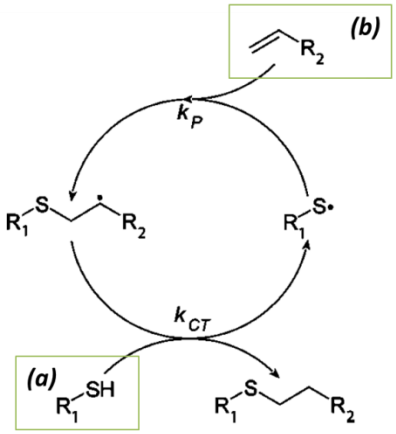

Figure I.40: Thiol-ene mechanism, the thiol group (a) reacts with the vinyl compound (b) [225]

Multicolor fluorescent labelling of cellulose nanofibrils was also achieved more recently through the thiol-Michael addition type of thiol-ene chemistry. Cellulose nanofibrils were first grafted with furan bearing compound through esterification in DMSO under thermal treatment. Diels alder reaction (described later) was used as an intermediate reaction step to graft a bis-maleimide molecule on furan modified CNF before subsequent thiol-ene click chemistry with thiol-bearing chromophore and alkene bond of maleimide [226]. This multistep grafting is a very innovative strategy of chemical surface modification of CNF but it still requires organic solvent in the first esterification. Thus, the multistep chemical surface modification of CNF suspensions in fully aqueous medium is then still a field with potential investigation.

3.3.2. Thiol-Yne

Thiol-yne reaction is a second type of thiol radical addition and complements the thiol-ene route since two thiols can be added to one alkyne function. Thiol-yne coupling thus combines in a very elegant way the building blocks of the most widely used click reaction (alkyne groups in CuACC) with the thiol-ene chemistry (same thiol addition) [218]. Moreover, the kinetic of the addition of the second thiol to the vinyl sulfide (first addition) is three times faster [227]. Thiol-yne coupling was recently re-introduced by Bowman and co-workers in 2009. Their work was inspired by almost forgotten reports on multiple radical additions of thiols to alkynes from the 1940's. The group investigated the mechanism and kinetics of thiol-yne photopolymerizations for the production of highly cross-linked polymers networks. The Figure I.41 shows the mechanism Bowman and co-workers came up with regarding the thiol-yne reaction.

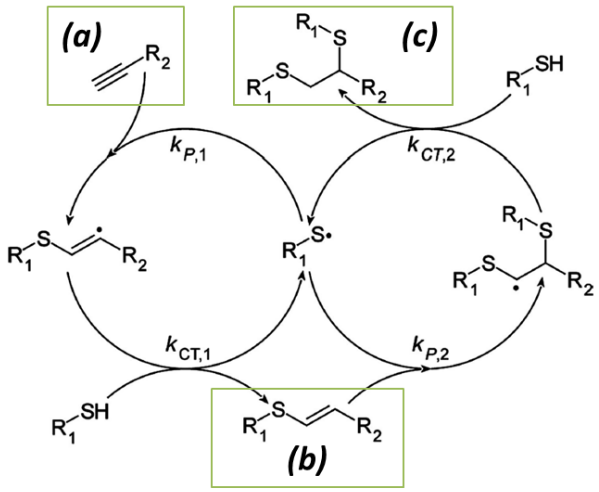

Figure I.41: Thiol-yne mechanism, each alkyne group (a) reacts first with a thiol to form the vinyl sulfide (b) which further reacts with a second thiol to yield the 1,2-disubstituted adduct (c) [225]

The thiol-yne reaction is triggered by the use of a chemical radical source or UV irradiation at ambient temperature and the presence of oxygen should be avoided. Although this last point is not really in accordance with click chemistry principles, thiol-yne coupling is still considered as a full potential strategy for the construction of tailored materials.

In July 2018, only two papers in the literature were dealing with thiol-yne chemistry related with cellulose substrates (a few other papers deal with cellulose derivatives). Researchers used thiol-ene and thiol-yne coupling procedures on cellulose paper in order to develop the covalent printing technique. Di-sulfide bridges containing compounds were first covalently immobilized on paper. Then the S-S bonds were cleaved to allow free thiol groups to react through either thiol-ene or thiol-yne click chemistry reactions with chromophoric small molecules which play the role of inks. The printed shapes were controlled by using a hidden pattern as a filter in between the sample and the light irradiation device [228]. This new substrate is supposed to find application as sensor in the field of medicine and anti-counterfeiting technique.

The only other paper on thiol-yne chemistry applied to cellulosic substrates describes the formation of dendritic-linear-dendritic (DLD) block copolymer hydrogels and their combination with cellulose nanocrystals (CNC). CNC were first functionalized with thiol groups and used as crosslinkers thanks to the thiol-yne coupling. A huge library of functional DLD block copolymers and CNC-based 3D networks were obtained and are suitable for biological applications [229].

Despite these preliminary works, thiol-yne click chemistry applied on cellulose nanofibrils seems to be an unaddressed field of research so far.

In this Ph.D. work, the use of thiol-ene and thiol-yne click chemistry will be the key steps to bind active principle ingredients to CNF.

3.3.3. Diels Alder

The Diels alder reaction has been extensively studied since its first description in 1928 by O. Diels and K. Alder in Germany. They both get the Nobel Prize in 1950 for their work on diene synthesis. The reaction involves a conjugated diene and a dienophile (alkene or alkyne) compounds. With a simple heat treatment, those compounds can undergo the [4+2]-cycloaddition that leads to the formation of new cyclic molecule: the adduct, as depicted on Figure I.42 below.

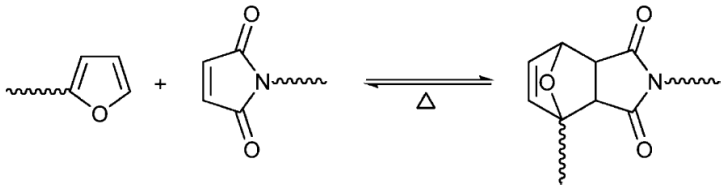

Figure I.42: The Diels–Alder equilibrium between furan and maleimide end groups [230]

The 4 π-electrons of the diene and the 2 π-electrons of the dienophile will form new σ-bonds that are energetically more stable than π-bonds. In one single step, the circular transfer of the six electrons creates two new σ-bonds. The diene must be in *s-cis* conformation in order to ensure a good overlapping of molecular orbital with the dienophile. However the *s-trans* conformation is usually more stable. This is why cyclic diene are really interesting compounds for Diels Alder reaction because the *s-cis* conformation is the only one available. The Diels-Alder reaction is thermally reversible. High temperature treatment gives back the initial diene and die nophile molecules through the so called *retro*-Diels-Alder reaction. The reaction can occur in many organic solvents and also in water.

In case of cyclic diene and dienophile (like furan and maleimide groups), *endo* and *exo* products can be obtained. Both molecules are in parallel plans but two configurations are possible as shown in Figure I.43 below.

The *endo*-product is considered as the kinetic product because favorable interaction occurs in addition to the [4+2] cycloaddition, which are not occurring in the *exo*-product formation. However, the *exo*-product is thermodynamically more stable since it avoids steric hindrance.

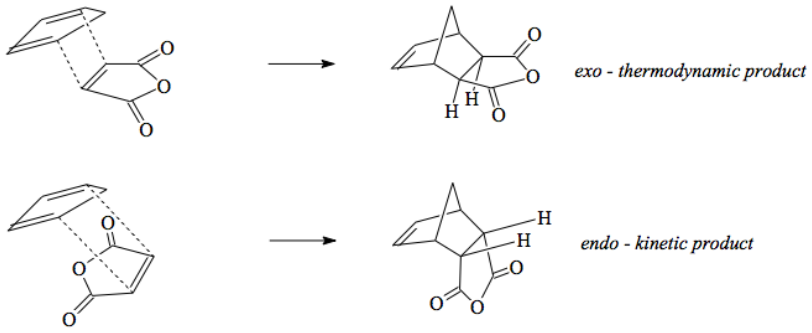

Figure I.43: The exo and endo products from Diels Alder reaction between furan and maleimide functions

Diels Alder reaction between furan and maleimide groups is of major importance. First, furan products mostly originate from furfural that is industrially extracted from vast array of agricultural and forestry wastes to several hundreds of thousand tons each year [231]. Furanic compounds are biobased products and then are in accordance with the green chemistry principles described earlier. Furan is considered as an electron-rich ring, explained by the existence of many mesomeric forms. On the contrary maleimide carbon double bond has a lower electron density due to the two carbonyl groups that are electron attractor. This configuration gives rise to a very effective Diels-Alder reaction. The frontier molecular orbital theory is the key to explain it: electron enriched diene has a highest occupied molecular orbital (HOMO) of higher energy level and deprived dienophile has a lowest unoccupied molecular orbital (LUMO) of lower energy level. The energy gap is smaller and the interaction is simpler.

Natural polymers are good platforms for the implementation of Diels Alder reactions as demonstrated by the review of A. Gandini recently very published. Vegetable oils, natural rubber and cellulose substrates are covered [232]. Many different cellulose substrates were utilized in order to perform Diels Alder reaction. Hydroxyethylcellulose was provided with pendant furan groups through esterification of furoyl chloride and acetic acid [233]. A bis-maleimide compound was then used for crosslinking through Diels-Alder reaction at 70°C. The retro-Diels-alder was also studied resulting in a material with on-demand self-healing properties and strong modulus and tensile strength.

Nanocelullose material was also appeared as a good candidate for new material designing. Partially modified gelatin was reacted with chondroitin sulfate through amidation with EDC/NHS coupling on one hand, and with maleimide functionalized cellulose nanocrystals (CNC) on the other hand. Bio-nanocomposite hydrogels with lower swelling ratios and stiffer networks (higher storage moduli) were thus obtained [234]. In the same spirit, self-healing nanocomposites hydrogels based on cellulose nanocrystals and poly(ethylene glycol) (PEG) chains were prepared [235]. Furyl-modified

CNC and maleimide functionalized PEG were covalently bind with Diels Alder reaction. Cyclic loading-unloading tests showed good self-recovery properties.

However, only a very few papers deal with Diels Alder reaction applied on CNF. The first one was published in 2015 by the group of L. Bergström from Sweden who successfully designed multicolor CNF thanks to fluorescent probes (7-mercapto-4-methylcoumarin and fluorescein diacetate 5-maleimide) that were covalently immobilized on CNF through Diels Alder reaction as shown in Figure I.44. These modified CNF brought innovative tool in biological imaging [226].

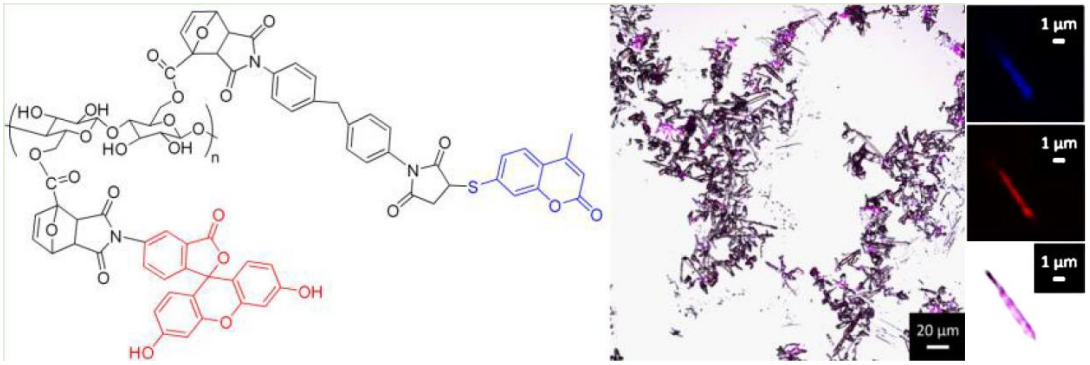

Figure I.44: Design of multicolor CNF through covalent immobilization of fluorescent probes by Diels Alder click chemistry (confocal microscopic images on the far right) [226]

The only other reported work was published in 2017 by A. Gandini et al. The researchers combined furan modified natural rubber and maleimide modified CNF in a reversible crosslinked composite system thanks to Diels Alder reaction. The successful results open the way to more easily recyclable elastomeric artefacts such as tires together with better thermal resistance [236]. These preliminary works show that there is room for endless application thanks to the versatile Diels Alder reaction and its implementation to CNF based systems.

In this Ph.D. work, novel procedure of Diels Alder reaction will be use to immobilize active principle ingredients on pre-functionalized CNF.

Conclusions to chapter I

As described in this chapter, a wide range of biobased polymers are suitable for biomedical applications. Among them collagen and cellulose deserve a particular attention. The former has excellent biological properties and perfectly mimics the extra cellular matrix medium that naturally involves collagen, the latter, especially cellulose nanofibrils, forms 2D and 3D biocompatible structures that have high potential in drug release and wound healing or tissue engineering applications. The general context of nanomaterials in medical devices appeals for health and toxicology assessment. For cellulose nanofibrils, a low or nonexistent toxicity has been proven and commonly admitted by the scientific community. However, complementary studies are still necessary for long term impacts since cellulose does not degrade in the human body and seemed persistent in pulmonary route. In order to be widely used in medical industry or any other field, nanocellulose often requires enhancement through surface modification for a better compatibility or new functionalities. A wide number of techniques are available: esterification, amidation and click chemistry strategies were introduced. Their use on CNC and mostly CNF were reviewed. Such techniques have potential to be used in water based systems with a limited use of organic solvents and energy demanding process. Green chemistry for surface modification of CNF is a promising way for the upscaling of processes associated with CNF industrialization. The growing market of nanocellulose was detailed in terms of patents and field of application and confirmed the tendency for the transition to these biobased compounds.

In line with this context and literature review, it seems very innovative to (i) functionalize the CNF surface with drugs through water based green chemistry approaches and (ii) use such material in combination with collagen for the design of new medical devices for topical or internal applications. These are the main objective of this Ph.D. project, as described on **Erreur ! Source du renvoi introuvable.**. The next chapter discusses the surface modification techniques applied to CNF with covalent drug immobilization purposes. Such modified CNF will be embedded in prototype medical devices, part of them involving collagen, and their release capacities will be evaluated as well as their antimicrobial activity, as detailed in the chapter III.

List of tables

List of figures

Bibliography

[1] R. P. Babu, K. O'connor, and R. Seeram, "Current progress on bio-based polymers and their future trends," *Progress in Biomaterials*, vol. 2, no. 1, p. 8, 2013.

[2] "European Bioplastics, Bioplastics market data." 2017.

[3] "Lead Market Initiative – speed up time-to-market of innovations and pilot new innovation policy in Europe - Growth - European Commission," *Growth*. [Online]. Available: /growth/content/lead-market-initiative-%E2%80%93-speed-time-market-innovations-and-pilot-new-innovation-policy-0_en. [Accessed: 07-Aug-2018].

[4] "BioPreferred|Site Map." [Online]. Available: https://www.biopreferred.gov/BioPreferred/faces/pages/AboutBioPreferred.xhtml. [Accessed: 07-Aug-2018].

[5] L. Avérous and E. Pollet, "Biodegradable Polymers," in *Environmental Silicate Nano-Biocomposites*, Springer, London, 2012, pp. 13–39.

[6] R. L. Reis, N. M. Neves, J. F. Mano, M. E. Gomes, A. P. Marques, and H. S. Azevedo, *Natural-Based Polymers for Biomedical Applications*. Elsevier, 2008.

[7] L. Bedian, A. M. Villalba-Rodríguez, G. Hernández-Vargas, R. Parra-Saldivar, and H. M. N. Iqbal, "Bio-based materials with novel characteristics for tissue engineering applications – A review," *International Journal of Biological Macromolecules*, vol. 98, pp. 837–846, May 2017.

[8] A. A. Hıncal and H. S. Kaş, *Biomedical Science and Technology: Recent Developments in the Pharmaceutical and Medical Sciences*. Boston, MA: Springer US, 1998.

[9] J. D. Enderle and J. D. Bronzino, *Introduction to Biomedical Engineering*. Academic Press, 2012.

[10] H. Pun, "Terminology for biorelated polymers and applications (IUPAC Recommendations 2012."

[11] R. Lanza, R. Langer, and J. Vacanti, *Principles of Tissue Engineering Ed. 4*. Elsevier Science, 2013.

[12] C. Murphy, D. Little, and A. Schindeler, "Cell-scaffold interactions in the bone tissue engineering triad," *European Cells and Materials*, vol. 26, pp. 120–132, Sep. 2013.

[13] M. A. Rice, B. T. Dodson, J. A. Arthur, and K. S. Anseth, "Cell-based Therapies and Tissue Engineering," *Otolaryngologic Clinics of North America*, vol. 38, no. 2, pp. 199–214, Apr. 2005.

[14] P. X. Ma, "Biomimetic materials for tissue engineering," *Advanced Drug Delivery Reviews*, vol. 60, no. 2, pp. 184–198, Jan. 2008.

[15] E. Pişkin, "Polymer based drug delivery systems," in *Biomedical Science and Technology: Recent Developments in the Pharmaceutical and Medical Sciences*, A. A. Hıncal and H. S. Kaş, Eds. 1998.

[16] D. F. Williams, "On the nature of biomaterials," *Biomaterials*, vol. 30, no. 30, pp. 5897–5909, Oct. 2009.

[17] M. Smyth, "Nanocellulose based materials for Cell Culture," phdthesis, Université Grenoble Alpes, 2017.

[18] B. J. Love, *Biomaterials : A Systems Approach to Engineering Concepts*. Elsevier Science, 2017.

[19] T. Srichana and A. J. Domb, "Polymeric Biomaterials," in *Biomedical Materials*, Springer, Boston, MA, 2009, pp. 83–119.

[20] A. P. C. Almeida, J. P. Canejo, S. N. Fernandes, C. Echeverria, P. L. Almeida, and M. H. Godinho, "Cellulose-Based Biomimetics and Their Applications," *Advanced Materials*, vol. 30, no. 19, p. 1703655, May 2018.

[21] T. T. Teeri, H. Brumer, G. Daniel, and P. Gatenholm, "Biomimetic engineering of cellulose-based materials," *Trends in Biotechnology*, vol. 25, no. 7, pp. 299–306, Jul. 2007.

[22] K. Hamad, M. Kaseem, H. W. Yang, F. Deri, and Y. G. Ko, "Properties and medical applications of polylactic acid: A review," *Express Polymer Letters*, vol. 9, no. 5, pp. 435–455, 2015.

[23] L.-T. Lim, R. Auras, and M. Rubino, "Processing technologies for poly(lactic acid)," *Progress in Polymer Science*, vol. 33, no. 8, pp. 820–852, Aug. 2008.

[24] D. da Silva *et al.*, "Biocompatibility, biodegradation and excretion of polylactic acid (PLA) in medical implants and theranostic systems," *Chemical Engineering Journal*, vol. 340, pp. 9–14, May 2018.

[25] B. Tyler, D. Gullotti, A. Mangraviti, T. Utsuki, and H. Brem, “Polylactic acid (PLA) controlled delivery carriers for biomedical applications,” *Advanced Drug Delivery Reviews*, vol. 107, pp. 163–175, Dec. 2016.
[26] Z. Li, J. Yang, and X. J. Loh, “Polyhydroxyalkanoates: opening doors for a sustainable future,” *NPG Asia Materials*, vol. 8, no. 4, pp. e265–e265, Apr. 2016.
[27] P. Jambunathan and K. Zhang, “Engineered biosynthesis of biodegradable polymers,” *J Ind Microbiol Biotechnol*, vol. 43, no. 8, pp. 1037–1058, Aug. 2016.
[28] J. Xu and B.-H. Guo, “Poly(butylene succinate) and its copolymers: Research, development and industrialization,” *Biotechnology Journal*, vol. 5, no. 11, pp. 1149–1163, Nov. 2010.
[29] M. Gigli, M. Fabbri, N. Lotti, R. Gamberini, B. Rimini, and A. Munari, “Poly(butylene succinate)-based polyesters for biomedical applications: A review,” *European Polymer Journal*, vol. 75, pp. 431–460, Feb. 2016.
[30] J. F. Kennedy, C. J. Knill, L. Liu, and P. S. Panesar, “Chapter 5. Starch and its Derived Products: Biotechnological and Biomedical Applications,” in *Polymer Chemistry Series*, P. A. Williams, Ed. Cambridge: Royal Society of Chemistry, 2011, pp. 130–165.
[31] A. J. Salgado, O. P. Coutinho, R. L. Reis, and J. E. Davies, “In vivo response to starch-based scaffolds designed for bone tissue engineering applications,” *Journal of Biomedical Materials Research Part A*, vol. 80A, no. 4, pp. 983–989, Mar. 2007.
[32] C. S. Pereira, A. M. Cunha, R. L. Reis, B. VÁzquez, and J. S. RomÁn, “New starch-based thermoplastic hydrogels for use as bone cements or drug-delivery carriers,” *Journal of Materials Science: Materials in Medicine*, vol. 9, no. 12, pp. 825–833, Dec. 1998.
[33] M. E. Gomes, J. S. Godinho, D. Tchalamov, A. M. Cunha, and R. L. Reis, “Alternative tissue engineering scaffolds based on starch: processing methodologies, morphology, degradation and mechanical properties,” *Materials Science and Engineering: C*, vol. 20, no. 1, pp. 19–26, May 2002.
[34] K. Y. Lee and D. J. Mooney, “Alginate: Properties and biomedical applications,” *Progress in Polymer Science*, vol. 37, no. 1, pp. 106–126, Jan. 2012.
[35] K. G. Mandel, B. P. Daggy, D. A. Brodie, and H. I. Jacoby, “Review article: alginate-raft formulations in the treatment of heartburn and acid reflux.,” *Aliment Pharmacol Ther*, vol. 14, no. 6, pp. 669–690, Jun. 2000.
[36] S. M. Selimoglu and M. Elibol, “Alginate as an immobilization material for MAb production via encapsulated hybridoma cells,” *Critical Reviews in Biotechnology*, vol. 30, no. 2, pp. 145–159, Jun. 2010.
[37] J. D. Lalau *et al.*, “Efficacy and tolerance of calcium alginate versus vaseline gauze dressings in the treatment of diabetic foot lesions,” */data/revues/12623636/00280003/223/*, Feb. 2008.
[38] O. Smidsrød and G. Skja˚k-Br1k, “Alginate as immobilization matrix for cells,” *Trends in Biotechnology*, vol. 8, pp. 71–78, Jan. 1990.
[39] R. Jayakumar, M. Prabaharan, P. T. Sudheesh Kumar, S. V. Nair, and H. Tamura, “Biomaterials based on chitin and chitosan in wound dressing applications,” *Biotechnology Advances*, vol. 29, no. 3, pp. 322–337, May 2011.
[40] J. Xie *et al.*, “Osteogenic differentiation and bone regeneration of iPSC-MSCs supported by a biomimetic nanofibrous scaffold,” *Acta Biomaterialia*, vol. 29, pp. 365–379, Jan. 2016.
[41] Y. Zhang, Q.-S. Wang, K. Yan, Y. Qi, G.-F. Wang, and Y.-L. Cui, “Preparation, characterization, and evaluation of genipin crosslinked chitosan/gelatin three-dimensional scaffolds for liver tissue engineering applications,” *Journal of Biomedical Materials Research Part A*, vol. 104, no. 8, pp. 1863–1870, Aug. 2016.
[42] M. D. Shoulders and R. T. Raines, “Collagen Structure and Stability,” *Annual Review of Biochemistry*, vol. 78, no. 1, pp. 929–958, Jun. 2009.
[43] K. E. Kadler, C. Baldock, J. Bella, and R. P. Boot-Handford, “Collagens at a glance,” *Journal of Cell Science*, vol. 120, no. 12, pp. 1955–1958, May 2007.
[44] P. Fratzl, “Cellulose and collagen: from fibres to tissues,” *Current Opinion in Colloid & Interface Science*, vol. 8, no. 1, pp. 32–39, Mar. 2003.

[45] J. Brinckmann, "Collagens at a glance," in *Collagen*, Springer, 2005, pp. 1–6.
[46] S. Ricard-Blum, F. Ruggiero, and M. van der Rest, "The Collagen Superfamily," in *Collagen*, Springer, Berlin, Heidelberg, pp. 35–84.
[47] J. Engel and H. P. Bächinger, "Structure, Stability and Folding of the Collagen Triple Helix," in *Collagen*, Springer, Berlin, Heidelberg, pp. 7–33.
[48] J. Bella, "Collagen structure: new tricks from a very old dog," *Biochemical Journal*, vol. 473, no. 8, pp. 1001–1025, Apr. 2016.
[49] D. E. Birk and P. Bruckner, "Collagen Suprastructures," in *Collagen*, Springer, Berlin, Heidelberg, pp. 185–205.
[50] A. Abe, Ed., *Polymer composites, polyolefin fractionation, polymeric peptidomimetics, collagens*. Heidelberg: Springer, 2013.
[51] Z. Yu, B. An, J. A. M. Ramshaw, and B. Brodsky, "Bacterial collagen-like proteins that form triple-helical structures," *Journal of Structural Biology*, vol. 186, no. 3, pp. 451–461, Jun. 2014.
[52] M. I. A. Rodríguez, L. G. R. Barroso, and M. L. Sánchez, "Collagen: A review on its sources and potential cosmetic applications," *Journal of Cosmetic Dermatology*, vol. 17, no. 1, pp. 20–26, 2017.
[53] K. Silvipriya, K. Kumar, A. Bhat, B. Kumar, A. John, and P. Lakshmanan, "Collagen: Animal Sources and Biomedical Application," *Journal of Applied Pharmaceutical Science*, pp. 123–127, 2015.
[54] E. Mocan, O. Tagadiuc, and V. Nacu, "Aspects of Collagen Isolation Procedure," p. 3.
[55] P. Montero and M. C. Gómez-Guillén, "Extracting Conditions for Megrim (Lepidorhombus boscii) Skin Collagen Affect Functional Properties of the Resulting Gelatin," *Journal of Food Science*, vol. 65, no. 3, pp. 434–438, 2000.
[56] "Structure and rheology of gelatin and collagen gels - IOS Press." [Online]. Available: https://content.iospress.com/articles/biorheology/bir30-3-4-05. [Accessed: 30-Jul-2018].
[57] M. C. Gómez-Guillén, B. Giménez, M. E. López-Caballero, and M. P. Montero, "Functional and bioactive properties of collagen and gelatin from alternative sources: A review," *Food Hydrocolloids*, vol. 25, no. 8, pp. 1813–1827, Dec. 2011.
[58] "Global Tissue Engineered Collagen Biomaterials Market: Rising Use of Collagen in Wound Healing Stokes Demand, finds TMR." [Online]. Available: https://www.transparencymarketresearch.com/pressrelease/tissue-engineered-collagen-biomaterials-market.htm. [Accessed: 30-Jul-2018].
[59] A. Sionkowska, S. Skrzyński, K. Śmiechowski, and A. Kołodziejczak, "The review of versatile application of collagen," *Polymers for Advanced Technologies*, vol. 28, no. 1, pp. 4–9, 2016.
[60] "Global Collagen Market Size By Source | Industry Analysis Report, 2025." [Online]. Available: https://www.grandviewresearch.com/industry-analysis/collagen-market. [Accessed: 30-Jul-2018].
[61] E. A. Sander and V. H. Barocas, "Biomimetic Collagen Tissues: Collagenous Tissue Engineering and Other Applications," in *Collagen*, Springer, Boston, MA, 2008, pp. 475–504.
[62] G. S. Offeddu, J. C. Ashworth, R. E. Cameron, and M. L. Oyen, "Multi-scale mechanical response of freeze-dried collagen scaffolds for tissue engineering applications," *Journal of the Mechanical Behavior of Biomedical Materials*, vol. 42, pp. 19–25, Feb. 2015.
[63] C. Dong and Y. Lv, "Application of Collagen Scaffold in Tissue Engineering: Recent Advances and New Perspectives," *Polymers*, vol. 8, no. 2, p. 42, Feb. 2016.
[64] Y. Bayon, P. Gravagna, and J.-L. Tayot, "Method for preparing two-layer bicomposite collagen material for preventing post-operative adhesions," US6596304B1, 22-Jul-2003.
[65] Y. Bayon, P. Gravagna, and A. Meneghin, "Biosynthetic Implant for Soft Tissue Repair," WO2009156866 (A2), 30-Dec-2009.
[66] A. Gandini and M. N. Belgacem, "Chapter 1 - The State of the Art," in *Monomers, Polymers and Composites from Renewable Resources*, M. N. Belgacem and A. Gandini, Eds. Amsterdam: Elsevier, 2008, pp. 1–16.
[67] A. C. O'sullivan, "Cellulose: the structure slowly unravels," *Cellulose*, vol. 4, no. 3, pp. 173–207, Jun. 1997.

[68] D. N.-S. Hon, "Cellulose: a random walk along its historical path," *Cellulose*, vol. 1, no. 1, pp. 1–25, 1994.
[69] W. N. Haworth, E. L. Hirst, and H. A. Thomas, "The Existence of the Cellobiose Residue in Cellulose," *Nature*, vol. 126, no. 3177, p. 438, Sep. 1930.
[70] H. Kang, R. Liu, and Y. Huang, "Cellulose derivatives and graft copolymers as blocks for functional materials," *Polym. Int*, vol. 62, no. 3, pp. 338–344, Mar. 2013.
[71] M. Jorfi and E. J. Foster, "Recent advances in nanocellulose for biomedical applications," *J. Appl. Polym. Sci.*, vol. 132, no. 14, p. n/a-n/a, Apr. 2015.
[72] N. A. Hoenich, "Cellulose for Medical Applications: Past, Present, and Future," *BioResources*, vol. 1, no. 2, pp. 270–280, Aug. 2007.
[73] T. Shibata, "Chapter 3:Cellulose and Its Derivatives in Medical Use," in *Renewable Resources for Functional Polymers and Biomaterials*, 2011, pp. 48–87.
[74] R. Ek, G. Alderborn, and C. Nyström, "Particle analysis of microcrystalline cellulose: Differentiation between individual particles and their agglomerates," *International Journal of Pharmaceutics*, vol. 111, no. 1, pp. 43–50, Oct. 1994.
[75] S. Dumitriu, *Polysaccharides in Medicinal Applications*. CRC Press, 1996.
[76] E. Sjostrom, *Wood Chemistry: Fundamentals and Applications*. Elsevier, 2013.
[77] S. Kamel, N. Ali, K. Jahangir, S. M. Shah, and A. A. El-Gendy, "Pharmaceutical significance of cellulose: A review," *Express Polymer Letters*, vol. 2, no. 11, pp. 758–778, 2008.
[78] J. Siepmann, H. Kranz, R. Bodmeier, and N. A. Peppas, "HPMC-Matrices for Controlled Drug Delivery: A New Model Combining Diffusion, Swelling, and Dissolution Mechanisms and Predicting the Release Kinetics," *Pharm Res*, vol. 16, no. 11, pp. 1748–1756, Nov. 1999.
[79] P. Colombo, R. Bettini, and N. A. Peppas, "Observation of swelling process and diffusion front position during swelling in hydroxypropyl methyl cellulose (HPMC) matrices containing a soluble drug," *Journal of Controlled Release*, vol. 61, no. 1, pp. 83–91, Aug. 1999.
[80] J. Siepmann and N. A. Peppas, "Modeling of drug release from delivery systems based on hydroxypropyl methylcellulose (HPMC)," *Advanced Drug Delivery Reviews*, p. 19, 2001.
[81] S.-Y. Lin and Y. Kawashima, "Drug Release from Tablets Containing Cellulose Acetate Phthalate As an Additive or Enteric-Coating Material," *Pharm Res*, vol. 4, no. 1, pp. 70–74, Feb. 1987.
[82] C. Chang and L. Zhang, "Cellulose-based hydrogels: Present status and application prospects," *Carbohydrate Polymers*, vol. 84, no. 1, pp. 40–53, Feb. 2011.
[83] X. Bourges, P. Weiss, G. Daculsi, and G. Legeay, "Synthesis and general properties of silated-hydroxypropyl methylcellulose in prospect of biomedical use," *Advances in Colloid and Interface Science*, vol. 99, no. 3, pp. 215–228, Dec. 2002.
[84] C. Demitri *et al.*, "Novel superabsorbent cellulose-based hydrogels crosslinked with citric acid," *Journal of Applied Polymer Science*, vol. 110, no. 4, pp. 2453–2460, Nov. 2008.
[85] R. A. Wach, H. Mitomo, F. Yoshii, and T. Kume, "Hydrogel of biodegradable cellulose de rivatives. II. Effect of some factors on radiation-induced crosslinking of CMC," *Journal of Applied Polymer Science*, vol. 81, no. 12, pp. 3030–3037, Sep. 2001.
[86] H. M. Nizam El-Din, S. G. Abd Alla, and A. W. M. El-Naggar, "Swelling and drug release properties of acrylamide/carboxymethyl cellulose networks formed by gamma irradiation," *Radiation Physics and Chemistry*, vol. 79, no. 6, pp. 725–730, Jun. 2010.
[87] T. Abitbol *et al.*, "Nanocellulose, a tiny fiber with huge applications," *Current Opinion in Biotechnology*, vol. 39, pp. 76–88, Jun. 2016.
[88] H. Kargarzadeh *et al.*, "Advances in cellulose nanomaterials," *Cellulose*, vol. 25, no. 4, pp. 2151–2189, Feb. 2018.
[89] O. Nechyporchuk, M. N. Belgacem, and J. Bras, "Production of cellulose nanofibrils: A review of recent advances," *Industrial Crops and Products*, Apr. 2016.
[90] J. Pérez, J. Muñoz-Dorado, T. de la Rubia, and J. Martínez, "Biodegradation and biological treatments of cellulose, hemicellulose and lignin: an overview," *International Microbiology*, vol. 5, no. 2, pp. 53–63, Jun. 2002.

[91] B. G. Rånby and E. Ribi, "Über den Feinbau der Zellulose," *Experientia*, vol. 6, no. 1, pp. 12–14, Jan. 1950.
[92] B. G. Rånby, "Fibrous macromolecular systems. Cellulose and muscle. The colloidal properties of cellulose micelles," *Discuss. Faraday Soc.*, vol. 11, no. 0, pp. 158–164, 1951.
[93] R. F. Nickerson and J. A. Habrle, "Cellulose Intercrystalline Structure," *Industrial & Engineering Chemistry*, vol. 39, no. 11, pp. 1507–1512, Nov. 1947.
[94] M. M. de S. Lima and R. Borsali, "Rodlike Cellulose Microcrystals: Structure, Properties, and Applications," *Macromolecular Rapid Communications*, vol. 25, no. 7, pp. 771–787.
[95] A. Dufresne, *Nanocellulose, From Nature to High Performance Tailored Materials*. Berlin, Boston: De Gruyter, 2017.
[96] "ISO/TS 20477:2017 - Nanotechnologies -- Standard terms and their definition for cellulose nanomaterial." [Online]. Available: https://www.iso.org/standard/68153.html. [Accessed: 09-Oct-2018].
[97] F. W. Herrick, R. L. Casebier, J. K. Hamilton, and K. R. Sandberg, "Microfibrillated cellulose: morphology and accessibility," *J. Appl. Polym. Sci.: Appl. Polym. Symp.; (United States)*, vol. 37, Jan. 1982.
[98] A. F. Turbak, F. W. Snyder, and K. R. Sandberg, "Microfibrillated cellulose, a new cellulose product: properties, uses, and commercial potential," *J. Appl. Polym. Sci.: Appl. Polym. Symp.; (United States)*, vol. 37, Jan. 1982.
[99] K. L. Spence, R. A. Venditti, O. J. Rojas, Y. Habibi, and J. J. Pawlak, "A comparative study of energy consumption and physical properties of microfibrillated cellulose produced by different processing methods," *Cellulose*, vol. 18, no. 4, pp. 1097–1111, Aug. 2011.
[100] A. Tejado, M. N. Alam, M. Antal, H. Yang, and T. G. M. van de Ven, "Energy requirements for the disintegration of cellulose fibers into cellulose nanofibers," *Cellulose*, vol. 19, no. 3, pp. 831–842, Jun. 2012.
[101] M. Pääkkö *et al.*, "Enzymatic Hydrolysis Combined with Mechanical Shearing and High-Pressure Homogenization for Nanoscale Cellulose Fibrils and Strong Gels," *Biomacromolecules*, vol. 8, no. 6, pp. 1934–1941, Jun. 2007.
[102] T. Saito, Y. Nishiyama, J.-L. Putaux, M. Vignon, and A. Isogai, "Homogeneous Suspensions of Individualized Microfibrils from TEMPO-Catalyzed Oxidation of Native Cellulose," *Biomacromolecules*, vol. 7, no. 6, pp. 1687–1691, Jun. 2006.
[103] I. Besbes, S. Alila, and S. Boufi, "Nanofibrillated cellulose from TEMPO-oxidized eucalyptus fibres: Effect of the carboxyl content," *Carbohydrate Polymers*, vol. 84, no. 3, pp. 975–983, Mar. 2011.
[104] C. Aulin, E. Johansson, L. Wågberg, and T. Lindström, "Self-Organized Films from Cellulose I Nanofibrils Using the Layer-by-Layer Technique," *Biomacromolecules*, vol. 11, no. 4, pp. 872–882, Apr. 2010.
[105] F. Rol, M. N. Belgacem, A. Gandini, and J. Bras, "Recent advances in surface-modified cellulose nanofibrils," *Progress in Polymer Science*, Sep. 2018.
[106] M. Henriksson, G. Henriksson, L. A. Berglund, and T. Lindström, "An environmentally friendly method for enzyme-assisted preparation of microfibrillated cellulose (MFC) nanofibers," *European Polymer Journal*, vol. 43, no. 8, pp. 3434–3441, Aug. 2007.
[107] O. Nechyporchuk, F. Pignon, and M. N. Belgacem, "Morphological properties of nanofibrillated cellulose produced using wet grinding as an ultimate fibrillation process," *J Mater Sci*, vol. 50, no. 2, pp. 531–541, Jan. 2015.
[108] L. R. Lynd, P. J. Weimer, W. H. van Zyl, and I. S. Pretorius, "Microbial Cellulose Utilization: Fundamentals and Biotechnology," *Microbiol. Mol. Biol. Rev.*, vol. 66, no. 3, pp. 506–577, Jan. 2002.
[109] N. J. Davis and S. L. Flitsch, "Selective oxidation of monosaccharide derivatives to uronic acids," *Tetrahedron Letters*, vol. 34, no. 7, pp. 1181–1184, Feb. 1993.
[110] A. Isogai, T. Saito, and H. Fukuzumi, "TEMPO-oxidized cellulose nanofibers," *Nanoscale*, vol. 3, no. 1, pp. 71–85, 2011.

[111] T. Saito *et al.*, "Individualization of Nano-Sized Plant Cellulose Fibrils by Direct Surface Carboxylation Using TEMPO Catalyst under Neutral Conditions," *Biomacromolecules*, vol. 10, no. 7, pp. 1992–1996, Jul. 2009.
[112] T. R. Garrett, M. Bhakoo, and Z. Zhang, "Bacterial adhesion and biofilms on surfaces," *Progress in Natural Science*, vol. 18, no. 9, pp. 1049–1056, Sep. 2008.
[113] D. Klemm *et al.*, "Nanocelluloses: A New Family of Nature-Based Materials," *Angew. Chem. Int. Ed.*, vol. 50, no. 24, pp. 5438–5466, Jun. 2011.
[114] S. Mohanty, S. K. Nayak, B. S. Kaith, and S. Kalia, *Polymer Nanocomposites based on Inorganic and Organic Nanomaterials*. John Wiley & Sons, 2015.
[115] D. Mamlouk and M. Gullo, "Acetic Acid Bacteria: Physiology and Carbon Sources Oxidation," *Indian J Microbiol*, vol. 53, no. 4, pp. 377–384, Dec. 2013.
[116] "Invention controls weavers of nanoscale biomaterials." [Online]. Available: https://vtnews.vt.edu/content/vtnews_vt_edu/en/articles/2008/11/2008-693.html. [Accessed: 30-Jan-2018].
[117] G. Helenius, H. Bäckdahl, A. Bodin, U. Nannmark, P. Gatenholm, and B. Risberg, "In vivo biocompatibility of bacterial cellulose," *J. Biomed. Mater. Res.*, vol. 76A, no. 2, pp. 431–438, Feb. 2006.
[118] N. Petersen and P. Gatenholm, "Bacterial cellulose-based materials and medical devices: current state and perspectives," *Applied Microbiology and Biotechnology*, vol. 91, no. 5, pp. 1277–1286, Sep. 2011.
[119] J. M. Rajwade, K. M. Paknikar, and J. V. Kumbhar, "Applications of bacterial cellulose and its composites in biomedicine," *Applied Microbiology and Biotechnology*, vol. 99, no. 6, pp. 2491–2511, Mar. 2015.
[120] R. J. Moon and E. J. Foster, "Current characterization methods for cellulose nanomaterials," 2018.
[121] Kangas, "Characterization of fibrillated celluloses. A short review and evaluation of characteristics with a combination of methods," *Nordic Pulp and Paper Research Journal*, vol. 29, no. 01, pp. 129–143, Mar. 2014.
[122] J. Desmaisons, E. Boutonnet, M. Rueff, A. Dufresne, and J. Bras, "A new quality index for benchmarking of different cellulose nanofibrils," *Carbohydrate Polymers*, vol. 174, pp. 318–329, Oct. 2017.
[123] Future Markets, Inc, "The Global Market for Nanocellulose 2017-2027." Jun-2017.
[124] M. Märtson, J. Viljanto, T. Hurme, P. Laippala, and P. Saukko, "Is cellulose sponge degradable or stable as implantation material? An in vivo subcutaneous study in the rat," *Biomaterials*, vol. 20, no. 21, pp. 1989–1995, Nov. 1999.
[125] M. Märtson, J. Viljanto, T. Hurme, and P. Saukko, "Biocompatibility of Cellulose Sponge with Bone," *ESR*, vol. 30, no. 6, pp. 426–432, 1998.
[126] M. Märtson, J. Viljanto, P. Laippala, and P. Saukko, "Connective Tissue Formation in Subcutaneous Cellulose Sponge Implants in the Rat," *ESR*, vol. 30, no. 6, pp. 419–425, 1998.
[127] T. Miyamoto, S. Takahashi, H. Ito, H. Inagaki, and Y. Noishiki, "Tissue biocompatibility of cellulose and its derivatives," *Journal of Biomedical Materials Research*, vol. 23, no. 1, pp. 125–133, 1989.
[128] S. K. Bowry and T. H. Rintelen, "Synthetically modified cellulose (SMC): a cellulosic hemodialysis membrane with minimized complement activation.," *ASAIO J*, vol. 44, no. 5, pp. M579-83, 1998.
[129] N. Lin and A. Dufresne, "Nanocellulose in biomedicine: Current status and future prospect," *European Polymer Journal*, vol. 59, pp. 302–325, Oct. 2014.
[130] T. Kovacs *et al.*, "An ecotoxicological characterization of nanocrystalline cellulose (NCC)," *Nanotoxicology*, vol. 4, no. 3, pp. 255–270, Sep. 2010.
[131] M. J. D. Clift *et al.*, "Investigating the Interaction of Cellulose Nanofibers Derived from Cotton with a Sophisticated 3D Human Lung Cell Coculture," 06-Sep-2011. [Online]. Available: http://pubs.acs.org/doi/abs/10.1021/bm200865j. [Accessed: 02-Aug-2018].

[132] H. Norppa, "Nanofibrillated cellulose: results of in vitro and in vivo toxicological assays," p. 29, 2012.
[133] J. Vartiainen *et al.*, "Health and environmental safety aspects of friction grinding and spray drying of microfibrillated cellulose," *Cellulose*, vol. 18, no. 3, pp. 775–786, Jun. 2011.
[134] K. J. Ong, J. A. Shatkin, K. Nelson, J. D. Ede, and T. Retsina, "Establishing the safety of novel bio-based cellulose nanomaterials for commercialization," *NanoImpact*, vol. 6, pp. 19–29, Apr. 2017.
[135] K.-S. Hannukainen, S. Suhonen, K. Savolainen, and H. Norppa, "Genotoxicity of nanofibrillated cellulose in vitro as measured by enzyme comet assay," *Toxicology Letters*, vol. Supplement, no. 211, p. S71, 2012.
[136] L. Alexandrescu, K. Syverud, A. Gatti, and G. Chinga-Carrasco, "Cytotoxicity tests of cellulose nanofibril-based structures," *Cellulose*, vol. 20, no. 4, pp. 1765–1775, Aug. 2013.
[137] K. Hua *et al.*, "Translational study between structure and biological response of nanocellulose from wood and green algae," *RSC Advances*, vol. 4, no. 6, pp. 2892–2903, 2014.
[138] C. Endes *et al.*, "A critical review of the current knowledge regarding the biological impact of nanocellulose," *Journal of Nanobiotechnology*, vol. 14, no. 1, p. 78, Dec. 2016.
[139] Kangas, "Environmental, Health & Safety (EHS) aspects of cellulose nanomaterials (CN) and CN-based products," *Nordic Pulp and Paper Research Journal*, vol. 31, no. 02, pp. 179–190, Jun. 2016.
[140] M. Pitkanën *et al.*, "Nanofibrillar cellulose – Assessment of cytotoxic and genotoxic properties in vitro," presented at the Tappi International conference on nanotechnology for the forest products industry, Espoo, Finland, 2010.
[141] P. Kollar *et al.*, "Cytotoxicity and effects on inflammatory response of modified types of cellulose in macrophage-like THP-1 cells," *International Immunopharmacology*, vol. 11, no. 8, pp. 997–1001, Aug. 2011.
[142] M. Pitkänen *et al.*, "Characteristics and safety of nano-sized cellulose fibrils," *Cellulose*, vol. 21, no. 6, pp. 3871–3886, Dec. 2014.
[143] A. B. Stefaniak, M. S. Seehra, N. R. Fix, and S. S. Leonard, "Lung biodurability and free radical production of cellulose nanomaterials," *Inhalation Toxicology*, vol. 26, no. 12, pp. 733–749, Oct. 2014.
[144] M. Čolić, D. Mihajlović, A. Mathew, N. Naseri, and V. Kokol, "Cytocompatibility and immunomodulatory properties of wood based nanofibrillated cellulose," *Cellulose*, vol. 22, no. 1, pp. 763–778, Feb. 2015.
[145] K. Hua, E. Ålander, T. Lindström, A. Mihranyan, M. Strømme, and N. Ferraz, "Surface Chemistry of Nanocellulose Fibers Directs Monocyte/Macrophage Response," *Biomacromolecules*, vol. 16, no. 9, pp. 2787–2795, Sep. 2015.
[146] M. Vikman, J. Vartiainen, I. Tsitko, and P. Korhonen, "Biodegradability and Compostability of Nanofibrillar Cellulose-Based Products," *J Polym Environ*, vol. 23, no. 2, pp. 206–215, Jun. 2015.
[147] K. Hua, M. Strømme, A. Mihranyan, and N. Ferraz, "Nanocellulose from green algae modulates the in vitro inflammatory response of monocytes/macrophages," *Cellulose*, vol. 22, no. 6, pp. 3673–3688, Dec. 2015.
[148] H. R. Nordli, G. Chinga-Carrasco, A. M. Rokstad, and B. Pukstad, "Producing ultrapure wood cellulose nanofibrils and evaluating the cytotoxicity using human skin cells," *Carbohydrate Polymers*, vol. 150, pp. 65–73, Oct. 2016.
[149] B. J. Harper *et al.*, "Impacts of chemical modification on the toxicity of diverse nanocellulose materials to developing zebrafish," *Cellulose*, vol. 23, no. 3, pp. 1763–1775, Jun. 2016.
[150] S. Tomić, V. Kokol, D. Mihajlović, A. Mirčić, and M. Čolić, "Native cellulose nanofibrills induce immune tolerance *in vitro* by acting on dendritic cells," *Scientific Reports*, vol. 6, p. 31618, Aug. 2016.
[151] J. Catalán *et al.*, "Genotoxic and inflammatory effects of nanofibrillated cellulose in murine lungs," *Mutagenesis*, vol. 32, no. 1, pp. 23–31, Jan. 2017.

[152] A. L. Menas *et al.*, "Fibrillar vs crystalline nanocellulose pulmonary epithelial cell responses: Cytotoxicity or inflammation?," *Chemosphere*, vol. 171, pp. 671–680, Mar. 2017.
[153] V. R. Lopes, C. Sanchez-Martinez, M. Strømme, and N. Ferraz, "In vitro biological responses to nanofibrillated cellulose by human dermal, lung and immune cells: surface chemistry aspect," *Particle and Fibre Toxicology*, vol. 14, no. 1, p. 1, Jan. 2017.
[154] A. Rashad, K. Mustafa, E. B. Heggset, and K. Syverud, "Cytocompatibility of Wood-Derived Cellulose Nanofibril Hydrogels with Different Surface Chemistry," *Biomacromolecules*, vol. 18, no. 4, pp. 1238–1248, Apr. 2017.
[155] J. Liu, M. Bacher, T. Rosenau, S. Willför, and A. Mihranyan, "Potentially Immunogenic Contaminants in Wood-Based and Bacterial Nanocellulose: Assessment of Endotoxin and (1,3)-β-d-Glucan Levels," *Biomacromolecules*, vol. 19, no. 1, pp. 150–157, Jan. 2018.
[156] C. Ventura, A. F. Lourenço, A. Sousa-Uva, P. J. T. Ferreira, and M. J. Silva, "Evaluating the genotoxicity of cellulose nanofibrils in a co-culture of human lung epithelial cells and monocyte-derived macrophages," *Toxicology Letters*, vol. 291, pp. 173–183, Jul. 2018.
[157] M. Ogonowski *et al.*, "Multi-level toxicity assessment of engineered cellulose nanofibrils in Daphnia magna," *Nanotoxicology*, vol. 12, no. 6, pp. 509–521, Jul. 2018.
[158] M. Ilves *et al.*, "Nanofibrillated cellulose causes acute pulmonary inflammation that subsides within a month," *Nanotoxicology*, vol. 0, no. 0, pp. 1–18, May 2018.
[159] G. Pyrgiotakis *et al.*, "Development of high throughput, high precision synthesis platforms and characterization methodologies for toxicological studies of nanocellulose," *Cellulose*, vol. 25, no. 4, pp. 2303–2319, Apr. 2018.
[160] S. F. Souza, M. Mariano, D. Reis, C. B. Lombello, M. Ferreira, and M. Sain, "Cell interactions and cytotoxic studies of cellulose nanofibers from Curauá natural fibers," *Carbohydrate Polymers*, vol. 201, pp. 87–95, Dec. 2018.
[161] M. Roman, "Toxicity of Cellulose Nanocrystals: A Review," *Industrial Biotechnology*, vol. 11, no. 1, pp. 25–33, Feb. 2015.
[162] A. F. P. D. F. Wouk, J. M. Diniz, S. M. CíRio, H. Dos Santos, E. L. Baltazar, and A. Acco, "Membrana biológica (Biofill) - estudo comparativo com outros agentes promotores da cicatrização da pele em suínos: aspectos clínicos, histopatológicos e morfométricos," *Archives of Veterinary Science*, vol. 3, no. 1, Dec. 1998.
[163] D. Klemm, D. Schumann, U. Udhardt, and S. Marsch, "Bacterial synthesized cellulose Ð arti®cial blood vessels for microsurgery," *Prog. Polym. Sci.*, p. 43, 2001.
[164] D. A. Schumann *et al.*, "Artificial vascular implants from bacterial cellulose: preliminary results of small arterial substitutes," *Cellulose*, vol. 16, no. 5, pp. 877–885, Oct. 2009.
[165] W. Czaja, A. Krystynowicz, S. Bielecki, and R. M. Brown, "Microbial cellulose—the natural power to heal wounds," *Biomaterials*, vol. 27, no. 2, pp. 145–151, Jan. 2006.
[166] W. K. Czaja, D. J. Young, M. Kawecki, and R. M. Brown, "The Future Prospects of Microbial Cellulose in Biomedical Applications," *Biomacromolecules*, vol. 8, no. 1, pp. 1–12, Jan. 2007.
[167] W. K. Czaja, D. J. Young, M. Kawecki, and R. M. Brown, "The Future Prospects of Microbial Cellulose in Biomedical Applications," *Biomacromolecules*, vol. 8, no. 1, pp. 1–12, Jan. 2007.
[168] S. Sheykhnazari, T. Tabarsa, A. Ashori, A. Shakeri, and M. Golalipour, "Bacterial synthesized cellulose nanofibers; Effects of growth times and culture mediums on the structural characteristics," *Carbohydrate Polymers*, vol. 86, no. 3, pp. 1187–1191, Aug. 2011.
[169] N. Halib *et al.*, "Potential Applications of Nanocellulose-Containing Materials in the Biomedical Field," *Materials*, vol. 10, no. 8, p. 977, Aug. 2017.
[170] S. Toivonen *et al.*, "Regulation of Human Pluripotent Stem Cell-Derived Hepatic Cell Phenotype by Three-Dimensional Hydrogel Models," *Tissue Engineering Part A*, vol. 22, no. 13–14, pp. 971–984, Jun. 2016.
[171] P. Laurén, "Biomedical applications of nanofibrillar cellulose (Ph.D. thesis)," 2018.
[172] R. Kolakovic, L. Peltonen, A. Laukkanen, J. Hirvonen, and T. Laaksonen, "Nanofibrillar cellulose films for controlled drug delivery," *European Journal of Pharmaceutics and Biopharmaceutics*, vol. 82, no. 2, pp. 308–315, Oct. 2012.

[173] R. Kolakovic *et al.*, "Evaluation of drug interactions with nanofibrillar cellulose," *European Journal of Pharmaceutics and Biopharmaceutics*, vol. 85, no. 3, Part B, pp. 1238–1244, Nov. 2013.
[174] H. Valo *et al.*, "Drug release from nanoparticles embedded in four different nanofibrillar cellulose aerogels," *European Journal of Pharmaceutical Sciences*, vol. 50, no. 1, pp. 69–77, Sep. 2013.
[175] G. Chinga-Carrasco and K. Syverud, "Pretreatment-dependent surface chemistry of wood nanocellulose for pH-sensitive hydrogels," *J Biomater Appl*, vol. 29, no. 3, pp. 423–432, Sep. 2014.
[176] R. Kolakovic, L. Peltonen, T. Laaksonen, K. Putkisto, A. Laukkanen, and J. Hirvonen, "Spray-Dried Cellulose Nanofibers as Novel Tablet Excipient," *AAPS PharmSciTech*, vol. 12, no. 4, pp. 1366–1373, Dec. 2011.
[177] G. Sarkar *et al.*, "Cellulose nanofibrils/chitosan based transdermal drug delivery vehicle for controlled release of ketorolac tromethamine," *New J. Chem.*, vol. 41, no. 24, pp. 15312–15319, Dec. 2017.
[178] J. Zhao, C. Lu, X. He, X. Zhang, W. Zhang, and X. Zhang, "Polyethylenimine-Grafted Cellulose Nanofibril Aerogels as Versatile Vehicles for Drug Delivery," *ACS Appl. Mater. Interfaces*, vol. 7, no. 4, pp. 2607–2615, Feb. 2015.
[179] P. Laurén, Y.-R. Lou, M. Raki, A. Urtti, K. Bergström, and M. Yliperttula, "Technetium-99m-labeled nanofibrillar cellulose hydrogel for in vivo drug release," *European Journal of Pharmaceutical Sciences*, vol. 65, pp. 79–88, Dec. 2014.
[180] A. A. Jack *et al.*, "The interaction of wood nanocellulose dressings and the wound pathogen P. aeruginosa," *Carbohydrate Polymers*, vol. 157, pp. 1955–1962, Feb. 2017.
[181] K. Syverud, S. R. Pettersen, K. Draget, and G. Chinga-Carrasco, "Controlling the elastic modulus of cellulose nanofibril hydrogels—scaffolds with potential in tissue engineering," *Cellulose*, vol. 22, no. 1, pp. 473–481, Feb. 2015.
[182] O. Aarstad, E. B. Heggset, I. S. Pedersen, S. H. Bjørnøy, K. Syverud, and B. L. Strand, "Mechanical Properties of Composite Hydrogels of Alginate and Cellulose Nanofibrils," *Polymers*, vol. 9, no. 8, p. 378, Aug. 2017.
[183] V. Kuzmenko, E. Karabulut, E. Pernevik, P. Enoksson, and P. Gatenholm, "Tailor-made conductive inks from cellulose nanofibrils for 3D printing of neural guidelines," *Carbohydrate Polymers*, vol. 189, pp. 22–30, Jun. 2018.
[184] K.-M. Chin, S. S. Ting, H. L. Ong, and M. Omar, "Surface functionalized nanocellulose as a veritable inclusionary material in contemporary bioinspired applications: A review," *Journal of Applied Polymer Science*, vol. 135, no. 13, p. 46065.
[185] Y. Habibi, "Key advances in the chemical modification of nanocelluloses," *Chem. Soc. Rev.*, vol. 43, no. 5, pp. 1519–1542, 2014.
[186] K. Missoum, M. N. Belgacem, and J. Bras, "Nanofibrillated Cellulose Surface Modification: A Review," *Materials*, vol. 6, no. 5, pp. 1745–1766, May 2013.
[187] K. Missoum, "Modification chimique de surface de NanoFibrilles de Cellulose (NFC)," phdthesis, Université Grenoble Alpes, 2012.
[188] "Introduction and Objectives," in *Esterification of Polysaccharides*, Springer, Berlin, Heidelberg, 2006, pp. 1–3.
[189] "Selected Examples of New Applications," in *Esterification of Polysaccharides*, Springer, Berlin, Heidelberg, 2006, pp. 181–193.
[190] T. Mekonnen, P. Mussone, H. Khalil, and D. Bressler, "Progress in bio-based plastics and plasticizing modifications," *J. Mater. Chem. A*, vol. 1, no. 43, pp. 13379–13398, Oct. 2013.
[191] J.-F. Sassi and H. Chanzy, "Ultrastructural aspects of the acetylation of cellulose," *Cellulose*, vol. 2, no. 2, pp. 111–127, Jun. 1995.
[192] P. Tingaut, T. Zimmermann, and F. Lopez-Suevos, "Synthesis and Characterization of Bionanocomposites with Tunable Properties from Poly(lactic acid) and Acetylated Microfibrillated Cellulose," *Biomacromolecules*, vol. 11, no. 2, pp. 454–464, Feb. 2010.

[193] K. Missoum, M. Naceur Belgacem, J.-P. Barnes, M.-C. Brochier-Salon, and J. Bras, "Nanofibrillated cellulose surface grafting in ionic liquid," *Soft Matter*, vol. 8, no. 32, pp. 8338–8349, 2012.
[194] M. Fumagalli, D. Ouhab, S. M. Boisseau, and L. Heux, "Versatile Gas-Phase Reactions for Surface to Bulk Esterification of Cellulose Microfibrils Aerogels," *Biomacromolecules*, vol. 14, no. 9, pp. 3246–3255, Sep. 2013.
[195] S. Saini, N. Belgacem, J. Mendes, G. Elegir, and J. Bras, "Contact Antimicrobial Surface Obtained by Chemical Grafting of Microfibrillated Cellulose in Aqueous Solution Limiting Antibiotic Release," *ACS Applied Materials & Interfaces*, vol. 7, no. 32, pp. 18076–18085, Aug. 2015.
[196] E. Valeur and M. Bradley, "Amide bond formation: beyond the myth of coupling reagents," *Chemical Society Reviews*, vol. 38, no. 2, pp. 606–631, 2009.
[197] C. A. G. N. Montalbetti and V. Falque, "Amide bond formation and peptide coupling," *Tetrahedron*, vol. 61, no. 46, pp. 10827–10852, Nov. 2005.
[198] A. El-Faham and F. Albericio, "Peptide Coupling Reagents, More than a Letter Soup," *Chemical Reviews*, vol. 111, no. 11, pp. 6557–6602, Nov. 2011.
[199] J. Araki, M. Wada, and S. Kuga, "Steric Stabilization of a Cellulose Microcrystal Suspension by Poly(ethylene glycol) Grafting," *Langmuir*, vol. 17, no. 1, pp. 21–27, Jan. 2001.
[200] M. Bodanszky, "Formation of the Peptide Bond," in *Peptide Chemistry*, Springer, Berlin, Heidelberg, 1993, pp. 55–73.
[201] N. Nakajima and Y. Ikada, "Mechanism of amide formation by carbodiimide for bioconjugation in aqueous media," *Bioconjugate chemistry*, vol. 6, no. 1, pp. 123–130, 1995.
[202] H. Mojarradi, "Coupling of substances containing a primary amine to hyaluronan via carbodiimide-mediated amidation," p. 49.
[203] E. Lasseuguette, "Grafting onto microfibrils of native cellulose," *Cellulose*, vol. 15, no. 4, pp. 571–580, Aug. 2008.
[204] S. Arola, T. Tammelin, H. Setälä, A. Tullila, and M. B. Linder, "Immobilization–Stabilization of Proteins on Nanofibrillated Cellulose Derivatives and Their Bioactive Film Formation," *Biomacromolecules*, vol. 13, no. 3, pp. 594–603, Mar. 2012.
[205] E. Karabulut, T. Pettersson, M. Ankerfors, and L. Wågberg, "Adhesive Layer-by-Layer Films of Carboxymethylated Cellulose Nanofibril–Dopamine Covalent Bioconjugates Inspired by Marine Mussel Threads," *ACS Nano*, vol. 6, no. 6, pp. 4731–4739, Jun. 2012.
[206] H. Orelma, L. Johansson, I. Filpponen, O. J. Rojas, and J. Laine, "Generic Method for Attaching Biomolecules via Avidin–Biotin Complexes Immobilized on Films of Regenerated and Nanofibrillar Cellulose," *Biomacromolecules*, vol. 13, no. 9, pp. 2802–2810, Sep. 2012.
[207] H. Orelma, I. Filpponen, L.-S. Johansson, M. Österberg, O. J. Rojas, and J. Laine, "Surface Functionalized Nanofibrillar Cellulose (NFC) Film as a Platform for Immunoassays and Diagnostics," *Biointerphases*, vol. 7, no. 1, p. 61, Dec. 2012.
[208] A. Benkaddour, K. Jradi, S. Robert, and C. Daneault, "Grafting of Polycaprolactone on Oxidized Nanocelluloses by Click Chemistry," *Nanomaterials*, vol. 3, no. 1, pp. 141–157, Mar. 2013.
[209] K. Junka, J. Guo, I. Filpponen, J. Laine, and O. J. Rojas, "Modification of Cellulose Nanofibrils with Luminescent Carbon Dots," *Biomacromolecules*, vol. 15, no. 3, pp. 876–881, Mar. 2014.
[210] R. Weishaupt *et al.*, "TEMPO-Oxidized Nanofibrillated Cellulose as a High Density Carrier for Bioactive Molecules," *Biomacromolecules*, vol. 16, no. 11, pp. 3640–3650, Nov. 2015.
[211] H. Orelma *et al.*, "Preparation of photoreactive nanocellulosic materials via benzophenone grafting," *RSC Advances*, vol. 6, no. 88, pp. 85100–85106, 2016.
[212] S. Gorgieva, L. Girandon, and V. Kokol, "Mineralization potential of cellulose-nanofibrils reinforced gelatine scaffolds for promoted calcium deposition by mesenchymal stem cells," *Materials Science and Engineering: C*, vol. 73, pp. 478–489, Apr. 2017.
[213] R. Hollertz, V. L. Durán, P. A. Larsson, and L. Wågberg, "Chemically modified cellulose micro- and nanofibrils as paper-strength additives," *Cellulose*, vol. 24, no. 9, pp. 3883–3899, Sep. 2017.

[214] Y. Zhang and O. J. Rojas, "Immunosensors for C-Reactive Protein Based on Ultrathin Films of Carboxylated Cellulose Nanofibrils," *Biomacromolecules*, vol. 18, no. 2, pp. 526–534, Feb. 2017.
[215] T. Kaldéus, M. Nordenström, A. Carlmark, L. Wågberg, and E. Malmström, "Insights into the EDC-mediated PEGylation of cellulose nanofibrils and their colloidal stability," *Carbohydrate Polymers*, vol. 181, pp. 871–878, Feb. 2018.
[216] M. Meldal and C. W. Tornøe, "Cu-Catalyzed Azide–Alkyne Cycloaddition," *Chemical Reviews*, vol. 108, no. 8, pp. 2952–3015, Aug. 2008.
[217] H. C. Kolb, M. G. Finn, and K. B. Sharpless, "Click Chemistry: Diverse Chemical Function from a Few Good Reactions," *Angewandte Chemie International Edition*, vol. 40, no. 11, pp. 2004–2021, Jun. 2001.
[218] R. Hoogenboom, "Thiol-Yne Chemistry: A Powerful Tool for Creating Highly Functional Materials," *Angewandte Chemie International Edition*, vol. 49, no. 20, pp. 3415–3417, May 2010.
[219] C. R. Becer, R. Hoogenboom, and U. S. Schubert, "Click Chemistry beyond Metal-Catalyzed Cycloaddition," *Angewandte Chemie International Edition*, vol. 48, no. 27, pp. 4900–4908, Jun. 2009.
[220] W. Xi, T. F. Scott, C. J. Kloxin, and C. N. Bowman, "Click Chemistry in Materials Science," *Advanced Functional Materials*, vol. 24, no. 18, pp. 2572–2590, May 2014.
[221] K. Solin, H. Orelma, M. Borghei, M. Vuoriluoto, R. Koivunen, and O. J. Rojas, "Two-Dimensional Antifouling Fluidic Channels on Nanopapers for Biosensing," *Biomacromolecules*, Dec. 2018.
[222] C. E. Hoyle, A. B. Lowe, and C. N. Bowman, "Thiol-click chemistry: a multifaceted toolbox for small molecule and polymer synthesis," *Chemical Society Reviews*, vol. 39, no. 4, p. 1355, 2010.
[223] A. Gress, A. Völkel, and H. Schlaad, "Thio-Click Modification of Poly[2-(3-butenyl)-2-oxazoline]," *Macromolecules*, vol. 40, no. 22, pp. 7928–7933, Oct. 2007.
[224] P. Tingaut, R. Hauert, and T. Zimmermann, "Highly efficient and straightforward functionalization of cellulose films with thiol -ene click chemistry," *Journal of Materials Chemistry*, vol. 21, no. 40, pp. 16066–16076, 2011.
[225] B. D. Fairbanks, T. F. Scott, C. J. Kloxin, K. S. Anseth, and C. N. Bowman, "Thiol–Yne Photopolymerizations: Novel Mechanism, Kinetics, and Step-Growth Formation of Highly Cross-Linked Networks," *Macromolecules*, vol. 42, no. 1, pp. 211–217, Jan. 2009.
[226] J. R. G. Navarro *et al.*, "Multicolor Fluorescent Labeling of Cellulose Nanofibrils by Click Chemistry," *Biomacromolecules*, vol. 16, no. 4, pp. 1293–1300, Apr. 2015.
[227] A. B. Lowe, C. E. Hoyle, and C. N. Bowman, "Thiol-yne click chemistry: A powerful and versatile methodology for materials synthesis," *Journal of Materials Chemistry*, vol. 20, no. 23, p. 4745, 2010.
[228] J. Rull-Barrull, M. d'Halluin, E. L. Grognec, and F.-X. Felpin, "Photoresponsive cellulose paper as a molecular printboard for covalent printing," *J. Mater. Chem. C*, vol. 5, no. 21, pp. 5154–5162, Jun. 2017.
[229] S. Mongkhontreerat, O. C. J. Andrén, A. Boujemaoui, and M. Malkoch, "Dendritic hydrogels: From exploring various crosslinking chemistries to introducing functions and naturally abundant resources," *Journal of Polymer Science Part A: Polymer Chemistry*, vol. 53, no. 21, pp. 2431–2439, Nov. 2015.
[230] A. Gandini, "The furan/maleimide Diels–Alder reaction: A versatile click–unclick tool in macromolecular synthesis," *Progress in Polymer Science*, vol. 38, no. 1, pp. 1–29, Jan. 2013.
[231] A. Gandini and M. N. Belgacem, "Chapter 6 - Furan Derivatives and Furan Chemistry at the Service of Macromolecular Materials," in *Monomers, Polymers and Composites from Renewable Resources*, M. N. Belgacem and A. Gandini, Eds. Amsterdam: Elsevier, 2008, pp. 115–152.
[232] A. Gandini, A. J. F. Carvalho, E. Trovatti, R. K. Kramer, and T. M. Lacerda, "Macromolecular materials based on the application of the Diels–Alder reaction to natural polymers and plant oils," *European Journal of Lipid Science and Technology*, vol. 120, no. 1, p. 1700091, 2018.
[233] J. Ax and G. Wenz, "Thermoreversible Networks by Diels–Alder Reaction of Cellulose Furoates With Bismaleimides," *Macromol. Chem. Phys.*, vol. 213, no. 2, pp. 182–186, Jan. 2012.

[234] C. García-Astrain *et al.*, "Maleimide-grafted cellulose nanocrystals as cross-linkers for bionanocomposite hydrogels," *Carbohydrate Polymers*, vol. 149, pp. 94–101, Sep. 2016.
[235] C. Shao, M. Wang, H. Chang, F. Xu, and J. Yang, "A Self-Healing Cellulose Nanocrystal-Poly(ethylene glycol) Nanocomposite Hydrogel via Diels–Alder Click Reaction," *ACS Sustainable Chemistry & Engineering*, vol. 5, no. 7, pp. 6167–6174, Jul. 2017.
[236] E. Trovatti, A. G. Cunha, A. J. F. Carvalho, and A. Gandini, "Furan-modified natural rubber: A substrate for its reversible crosslinking and for clicking it onto nanocellulose," *International Journal of Biological Macromolecules*, vol. 95, pp. 762–768, Feb. 2017.

Chapter II

Immobilization of active principle ingredients on cellulose nanofibrils

Table of Content

II. Immobilization of active principle ingredients on cellulose nanofibrils

Introduction to chapter II

The functionalization of cellulose nanofibrils (CNF) appears to be necessary to improve its potential for new demanding fields of application, such as biomedical. Chapter I reviewed how the high specific surface area of CNF, combined with its chemical versatility can offer a wide range of functionalization strategies to immobilize active principle ingredients (API). Accordingly, in the experimental part, different chemical routes can be applied whether if CNF films or suspensions are used.

Indeed, the first part of the chapter II describes the simple covalent bonding strategy that is used to graft Ciprofloxacin directly onto CNF films. The antibacterial activity of such modified films is investigated in order to confirm its contact active properties. Such films present potential use in topical application medical devices.

The second part will focus on more complex immobilization strategies for CNF suspensions. A two-step chemical modification was performed on TEMPO oxidized cellulose nanofibrils (CNF-t) suspensions in water. In the first step, CNF-t is provided with pending alkyne functions through amidation that are supposed to react, in the second step, with a thiolated prodrug of metronidazole through thiol-yne click chemistry. In the third part of this chapter, a similar approach is proposed. CNF-t are first provided with furan functions that subsequently react with the maleimide function of another prodrug of metronidazole. The Figure II.1 summarizes the chapter II structure. Highly innovative characterization tool as dynamic nuclear polarization enhanced nuclear magnetic resonance (DNP-NMR) is used for the first time to investigate cellulose nanofibrils in order to detect modifications that are usually not visible with traditional tools.

Throughout these findings, API enhanced CNF can be designed and tailored to match the required functionalities of different types of medical devices, namely external or internal treatments.

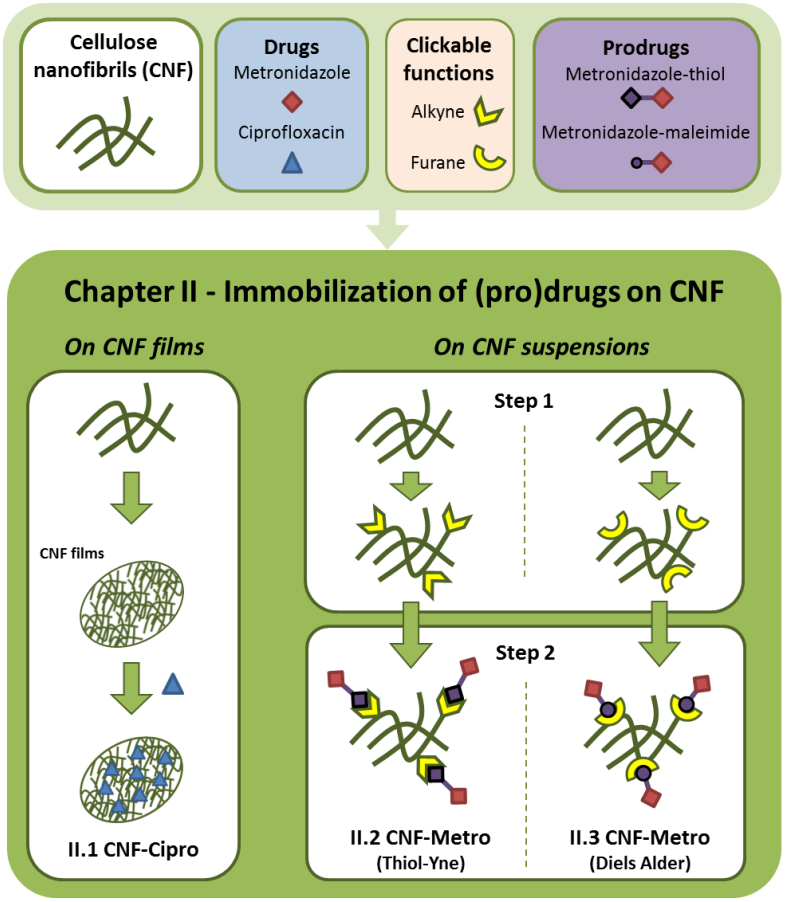

Figure II.1: Graphical representation of chapter II structure

1. Single step immobilization of Ciprofloxacin on cellulose nanofibrils films for antimicrobial membrane development

This section is adapted from "H. Durand, C. Darpentigny, E.Zeno, N. Belgacem, J. Bras - Single step immobilization of Ciprofloxacin on cellulose nanofibers for antimicrobial membrane development", submitted in Material Science Engineering: C in November 2018

Abstract

The combination of nanocellulosic material with active principle ingredients appear like a promising strategy for the development of next generation active medical device. The high specific surface and tunable surface chemistry are properties of high interest when it comes to immobilize molecules on cellulose nanofibers. Proved biodegradability and biocompatibility are al so key properties when such materials are intended to be used in the biomedical field. Here we demonstrate immobilization of Ciprofloxacin on the surface of cellulose nanofibers films through a green solvent-free esterification procedure. Surface and bulk analyses were performed in order to reveal the presence of Ciprofloxacin on the CNF films. Complementary antimicrobial testing was set up to assess the activity of the prototype medical device. The immobilization of Ciprofloxacin was proven to be successful and a prolonged activity of CNF films grafted with the active molecule confirmed the covalent nature of the immobilization. This work further strengthens the potential of cellulose nanofibers as a high added value platform for the design of medical devices with long-term active properties.

Keywords: cellulose nanofibrils, Ciprofloxacin, green functionalization, antibacterial activity

1.1 Introduction

Cellulose is the most abundant polymer on earth with an estimated quantity of 7.5 $x10^{10}$ tons produced by photosynthesis each year [1]. This is seventeen times more than the global oil extraction in 2016 [2]. Thus cellulose appears like one of the key alternative material to fossil resources products. Cellulose is renewable, biodegradable and biocompatible, it is available globally and its extraction processes are continuously under intensive investigation to reduce environmental impact and become more sustainable.

Moreover, in the 1980's, cellulose nanofibers (CNF) were discovered and isolated from cellulose fibers [3], [4]. CNF are composed of the elementary fibrils of the cellulose fiber and comprises amorphous and crystalline region. Their isolation process is still under optimization in order to reach suitable energy consumption and reduce environmental impact. Today, several books [5], [6], reviews [7], [8], and conferences (TAPPI Nano, ACS Cellulose division), are dedicated to the investigation of these cellulose nanofibrils and the best ways to produce and characterize them [9]–[11].

CNF can be used in many different fields, from papermaking industry in order to reinforce structures or improve barrier properties [6], [12], [13], to nanocomposites [14], electronics [15]–[17], the cosmetics or even the medical industry [18]–[21]. A couple of applications already exist on the market like skin care patch or even hygiene pads.

In the medical field, CNF have great opportunities thanks to their biocompatibility as recently reported [18], [22], [23]. CNF were proposed for the first time in early 2010 to prepare long lasting drug release tablets and films [24], [25]. Cellulose nanofibrils were also coated on substrates in order to develop nanostructured network which sustained release of various molecule like caffeine or chlorhexidine digluconate [26], [27]. The same authors also associated CNF suspensions with β-cyclodextrins in order to further improve the molecule encapsulation capabilities of the nano-structured CNF networks [28].

Also, CNF have a huge specific surface area with a tunable surface chemistry which allows for a wide range of functionalization strategies. However, a very few publication investigated the direct covalent immobilization of active pharmaceutical ingredients (API) on CNF substrates. This type of strategy could help to develop new active products for the medical field. In 2015, researchers managed to chemically graft penicillin of CNF films and suspensions. The grafting was also confirmed by antimicrobial testing against gram positive and gram negative bacteria strains. The substrates

proved to be successfully contact-active non-leaching packaging prototypes. [29] Nisin, another antimicrobial molecule, was also anchored to carboxylated CNF through an amidation reaction resulting into active systems for prolonged-release antimicrobial properties[30].

In this paper, we investigated the chemical immobilization of Ciprofloxacin, an API that is suitable for the medical field (Figure II.2).

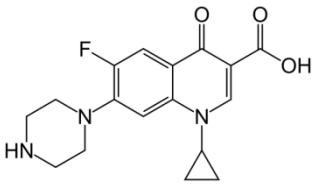

Figure II.2: Ciprofloxacin molecular structure

Ciprofloxacin is a synthetic antibiotic with a broad spectrum activity which was patented in 1981. It is part of the second generation of fluoro-quinolones that have a therapeutic activity principle based on the inhibition of enzymes involved in DNA synthesis and cell division which unwind the DNA supercoil structure prior to replication. The fluoroquinolones inhibits the action of this enzyme and stop the DNA replication process which leads to bacteriostasis and eventually cell death [31].

The broad spectrum activity of Ciprofloxacin is explained by the combination of the fluorine atoms, which improves activity against gram positive bacteria. The piperazin ring is known to bring a better ability to penetrate the bacterial cell wall and the cyclopropyl side chain increases the bioavailability of the compound. This improves the activity against gram negative bacteria [32].

In previous work, penicillin was used, but in the late 90's bacterial resistance started to be monitored. The intense use of this molecule for more than 50 years now explains the resistance development and the need for alternative solutions[33]. For this study Ciprofloxacin was chosen because second generation fluoroquinolones show less resistance of micro-organisms with a much wider spectrum activity than penicillin. It is active against both gram positive and gram negative strains revealing a potent antimicrobial activity [34]. Moreover, the availability of a carboxylic group allows for esterification reaction with hydroxyls of cellulose nanofibers surface. The presence of Ciprofloxacin on CNF substrates can also be confirmed thanks to its three nitrogen atoms that can be easily traced with elemental analysis.

In this paper, Ciprofloxacin was covalently immobilized on CNF films thanks to its carboxyl groups through esterification with hydroxyls groups available on cellulose. The grafting was confirmed and the antimicrobial activity of the sample was assessed. The general procedure is described on Figure

II.3. The modified CNF films are believed to be high-added value starting materials for the development of innovative medical devices for topical application.

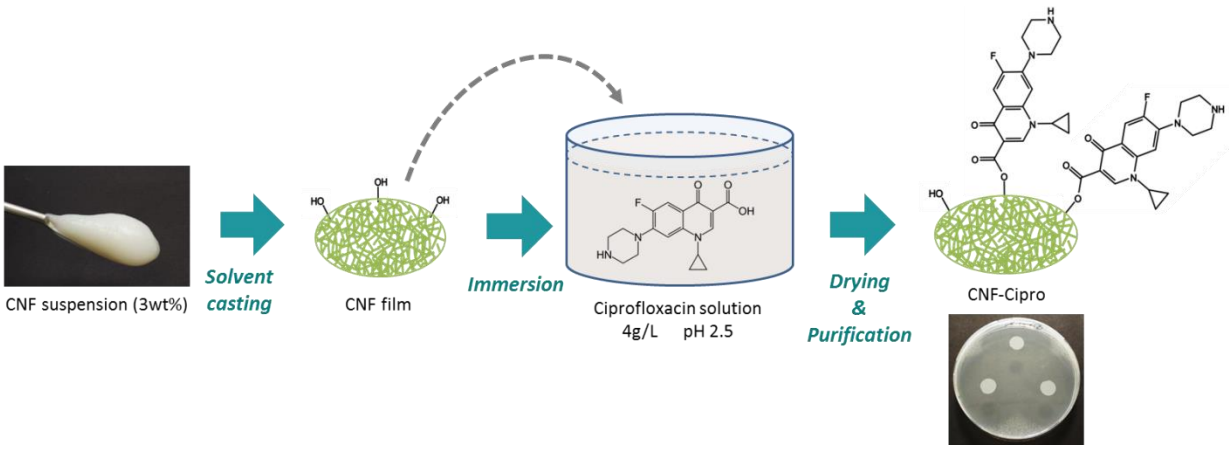

Figure II.3: Graphical description of the immobilization strategy of Ciprofloxacin on cellulose nanofibrils films to prepare medical devices for topical application with antimicrobial activity

1.2 Experimental procedures

1.2.1. Materials

The cellulose nanofibers (CNF) suspension was provided by the Centre Technique du Papier (CTP, Grenoble, France) and was produced by enzymatic pre-treatment of a bleached birch pulp followed by strong refining (80°SR) and homogenization: 3 passes at 1500 bars in an Ariete homogenizer from GEA (Italy). Ciprofloxacin (≥98.0%, CAS: 85721-33-1) was purchased from Sigma-Aldrich as a white powder and used as received.

Bacillus subtilis (BGA) spore suspension were provided by SIGMA-Aldrich (MERCK) at a concentration range of 8.10^6 – 5.10^7 CFU/ml and were used as received to prepare inoculations.

Staphylococcus aureus and Escherichia coli were purchased from Thermo Scientific (ATCC 6538 and 8739 respectively) in the form of freeze-dried suspensions. Rehydrating procedure was followed according to supplier's information. Pre-inoculum were prepared in a commercial Nutrient Broth solution (composed of peptone, yeast extract, sodium chloride, and glucose) and sterilize in autoclave (121°C, 15min) in which bacteria were grown for 16h in a 37°C incubator. Difco™ Nutrient Agar from Becton Dickinson was used and also submitted to autoclave sterilization. Sterile polystyrene petri dishes (90mm diameter) purchased from Carl Roth were utilized in every microbiological testing.

1.2.2. Methods

1.2.2.a. Preparation of CNF-e films

The CNF suspension was diluted with deionized water from 3% w/w (gel state) to 1% w/w (more liquid and stirrable fluid) and magnetically stirred for 5 minutes at 300 rpm. The high shear stirrer Ultra-Turrax (IKA, USA) was used on the suspension to ensure a homogeneous dispersion of the CNF: 30 seconds at 10 000 rpm. The suspension was casted in polystyrene petri dish and let to dry in a controlled condition room (23°C and 50%RH) until films can be easily collected (around 5 days). The resulting films were recovered from the petri dish and stored in the same controlled condition room before any characterization.

1.2.2.b. Immobilization of Ciprofloxacin on CNF films

An aqueous solution of Ciprofloxacin was prepared in 0.1N HCl in order to favor the solubility of the drug. CNF films were then immersed in the solution for 15 minutes. The films were then carefully recovered and put in contact with blotting papers in order to remove the excess liquid. A thermal treatment was applied under vacuum in a buchï oven, for 24 hours at 50°C under vacuum for the activation of the esterification reaction. The temperature was kept rather low in comparison with similar previous work where thermal treatment was performed in an oven at 150°C [29]. Our objective is to avoid potential degradation of the Ciprofloxacin that is likely occurring at 150°C [35]. The films were purified with soxhlet extraction with high purity acetone first and also deionized water for a duration corresponding to at least 100 washes for each solvent so that the non-covalently bound Ciprofloxacin was removed from the CNF film. Non-modified CNF films were also exposed to the heat treatment in Buchï oven and soxhlet extraction to produce relevant references without Ciprofloxacin. Finally, the modified films (CNF-Cipro) and reference films (CNF-ref) were stored in a controlled condition room (23°C, 50%RH) for at least 24h before any characterization.

1.2.2.c. Scanning Electron Microscopy

Scanning Electron Microscopy (SEM) pictures of CNF films surfaces and cross-sections were obtained on a Quanta200®. Carbon tape was used to immobilize samples on supports and they were then coated with a thin layer of pure carbon thanks to an EMITECH® K450X carbon coater. The working distance during SEM image acquisition was in between 9.8 and 10.1 mm with a voltage of 10 kV and a magnitude of x250 for films surface and x1000 for cross-sections. At least ten pictures per sample were recorded and the most representative were kept for the discussion.

1.2.2.d. Infrared spectroscopy, ATR mode

Fourier Transformed Infrared (FTIR) spectra of the CNF films and Ciprofloxacin powder were obtained on a Perkin Elmer Spectrum One spectrometer (Waltham, Massachusetts, USA) in attenuated total

reflectance (ATR) mode. At least 5 measurements of 16 scans with a resolution of 2 cm^{-1} between 600 and 4000 cm^{-1} on each side of the films and different locations were performed. Spectra were normalized at 1110 cm^{-1}, the wavenumber of C-O-C bonds in cellulosic substrates. The most representative spectra were chosen for discussion.

1.2.2.e. Elemental analysis - CHNS

Elemental Analysis (EA) was performed on a vario Micro Cube device from Elementar. Carbon, Hydrogen, Nitrogen and Sulfur mass proportion of CNF-Cipro and CNF-ref films were measured. Film pieces of 4 to 7 mg were weighed on a *micro-balance*. An average of four measurements was obtained for each sample. The Ciprofloxacin loading X_{cipro} can be calculated (equation (II-1)) by considering nitrogen and the drug molar masses. This value gives the actual weight proportion of Ciprofloxacin in CNF films.

$$X_{cipro} = \frac{\%N \times M(cipro)}{3 \times M(N)} \qquad \textbf{(II-1)}$$

where $M(cipro)$ is the molar mass of Ciprofloxacin (331.198 g/mol) and the value 3 corresponds to the number of nitrogen atoms in Ciprofloxacin.

1.2.2.f. Minimum Inhibitory Concentration

The Minimum Inhibitory Concentration (MIC) is defined as the lowest concentration of a drug that inhibits the visible growth of an organism after overnight incubation [36]. Several series of dilution of the Ciprofloxacin solution were prepared in Eppendorf pipettes. The first series covered a wide range of concentration from 4.10^{-1} to 4.10^{-10} mg/ml. On the other hand an agar solution was prepared for subsequent inoculation with the bacteria at 10^4 CFU/ml with B. subtilis spore suspension. The test objective was to put the inoculated agar in contact with all the Ciprofloxacin solution dilutions prepared beforehand inside petri dishes. A 100µl of each diluted solution was mixed with 10ml of inoculated agar medium. The petri dishes were cooled down until the agar turn to gel state and then put in an incubator at 37°C for 24h. All the petri dishes were then analyzed: those without any visible bacterial growth have a concentration of Ciprofloxacin that was superior to the MIC. The lowest concentration resulting in bacterial growth inhibition was used to determine a first value of MIC. The procedure was repeated in a narrower range of concentrations below the first obtained value. It also helps to refine the MIC value by duplicating the measurement.

1.2.2.g. Influence of temperature on Ciprofloxacin stability

The immobilization procedure of Ciprofloxacin on CNF film required a 24h-long exposition to a temperature of 50°C. This thermal treatment might have affected the stability of the active molecule itself. The thermal stability of Ciprofloxacin was then to be assessed. In literature, little degradation of Ciprofloxacin in acidic solution is observed at 90°C [37]. MIC measurements were chosen as a tool to follow influence of temperature on Ciprofloxacin: solutions of 4g/l Ciprofloxacin were exposed to different thermal treatment for 24h: 5°C, room temperature (20°C), 50°C and 70°C in closed container. MICs of the thermally treated solution were then measured in order to study the heat effect on the MIC values of Ciprofloxacin and unveil hints on its thermal stability in solution.

1.2.2.h. Zone of Inhibition (ZOI) of CNF films

The test mostly follows AFNOR EN 1104 guidelines. CNF-Cipro and CNF-ref films were tested against gram positive Bacillus subtilis and Staphylococcus aureus and gram negative *Echireschia* coli strains. CNF-Cipro and CNF-ref discs of 10 mm diameter were dry sterilized for more than 16 h in an oven at 50°C. Three solutions of agar were respectively inoculated with E. coli, B. subtilis and S. aureus. Petri dishes were prepared with about 10 ml of agar solutions. When the inoculated agar turned into gel state after cooling down, samples discs were deposited on the surface. After incubation during 3 days at 37°C, petri dishes are observed to detect inhibition zones, which could indicate if Ciprofloxacin has leached out of the films. In this case, radiuses of inhibitions zones were measured. At least triplicates were performed for each sample and two types of references, i) non modified CNF films (negative reference) and ii) blotting paper discs impregnated in a Ciprofloxacin solution (positive reference) in order to confirm the validity of the experiment.

A modified version of the previous test was also implemented: successive zone of inhibition assessment. The objective of this test was to expose several times the same 10 mm diameter disc samples to a new inoculated medium. Bacterial suspensions of Escherichia coli and Staphylococcus epidermidis were prepared at a 10^8CFU/ml concentration in a Mueller Hinton broth. These bacterial suspensions were spread onto the surface of agar containing petri dishes. The incubation was performed at 37°C for 24 h before discs were recovered and transferred to new identically prepared petri dishes for another 24 h. Radius of inhibitions zones were collected for analysis. Four cycles of 24h were performed in order to assess the extent of activity of the samples. At the end of each cycle, once the samples were transferred to the next medium, zones of inhibition were examined and radiuses were measured. Three discs for each sample were used for repeatability.

1.3 Results and discussions

1.3.1. CNF and CNF films morphology and characterization

The CNF used in this study were produced from the Centre Technique du Papier (CTP, Grenoble, France). It is well known in the scientific community that several grades of CNF can be obtained from different wood sources and production procedures. A short description of their quality before any use is relevant if researchers want to compare our procedures and results to other works available in the literature. The CNF used in this study are considered of high quality, i. e. high homogeneity and amount of nanoscaled fibers versus microscale fibers. This is confirmed by the Figure II.4. The CNF suspension is a thick gel at only 3 wt% concentration indicating a high proportion of hydrogen bonding interactions in between nano and micro fibers. The CNF films obtained by film casting are transparent and homogeneous (Figure II.4b). Optical microscopy shows a very small proportion of remaining micro-sized fibers in Figure II.4c while Figure II.4d confirms the nano-sized dimensions of the fibrils.

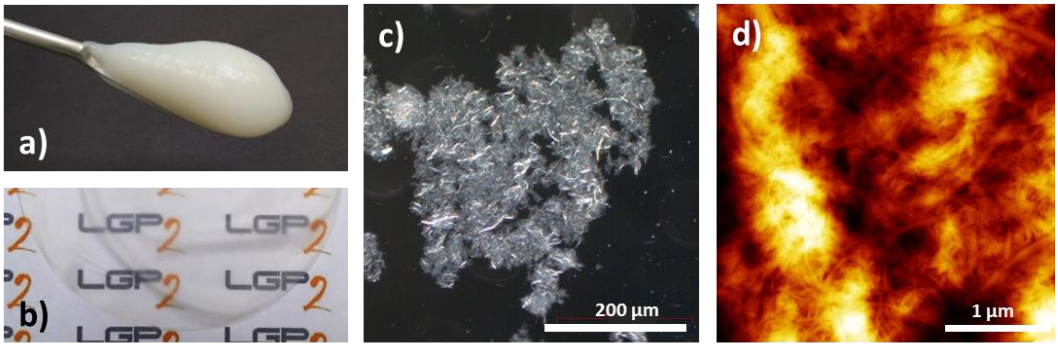

Figure II.4: Characterization of the CNF used in this study, a) thick CNF gel at 3 wt%, b) 90 mm diameter film (ca. 30 µm thick) with high transparency and c) optical microscopy of 1 wt% CNF suspension (x20) and d) height sensor AFM image of CNF films surface

The influence of the chemical grafting procedure on the structure of the CNF films was investigated by SEM. Figure II.5 shows pictures of cross sections and surfaces of the CNF-ref (A, C) and CNF-cipro samples (B, D). The thicknesses of the films are roughly the same, 23 ± 1 µm and 20 ± 2 µm and cross sections seem not to be affected by the immersion in Ciprofloxacin solution or purification steps with soxhlet extraction with pure acetone and deionized water. The surfaces of the films also seem to be very close before and after the treatment in terms of apparent topology. The swelling that occurs upon solvent absorption and the subsequent drying steps do not change the structure of the CNF films according to SEM analysis.

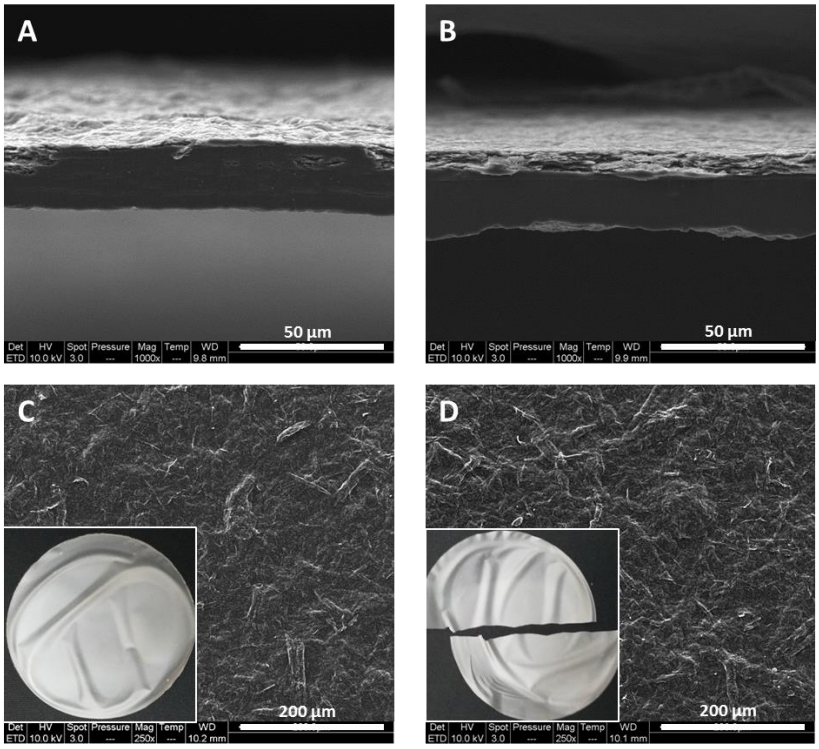

Figure II.5 : SEM pictures of A & C CNF-ref cut B & D CNF-CIPRO

1.3.2. Surface analysis of functionalized CNF films

Figure II.6 shows FTIR-ATR spectra of the samples characterized in this work. The FTIR-ATR spectrum of Ciprofloxacin powder is shown as well as spectra of "CNF-ref", "CNF-Cipro before extraction" and CNF-"Cipro after extraction" films.

Typical absorption peaks of cellulose polymer are present on the three curves refe rring to cellulosic substrates: stretching of –OH and –CH– bonds respectively at 3300 cm^{-1} and 2900 cm^{-1}. Peaks at 1160 cm^{-1} and 1106 cm^{-1} are attributed to anti-symmetrical -C-O-C- bridge stretching and anti-symmetrical anhydroglucose ring breathing, respectively [38], [39]. The highest peaks at 1050, 1027, 1003 and 982 cm^{-1} were assigned to -C-O- stretching [40]. Finally the peak at 896 cm^{-1} refers to cellulose C_1 and its four surrounding atoms [40]. The three CNF-related spectra show a peak in the 1640 cm^{-1} region which is related to the stretching of –OH bonds of bound water. The CNF-ref curves thus show very similar peak when compared to the above cited literature. This confirms that the acidic conditions encountered during the ciprofloxacin immobilization procedure do not affect the chemical structure of CNF membrane surfaces.

Regarding Ciprofloxacin spectrum, a typical peak of C=O carbonyl bond stretching can be found at 1617 cm^{-1}. COO^- carboxyla te systems give an anti-symmetrical signal at 1590 cm^{-1} and a symmetrical signal at 1375 cm^{-1}. The 3000-3100 cm^{-1} region evidences the presence of aromatic nucleus C-H bonds with stretching signals, especially at 3045 cm^{-1}. The existence of these bonds is further

confirmed by the 868 cm^{-1} peak which is attributed to bending modes of C-H bonds in aromatic nucleus. The three peaks at 1543, 1499 and 1475 cm^{-1} indicate the presence of C=C stretching modes of aromatic nucleus and also bending modes of N-H bonds. [41] All those peaks confirmed the structure of Ciprofloxacin.

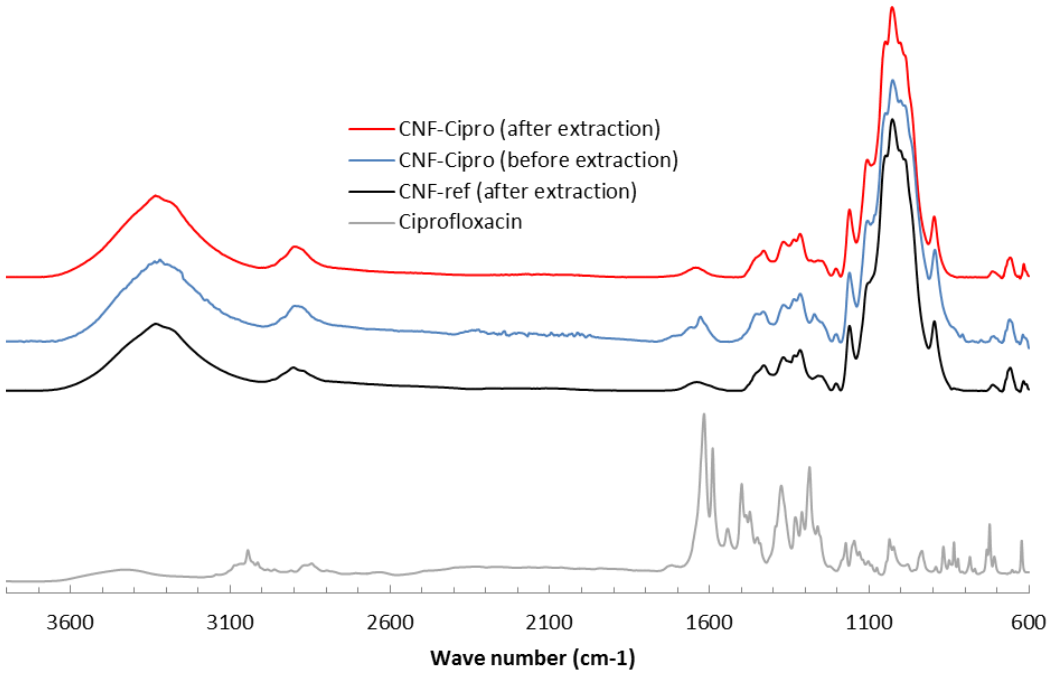

Figure II.6: FTIR-ATR spectra of Ciprofloxacin, CNF-ref film after extraction and CNF-cipro before and after soxhlet extraction

On CNF-Cipro (before extraction) spectrum a significant peak arises at 1628 cm^{-1} and 1657 cm^{-1} which are believed to be associated with C=O bonds of Ciprofloxacin. The ester function formed during esterification between CNF and Ciprofloxacin also seems to appear at 1720 cm^{-1}.

On CNF-Cipro (after extraction) spectrum, no significant peak is present. The spectrum matches with CNF-ref signal. The objective of the soxhlet extraction was to remove as much as possible of the non-covalently immobilized Ciprofloxacin from the CNF film. The amount of remaining immobilized Ciprofloxacin is probably very low and could not be detected with FTIR-ATR technique. This is why further bulk characterization tools were required to confirm the presence of the molecule.

1.3.3. Bulk analysis of functionalized CNF films

Elemental analysis experiments were conducted on CNF films. Carbon, Hydrogen, Nitrogen and Sulfur bulk weight proportion were recorded and are presented in Table II.1. CNF-ref samples show values of Carbon and Hydrogen contents slightly lower than pure cellulose (C 44.4% and H 6.2%), this is attributed to the presence of inorganic contaminants. The increase of carbon content between CNF-ref and CNF-Cipro (after extraction) reaches about 3 %C. As CNF-ref samples were subjected to the

exact same purification procedure as CNF-Cipro, we can consider this difference due to the presence of Ciprofloxacin. Moreover, on the CNF-Cipro samples, the increase of Nitrogen content clearly confirms the presence of Ciprofloxacin since its molecular structure includes three atoms of nitrogen. Similar analysis based on the nitrogen increase have been conducted with success before [29], [42]. Considering the extensive purification steps performed by soxhlet extraction with pure acetone and deionized water, the remaining Ciprofloxacin is likely to be strongly immobilized on CNF films.

Table II.1: Elemental analysis of carbon, hydrogen, nitrogen and sulfur and degree of substitution for modified CNF films based on the increase of nitrogen

	% C	± sd	% H	± sd	% N	± sd	% S	± sd
CNF-ref	**42.73**	*0.45*	**6.35**	*0.14*	**<0.10**	-	**<0.20**	-
CNF-Cipro	**43.15**	*0.05*	**6.345**	*0.18*	**0.115**	*0.02*	**<0.20**	-
Ciprofloxacin ***(theoretical values)***	**61.57**	-	**5.43**	-	**12.68**	-	**0.00**	-

Out of these results and by using equation **Erreur ! Source du renvoi introuvable.**, the achieved Ciprofloxacin loading X_{cipro} can be calculated. By considering molar masses of nitrogen and Ciprofloxacin we can easily obtain the actual mass proportion of the drug immobilized on the CNF film. A value of 0.91 wt% of Ciprofloxacin loading is obtained which is consistent with literature drug loaded systems loadings starting around 1 wt% [43]–[46].

1.3.4. Influence of temperature conditions on Ciprofloxacin stability

Minimum Inhibitory Concentration (MIC) was measured on a 4 g/l Ciprofloxacin solution with two series of dilutions according to the afore-mentioned protocol. The result for the intrinsic value of MIC for Ciprofloxacin was 8 µg/ml measured against B. subtilis strain after the second dilution series. This result is in accordance with the literature where values ranging from 0.5 to 64 µg/ml for similar gram positive bacteria are reported [47], [48]. The MIC measurement against B. subtilis was chosen as a way to assess the thermal stability of Ciprofloxacin in aqueous solution. For thermal treatment equal to or lower than 50°C, the measured MIC values remain stable at 12 µg/ml, as shown in Figure II.7. This value is in accordance with the initial result where an 8mg/l MIC is measured after the second series of dilution. For the thermal stability, the dilutions of the series were different (two fold dilutions against ten-fold dilutions) and this explains why the value is slightly different (8 against 12 mg/l) but fairly comparable. However, at 70°C, a higher value of MIC is measured indicating a slight loss of activity of the active molecule. This value is still in the range of common values found in literature mentioned above. From these result, the thermal treatment of 50°C applied during the

immobilization of Ciprofloxacin on CNF films should not affect the active molecule antimicrobial activity.

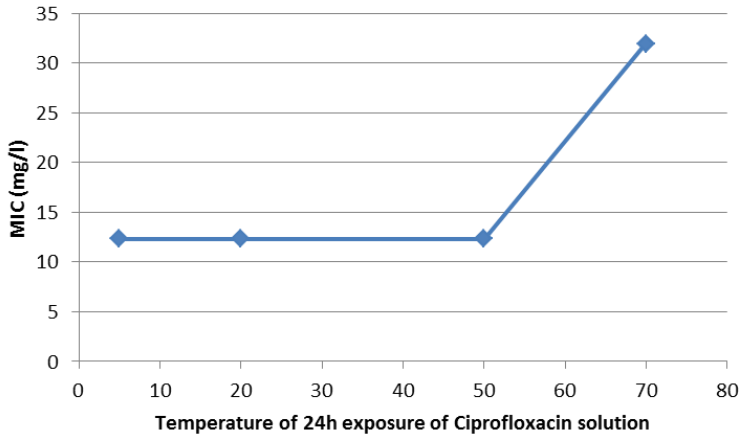

Figure II.7: MIC measurements for Ciprofloxacin solution exposed overnight to different temperatures

1.3.5. Antimicrobial activity of functionalized CNF films

Zone of inhibition test is the simplest antimicrobial activity test for 2D samples when it comes to assess qualitatively the leaching of an active compound in static conditions. CNF films were put in contact with the inoculated agar before 72h of incubation at 37°C. Figure II.8 shows the petri dish of most representative results for each sample. Picture A confirmed the growth of B. subtilis in the test conditions. Picture B confirmed the fact that Ciprofloxacin has a growth inhibition effect on B. subtilis strain: large zones of inhibitions surround the three Ciprofloxacin solution impregnated paper discs. On picture C, CNF-ref discs are fully covered with bacteria, the inset shows in addition that no contact activity is detected around or onto the discs. Finally, the picture D shows large areas of growth inhibition for CNF-Cipro samples, confirming the antimicrobial activity of functionalized CNF films. However, such zone of inhibition is surprising if we expect Ciprofloxacin to be only covalently immobilized on CNF films. This result has been confirmed with ZOI test against other bacteria strains, i.e. S. aureus and E. coli as shown on the table in Figure II.8.

The only phenomenon that can explain the presence of these large zones of inhibition is that not covalently bound Ciprofloxacin are still present in the sample, even after the washing through soxhlet extraction with acetone 99+% and deionized water. Similar observations are found in the literature when researchers grafted Nisin on oxidized cellulose nanofibrils films [30].

Ciprofloxacin is leaching out the CNF substrate and further antimicrobial testing is necessary for the evaluation of the sample activity on long term behavior and specifically on the leaching phenomenon.

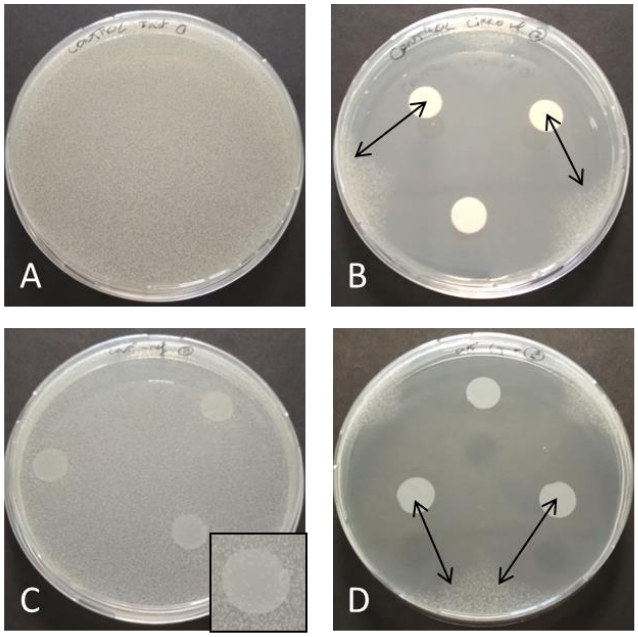

Bacteria strain type and name		ZOI radius (cm)	
		CNF-ref (C)	CNF-cipro (D)
Gram-positive	*B. subtilis*	0	2.60
	S. aureus	0	1.75
Gram negative	*E. coli*	0	2.00

Figure II.8: LEFT, zone of Inhibition testing against B. subtilis. A: negative control, B: positive control (Ciprofloxacin solution on paper discs), C: CNF-ref films, D: CNF-cipro films, and RIGHT, Zone of Inhibition radius for CNF-ref and CNF-cipro against both types of bacterial strain

The long-term activity of CNF-cipro samples was also assessed through the use of zone of inhibition testing. Four cycles of successive 24 h exposition to inoculated media were performed on CNF-cipro samples. Gram positive strain Staphylococcus Epidermidis and gram negative strain Escherichia coli were used to inoculate the agar medium on which CNF-cipro films samples were deposited. A clear zone of inhibition was detected after cycle 1 with a 1 cm radius zone of inhibition for both strains. Upon next cycle of exposition to a new inoculated medium, zones of inhibition seemed to disappear but the CNF-cipro films were still active against the two strains since underneath the sample, zones that are clear of any kind of bacterial growth were revealed as depicted on Figure II.9. A stable zone of inhibition matching the size of the disk sample is detected up to four cycles of 24h of incubation, and for both types of strains confirming the long term activity potential of CNF-cipro samples and also the contact antimicrobial activity which finally reveals indirectly the covalent immobilization of Ciprofloxacin. Indeed, if the Ciprofloxacin was only adsorbed for CNF-cipro samples, the ZOI would decrease and give the same result as CNF-ref films where bacteria are found even onto the films.

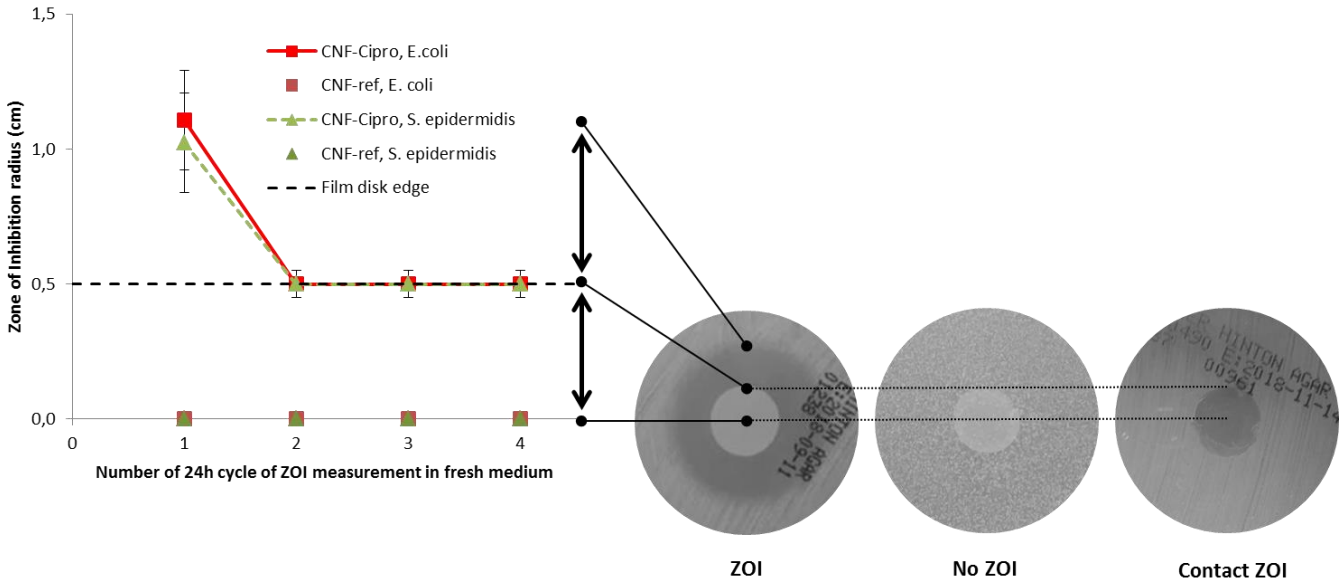

Figure II.9: Successive zone of inhibition test for CNF-ref and CNF-cipro

This result is very promising and proves that it is possible to graft APIs onto CNF film membranes to obtain long term contact active device which are suitable for topical applications. What is of particular interest is that such biocompatible membrane is equally contact active against both gram positive and gram negative bacteria strains.

1.4 Conclusions

This work reveals the possibility of strong immobilization of the fluoroquinolone Ciprofloxacin on CNF films through simple esterification reaction conducted under vacuum and in aqueous medium reaching green chemistry standards. The influence of the immobilization procedure and purification steps on CNF films structure were evaluated with SEM technique and no changes were observed. The influence of temperature on Ciprofloxacin solution and Ciprofloxacin activity was also assessed through MIC measurements in order to be sure that immobilization procedure did not affect the drug efficiency. The immobilization procedure success was proven by elemental analysis. Plus, antimicrobial activity testing proved the samples to be active against the four strains B. subtilis, S. aureus and S. epidermidis (gram-positives) and E. coli (gram-negative). Moreover, a prolonged activity shifting from release active device to contact active device over 4 days was confirmed. These results increase CNF potential for medical applications and show how versatile CNF substrates can be thanks to surface modification opportunities and film forming capacities.

2. Two-step immobilization of prodrug on TEMPO cellulose nanofibrils through thiol-yne click chemistry

This section is adapted from "H. Durand, E. Zeno, M. Demeunynck, I. Baussanne, M. Bardet, J. Vigier-Gravel, L. Emsley, N. Belgacem, J. Bras - Two-step immobilization of prodrug on TEMPO cellulose nanofibrils through thiol-yne click chemistry", submitted in Chemical Communication in November 2018

Abstract

The surface functionalization of nanocellulosic substrates is often required in order to take benefit from their outstanding properties such as high specific surface, biodegradability and biocompatibility. The potential of cellulose nanofibrils for the medical field is currently increasing. Nowadays, drug encapsulation and drug release from cellulose nanofibrils systems are intense research topics. On the other end, prodrugs that improve drug availability and tune their functionalities can now be designed. In this work, we present an ester-containing prodrug of metronidazole that is covalently bound to cellulose nanofibrils in aqueous suspension through a two-step immobilization procedure: amidation and thiol-yne click chemistry reactions are used. The presence of the drug is confirmed by several characterization tools and methods such as Raman spectroscopy, Elemental analysis, Dynamic Nuclear Polarization enhanced NMR. DNP enhanced NMR, up to our knowledge, has been used for the first time to study cellulose nanofibrils substrates and was the ultimate tool to confirm the covalent nature of the binding. The ester function of the immobilized prodrug can be cleaved by specific enzyme activity and allow for an on-site controlled drug release.

2.1 Introduction

Among cellulosic nanomaterials, cellulose nanofibrils (CNF) are considered as one of the best starting platform material for the development of unique systems. The tremendous enthusiasm in the scientific community for this material arises from the general characteristics of cellulose nanomaterials such as widespread availability, biodegradability, biocompatibility, excellent mechanical properties and tunable surface chemistry [11]. Today, such CNF can be used in several and various applications (i.e. paper and packaging [6], [12], [13], [49], electronics [50], composites [14] medical and cosmetics [18]–[21] industries) as reinforcement agent, rheology modifier or nanostructured networks and membranes. Among identified CNF grades, TEMPO oxidized CNF (CNF-t) has enhanced features such as chemical reactivity together with specific rheological properties, both explained by the presence of carboxylic acid moieties along the cellulose nanofibers.

Industrial production of CNF-t is under development in different places of the globe. Pioneer research investigations on TEMPO oxidation of cellulose by the group of Professor Akira Isogai in Japan [51], [52] led to the apparition of CNF-t production facilities while in Europe and North America, small companies are starting to sell CNF-t.

The growing production facilities come along with novel and promising applications of CNF-t such as the biomedical field. A couple of reviews deal with the use of CNF-t (together with other cellulose nanomaterials) for biomedical application and describe the potential of this material for the design of new innovative healthcare systems [18], [20], [53]. CNF-t draws specific attention since it is possible to produce it in an ultrapure form with low endotoxin content making them suitable for wound healing when freeze-dried into aerogels: Low cytotoxicity was also confirmed in addition with really high water holding capacity [54]. Hydrogels of CNF-t were also crosslinked with diamines of different carbon chain length by exploiting the aldehydes groups produced with the TEMPO-mediated oxidation through Schiff base formation. Researchers were able to control the elastic modulus and transform reversible hydrogels into irreversible hydrogels. Such systems are of particular interest in the tissue engineering field [55].

CNF-ts were also investigated to be used as drug carriers. The ability to deliver Ibuprofen through the skin from CNF-t-Ibuprofen gel formulations was assessed *in-vitro* and *in-vivo* against commercial available solutions. CNF-t systems were able to match with commercial references while including five times lower drug loading proving a more efficient and optimized use of drug [56]. Aerogels of different kind of cellulose nanofibrils suspensions mixed with beclomethasone dipropionate (BDP) nanoparticle coated with hydrophobin proteins were also produced through freeze drying. CNF-t

based systems showed a sustained drug release. The CNF three-dimensional structure was tunable by varying the freeze drying parameters allowing for a controlled release of the drug [57].

Metronidazole is part of the nitroimidazole antibacterials. It is used to fight diseases concerning different organs and especially in gastrointestinal tract and reproductive system, mainly against anaerobic micro-organisms. The mechanism of action of metronidazole involves the penetration into the anaerobic bacteria and its chemical transformation (reduction) by proteins to an active product that will cleave DNA strands and thereby inhibits the replication mechanism and prevent cell growth [58], [59]. Since the 1980's, Metronidazole have been successfully used with cellulose derivatives tableting compounds such as hydroxypropyl methyl cellulose [60], methyl cellulose [61] and cellulose acetate phthalate [62].

Recently, lignin-containing and delignified cellulose fibers were used to produce partially fibrillated microcrystalline cellulose that was investigated to develop drug release system. Stable hydrogel-like materials were obtained thanks to the entanglement of the available micro and nanofibrils as confirmed by rheological studies. Metronidazole was encapsulated in such materials and drug release studies were performed. It was shown that both viscosity and lignin content of the hydrogel-like material influenced the release dynamics. As a conclusion such matrix carriers emerged as interesting alternatives to previously cited cellulose derivatives [63]. Up to our knowledge, only one publication deals with the use of CNF-t and metronidazole. CNF-t hydrogels were used as matrix for encapsulation of 6 different active principle ingredients, including metronidazole. Researchers investigated the effect of freeze drying and subsequent rehydration on rheological properties and the drug release profiles. Results suggested that the CNF-t hydrogels were successfully rehydrated and release profiles were equivalent, before and after freeze drying, confirming their potential for controlled release applications [64].

These uses of metronidazole relied only on physical adsorption of the drug onto the cellulosic substrates. Micro and nanosized three dimensions structures of the developed systems allowed for a diffusion-controlled release mechanism. The purpose of this work is to investigate a complementary anchoring strategy of the drug to the cellulosic substrates. The covalent immobilization of metronidazole on CNF-t surface is expected to allow for a better control of the release with an "on-demand" release thanks to the presence of esterase in infected zones of living tissues. For this purpose, a prodrug will be designed with metronidazole: a cleavable ester bond and a reactive thiol group for anchoring will be introduced on metronidazole. The prodrug will thus bind to CNF-t by reaction of the thiol group. The presence of ester will allow the liberation of the drug by ester-specific enzymes (present in fat tissues and on infection sites [65]) on the targeted site of treatment.

To achieve this goal, efficient chemical modification of the CNF surface is required. It should be noted that surface modification of CNF is still an intense and challenging field of research. The very large specific surface area of CNF, together with their high amount of reactive hydroxyls, or carboxylic acid groups in the case of CNF-t, lead to a wide range of strategies for surface modifications. Reactions such as etherification, esterification, silylation and amidation have been performed to covalently bind small molecules or polymer chains to CNF as described in relevant reviews [66]–[68]. The use of sustainable materials such as CNF goes hand in hand with the increasing need for low-environmental impact processes and green chemistry procedures for CNF surface functionalization. In this context, click chemistry is of particular interest. Sharpless et al. introduced in 2001 the concept of click chemistry that gathers reactions that are efficient, stereospecific, modular, requiring simple conditions (not sensible to oxygen and water), and results quickly in very high yields while involved reagents must be readily available [69]. Click chemistry was seldom used to modify cellulosic nanofibrils. CuAAC and thiol-ene click chemistry were applied to CNF films in order to immobilize fluorescent compounds [70], [71]. So far, thiol-yne strategy has not been attempted with CNF. In this work a multistep covalent immobilization of metronidazole through amidation and thiol-yne click chemistry were performed in order to covalently bind the prodrug, i.e. thiol-metronidazole, to the CNF as described on Figure II.10. To our best knowledge this work constitutes the first example of a sophisticated strategy towards active on-demand CNF based materials.

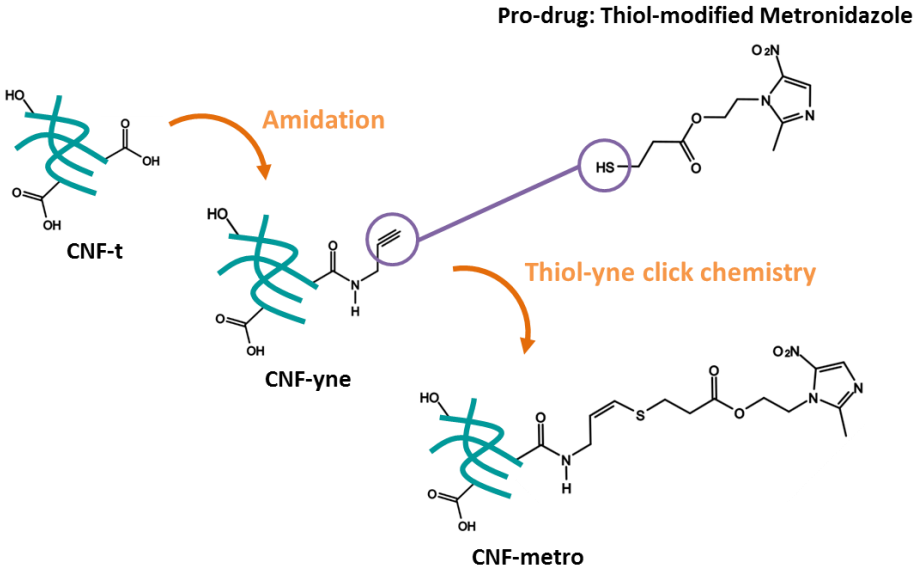

Figure II.10: General multistep immobilization procedure of thiol modified metronidazole prodrug on CNF-t. Note that thiol-yne click reaction can give a double addition of thiol compound. However, due to steric hindrance, the second addition is less likely to happen so that only the "one-addition" product is depicted.

2.2 Experimental procedure

2.2.1. Materials

The cellulose nanofibrils (CNF) suspensions were provided by the Centre Technique du Papier (CTP, Grenoble, France). A first suspension referred as CNF-e was produced by a 2h enzymatic pre-treatment of a pre-refined (40°SR) bleached birch pulp followed by homogenization: 3 passes at 1500 bars in an Ariete homogenizer from GEA. The second suspension, which is referred as CNF-t, was also produced the Centre Technique du Papier (CTP, Grenoble, France). The TEMPO mediated oxidation was performed on a pre-refined (40°SR) bleached bisulfite pulp provided by TEMBEC following classical procedure developed by A. Isogai's team in the end of 2000s [51], [52]. The cellulose fiber pulp concentration was set at 1.5 wt% and the pre-treatment was done at pH 10 for 2h and involved NaBr, NaClO and the TEMPO reagent. The oxidized pulp was then subjected to the high pressure homogenizer (GEA Niro Soavi) to produce the CNF-t suspension (1.7 mmol/g of carboxyl groups, as presented later on).

Propargyl-amine (CAS: 2450-71-7), propargyl-bromide (CAS: 106-96-7), N-(3-dimethylaminopropyl)-N'-ethylcarbodiimide hydrochloride (EDC, CAS: 25952-53-8), N-hydroxysuccinimide (NHS, CAS: 6066-82-6), sodium hydroxide (NaOH, CAS: 1310-73-2), and hydrogen chloride (HCl, CAS: 7647-01-0) 4-(dimethylamino)pyridine (DMAP, CAS: 1122-58-3), N,N-Dicyclohexylcarbodiimide (DCC, CAS: 538-75-0), trifluoroacetic acid (TFA, CAS: 76-05-1), triisopropylsilane (TiPS, CAS: 6485-79-6) were purchased from Sigma Aldrich and used as received. Isopropanol (CAS: 67-63-0) was purchased from ACROS Organics. Tris(2-carboxyethyl)phosphine hydrochloride (TCEP, >98 %, CAS: 51805-45-9) was purchased from ThermoFisher Scientific. Biocompatible photoinitiator lithium phenyl(2,4,6-trimethylbenzoyl)phosphinate (LAP, >98 %, CAS: 85073-19-4) was purchased from Tokyo Chemical Industry. The biradical 15-{[(7-oxyl-3,11-dioxa-7-azadispiro[5.1.5.3]hexadec-15-yl)carbamoyl][2-(2,5,8,11-tetraoxatridecan-13-ylamino)}-[3,11-dioxa-7-azadispiro[5.1.5.3]hexadec-7-yl])oxidanyl (AMUpol) was obtained from ICR (Aix-Marseille University, UMR7273, France). Deionized water was used for every experiment.

2.2.2. Methods

2.2.2.a. Alkynation of CNF-t through amidation

The CNF-t suspension concentration was decreased from 1.5 wt% to 0.4 wt% in order to be easily stirrable. Deionized water was added before homogenization with an IKA Ultra-Turrax high shear mixer (China) for 1 minute at 10 000 rpm. The pH of the suspension was then adjusted to 4 under magnetic stirring using a 0.5 M HCl solution.

A solution of the coupling agents EDC and NHS was prepared in deionized water. After complete dissolution the solution was added to the suspension of CNF-t. A molar ratio of 4 equivalents of EDC and NHS for 1 equivalent of carboxyl group of CNF-t was used. The mixture was magnetically stirred for 30 min at room temperature in order to activate the carboxyl groups of the CNF-t. The pH was maintained at 4 during the reaction with 0.5M HCl or NaOH solution droplets addition. This pH favors the EDC carbocation availability and acid form of the carboxyl groups that are both required for a more efficient reaction.

The pH was then increased with 0.5M NaOH solution to 8.5 for the second part of the reaction i.e. the amine addition. A solution of propargyl amine was prepared in deionized water and added to the mixture. Again, a molar ratio of 4 equivalents for 1 equivalent of carboxyl groups of CNF-t was used. The mixture was magnetically stirred for 72h at room temperature and the pH was kept at 8.5 with 0.5M HCl or NaOH solution droplets addition.

After 72h of reaction, the mixture was washed by centrifugation and dialysis. First, the reaction was quenched by decreasing the pH to 2-2.5 with 0.5M HCl solution. Then, centrifugation – re-dispersion cycles were applied to the suspension: centrifugations were operated during 10 minutes at 20 000 g (about 11 100 rpm) and re-dispersions were done in acidic water (pH 2-2.5) in order to remove all the non-covalently bound chemicals (EDC, NHS and free amine). In between each centrifugation cycle, re-dispersions were done using high shear mixer (Ultra-turrax, IKA) for 1 min. A total of 6 centrifugation – re-dispersion cycles were performed to ultimately isolate the alkyne modified CNF-t, referred as CNF-yne. The last dispersion was done in neutral water.

The last step of purification consisted in a dialysis of the CNF-yne suspension against neutral water with 6-8 kDA MWCO membranes (Spectra/Por® 1 Standard RC Tubing, SPECTRUM) for at least 5 days under slow magnetic stirring and renewal of the medium twice a day.

2.2.2.b. Synthesis of Metro-SH compound

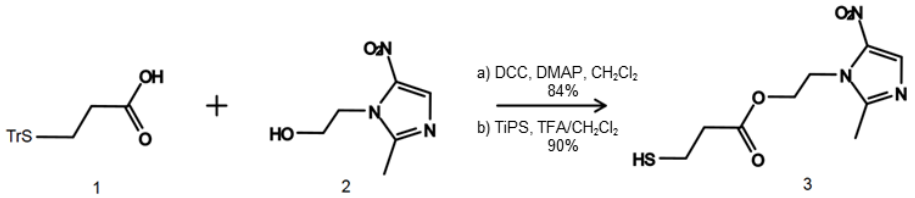

Figure II.11: Synthesis path of metronidazole-thiol (3) from metronidazole (2) and S-trityl-3-(mercaptopropionic acid (1)

S-Trityl-3-mercaptopropionic acid was synthesized according to a procedure designed by Sharma et al [72]. This product **1** (1050 mg, 3.0 mmol), metronidazole **2** (467 mg, 2.7 mmol) and DMAP (24 mg,

0.2 mmol) were dissolved in 30 ml of CH_2Cl_2 at 0°C. DCC (618 mg, 3.0 mmol) was added in the solution after 15 minutes. The reacting mixture was stirred during 3 h at room temperature, then filtered and concentrated under vacuum. The crude product was purified by flash chromatography on silica gel with CH_2Cl_2 as eluent to give the protected compound as a white solid (1.15 g, 2.3 mmol, 84 %). 1H NMR (400 MHz, CDCl3) δ 7.86 (s, 1H, CH imidazole), 7.33-7.31 (m, 6H, CH arom.), 7.22-7.19 (m, 6H, CH arom.), 7.15 (m, 3H, CH arom.), 4.45 (t, J = 5.2 Hz, 2H, OCH2), 4.29 (t, J = 5.2 Hz, 2H, NCH2), 2.36 (t, J = 7.2 Hz, 2H, CH2CO), 2.35 (s, 3H, CH3), 2.07 (t, J = 7.2 Hz, 2H, SCH2); 13C NMR (101 MHz, CDCl3) δ 171.3, 150.8, 144.7, 144.5, 133.2, 129.6, 128.0, 127.9, 126.8, 126.7, 67.0, 62.7, 45.0, 33.4, 26.6, 14.4.

The tritylated compound was dissolved at 0°C in 30 ml of CH_2Cl_2 and 15 ml of TFA. After 10 minutes, TiPS (1 ml, 4.87 mmol, 2 equiv.) was added to the solution that was allowed to warm up to room temperature and stirred for 1 h. The solution was concentrated under vacuum and the TFA was co-evaporated twice with methanol. The residue was washed three times with cold cyclohexane and dried under vacuum. The amorphous solid was purified by flash chromatography on silica gel with CH_2Cl_2/MeOH: 97/3 as eluent to give the compound **3** (see Figure II.11) as a rosy amorphous solid. (568 mg, 95 %).

2.2.2.c. Immobilization of Metro-SH on CNF substrates through thiol-yne click chemistry

Metro-SH **3** (62.5 mg, 0.25 mmol) was dissolved in a mixture of 15 g deionized water and ethanol (50:50 v/v ratio). To this solution was added 5 ml of deionized water containing a 5 % molar ratio relative to the thiol groups of **3** of tris-(2-carboxyethyl)phosphine (TCEP) to prevent the air oxidation of the thiol into disulfide, and lithium phenyl(2,4,6-trimethylbenzoyl)phosphinate (LAP), a biocompatible photoinitiator required to activate the thiol-yne click reaction, at a quantity of 0.01 wt% relative to the CNF-yne mass. Then the resulting mixture was added to the CNF-yne suspension. The whole mixture was transferred to a UV transparent two necked balloon and put under magnetic stirring. The suspension was exposed to UV radiation with a UV lamp (Fire Edge™ FE300, Phoseon Technology USA, wavelength 345-385nm) and a nitrogen flux was used to remove the dioxygen from the free volume of the balloon. The UV-exposure and nitrogen flux were maintained for 4 h. The modified CNF (CNF-Metro), was purified by several centrifugation – re-dispersion steps as described before: three steps of washing with water/ethanol mixture (50/50 v/v) and two steps with deionized water only. Washed suspensions were further purified by dialysis against deionized water under slow magnetic stirring for 5 days with daily renewal of dialysis medium in order to completely remove non-covalently bound compounds. Dialysis membranes were 6-8 kDA MWCO membranes (Spectra/Por® 1 Standard RC Tubing, SPECTRUM). CNF-Metro suspensions were stored in the fridge

at 5°C before characterization. The corresponding CNF films were produced by solvent casting in Teflon molds and let dry overnight in an oven at 40°C, these films were used for solid state characterization.

2.2.2.d. Infrared spectroscopy, ATR mode

Fourier Transformed Infrared (FTIR) spectra of the films were obtained on a Perkin Elmer Spectrum One spectrometer (Waltham, Massachusetts, USA) in attenuated total reflectance (ATR) mode. At least 5 measurements of 16 scans with a resolution of 2cm^{-1} between 600 and 4000 cm^{-1} on each side of the CNF films were performed. Spectra were normalized at 1110 cm^{-1}, the approximate wavenumber of C-O-C bonds in cellulosic substrates. The most representative spectra were chosen for discussion.

2.2.2.e. Raman spectroscopy

Raman spectra were recorded on a Renishaw (INVIA, UK) spectrometer equipped with a 1200 lines/mm grating and a CCD detector. Excitation wavelength was 785 nm and the beam power was adjusted to avoid sample degradation. The incident beam was focused on the samples through an x50 ultra-long working distance objective which resulted in a spot size of an approximate diameter of 2 µm. The spectra were recorded between 0 and 3600 cm^{-1}.

2.2.2.f. Conductometric titration and *DO/DS* calculation

The carboxylic content of the CNF-t suspension was measured before and after the first step of functionalization by conductometric titration. The amount of CNF-t suspension corresponding to 50 mg of dry material was precisely diluted to 200 ml with de-ionized water. Magnetic stirring and high shear mixer Ultra-Turrax (IKA) were used to produce a homogeneous dispersion. The pH was decreased around 2.5 with 0.1 M HCl to turn every remaining carboxylate moieties of CNF surface into the acid form of the carboxylic acids, and the volume of added HCl solution was recorded. The titration was done with a 0.01 M NaOH solution, which precise concentration was measured with 3 colorimetric titrations before the titration of the CNF suspensions. The conductivity of the suspension was recorded after stabilization of the value. NaOH added volumes were reduced when the curve indicated changes in order to improve the assessment of the transitions. The titration curves typically display three regions, a first slope showing the decrease of the conductivity that corresponds to the neutralization of the remaining strong acid, a plateau where the weak acid groups are titrated (carboxylic groups of CNFs) and a last part where conductivity increases when all acids are titrated.

The degree of oxidation (*DO*) represent the number of carboxylic groups per anhydroglucose unit (AGU) on oxidized CNF. It can be calculated with equation (II-2) according to Da Silva Perez et al. [73].

$$DO = \frac{162 \times C \times (V_{eq1} - V_{eq2})}{m - 36 \times C \times (V_{eq1} - V_{eq2})} \quad \textit{(II-2)}$$

The value of 162 (g/mol) is the molar mass of the AGU. The precise concentration of the NaOH solution is *C*. The CNF dry quantity is *m*. The value 36 (g/mol) is the difference between the molar mass of the carboxylate form of the carboxylic groups including the sodium counter ion (198 g/mol) and the molar mass of the AGU (162 g/mol). This term arises from the partial replacement of primary hydroxyl groups by carboxylate groups during the TEMPO mediated oxidation process. The two NaOH solution equivalent volumes V_{eq1} and V_{eq2} are extracted at the edge of the plateau on the titration curve by calculating the intersections of the first (decreasing slope) and third (increasing slope) part of the curve with the plateau.

The carboxylic group content X_{ox} on CNF-t can be calculated with equation (II-3).

$$X_{ox} = \frac{C \times (V_{eq1} - V_{eq2})}{m} \quad \textit{(II-3)}$$

The terms are the same used in equation (II-2) and X_{ox} is expressed in micro-mole of carboxylic group per gram of dry CNF (µmol/g).

After the amidation reaction with propargyl amine, the remaining carboxylic groups were also quantified by conductometric titration and the residual degree of oxidation DO_{res} was calculated with equation (II-4) by integrating the molecular weight M of the propargylamine and the same previous terms as it was done before for amidation on CNC [74].

$$DO_{res} = \frac{(162 + (M - 40) \times DO) \times C \times (V_{eq1} - V_{eq2})}{m - (M - 40) \times C \times (V_{eq1} - V_{eq2})} \quad \textit{(II-4)}$$

The value 40 (g/mol) correspond to the loss of sodium and oxygen atoms on CNF and hydrogen atom from the amine group of propargyl amine.

While equation (II-3) was used to characterize CNF-t before the amidation reaction to calculate the quantities of required chemicals, equations (II-2) and (II-4) were used to compare the *DO* before and after the amidation reaction. The proportion of carboxylic groups ($\%COOH_{conv.}$) that was converted during the amidation reaction can thus be assessed with equation (II-5).

$$\%COOH_{conv.} = \frac{DO - DO_{res}}{DO} \times 100 \quad \textit{(II-5)}$$

All titrations were repeated at least three times.

From the values of X_{ox} and $\%COOH_{conv}$ it was possible to calculate a degree of substitution based on conductometric titration measurements DS_{cond}. By considering one gram of dry CNF-t, X_{ox} give access

to the molar quantity of oxidized anhydroglucose units (AGU) before amidation and so, non-oxidized AGU mass can be determined by subtraction (*n[AGU-OH]*). Through amidation of CNF-t, only oxidized AGU will react and $\%COOH_{conv}$ gives access to the molar quantity of converted oxidized AGU (*n[AGU-YNE]*) and non-reacted oxidized AGU ($n[AGU\text{-}COOH_{nr}]$) by subtraction again. Equation (II-6) gives the degree of substitution:

$$DS_{cond} = \frac{n[AGU-YNE]}{n[AGU-OH] + n[AGU-COOH_{nr}] + n[AGU-YNE]} \qquad \textbf{(II-6)}$$

where

$$n[AGU-YNE] = \%COOH_{conv.} \times X_{ox}$$

$$n[AGU-OH] = \frac{1 - X_{ox} \times M_{AGU-COOH}}{M_{AGU-OH}}$$

$$n[AGU-COOH_{nr}] = 1 \times X_{ox} - n[AGU-YNE]$$

with $M_{AGU\text{-}COOH}$ the molar mass of an oxidized AGU (176.1 g/mol), $M_{AGU\text{-}OH}$ the molar mass of an AGU (162.1 g/mol). In $n[AGU\text{-}COOH_{nr}]$ formula, the dimension of the figure 1 is a mass, one gram of modified CNF is considered for the DS_{cond} calculation.

2.2.2.g. Elemental analysis

CNF films were prepared by solvent casting from CNF suspensions. The suspensions were poured into Teflon molds and evaporated overnight in an oven at 40°C. Elemental Analysis (EA) was performed on a vario Micro Cube device from Elementar. Carbon, Hydrogen, Nitrogen, Sulfur and Oxygen mass proportion of CNF films were measured. Films pieces of 4 to 7 mg were weighted on a *micro-balance*. An average of four measurements was made for each sample. A degree of substitution from elemental analysis (DS_{EA}) was then calculated based on the detection of the increase of Nitrogen content from the CNF-t film to the CNF-yne film. Equation (II-7) was used.

$$DS_{EA} = \frac{162{,}1406 \times \%N}{n(N\ in\ grafted\ mol) \times M(N) - M(grafted\ mol) \times \%N} \qquad \textbf{(II-7)}$$

where 162.1406 is the precise molar mass of anhydro-glucose unit (AGU), *%N* the mass proportion of nitrogen detected by elemental analysis, *n(N in grafted mol)* the number of nitrogen atom in the grafted molecule (i.e. propargylamine), *M(N)* the molar mass of nitrogen, *M(grafted molecule)* the molar mass difference between grafted and non-grafted AGU. This DS_{EA} represents the quantity of AGU modified with a propargylamine molecule within the bulk material.

2.2.2.h. Atomic force microscopy

Atomic force microscopy (AFM) images were recorded on a Dimension icon® (Bruker, USA). The suspension concentration was adjusted at $7.5x10^{-4}$ wt% by several dilution of the gel using high shear mixer Ultra-Turrax (IKA). A drop of this suspension was deposited on freshly cleaved mica plate before drying overnight under fumehood at room temperature. The acquisition was performed in tapping mode using a silica coated cantilever (OTESPA® 300 kHz – 42 N/m, Bruker, USA). Zones of 3,3*3,3 µm² were analyzed.

2.2.2.i. Liquid ^{1}H and ^{13}C nuclear magnetic resonance

In liquid nuclear magnetic resonance (NMR) analysis was performed at DPM on the prodrug in order to confirm its chemical structure. ^{1}H and ^{13}C NMR spectra were obtained at 400 and 101 MHz respectively, using a Bruker Advance DRX 400 spectrometer. Solvent residual peaks were used as reference and calibrated as follows; CDCl3: 7.26ppm; MeOD-d4: 3.31ppm; DMSO-d6: 2.50 ppm.

J-modulated (JMOD) spin echo sequence was applied to ^{13}C NMR spectra in order to obtain quaternary and secondary carbons signal with an opposite phase to those of primary and tertiary carbons.

2.2.2.j. Solid state ^{13}C nuclear magnetic resonance

Solid state ^{13}C nuclear magnetic resonance (^{13}C ssNMR) analyses were performed at the « Institute for Nanoscience and Cryogenics (INAC) » in the «French Alternative Energies and Atomic Energy Commission (CEA) » at Grenoble, on a Bruker AVANCE400 spectrometer. Acquisition, data treatment and peaks deconvolution were done using the LINUX TopSpin 3.2 software. Samples were placed in 4 mm ZrO2 rotors. All spectra were recorded using a combination of cross-polarization, high power proton decoupling and magic angle spinning (CP/MAS). ^{13}C NMR spectra were acquired at 298 K, with a 4 mm probe operating at 100.13 MHz. The chemical shift values were measured with respect to TMS via glycine as a secondary reference with the carbonyl signal set to 176.03 ppm. MAS was performed at 14 kHz. The number of scans was 15 000 with a recycle delay of 2 s and CP time of 1.5 ms.

2.2.2.k. Dynamic nuclear polarization enhanced nuclear magnetic resonance

Dynamic nuclear polarization enhanced nuclear magnetic resonance (DNP-NMR) experiments were performed on a 263 GHz/400 MHz AVANCE III Bruker DNP system. The spectrometer is equipped with a low temperature MAS probe and a 263 GHz capable of outputting ca. 5-10 W of CW microwaves. The probe was configured in double mode 1H/13C. The sweep coil of the main magnetic field was optimized so that microwave irradiation gave the maximum positive proton DNP enhancement for AMUPol (a biradical polarizing agent). DNP enhancements were determined by

comparing the intensity of the spectra acquired with and without microwave irradiation, and the ^{1}H and ^{13}C enhancements are tabulated in the supporting information (SI) for all samples studied.

DNP enhanced ^{1}H and ^{13}C Solid-State NMR

For ^{13}C NMR experiments, the recycle delays were 3 or 4 s. The ^{1}H π /2 pulse length used for the variable amplitude CP experiments was 2.5 µs to afford 100 kHz ^{1}H decoupling using SPINAL-64. The contact time was typically 5 ms. The MAS frequency used is 12.5 kHz.

For DNP experiments, 30 mg of sample is impregnated with 16 µl of 10 mM AMUPol in D_2O/H_2O (9/1 v/v). The DNP sample is then packed in a 3.2 mm sapphire rotor and capped with a Teflon plug and zirconia cap. The filled DNP rotor was then spun at room temperature in the spinning station up to 12.5 kHz before being inserted into the pre-cooled (ca. 100 K) 3.2 mm low temperature MAS NMR probe, where the sample is frozen within a few seconds.

For the 1D and 2D INADEQUATE experiments the corresponding sequences are those of TOPSPIN, the NMR software proposed by Bruker Corporation. The 2D INADEQUATE, SQ-2Q 13C-13C, is the version proposed by Lesage et al. adding DNP conditions [75]. The number of scans was set to 64 and the number of experiments in the indirect dimension to 128 and the recycling delay to 3s leading to an experiment time in the range of height hours.

2.3 Results and discussions

2.3.1. Characterization of CNF materials

Considering the numerous commercially available CNF types and the wide variety of lab-scale produced CNF, it is of high importance to precisely describe the properties and characteristics of the CNF that are used in this work. Cellulose nanofibrils suspensions are often a mixture of nanoscale particles, microfibrillated fibers, aggregates and residual fibers. The objective is to better know the starting material and be able to draw relevant conclusions from the presented results.

The CNF-t suspension that was produced by the CTP has a thick transparent gel appearance at 1.6 wt% concentration as shown in Figure II.12. AFM images of the low concentrated CNF-t suspension were also recorded in order to confirm the nanosize morphology of cellulose nanofibrils.

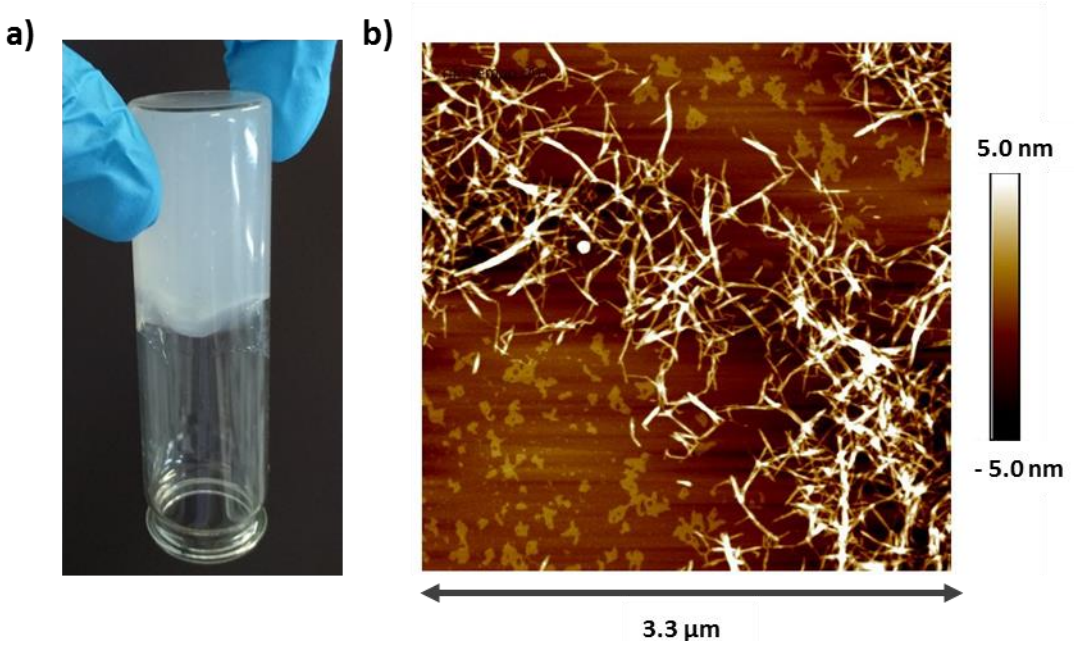

Figure II.12: CNF-t suspension appearance and morphology on a) a picture of the 1.6 wt% gel and b) an AFM height sensor image of a 1.5x10^{-4} wt% suspension

In order to assess the chemical reactivity of the CNF-t suspension, conductometric titration was performed to measure the degree of oxidation *DO* and initial carboxylic acid group content X_{ox}. A degree of oxidation of 29.9 % and quantity of 1.7 mmol/g ± 0.1 was detected, which confirmed the high surface charge due to TEMPO-mediated oxidation.

2.3.2. Prodrug characterization

The prodrug compound structure was confirmed by liquid ^{1}H and ^{13}C NMR analysis. As shown in Figure II.13, the full attribution of the carbon signals was successful and consistent with the expected chemical structure of the compound. The JMOD sequence revealed the presence of -C-H and –CH_3 carbons as negative signals (C8 and C7). Regarding the ^{1}H NMR, here are the main peak detected: δ 7.98 (s, 1H, CH imidazole), 4.61 (t, J = 4.8 Hz, 2H, OCH2), 4.43 (t, J = 5.2 Hz, 2H, NCH2), 2.68-2.63 (m, 2H, SCH2), 2.57 (s, 3H, CH3), 2.58-2.53 (m, 2H, CH2CO), 1.53 (t, J = 8.0 Hz, 1H, SH).

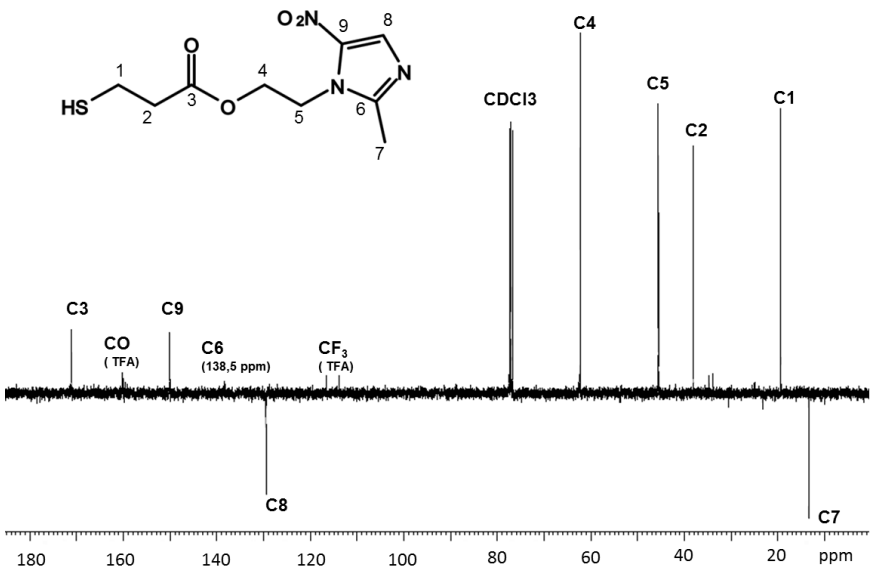

Figure II.13: Liquid ^{13}C NMR spectrum of thiol modified metronidazole and carbon attributions, TFA related detected carbons is a reaction intermediate, $CDCl_3$ is the solvent for NMR analysis. The structure is also confirmed with ^{1}H NMR (not shown).

2.3.3. First step: Introduction of alkyne function through amidation

The amidation reaction was performed on the CNF-t gel. After purification procedures, characterization of the grafting was possible, first by analyzing the resulting CNF-yne suspension and then dry films produced by solvent casting. The residual carboxylic acid content (DO_{res}) was determined by conductometric titration after the amidation reaction. A value of 9 % of residual carboxylic acid groups was detected (see Figure II.14) that gives, thanks to equation (II-4) and (II-5) a total of 68.8 % of initial carboxylic acid groups converted to amide function ($\%COOH_{conv.}$). This first quantitative result indicates that more than two-third of the carboxylic acid moieties reacted to become amide group. The degree of substitution DS_{cond} based on conductometric titration was calculated with equation (II-6) and was found to be $DS_{cond} = 0.19$. The CNF-yne suspension was then evaporated in Teflon molds in order to perform complementary characterizations.

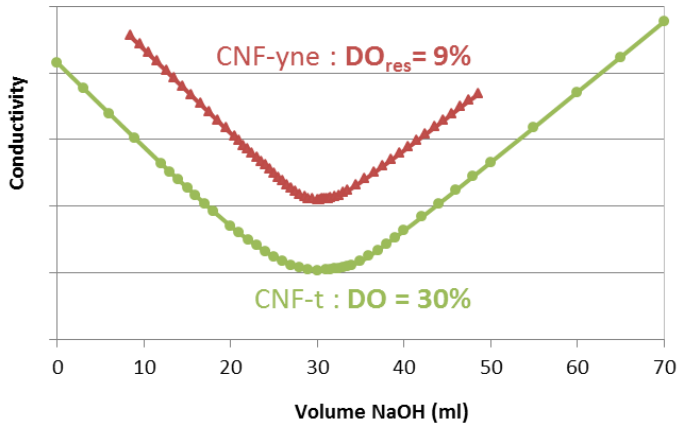

Figure II.14: Conductometric titration of CNF-t and CNF-yne (axis values are not shown since curves have been shifted for clarity)

Chemical structure of the resulting CNF-yne dry films was investigated through FTIR spectroscopy in ATR mode. The surface of the films was then analyzed in order to reveal new chemical bonds. Figure II.15 shows FTIR spectra of CNF-t, CNF-yne and CNF-metro. The three spectra showed classical peaks for cellulose backbone: stretching of O-H and C-H bonds around 3300 cm^{-1} and 2900 cm^{-1}, C-O-C glycosidic bond stretching at 1160 cm^{-1} and C-O bonds at 1100, 1050 and 1030 cm^{-1}[76]. CNF-t IR spectrum also showed two clear peaks at 1602 cm^{-1} and 1715 cm^{-1} which were respectively associated with C=O of carboxylate and carboxylic acid groups.

The pH of the CNF-t suspension was adjusted to 3 before producing films for analysis, which explains the presence of carboxylic acid signal. CNF-yne also showed the same peaks but with a lower intensity. Moreover, another peak arising around 1655 cm^{-1} was attributed to the C=O bond of amide I function, and a weak signal around 1550 cm^{-1} was due to the C-N bond of amide I function [74]. These data qualitatively proved the successful amidation reaction. Recent papers on amidation of CNF-t showed similar behavior in FTIR experiments and based their main conclusions on this characterization tool [77]. In our case, as the peak shifts were limited, complementary characterizations were performed.

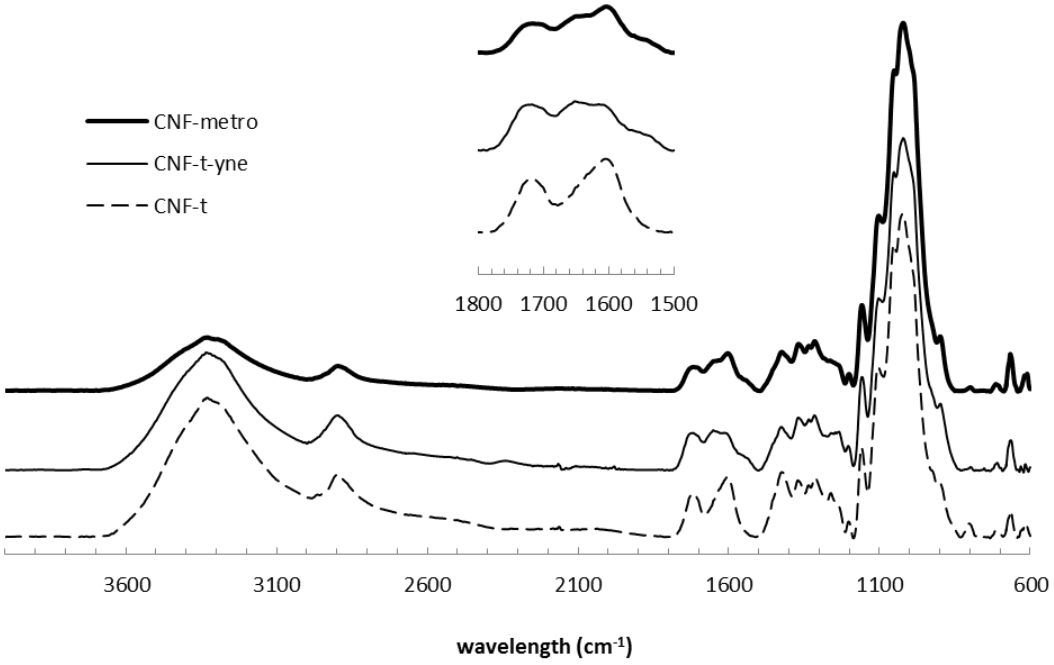

Figure II.15: FTIR-ATR spectra of CNF-t, CNF-yne and CNF-Metro

While FTIR spectroscopy relies on the study of absorption or transmission of light in a wide range of wavelengths, Raman spectroscopy relies on the study of the inelastic scattering of a specific wavelength light beam. This technique is complementary to the FTIR spectroscopy because some chemical bonds are much more active in Raman spectroscopy and could hardly be detected with FTIR spectroscopy and vice versa, especially when the proportion of the expected bond is low. This is the

case of alkyne bonds, which appeared to be more sensitive to Raman spectroscopy than in FTIR [78]. The Raman spectroscopy spectra are shown on Figure II.16. Both spectra showed characteristic peaks of cellulosic materials: C-H stretching at 2900 cm^{-1} and C-O bridges around 1100 cm^{-1} [79]. On CNF-t spectrum, the peak at 1660 cm^{-1} referred to the C=O of carboxylic acid groups. A clear signal appearing at 2120 cm^{-1} was attributed to the C≡C bond on the grafted propargyl-amine moiety [78]. This signal was not detected on the ATR-FTIR spectra. Moreover, the signal of the C=O of the carboxylic acid was slightly flattened indicating its partial conversion to amide group. This RAMAN spectroscopy analysis further confirmed the success of the amidation.

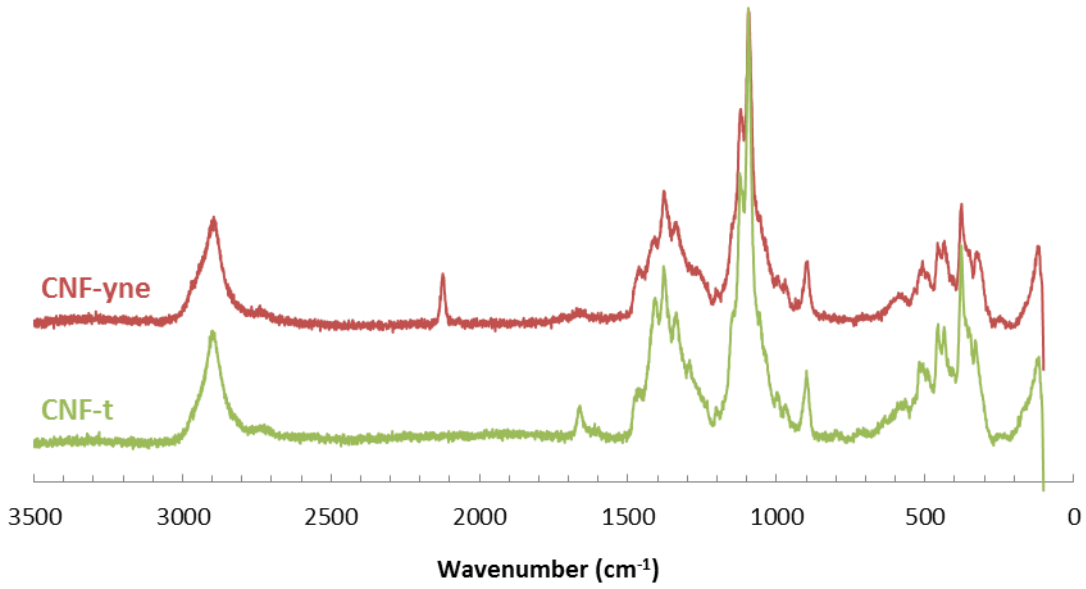

Figure II.16: RAMAN spectra of CNF-t and CNF-yne

Together with previously described conductometric titration, elemental analysis provided a second quantitative result which also confirmed grafting. Carbon, hydrogen, nitrogen and sulfur mass proportion were measured for each samples (Table II.2). The amidation reaction introduces a nitrogen atom on the cellulosic substrate, this element is thus more relevant to track. In Table II.2 we can see a significant increase of the nitrogen mass proportion for the CNF-yne sample. Coupling agents EDC and NHS also contain nitrogen in their molecular structures but it is proven to be insignificant thanks to thorough purification steps. The increases in carbon and hydrogen mass proportions also suggested the success of the grafting. The degree of substitution DS_{EA} was calculated according to equation (II-7) and gave a value of 0.14 which is slightly lower than the value DS_{cond} extracted from conductometric titration (0,19), but still in a very close order of magnitude.

Table II.2: Elemental analysis results for carbon, hydrogen, nitrogen and sulfur mass proportion of the various CNF samples

	% C	*sd*	% H	*sd*	% N	*sd*	% S	*sd*
CNF-t	**37,04**	*0,02*	**5,34**	*0,18*	**< 0,10**	-	**< 0,10**	-
CNF-yne	**40,59**	*0,13*	**5,69**	*0,22*	**1,15**	*0,05*	**< 0,10**	-
CNF-metro	**40,99**	*0,04*	**6,02**	*0,09*	**1,42**	*0,03*	**0,37**	*0,01*

Solid state NMR was also used to identify the composition of CNF-t and CNF-yne. The signals of solid state ^{13}C NMR are displayed on Figure II.17. The carbons contributions of the cellulose backbone are clearly identified on CNF-t spectrum. The intense peak between 100 and 110 ppm was attributed to C1, both peaks around 80-90 ppm come from the amorphous (right) and crystalline (left) C4. Carbon C2, C3 and C5 gave the intense peaks around 70-80 ppm while the peaks around 60 ppm were attributed to the C6 [80].

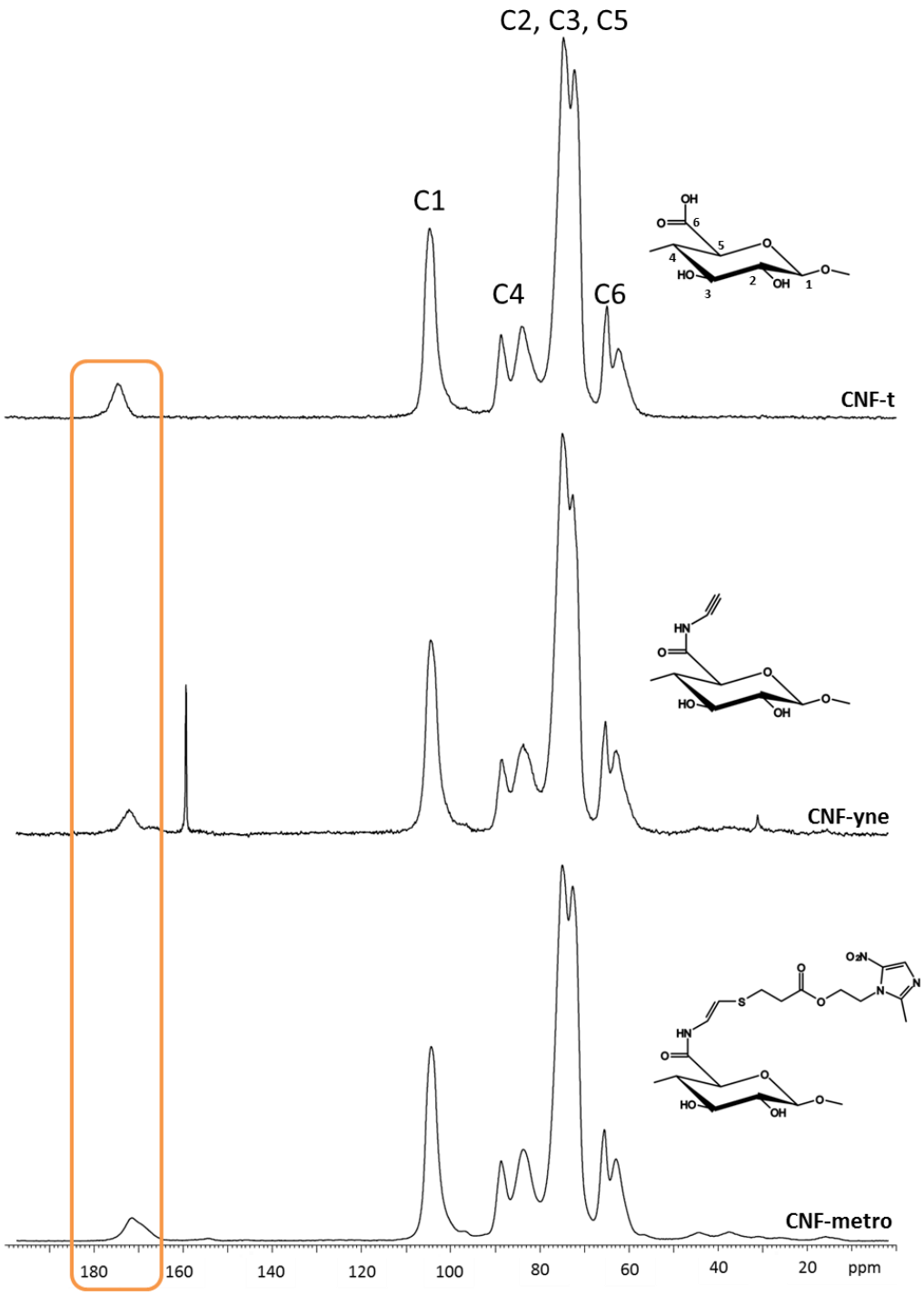

Figure II.17: Solid state ^{13}C NMR spectra of CNF-t, CNF-yne and CNF-metro

The ^{13}C spectrum of CNF-yne sample was quite similar regarding the regions that describe the cellulose backbone. The very sharp peak at 160 ppm was attributed to remaining EDC coupling agent according to previous results (not shown). However, this peak is no longer visible on the CNF-metro spectrum indicating that the last step of the immobilization procedure and the complementary purification steps removed all the remaining EDC coupling agents. This potential residue could be considered as an issue when calculating DS_{EA}. However, nitrogen was still detected in quantitative

amounts on CNF-metro whereas no more EDC was visible on NMR spectra. The presence of EDC was thus considered very limited on CNF-yne. The peak at 174 ppm was associated with the carbon of the carboxylic acid groups of CNF-t [81]. This peak was slightly shifted on CNF-yne signal, indicating a change of chemical environment due to the amidation reaction. A deconvolution technique was applied to unveil the contributions that explain this shift. The CNF-yne model signal displayed on Figure II.18A is a combination of carboxylic acid and amide model contributions. The overlap obtained was as high as 98.72 %, confirming the formation of the amide function on the CNF-t and the successful covalent immobilization of alkyne function on CNF.

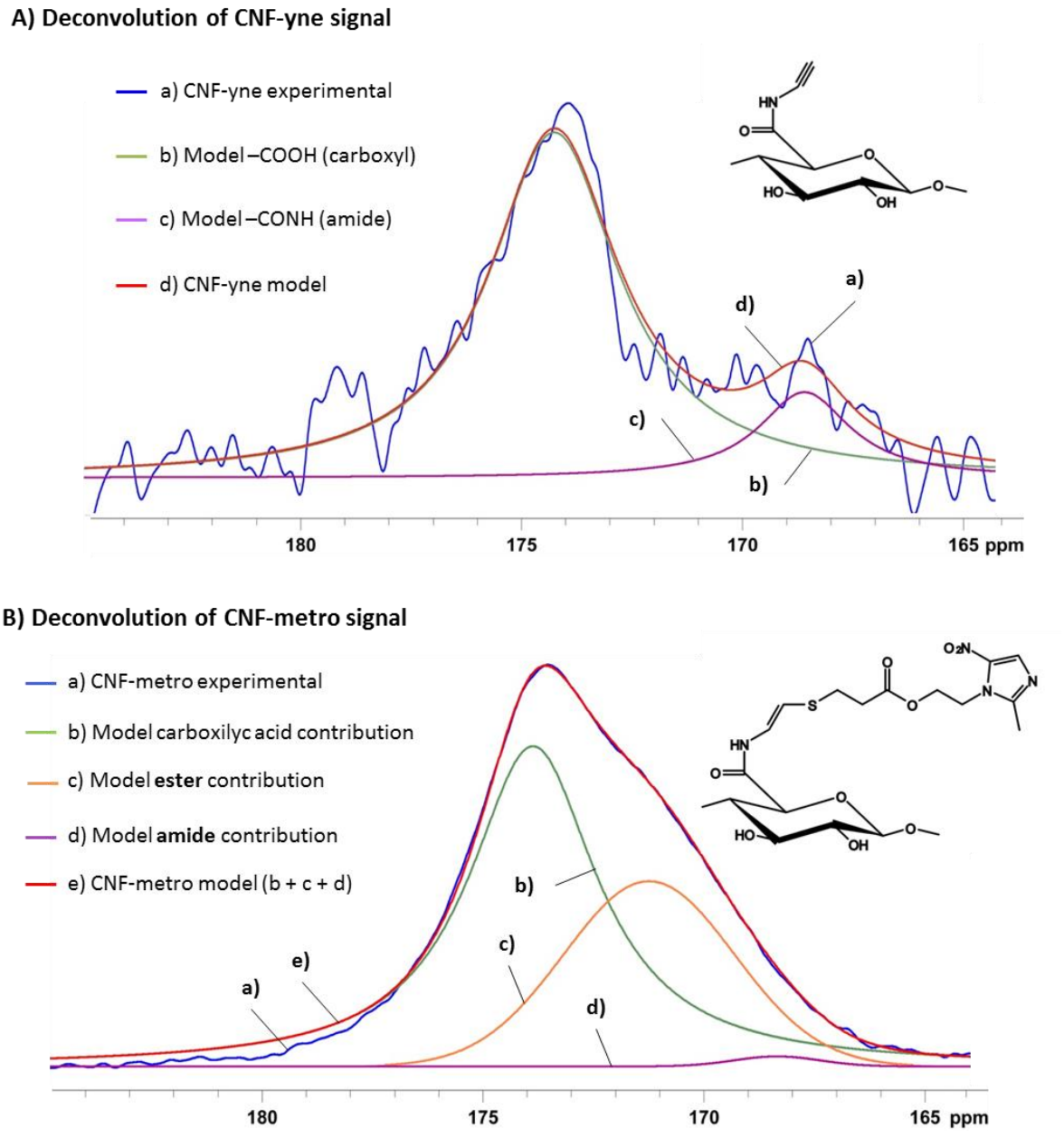

Figure II.18: Deconvolution of solid state ^{13}C NMR signal for A) CNF-yne with the amide contribution and B) CNF-metro with both the amide (small) and ester (big) contribution

Dynamic nuclear polarization enhanced NMR (DNP-NMR) was also performed on the three samples. This hyperpolarization method can increase the sensitivity of solid state NMR by several orders of magnitude [82]. As a proof of its potential, Figure II.19 compares the spectra of CNF-t without and with the microwave (MW) irradiation that allows the dynamic nuclear polarization transfer. The acquisition time of such signals is also very short in comparison with conventional solid state NMR. When several hours are necessary to reduce signal-to-noise ratio in conventional solid-state NMR, only minute-long acquisition of DNP enhanced NMR result in sharp and fine signals. As a matter of fact, in this example we could reach a 55 fold enhancement of signal to noise ratio. From a practical point of view, in order to reach similar signal-to-noise ratio without the DNP technique, it would have been necessary to multiply the number of accumulated transients by 3000. This is the reason why 2D ^{13}C INADEQUATE experiments in the solid phase become possible in natural abundance.

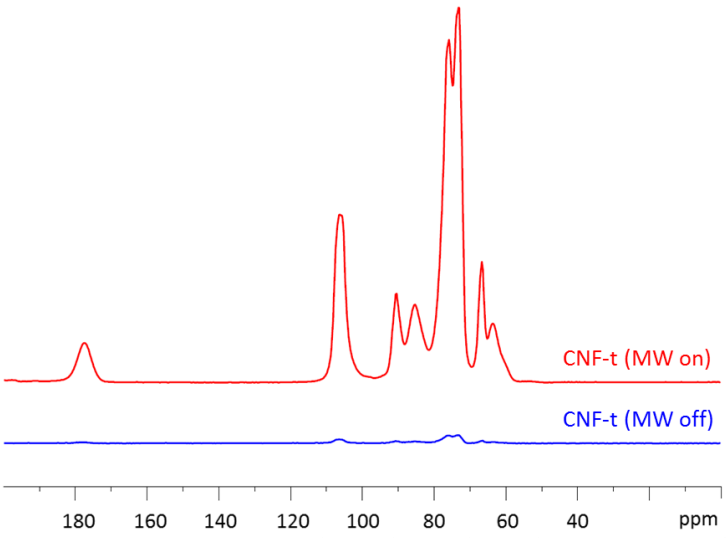

Figure II.19: ^{13}C DNP-NMR spectra for CNF-t, with (red) and without(blue) microwave irradiation(µwave)

The first result arising from DNP enhanced NMR was a further confirmation of the success of the amidation. Well defined signals appeared on CNF-yne spectra of Figure II.20a. Two peaks around 32 and 38 ppm were attributed to the aliphatic -CH_2- carbons introduced with propargylamine immobilization on CNF-t. These peaks were barely visible on conventional solid-state NMR. Moreover, as explained above, DNP enhanced NMR permit the acquisition of 2D INADEQUATE ^{13}C-^{13}C analysis with ^{13}C natural abundance. For instance, this analysis was used to study the region of carbons involved in carbonyls of CNF-t and CNF-yne samples. Figure II.20b shows the shift in the signal indicating the presence of a new type of carbon. This result confirmed the deconvolution treatment described before regarding the apparition of a signal due to the amidation reaction. This further proves the success of the amidation reaction.

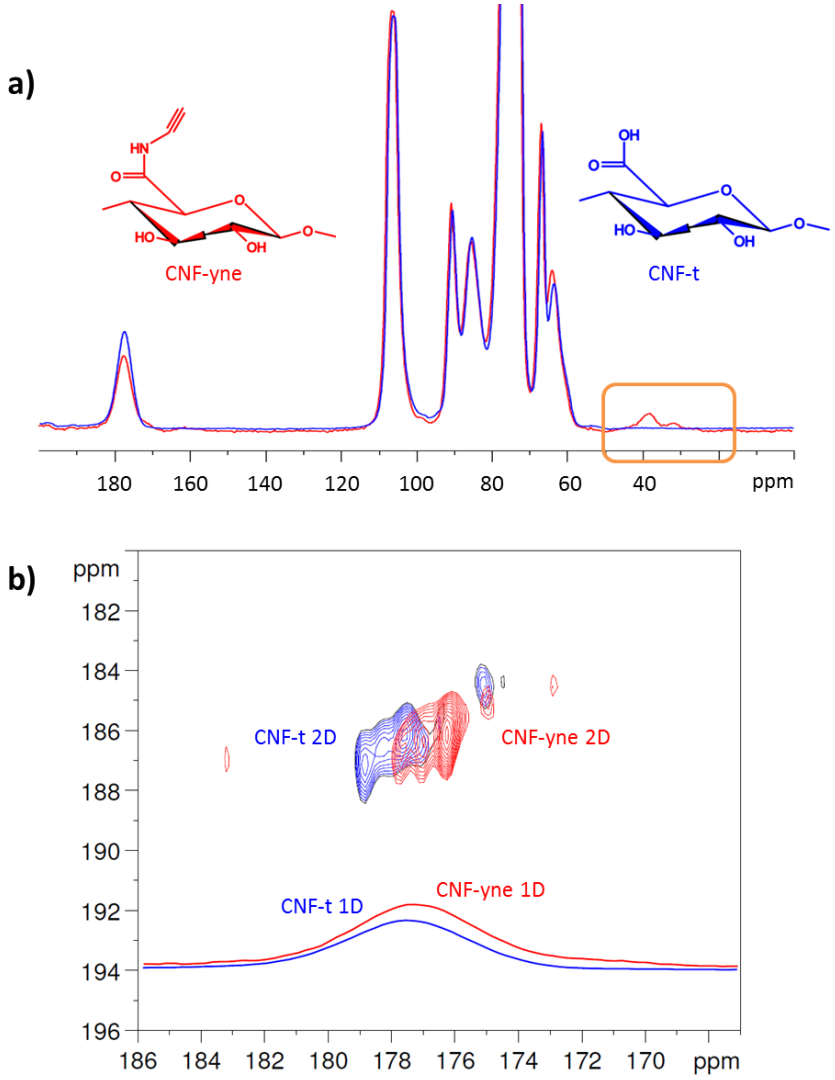

Figure II.20: a) ^{13}C DNP-NMR spectra of CNF-t and CNF-yne. Aliphatic -CH_2- carbons arises from CNF-yne signal. b) 2D inadequate ^{13}C-^{13}C DNP-NMR analysis of CNF-t and CNF-yne. The shift indicates the apparition of a carbon involved in an amide function.

In order to complement the analysis of CNF-t and CNF-yne samples with the DNP-NMR technique, 2D SQ-2Q ^{13}C-^{13}C correlation experiments are reported in Figure II.21. The one of pristine cellulose is not reported since it is alike to those already published. The only difference that could be noticed is that the NMR lines are a little broader in our case but it is due to the fact that we are working with nanocellulose fibers and not on regenerated cellulose. In any case the assignment is straightforward with a remarkable feature concerning the signal of C5 that overlaps with both signals assigned to C3 and C2. This feature is probably induced by the TEMPO mediated oxidation.

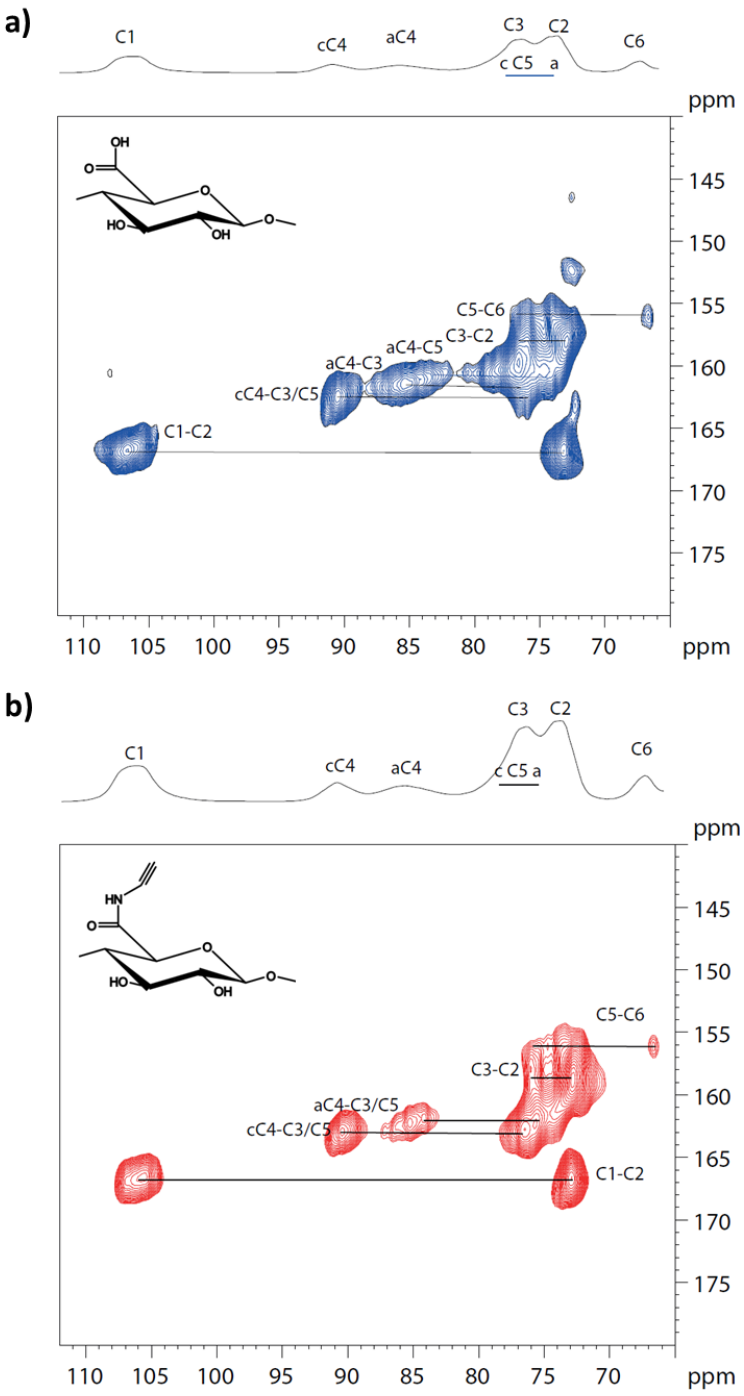

Figure II.21: 2D SQ-2Q ^{13}C-^{13}C correlation experiments, A) CNF-t reference material and B) CNF-yne after amidation reaction and immobilization of propargylamine

At first the 2D SQ-2Q ^{13}C-^{13}C recorded on CNF-yne appears to be very similar to the CNF-t. And the assignments can be easily carried out. It appears that the signal of C5 is narrower than in the CNF-t and overlaps mainly with the signal of C3. If the two 2D contour plots are displayed on the same map (CNF-yne in red and CNF-t in blue in Figure II.22) two differences indicated by arrows can be noticed. These changes in the position of the corresponding correlations can be interpreted by significant changes in the chemical shifts of C3 and C4 of amorphous celluloses. The corresponding correlation

between C6 and C5 does appear to be affected too. This is consistent with the expected reaction of amidation on C6. These effects are probably due to both chemical shifts induced by the amidation. The interesting point is that only the signal assigned to C4 in amorphous cellulose is affected, which indicates that the oxidation has occurred mainly on amorphous part of nanocellulose fibers.

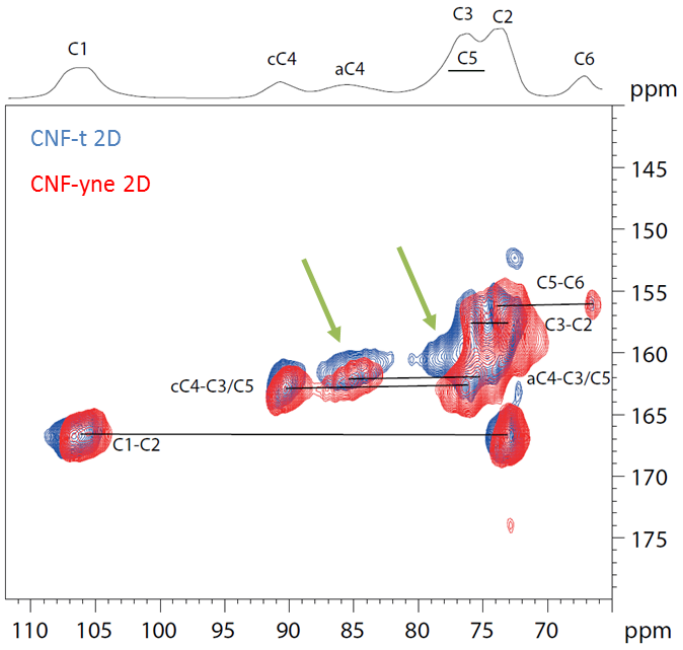

Figure II.22: 2D SQ-2Q ^{13}C-^{13}C correlation experiments, superposition of two sample experiments, CNF-t (blue) and CNF-yne (red)

Despite the use of DNP it was not possible to observe any correlation between the signal at 175 ppm assigned to carbonyl of amide and carbons of celluloses. However the pattern of these signals of the 2D map is interesting because due to the effect of coherence transfers and echo delays involved in the sequence their 2D correlations appears much resolved than on the corresponding 1D signals that allow to clearly observe chemical shifts induced by the amidation. Again, this clearly demonstrates the success of the reaction.

2.3.4. Second step: thiol-yne click chemistry reaction

The second step of the grafting strategy involved a click reaction to anchor the thiol-modified Metro-SH to the CNF-yne. In Figure II.10, the CNF-metro product displays only one molecule of thiol-modified drug per residue while the alkyne group is supposed to bind up to two thiol containing molecules by thiol-yne click reaction. However, considering the strong steric hindrance and the heterogeneous conditions of the chemistry that happened here, the binding of two molecules are on the alkyne group is probably strongly disfavored. We therefore depicted the result of the single addition even if double addition was not completely ruled out.

After the purification steps, ATR-FTIR analysis was performed on films produced by solvent casting from the modified CNF suspension. In Figure II.15, the peak at 1600 cm^{-1} was increased compared to the CNF-yne signal at the same wavelength, and could be attributed to the contribution of the stretching of NO_2 group of metronidazole molecule. This suggests the presence of the prodrug on the CNF.

Considering the significant amount of nitrogen and sulfur atoms that were introduced at this step, elemental analysis appeared again as a very relevant tool to characterize the presence of the Metro-SH on the CNF-yne. In fact on Table II.2, a significant increase of nitrogen content in comparison with the CNF-yne was detected, going from 1.15 % ±0.05 to 1.42 % ±0.03. In parallel, sulfur was also detected at 0.37 % ±0.01 while it was not detectable on CNF-yne. Also, the final ratio between the quantity of nitrogen and sulfur atoms must be close to 4 according to the chemical structure of CNF-Metro described on Figure II.10. The elemental analysis results gave a ratio of 1.42/0.37 = 3.8, which fits with the expected result. The progressive increase of nitrogen and the detection of sulfur both confirmed the immobilization of the Metro-SH onto the CNF.

Solid state ^{13}C NMR was used to further identify the composition of CNF-metro sample. On Figure II.17, in the region corresponding to carbons involved in C=O around 170 ppm, we noticed a difference of the shape of the CNF-yne signal suggesting a new chemical environment. The deconvolution technique was used again to clarify this result. The CNF-metro model signal (red) displayed on Figure II.18b perfectly fits with the low signal to noise experimental signal of CNF-metro (blue). A combination of model carboxylic acid, amide and ester contributions allowed the overlap to reached 98.9 % confirming the presence of an ester function. The thiol-modified drug is the only compound that contained such a chemical function. This is a complementary proof that the immobilization of the modified metronidazole on the cellulosic substrate was successful. However the covalent grafting of the prodrug molecule was still to be confirmed.

CNF-metro was also analyzed with DNP-NMR that allow for the access to the superfine signals hidden in the noise of conventional solid state NMR. On Figure II.23a, the same shift can be noticed in the carbonyls region that is in agreement with the deconvolution analysis performed earlier. Figure II.23b shows the peaks that arise around 12 ppm, 128 ppm and 148 ppm that were also detected on the liquid NMR spectrum of thiol-modified metronidazole displayed in red (corresponding to carbon C7, C8 and C9), which indicates again the presence of the molecule on the CNF-metro samples.

Moreover, the C1 signal at 21 ppm on Figure II.23b was not visible anymore on the spectrum of CNF-metro despite the enhanced sensitivity due to DNP. However we can observe a wider signal for -CH2- in comparison with CNF-yne spectrum between 25 and 45 ppm. The C1 signal has been shifted to

higher chemical shifts and this behavior is fully consistent with the thiol-yne reaction that replace the proton on the sulfur atom by an -CH=CH- group. These results are a good indication of the covalent binding of the prodrug molecule to the alkyne groups of the CNF substrate through thiol-yne click chemistry. This study also highlighted the strong interest of DNP-NMR to detect very small differences in solid functionalization. The two-step covalent immobilization of the prodrug on cellulose nanofibrils substrate in aqueous media was finally assessed thanks to this technique.

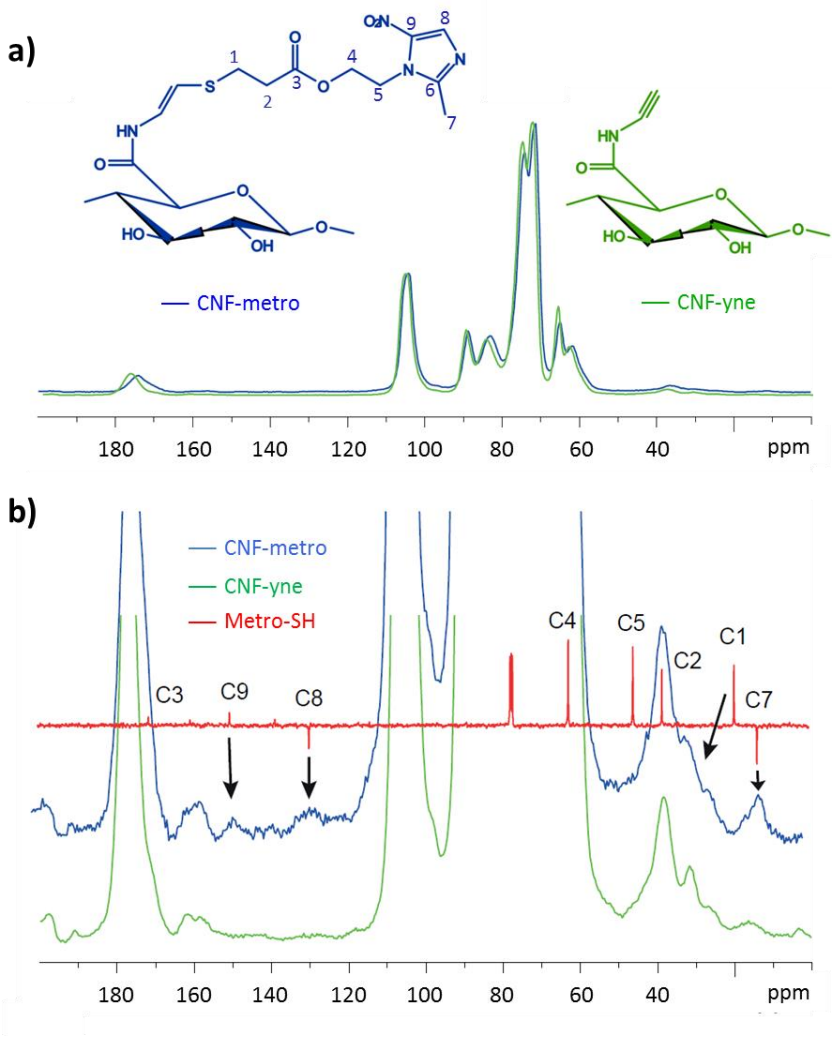

Figure II.23: a) ^{13}C DNP enhanced NMR of CNF-yne and CNF-metro samples and b) the same spectra combined with liquid ^{13}C NMR spectrum of the prodrug containing the metronidazole molecule on which a JMOD sequence was applied that gives negative -CH- and $-CH_3-$ signals

2.4 Conclusion

In this work, a multistep immobilization procedure was proposed to graft thiol modified metronidazole prodrug onto TEMPO oxidized cellulose nanofibrils. The first step was a successful amidation reaction between carboxylic acid groups of CNF-t confirmed by conductometric titration, FTIR-ATR, elemental analysis and both types of solid state NMR (conventional and DNP). An alkyne function was thus introduced at the surface of CNF. The second step of the grafting was the thiol-yne click chemistry reaction between the alkyne function and the thiol group of the modified metronidazole prodrug. The presence of the prodrug was then confirmed by elemental analysis, conventional solid-state NMR and DNP enhanced NMR. The obtained complex system is now suitable for drug release analysis in esterase enzyme containing medium and can be used in the development of innovative medical device prototypes with on-site triggered release of the compound thanks to the cleavable ester link of the prodrug.

3. Investigation of active principle ingredient grafting on cellulose nanofibrils through Diels Alder reaction with DNP-enhanced ssNMR

This section is adapted from "H. Durand, C. Balsollier, S. Fort, M. Demeunynck, I. Baussanne, D. Lee, G. de Paepe, A. Kumar, E. Zeno, N. Belgacem, J. Bras – Investigation of active principle ingredient grafting on cellulose nanofibrils through Diels Alder reaction with DNP-enhanced ssNMR", submitted in ACS Applied Nano Materials in November 2018

Abstract

This work deals with the covalent binding of a drug onto cellulose nanofibrils for a drug release application. More precisely, a Diels Alder reaction for a two-step covalent binding of Metronidazole to oxidized cellulose nanofibers (CNF-t) has been performed. CNF-t were first modified with furfurylamine in order to provide them with pending furan groups. Meanwhile, metronidazole molecule was chemically modified with maleimide and ester-containing compound. Diels Alder reaction was then triggered by heat to bind furan modified CNF-t with metronidazole-maleimide. Each chemical grafting step has been proved by the use of numerous techniques like FTIR, conductometric titration, elemental analysis and NMR (liquid and solid state). More innovatively, DNP-NMR was performed to confirm the click reactions for the first time onto nanocellulose. This new CNF-t based systems represent an innovative drug carrier formulation with "on-demand" API release abilities in presence of esterase enzyme.

3.1 Introduction

Wood derived cellulose finds industrial applications in a wide range of field, from paper products to buildings, cosmetics, foodstuffs or medical industry [83]. Numerous kinds of cellulosic materials are industrially produced for decades. In the beginning of the 1980s researchers isolated a new type of cellulosic materials, cellulose nanofibers thanks to the pioneer work of Turbak and co-workers [3], [4]. Since then, a huge scientific enthusiasm progressively raised on the topic of cellulose nanofibers (CNF), its isolation process and numerous potential uses resulting in exponentially growing number of papers published. Inheriting from cellulose characteristics such as widespread availability, biodegradability and biocompatibility, cellulose nanofibers also present excellent mechanical properties and high specific area that results in extended tunable surface chemistry [11]. These features led to the use of CNF for various end-applications like paper and packaging products [6], [12], [13], [49], composites [14], printed electronics industry [50] as well as cosmetics and medical field [18], [19], [21], [84]. Cellulose nanofibers can be organized into different 2D and 3D nano-structures such as film, membranes, hydrogels or aerogels.

Special grade of CNF was designed thanks to oxidation pretreatment of the cellulose fiber suspension before CNF production in order to limit energy consumption. TEMPO-mediated oxidation of cellulose fibers was adapted to CNF production by A. Isogai and co-workers [52], [85] end of 2000's. TEMPO oxidized CNF (CNF-t) bear carboxylic acid groups at the nanofiber surface that pave the way to new functionalization strategies.

One of the latest identified fields of potential application for CNF-t is the biomedical industry. Several reviews already describe the future use of CNF-t as a new platform for the development of enhanced medical devices [18], [84]. This goes in hand with biocompatibility and toxicity assessment that demonstrate the safety of CNF when they are intended for medical use: In-vitro testing against human fibroblast strains exhibit low or inexistent cytotoxicity for 3D structure or films of TEMPO oxidized CNF [22], [86]. Among biomedical science, drug delivery is a field where CNF-t displays particular potential. With only 20 % of ibuprofen compared to commercial products, CNF-t gel formulations exhibited equivalent performance providing proof of concept that CNF-t improve the efficiency of drug delivery [56]. Tunable aerogel 3D structure of different types of CNF, including CNF-t were also produced and mixed with beclomethasone di-propionate. A sustained release was revealed for CNF-t based systems [57]. Encapsulation of 6 active principle ingredients (API) was done in CNF-t hydrogels structure. The influence of freeze-drying and subsequent rehydration on the rheology of the 3D systems and API release profiles was monitored. Results exhibited successful

rehydration and did not show any difference before or after the freeze drying an rehydration process regarding the release profiles [64].

This last study used Metronidazole, a nitro-imidazole antibacterial compound that has been used since the 1980's to treat anaerobic micro-organisms in many areas of the body such as gastrointestinal tract and reproductive systems. Once absorbed by the bacteria and reduced by protein activity, Metronidazole can cleave DNA and prevent the replication mechanism that eventually leads to stop the cell growth [59]. Metronidazole loaded formulations were design with cellulose derivatives such as hydroxypropyl methyl cellulose, methyl cellulose and cellulose acetate phthalate in order to better control the delivery of this API [60]–[62]. More complex systems were developed with the AaltoCell™ partially fibrillated microcrystalline cellulose. Metronidazole was loaded in the entangled nano/microfibrils of the cellulose particles and drug release experiments were performed. A diffusion controlled release mechanism was proven, confirming the ability of metronidazole loaded cellulose based systems to be high-performing materials [63]. These works only rely on drug adsorption mechanisms. The objective of this paper is to investigate a new method for the loading of drugs onto CNF-t by developing functionalization for a release on-demand.

Covalent binding of molecules onto cellulosic nanomaterials is an intensive field of research. Surface chemical modification of CNF-t is possible thanks to the availability of hydroxyls and carboxylic acid groups that is increased by the high specific surface of these nanomaterials. Small molecules or polymer can be covalently linked to CNF surface through etherification, amidation, esterification and silylation according to the relevant reviews available in the literature [66], [68], [87]. The growing concerns about fossil resource depletion and environment impact have compelled researchers to investigate more sustainable modification procedures. As a green chemical route, click chemistry is foreseen to be more and more applied in material science. Click chemistry principles were described by Sharpless et al in 2001. Reactions are classified among click chemistry if they are stereospecific, modular, if they proceed in simple conditions (no sensitivity to water or oxygen), and result in very high yields with readily available reagents [88]. Diels Alder reactions match with click chemistry principles and are also metal-free reactions, confirming their wide applicability and physiological compatibility [89]. Natural polymers have been used to build up new materials thanks to Diels Alder reaction, especially the furan-maleimide strategy, as depicted in the recent review of A. Gandini and co-workers [90]. However, only a very few publications deal with the modification of cellulose nanofibers with Diels Alder reaction. Multicolor fluorescent probe were covalently linked to CNF through Diels Alder reaction that resulted in improved materials for biological imaging [70]. The reversible crosslinking of natural rubber was also performed thanks to the introduction of CNF and subsequent crosslinking based on Diels Alder furan-maleimide cycloaddition. Increased mechanical

properties and easier recycling process are the main outcomes of this work [91]. Recently, this strategy was recently used to produce enzymatically activated oligosaccharide-prodrugs of Doxorubicin and shown the Diels Alder reaction usefulness for complex handling compounds [92].

In this work, the implementation of Diels Alder reaction for a two-step covalent binding of Metronidazole to CNF-t is investigated. CNF-t were first modified with furfurylamine in order to provide them with pending furan groups. Meanwhile, metronidazole molecule was chemically modified with maleimide and ester functions containing compound. Diels Alder reaction was then triggered by heat to bind furan modified CNF-t with metronidazole-maleimide as depicted on Figure II.24. The ester function introduced in between the CNF substrates and the metronidazole molecule is expected to be sensitive to enzyme activity or slow hydrolysis as already proven in the literature [93]–[95]. Esterase are indeed available on fat tissues and infection sites [65]. This new CNF-t based systems represent an innovative drug carrier formulation with "on-demand" API release abilities in presence of esterase.

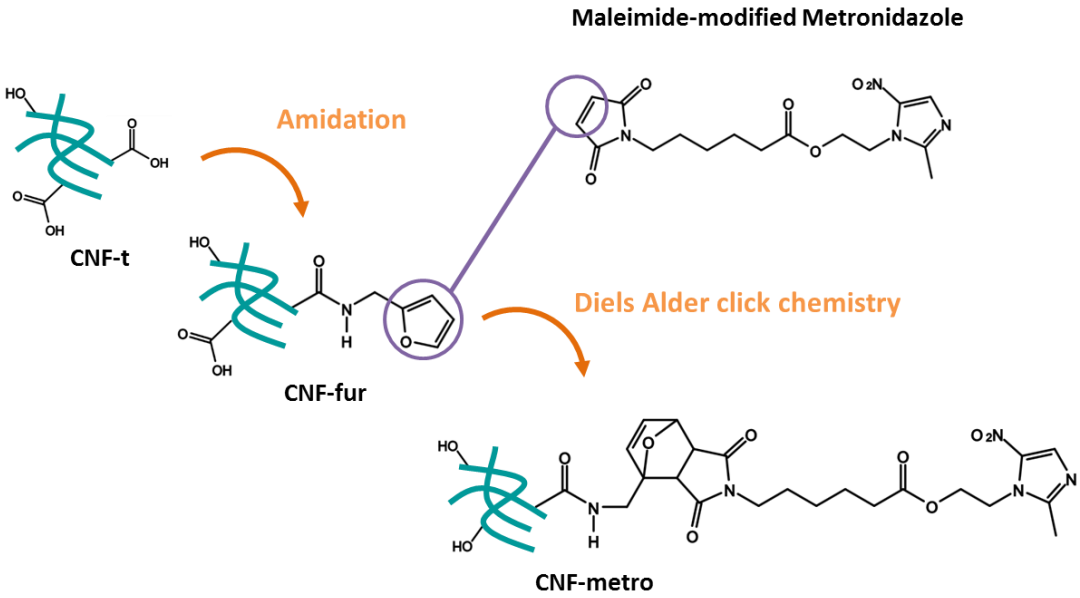

Figure II.24: General multistep immobilization procedure of maleimide-modified metronidazole on CNF-t

3.2 Experimental procedures

3.2.1. Materials

The cellulose nanofibrils (CNF) suspension was provided by the Centre Technique du Papier (CTP, Grenoble, France). The suspension which is referred as CNF-t was produced by TEMPO mediated oxidation of a pre-refined (40°SR) bleached bisulfite pulp provided by TEMBEC. The pulp concentration was adjusted to 1.5 wt% and the oxidation was performed at pH 10 for 2 hours in presence of NaBr, NaClO and the TEMPO reagent. High pressure homogenizer from GEA (Niro, Soavi,

Italy) was used to defibrillate the oxidized the cellulose fibers and produce the CNF-t suspension. 4-(Dimethylamino)pyridine (DMAP, CAS: 1122-58-3), N,N-Dicyclohexylcarbodiimide (DCC, CAS: 538-75-0), trifluoroacetic acid (TFA, CAS: 76-05-1), metronidazole (CAS: 443-48-1) were purchased from Sigma Aldrich, Alfa Aesar or Acros Organics and used without further purification. Furfurylamine (CAS: 617-89-0) was purchased from ACROS ORGANICS. N-(3-Dimethylaminopropyl)-N'-ethylcarbodiimide Hydrochloride (EDC, CAS: 25952-53-8), N-Hydroxysuccinimide (NHS, CAS: 6066-82-6), Sodium Hydroxide (NaOH, CAS: 1310-73-2), Hydrogen chloride (HCl, CAS: 7647-01-0) were purchased from Sigma Aldrich and used as received. The biradical 15-{[(7-oxyl-3,11-dioxa-7-azadispiro[5.1.5.3]hexadec-15-yl)carbamoyl][2-(2,5,8,11-tetraoxatridecan-13-ylamino)}-[3,11-dioxa-7-azadispiro[5.1.5.3]hexadec-7-yl])oxidanyl (AMUpol) was purchased from Cortecnet (France) and used in D_2O obtained from Sigma Aldrich (CAS: 7789-20-0). Deionized water was used for every experiment.

3.2.2. Methods

3.2.2.a. Synthesis of Metronidazole-maleimide

As represented in Figure II.25, 6-maleimidehexanoic acid (**1**, 753 mg, 3.6 mmol), metronidazole (**2**, 626 mg, 3.6 mmol) and DMAP (40 mg, 0.36 mmol) were dissolved in CH_2Cl_2 (25 mL) at 0°C. DCC (905 mg, 4.4 mmol) was added after 15 minutes [96], [97]. The reacting mixture was stirred 4 hours at room temperature, then filtered and concentrated under vacuum. The crude product was purified by flash chromatography on silicagel with CH_2Cl_2/MeOH: 98/2 as eluent to give the compound **3**, metronidazole-maleimide (Metro-MAL) as a yellow amorphous solid (669 mg, 1.83 mmol, 51 %).

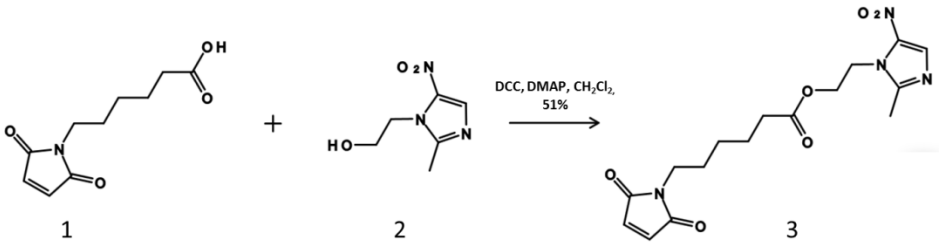

Figure II.25: Synthesis path of metronidazole-maleimide (Metro-MAL) (3) from metronidazole (2) and 6-maleimidehexanoic acid (1)

3.2.2.b. Immobilization of furan group on CNF-t through amidation

The CNF-t suspension concentration was decreased from 1.5 wt% to 0.4 wt% in order to be easily stirred. Deionized water was added before homogenization with an IKA Ultra-Turrax high shear mixer for 1 minute at 10 000 rpm. The pH of the suspension was then adjusted to 4 under magnetic stirring using a 0.5 M HCl solution.

A solution of the coupling agents EDC and NHS was prepared in deionized water. After complete dissolution the solution was added to the suspension of CNF-t. A molar ratio of 4 equivalents of EDC and NHS for 1 equivalent of carboxyl group of CNF-t was used. The mixture was magnetically stirred for 30 minutes at room temperature in order to activate the carboxyl groups of the CNF-t. The pH was maintained at 4 during the reaction with 0.5M HCl or NaOH solution droplets addition. This pH favors the EDC carbocation availability and acid form of the carboxyl groups which are both required for the activation reaction.

The pH was then increased to 8.5 for the second part of the reaction, the amine addition. Pure furfurylamine was mixed with 5ml of deionized water and added to the mixture. Again, a molar ratio of 4 equivalents for 1 equivalent of carboxyl groups of CNF-t was used. The mixture was magnetically stirred for 72h at room temperature and the pH was kept at 8.5 with 0.5M HCl or NaOH solution droplets addition.

After 72h of reaction, the washing of the mixture was performed by centrifugation and dialysis. First, the reaction was quenched by decreasing the pH to 2-2.5 with 0.5M HCl solution. Then, centrifugation washings were applied on the suspension: centrifugations were operated during 10 minutes at 20 000 g (about 11 100 rpm) and redispersions were done in deionized water in order to remove all the not covalently bound chemicals (EDC, NHS and free amine). In between each centrifugation cycle, the redispersions were done with the high shear mixer (Ultra-turrax, IKA) for 1 min at RT. A total of 6 centrifugation/redispersion operations were performed in order to recover the furan modified CNF-t, referred as CNF-fur. The last redispersion was done in neutral water.

The last step of purification consisted in a dialysis of the CNF-fur suspension against neutral water with 6-8 kDA MWCO membranes (Spectra/Por® 1 Standard RC Tubing, SPECTRUM) for at least 5 days under slow magnetic stirring and renewal of the medium twice a day.

3.2.2.c. Diels Alder reaction with model compounds

The conditions for Diels Alder reaction between CNF-fur and Metro-MAL were tested on model compounds to confirm their validity. First, furfurylamine (Fur) and 6-maleimido-hexanoic acid (6-MHA) were mixed in an equimolar ratio in a mixture of ethanol and deionized water (50/50 v/v). The solution was kept at 40°C to trigger the Diels Alder reaction and the pH was controlled over 4 hours to confirm its stability (around 6 ± 0.05). Secondly, the experiment was repeated from the beginning and set up in situ in a liquid NMR tubes under analysis in order to record spectra over time and assess the kinetic of the reaction. Spectra were recorded at 15 min, 1 h, 5 h, 24 h, 48 h and 72 h.

3.2.2.d. Immobilization of Maleimide-metronidazole on CNF-fur

Metro-MAL compound (95.2 mg) was dissolved in a 40 ml mixture of deionized water and ethanol at 50:50 v/v. The dissolution was assisted by an ultrasound bath (IKA, USA) and magnetic stirring. The CNF-fur suspension was diluted at a 0.15 wt% concentration and 9.42 ml of the Metro-MAL solution was added drop by drop under magnetic stirring in order to reach 1 molar equivalent of Metro-MAL compound to the furan groups available on the CNF substrate. Diels alder reaction was triggered by heating the system at 40°C for 24 h under continuous magnetic stirring. The reaction was followed with UV spectroscopy. The modified CNF-fur (now referred as CNF-metro) were purified with several centrifugation/redispersion steps with almost the same procedure than before: three steps of washing used 50/50 v/v water/ethanol mixture and two steps used deionized water only. Washed suspensions were further purified with dialysis against deionized water under slow magnetic stirring for 5 days with daily renewal of dialysis medium in order to completely remove non-covalently bound compounds. Dialysis membranes were a 6-8 kDA MWCO membranes (Spectra/Por® 1 Standard RC Tubing, SPECTRUM). CNF-metro suspensions were stored in the fridge at 5°C before any characterization.

Thin films were produced by solvent casting in petri dishes from the three CNF suspensions (CNF-t, CNF-fur and CNF-metro) at 0.1 wt% in order to obtain a 30g/m² film. Then, it was let dry overnight in an oven at 40°C. Also, the CNF suspensions were freeze dried to obtain another dry form of the products. These films and aerogels were used for solid state characterization.

3.2.2.e. Atomic force microscopy

Atomic force microscopy (AFM) images were recorded on a Dimension icon® (Bruker, USA). A $7.5.10^{-4}$ wt% suspension was prepared by several dilutions of the gel using high shear mixer Ultra-Turrax (IKA) in order to maintain the homogeneity even at low concentration. A drop of this suspension was deposited on freshly cleaved mica plate before drying overnight under fume hood at room temperature. The acquisition was performed in tapping mode using a silica coated cantilever (OTESPA® 300 kHz – 42 N/m, Bruker, USA). Zones of 3.3*3.3 µm² were analyzed. At least five images on two different samples were performed and the most representative were selected for the discussion.

3.2.2.f. Infrared spectroscopy

Fourier Transformed Infrared spectroscopy (FTIR) spectra of the CNF suspensions were obtained on a Perkin Elmer Spectrum One spectrometer (Waltham, Massachusetts, USA). KBr pellets were prepared with one drop of CNF suspensions. At least 3 pellets with measurements of 16 scans with a resolution of $2cm^{-1}$ between 600 and 4000 cm^{-1} were performed for each sample. Spectra were

normalized at 1110cm^{-1}, the wavenumber of C-O-C bonds in cellulosic substrates. The most representative spectra were chosen for discussion.

3.2.2.g. Conductometric titration and *DO/DS* calculation

The carboxylic content of the CNF-t suspension was measured before and after the first step of functionalization through conductometric titration. The amount of CNF-t suspension corresponding to 50mg of dry material was precisely diluted to 200ml with de-ionized water. Magnetic stirring and high shear mixer Ultra-Turrax (IKA) were used to produce a homogeneous dispersion. The pH was decreased around 2.5 with 0.1M HCl to turn every remaining carboxylate moieties of CNF surface into the acid form of carboxylic acid and the volume of added HCl solution was recorded. The titration was done with a 0.01M NaOH solution, which precise concentration was measured with 3 colorimetric titrations before the titration of the CNF suspensions. The conductivity of the suspension was recorded after stabilization all along NaOH addition and added volumes of NaOH were reduced when the curve indicated changes in the slopes to improve the assessment of the transitions. The titration curves typically display three regions, a first slope showing the decrease of the conductivity that correspond to the neutralization of the remaining strong acid, a plateau where the weak acid groups are titrated (carboxylic groups of CNFs) and a last part where conductivity increases when all acids are titrated.

The degree of oxidation (*DO*) represent the number of carboxylic groups per anhydroglucose unit (AGU) on oxidized CNF. It can be calculated with equation (II-8) according to Da Silva Perez et al. [73].

$$DO = \frac{162 \times C \times (V_{eq1} - V_{eq2})}{m - 36 \times C \times (V_{eq1} - V_{eq2})} \qquad \textbf{(II-8)}$$

The value of 162 (g.mol^{-1}) is the molar mass of the AGU. The precise concentration of the NaOH solution is *C*. The CNF dry quantity is *m*. The value 36 g.mol^{-1} is the difference between the molar mass of the carboxylate form of the carboxylic groups including the sodium counter ion (198 g.mol^{-1}) and the molar mass of the AGU (162 g.mol^{-1}). This term arises from the partial replacement of primary hydroxyl groups by carboxylate groups during the TEMPO mediated oxidation process. The two NaOH solution equivalent volumes V_{eq1} and V_{eq2} are extracted at the edge of the plateau on the titration curve by calculating the intersections of the first (decreasing slope) and third (increasing slope) part of the curve with the plateau.

The carboxylic group content X_{ox} on CNF-t can be calculated with equation (II-9).

$$X_{ox} = \frac{C \times (V_{eq1} - V_{eq2})}{m} \qquad \textbf{(II-9)}$$

The terms are the same used in equation (II-8) and X_{ox} is expressed in micro-mole of carboxylic group per gram of dry CNF (µmol.g^{-1}).

After the amidation reaction with furfurylamine, the amount of remaining carboxylic group can also be assessed by conductometric titration and the residual degree of oxidation DO_{res} is calculated with equation (II-10) by integrating the molecular weight *M* of the furfurylamine and the same previous terms as it was done before for amidation on CNC [74].

$$DO_{res} = \frac{(162 + (M - 40) \times DO) \times C \times (V_{eq1} - V_{eq2})}{m - (M - 40) \times C \times (V_{eq1} - V_{eq2})} \qquad \textbf{(II-10)}$$

The value 40 (g.mol^{-1}) correspond to the loss of sodium and oxygen atoms on CNF and hydrogen atom from the amine group of furfurylamine.

While equation (II-9) is used to characterize CNF-t before the amidation reaction to calculate the quantities of required chemicals in order to match targeted corresponding molar equivalent, equation (II-8) and (II-10) are used to compare the *DO* before and after the amidation reaction. The proportion of carboxylic groups ($\%COOH_{conv.}$) that were converted during the amidation reaction can thus be assessed with equation (II-11).

$$\%COOH_{conv.} = \frac{DO - DO_{res}}{DO} \times 100 \qquad \textbf{(II-11)}$$

All titrations were repeated at least three times.

From the values of X_{ox} and $\%COOH_{conv}$ it is possible to calculate a degree of substitution based on conductometric titration measurements DS_{cond}. By considering one gram of CNF-t, X_{ox} gives access to the molar quantity of oxidized anhydroglucose units (AGU) before amidation and so, non-oxidized AGU mass can be determined by subtraction ($n[AGU\text{-}OH]$). Through amidation of CNF-t, only oxidized AGU will react and $\%COOH_{conv}$ gives access to the molar quantity of converted oxidized AGU ($n[AGU\text{-}FUR]$) and non-reacted oxidized AGU ($n[AGU\text{-}COOH_{nr}]$) by subtraction again. Equation (II-12) gives the degree of substitution:

$$DS_{cond} = \frac{n[AGU - YNE]}{n[AGU - OH] + n[AGU - COOH_{nr}] + n[AGU - YNE]} \qquad \textbf{(II-12)}$$

where

$$n[AGU - YNE] = \%COOH_{conv.} \times X_{ox}$$

$$n[AGU - OH] = \frac{1 - X_{ox} \times M_{AGU-COOH}}{M_{AGU-OH}}$$

$$n[AGU - COOH_{nr}] = 1 \times X_{ox} - n[AGU - YNE]$$

with $M_{AGU\text{-}COOH}$ the molar mass of an oxidized AGU (176.1 g/mol), $M_{AGU\text{-}OH}$ the molar mass of an AGU (162.1 g/mol). In $n[AGU\text{-}COOH_{nf}]$ formula, the dimension of the figure 1 is a mass, one gram of modified CNF is considered for the DS_{cond} calculation.

3.2.2.h. Elemental analysis

CNF films were prepared by solvent casting from purified CNF suspensions. The suspensions were poured into Teflon molds and evaporated overnight in an oven at 40°C. Elemental Analysis was performed on a vario Micro Cube® device from Elementar (Germany). Carbon, Hydrogen, Nitrogen, Sulfur and Oxygen mass proportion of CNF films were measured. Films pieces of 4 to 7 mg were weighted on a *micro-balance*. An average of four measurements was obtained for each sample. A degree of substitution from elemental analysis (DS_{EA}) was then calculated based on the detection of the increase of Nitrogen content from the CNF-t film to the CNF-fur film. Equation (II-13) was used.

$$DS_{EA} = \frac{162{,}1406 \times \%N}{n(N\ in\ grafted\ mol) \times M(N) - M(grafted\ mol) \times \%N} \qquad \textbf{(II-13)}$$

where 162.1406 is the precise molar mass of anhydro-glucose unit (AGU), *%N* the mass proportion of nitrogen detected by elemental analysis, *n(N in grafted mol)* the number of nitrogen atom in the grafted molecule (i.e. furfurylamine), *M(N)* the molar mass of nitrogen, *M(grafted molecule)* the molar mass difference between grafted and non-grafted AGU. This DS_{EA} represents the quantity of AGU modified with a furfurylamine molecule within the bulk material.

3.2.2.i. Liquid ^{1}H and ^{13}C nuclear magnetic resonance on MetroMAL prodrug

For the prodrug characterization, nuclear magnetic resonance (NMR) spectra were recorded at room temperature in 5 mm tubes on a Bruker AC 400 MHz spectrometer (NMR facility, PCN-ICMG, Grenoble). Chemical shifts (δ) are reported in parts per million (ppm) from low to high field and referenced to residual non-deuterated solvent relative to Me_4Si. Standard abbreviations for multiplicity were used as follows: s = singlet; d = doublet; t = triplet; m = multiplet.

3.2.2.j. Liquid ^{13}C nuclear magnetic resonance on model Diels Alder reaction mixture

The model Diels Alder reaction kinetic was followed by liquid ^{13}C nuclear magnetic resonance analyses (^{13}C NMR) that were performed at the « Institute for Nanoscience and Cryogenics (INAC) » in the «French Alternative Energies and Atomic Energy Commission (CEA) » at Grenoble, on a Bruker AVANCE400 spectrometer. Acquisition and data treatment was done using the LINUX TopSpin 3.2 software. Furfurylamine (Fur) and 6-maleimido-hexanoic acid (6-MHA) were mixed in an equimolar ratio in a mixture of ethanol and deionized water (50/50 v/v). Chromium (III) acetylacetonate relaxing agent was added in 10 mg/ml final concentration. In 10 mm quartz liquid NMR tube, *in-situ*

acquisitions of spectra was done over time to assess the kinetic of the reaction. A 10 mm BB (broad band) probe was used for the acquisitions, at 313 K. Spectra were acquired at every 15 min the first 90 min, every hour during the following twelve hours and every 2 hours from 12 to 24 hours of reaction. Last spectra were acquired at 48 and 72 hours. The number of scans (NS) was also increased over time. The Bruker *INVGATE* sequence was used for quantitative analysis. The experiments were conducted with 1.3 s acquisition time, 5 s relaxation delay and a 30° pulse using a 250 ppm spectral width (relaxant agent in the mixture). Proton broad band decoupling was applied only during acquisition time. 64 k data points were used for data acquisition. Prior to Fourier transformation, zero-filling at 128 K was applied, followed by apodization with a 2 Hz exponential. Chemical shifts are given relative to TMS (tetramethylsilane, $\delta = 0$ ppm). The positions of the peaks were referred to the residual solvent signal. To discriminate unambiguously the -CH / -CH3 from the -CH2, the Bruker *DEPT* sequence was used. The experiments were conducted with 0.648 s acquisition time, 3.0 s relaxation delay, a last pulse at 135° to select CH2 carbons reversed compared to CH and CH3, with a 145 Hz coupling constant.

3.2.2.k. Solid state ^{13}C nuclear magnetic resonance

Solid-state ^{13}C nuclear magnetic resonance (^{13}C ssNMR) experiments were performed at the Centre de Recherches sur les Macromolécules Végétales (CERMAV-CNRS, Grenoble, France). Spectra were acquired using a Bruker Avance III 400 MHz spectrometer operating at 100.62 MHz for ^{13}C, using the combination of the cross-polarization, high-power proton decoupling and magic angle spinning (CP-MAS) method. The spinning speed was set at 12,000 Hz. The ^{1}H radio-frequency field strength was set to give a 90° pulse duration of 3.1 µs. The ^{13}C radio-frequency field strength was obtained by matching the Hartman-Hahn conditions at 60 kHz. At least 3,000 scans were integrated with a contact time of 2 ms using a ramp CP protocol and a recycle delay of 2 s. The acquisition time was 35 ms and the sweep width set at 29,761 Hz. The chemical shifts were calibrated with respect to the carbonyl peak of glycine (176.03 ppm).

3.2.2.l. Dynamic nuclear polarization enhanced nuclear magnetic resonance

Dynamic nuclear polarization enhanced nuclear magnetic resonance (DNP-NMR) was used to further characterize the samples. Impregnation with 10 mM AMUPol was done in D_2O only [98]. The wetted sample was then fully packed in a 3.2 mm outer-diameter sapphire rotor (28 mg of CNF-t sample and 40 µL of 10 mM AMUPol in D_2O). For CNF-fur and CNF-metro, 30 mg of sample and 80 µL of 10 mM AMUPol in D_2O were used. The samples were prepared in D_2O only, instead of using a glycerol/water glass forming matrix, in order to avoid any overlap from solvent ^{13}C resonances.

All experiments were performed on a Bruker Avance™ III 400 MHz DNP-NMR spectrometer equipped with 263 GHz gyrotron for microwave irradiation, a corrugated transmission line and a low temperature 3.2 mm MAS probe used in double-resonance mode [99]. For the cross-polarization magic angle spinning (CPMAS) experiment, a radio frequency (RF) field strength of 50 kHz for ^{13}C and 100 kHz for ^{1}H for all the pulses was used, unless otherwise stated. A CP contact time of 2 ms and a 50-100 % ramp on the proton during CP4 spin-lock was used in all cases [100], [101]. CP spin-lock was optimized for ^{13}C to match the Hartman-Hahn condition under MAS. All experiments were performed at 100 K. The MAS frequency for experiments was set to 13.3 kHz for all samples. The recycle delays set to 3.0 s for CNF-t, 2.5 s for CNF-fur and 1.9 s for CNF-metro, respectively. All experiments were processed and analyzed using Bruker Topspin 3.0.

3.3 Results and discussions

3.3.1. Characterization of CNF starting material

Cellulose nanofibrils suspensions are often a mixture of nanoscale particles, microfibrillated fibers, aggregates and residual fibers. Nowadays a wide range of CNF types are commercially available, from lab-scale production to pilot scale facilities. Properties and characteristics of CNF can differ from a supplier to another. It is now relevant to provide the reader with basic description of the CNF that are used in this work for helping comparisons with literature. The objective is to better know the starting material in order to draw relevant conclusions from the presented results.

The CNF-t suspension produced has a thick transparent gel appearance at 1.6 wt% concentration as depicted on Figure II.26. AFM images of the low concentrated CNF-t suspension were also recorded in order to confirm the nanosize morphology of cellulose nanofibrils.

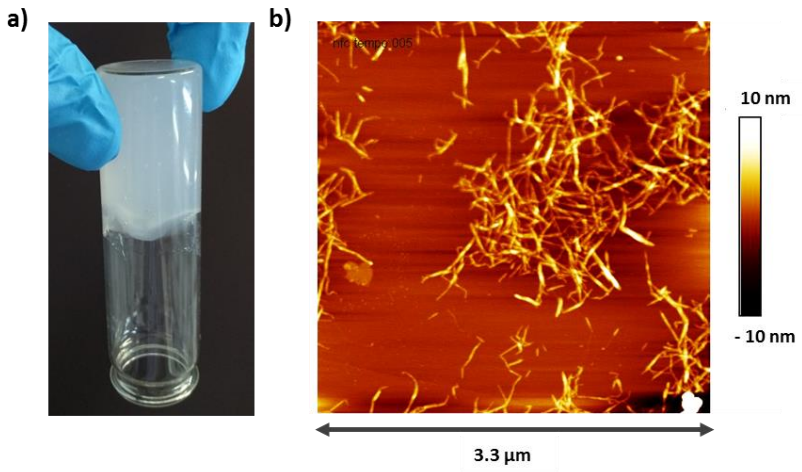

Figure II.26: CNF-t suspension appearance and morphology on a) a picture of the 1.6 wt% gel and b) an AFM height sensor image of a 1.5x10^{4} wt% suspension

Conductometric titrations were performed on the CNF-t suspension in order to assess the degree of oxidation *DO* and initial carboxylic acid group content X_{ox} related to the chemical reactivity of the material. A degree of oxidation *DO* of 29.9 % and a carboxylic content X_{ox} of 1.7 mmol/g ± 0,1 were calculated, which confirmed the high surface charge and surface chemical reactivity introduced on CNF surface through the TEMPO mediated oxidation treatment.

3.3.2. Prodrug synthesis and its characterization

Chemical structure of the Metro-MAL was elucidated thanks to ^{1}H and ^{13}C liquid NMR. The spectra exposed on Figure II.27 describe the full attribution of hydrogen and carbon atoms of the compound and confirms the success of the intended synthesis. The key result is the presence of the C_1, C_4 and C_2, C_3 peaks at 172.7 ppm and 134.1 ppm respectively. They prove that the prodrug chemical structure is suitable for the Diels Alder reaction since the maleimide group is indeed available on the isolated molecule.

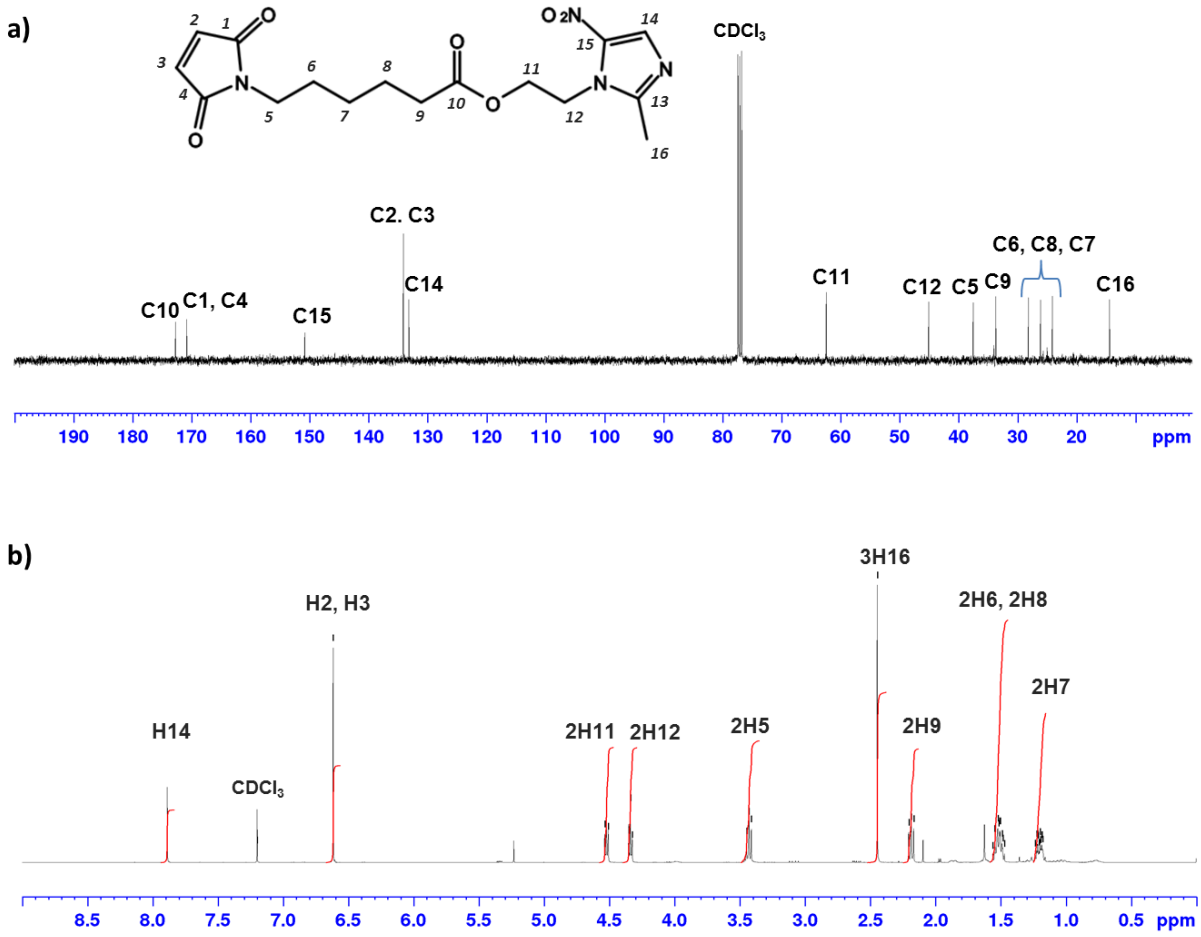

Figure II.27: Liquid ^{1}H and ^{13}C NMR spectrum of metronidazole maleimide (Metro-MAL) and carbon atoms attributions, $CDCl_3$ detected at 77ppm on ^{13}C spectrum is the solvent used for NMR analysis

3.3.3. Introduction of furan groups on CNF-t through amidation with furfurylamine

The covalent immobilization of furan groups was done on CNF-t suspensions. FTIR analysis was performed on CNF-t, CNF-fur and CNF-metro suspensions. Figure II.28 shows conventional peaks of cellulosic material for CNF related spectra. Stretching of O-H and C-H bonds at 3300 cm^{-1} and 2900 cm^{-1} respectively, -C-O-C- glycosidic bond stretching gives intense peaks in the 1100 cm^{-1} region together with C-O bonds at 1030, 1060 and 1110 cm^{-1} [10]. The CNF-t spectrum shows a sharp peak of strong intensity at 1740 cm^{-1} that corresponds to the acidic form of the carboxylic groups introduced by the TEMPO-mediated oxidation. At 1640 cm^{-1} the peak of medium intensity is associated with the O-H bonds of absorbed water molecules. In this region, on the CNF-fur spectrum, the shape of the detected peak is much wider. This is explained by the apparition of an amide function resulting from the bonding of furfurylamine to carboxylic groups of CNF-t. Around 1650 cm^{-1} the signal reveals the presence of a C=O bond that is involved in an amide I function. On the other side of this peak the observed widening is believed to be explained by C-N bond of the amide I that usually appears around 1550 cm^{-1}, which indicates the formation of an amide bond. This result qualitatively proves the presence of amide function on CNF substrate and the availability of furan groups. However, further confirmation and quantification of furan groups on CNF is required for subsequent reaction.

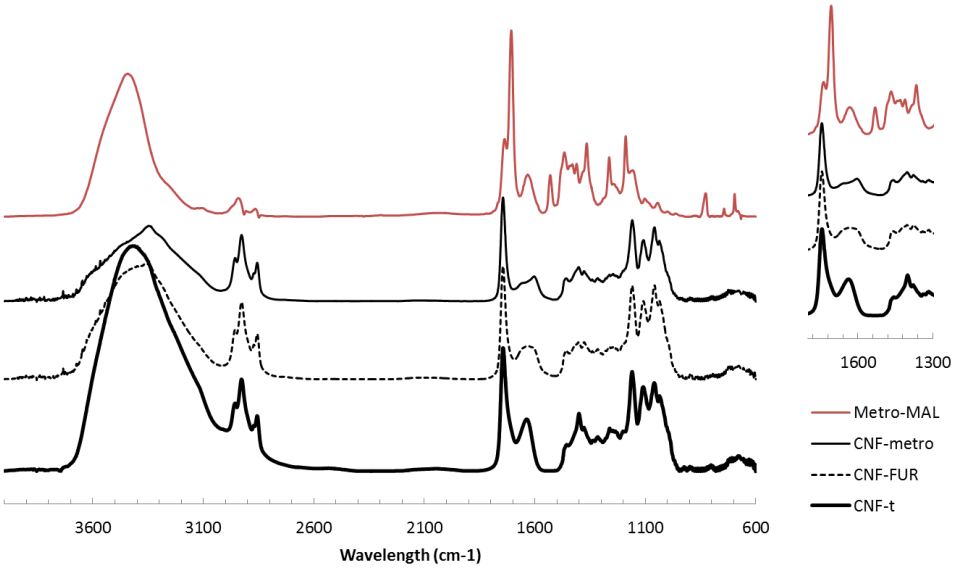

Figure II.28: FTIR spectra for CNF-t, CNF-fur after amidation, CNF-metro after Diels Alder reaction and Metro-MAL molecule. All spectra were measured through KBr disc preparation.

Conversion of carboxylic groups of CNF-t to amide function was mainly confirmed by conductometric titrations that were performed after the amidation and purification steps. The objective was to assess the amount of unreacted carboxylic acid groups and calculate the residual degree of oxidation DO_{res}. Figure II.29 shows the most representative curves obtained after conductometric titrations and

the values of *DO* and DO_{res} obtained before and after the reaction and calculated with equations (II-8) and (II-10). The residual degree of oxidation measured for CNF-fur is 18.3 % compared to 30.1 % for initial CNF-t suspension. The proportion of converted carboxylic group $\%COOH_{conv}$ can thus be calculated with equation (II-11) and gives a value of 39.1 %. This value can further be translated into a degree of substitution DS_{cond} thanks to equation (II-12) that provide us with the following result, DS_{cond} = 0.11.

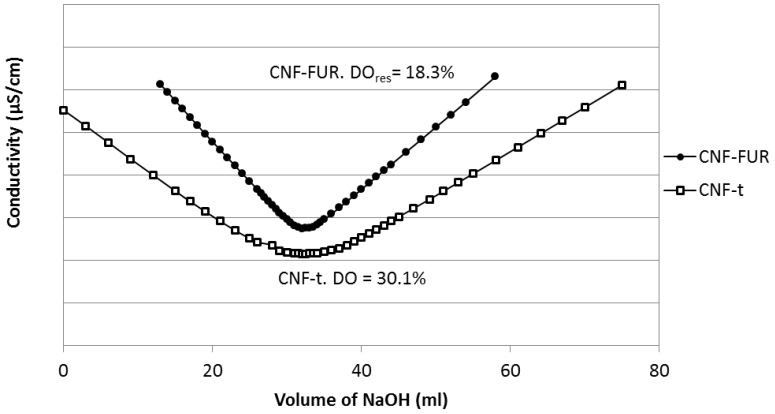

Figure II.29: Conductometric titration of CNF-t and CNF-fur suspension

The CNF solid films were then used to performed bulk elemental analysis experiments. In our case this analysis gives access to the mass proportion of carbon, hydrogen, nitrogen and sulfur content of the CNF films. On Table II.3, the mass proportion of carbon and hydrogen for CNF-t sample are lower than the theoretical values of pure cellulose (C 44.4 % and H 6.2 %). This can be explained by the presence of inorganic contaminants coming from the TEMPO oxidation and production process of CNF. However, the amount of oxygen is slightly superior to theoretical values of cellulose (49.3 %), remaining bound water is believed to explain this shift.

The amidation reaction is supposed to give an increase in the nitrogen quantity since furfurylamine involves a nitrogen atom in its chemical structure. This is clearly confirmed by elemental analysis results in Table II.3. However the use of EDC/NHS coupling agents that also have nitrogen atoms in their chemical structures could be detrimental to the outcome of elemental analysis. Intense purification strategies through both successive centrifugation/redispersion and days-lasting dialysis are believed to strongly reduce the amount of remaining EDC or NHS compound to an insignificant level. The nitrogen mass proportion for CNF-fur sample is 0.47 % while nothing is detected for CNF-t, which again confirms the presence of the furfurylamine molecule and its possible immobilization by covalent bonding thanks to the amidation. By measuring the oxygen content C/O ratio can also be calculated. Table II.3 shows in the last column that the C/O slightly increases. This is explained by a more numerous proportion of anhydroglucose unit (AGU) that bears a carbon rich furan moiety after

the amidation reaction. The equation (II-13) can be used to calculate a degree of substitution from elemental analysis values. It gives DS_{EA} = 0.06. This value is slightly lower than DS_{cond} (0.11) that is calculated from conductometric results. However, considering the very different nature of these characterization techniques and the low amount of immobilized furfurylamine on CNF-t, DS_{EA} and DS_{cond} values can be considered to be in the same order of magnitude. The combination of FTIR, conductometric titration and elemental analysis confirmed the availability of furan groups at the surface of cellulose nanofibers. This CNF-fur material is then suitable for Diels Alder click chemistry reaction for the binding of prodrug molecule, Metronidazole-maleimide. However, this reaction is supposed to take place in heterogeneous conditions and with moderate amount of furan groups, which could make the reaction less likely to occur. A model set up of this reaction was then implemented by reacting furfurylamine with 6-maleimido-hexanoic acid to validate the reaction conditions.

Table II.3: Results of elemental analysis for mass proportion of carbon, hydrogen, nitrogen and sulfur of CNF films

	% C	*sd*	% H	*sd*	% N	*sd*	% S	*sd*	% O	*sd*	C/O
CNF-t	**35.82**	*0.18*	**5.69**	*0.15*	**< 0.10**	-	**< 0.10**	-	**52.11**	-	**0.69**
CNF-fur	**39.23**	*0.68*	**6.12**	*0.12*	**0.47**	*0.01*	**< 0.10**	-	**51.66**	-	**0.76**
CNF-metro	**39.78**	*0.02*	**6.12**	*0.03*	**0.68**	*0.01*	**< 0.10**	-	**50.55**	*0.03*	**0.79**

3.3.4. Validation of click chemistry Diels Alder reaction conditions in homogeneous phase

Furfurylamine and 6-maleimido-hexanoic acid were reacted together at 40°C in a NMR tube under analysis in order to follow the evolution of the mixture and confirm that Diels Alder reaction is triggered upon these conditions. The carbons of the diene that is involved in the Diels Alder cycloaddition give a different signal after the reaction since they are actually among the carbons that undergo the strongest modification of chemical environment. On Figure II.30 is displayed the evolution of the liquid ^{13}C NMR spectra in the region from 79 to 92 ppm over reaction time together with the chemical compounds involved in the reaction and the expected product. This very narrow region reveals apparition of characteristic peaks that indicate the success of Diels Alder reaction, according to unpublished data acquired on similar reaction and conditions. After 1h of reaction at 40°C we can see peaks that arise from the baseline and they get stronger and more defined at 5 h and 24h. At 48 h and 72h the signals remain stable. Signals at 88 ppm and multiplet centered on 91 ppm are associated with the C10 carbon of new product while the peaks at 79 ppm and 81 ppm

correspond to the C13 carbon. The apparition of these signals confirms that Diels Alder reaction is occurring under the selected conditions in homogeneous phase. Even if it is obvious that heterogeneous conditions will have a lower kinetics, this experiment gives a rough idea of the time required to activate the Diels Alder reaction in these conditions. Based on these preliminary results, we have decided to perform our reaction on CNF-fur during at least 24h.

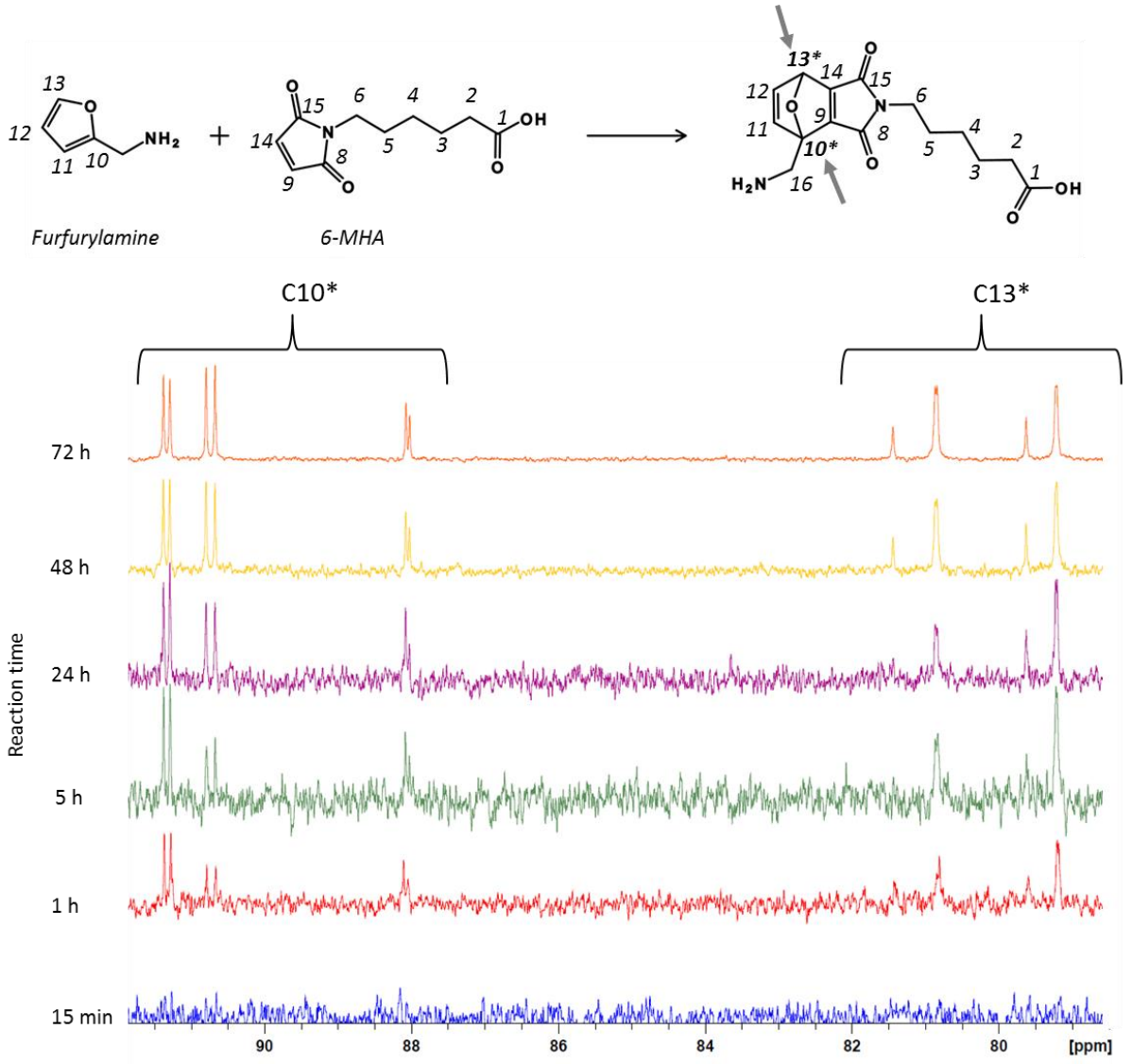

Figure II.30: Liquid ^{13}C NMR spectra of reaction mixture for Diels Alder reaction between furfurylamine and 6-maleimido-hexanoic acid in a 50/50 v/v ethanol/deionized water solvent

3.3.5. Immobilization of Metronidazole-maleimide prodrug on CNF-fur

On CNF-metro FTIR spectrum of Figure II.28 we can see that peaks at 1660 cm^{-1} and 1600 cm^{-1} clearly differs from the wide peak described above for CNF-fur spectrum in the same region. The spectrum of the Metro-MAL molecule is plotted against CNF substrates. Many of its characteristic peaks are overlapped with those of the CNF substrates and the potentially very low amount of immobilized drug is not visible with this technique.

Bulk analysis of the CNF-metro samples was performed with elemental analysis. Again, the increase of nitrogen mass proportion indicated by Table II.3 confirms the immobilization of the prodrug onto the CNF substrates since it is the only nitrogen containing molecule that was added in the reaction mixture. A significant proportion of 0.21 % ±0.01 of nitrogen can be attributed to the immobilization of the prodrug. Moreover, the decrease of oxygen proportion is in accordance with presence of metronidazole-maleimide since its chemical structure is less rich in oxygen atoms when compared to cellulose substrates (31 % vs. 49 % of oxygen mass proportion). The increase observed for C/O ratio confirms this result and is explained by the addition of even more carbon-rich structure like Metro-MAL compound on CNF-fur.

The final drug loading can be calculated from the shift of 0.21 % ±0.01 of nitrogen that is attributed to the prodrug presence. A value of 1.8 % of prodrug mass proportion in CNF films is obtained. This drug loading is consistent with values found in the literature when metronidazole is used [64] and could be released on demand with the presence of enzymes.

The Diels-Alder reaction has been also qualitatively followed by UV spectroscopy. Indeed, UV is preferably used for molecule in solutions but recent papers prove that UV absorbance can occur when nanoparticles are concerned, for example with silver nanowires [102], [103]. On Figure II.31, the UV-vis spectrum of Metro-MAL solution is displayed with spectrum of diluted CNF-fur suspension and spectra of the evolution of the Diels Alder reaction mixture over time. The two wide peaks centered on 220 nm and 320 nm are attributed to the absorbance of the metronidazole moiety as described in recent works [104], [105]. The contribution of maleimide function, that is usually detected around 300 nm when dealing with Diels Alder reaction [106], probably overlaps with the metronidazole signal.

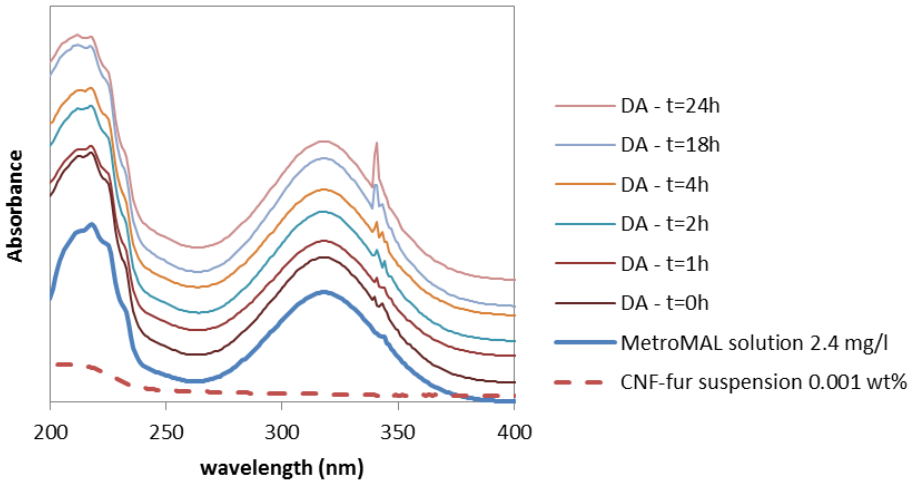

Figure II.31: UV spectroscopy following of the Diels-Alder (DA) reaction over time. Spectra from t =0h to t=24h have been shifted up for clarity

In our case, a peak that was observed neither for the Metro-MAL nor for the CNF-fur is clearly detected at 340 nm. This peak intensity grows over time and becomes more and more significant over 24 hours of Diels Alder reaction. This peak is believed to arise from the Diels Alder reaction and calls for further characterization of the obtained CNF suspension.

The conventional solid state ^{13}C NMR was used to characterize the product of the Diels Alder reaction. NMR peak assignments are provided for most of the resonances that could be assigned without ambiguity and are consistent with previously published data [80], [81]. The cellulose ^{13}C resonances at 66 and 89 ppm stem from C4 and C6 carbons of crystalline cellulose, respectively, whereas those at 64 and 84 ppm are assigned to amorphous C4 and C6 (Figure II.32). The ^{13}C resonance at 175 ppm confirms the presence of carbonyls from carboxylic groups in CNF-t.

CNF-fur spectrum confirms the formation of an amide bond during the first step of reaction since the peak of C=O bond at 175 ppm shifts to 170 ppm, similarly to the results obtained from the deconvolution technique used to confirm the formation of the amide bond, when propargylamine was grafted on CNF-t in the previous sub-chapter. Unfortunately, no obvious presence of MetroMAL can be observed on CNF-metro spectrum. This suggests that the achieved degree of substitution of the furan function by the MetroMAL molecule is under the limit of detection of conventional solid state NMR. Therefore, the innovative DNP-enhanced NMR technology is expected to bring further characterization of the CNF samples.

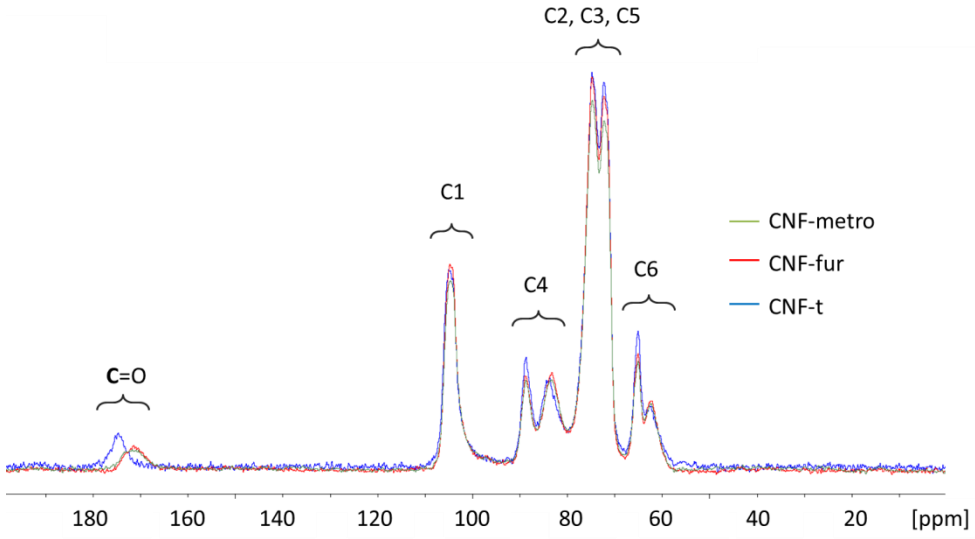

Figure II.32: Conventional solid state 13C NMR of CNF-t, CNF-fur and CNF-metro samples. Acquisition time was 2h

DNP-enhanced solid state NMR technique was used to go deeper in the chemical analysis of the three samples. Up to our knowledge, only a very few papers used such a technology with cellulose

based materials and this study is one of the first with nanocellulose. DNP was found to work efficiently on all CNF samples, with enhancements ($\varepsilon_{on/off}$) above 23 as illustrated by Figure II.33 for CNF-metro sample. This provides high NMR sensitivity and allows the fast observation of the scarce carbon species of furan and maleimide-modified metronidazole and especially confirmation of CNF-metro successful preparation.

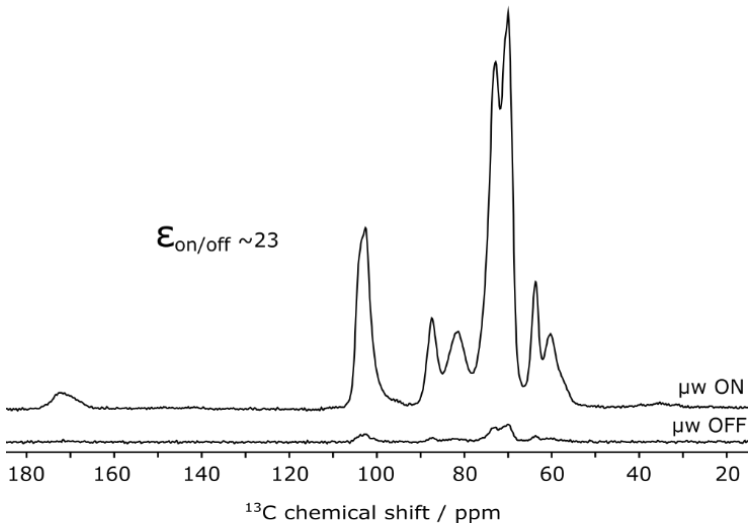

Figure II.33: 13C CPMAS NMR spectra with and without the application of microwave irradiation suitable for DNP enhancement on CNF-metro. The DNP enhancement factor (εon/off) is given in the figure.

DNP-enhanced ^{13}C cross-polarization magic angle spinning (CPMAS) spectra of the starting CNF material (CNF-t), furan-modified CNF (CNF-fur), and maleimide-metronidazole modified CNF (CNF-metro) are shown on Figure II.34. The ^{13}C NMR spectrum of CNF-fur along with insets of magnified chemical shift regions (0- 50 and 115-165 ppm) are displayed on Figure II.34b. The region 115-165 ppm shows two ^{13}C resonances from the furan ring at 144 and 151 ppm. The two other carbons from the same furan lie between 100-115 ppm, and one can be seen as a shoulder to the C1 cellulose resonance (see Figure II.35b) while the remaining furan ^{13}C resonance could not be observed directly because of resonance overlap with cellulose at 105 ppm. Deconvolution of the ^{13}C resonances between 165-180 ppm of the CNF-fur spectra, shown in Figure II.35a, gives the confirmation of the grafting of at least a part of the furan functions available on the CNF-t. The peak at 172 ppm results from the amide, and integration of this peak gives an estimate for the furan grafting at ~35 %. This value clearly correlates with the range of the value obtained from conductometric titration (39.1 %).

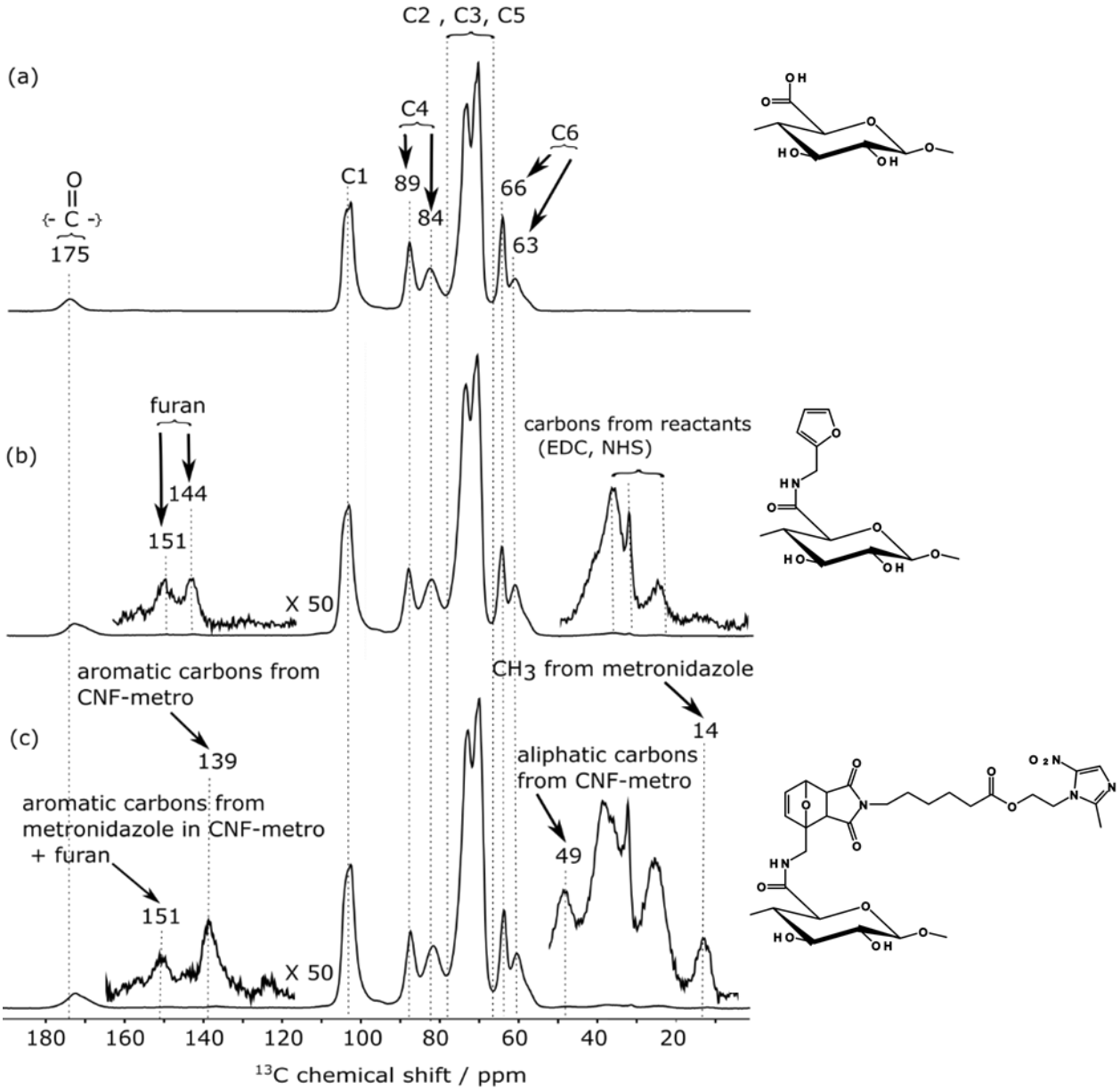

Figure II.34: DNP-enhanced solid-state NMR of surface-modified cellulose nanofibrils (CNF): 13C CPMAS spectra of (a) initial cellulose nanofibrils (CNF-t), (b) furoated cellulose nanofibrils (CNF-fur), and (c) maleimide-modified metronidazole grafted on cellulose nanofibrils (CNF-metro). The Cellulose 13C resonance assignment for (a), (b), and (c) is shown. The insets in (b) and (c) shows magnified spectra for the 0 – 50 ppm and 115 – 165 ppm spectral window, with the corresponding 13C resonance assignment.

The ^{13}C signals between 0-50 ppm in Figure II.34b can be assigned to carbons from N-(3-Dimethylaminopropyl)-N'-ethylcarbodiimide hydrochloride (EDC) and N-hydroxysuccinimide (NHS), which are remaining. The CH_2 moiety between the amide and furan should appear between 38-42 ppm, but cannot be identified unambiguously because of overlap from reactant carbons in the same region.

In Figure II.34c, the ^{13}C resonance at 139 ppm belongs to aromatic carbons next to nitro group from metronidazole in CNF-metro, demonstrating the presence of this function. Furthermore the decrease

in intensity of the ^{13}C resonance at 110 ppm from the furan, shown in Figure II.35b, confirms that the maleimide from CNF-metro has reacted with the furan from CNF-fur. The change in relative intensity of this ^{13}C resonance at 110 ppm, gives an estimate of about 50 % for the grafting of maleimide-modified metronidazole on CNF-fur furan rings.

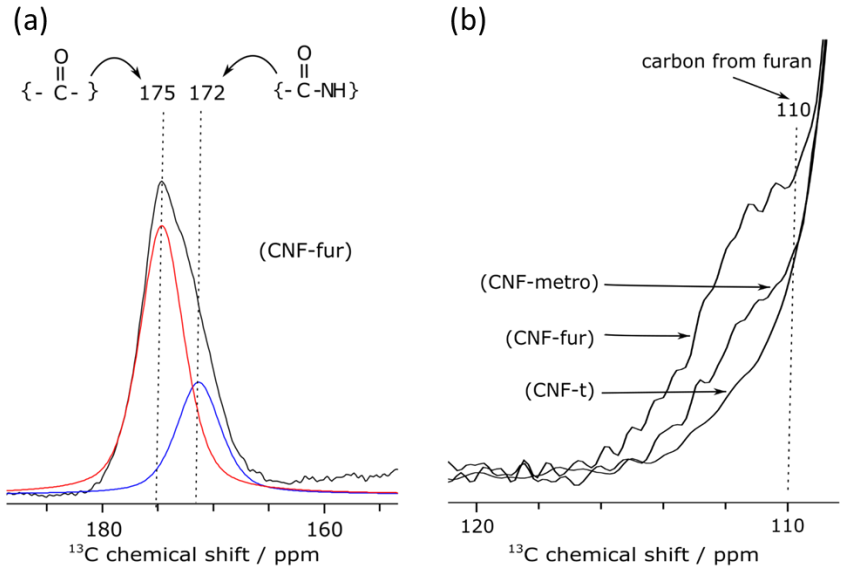

Figure II.35: (a) Deconvolution of resonances between 170 -180 ppm from CNF-fur sample, showing two distinct peaks corresponding to a carbonyl of carboxyl function and carbonyl from an amide function. (b) Extracted region from the ^{13}C CPMAS spectra of Figure II.34a, highlighting the evolution of the furan carbon at 110 ppm.

These results demonstrate the success of this complex two-steps covalent immobilization strategy thanks to this high performance enhanced NMR technique.

3.4 Conclusion

This study proposed for the first time a two-step strategy using amidation and Diels Alder click chemistry to covalently bind a prodrug onto oxidized CNF. The MetroMAL prodrug structure was confirmed by liquid NMR. Then, the amidation was first confirmed by conductometric titration, elemental analysis with the increase of nitrogen quantity and solid state NMR. The success of the Diels Alder reaction was proven both by elemental analysis and DNP-enhanced NMR experiments, which demonstrated to be a highly innovative technique suitable for CNF characterization. Very similar ranges of values for proportion of grafted anhydroglucose unit were obtained from these different techniques. These functionalized CNF could be used in medical device for drug release. The ester function that binds metronidazole to the CNF system being cleavable by esterase enzyme activity, “on-demand” drug release material was successfully designed.

***NB**: Authors would like to acknowledge Isabelle Jeacomine and Laurent Heux from Centre de Recherche sur les Macromolécules Végétales (CERMAV) for the ssNMR experiments and their expertise in this field.*

Conclusions of chapter II

The aim of this chapter was to propose new chemical immobilization strategies of active principle ingredients (API) on cellulose nanofibrils. Three different strategies were successfully applied on both CNF-e films and CNF-t suspensions.

In **chapter II-1**, CNF-e films were first immersed in water based Ciprofloxacin solution and an esterification reaction was then triggered upon heat treatment under vacuum. These CNF films demonstrated prolonged antibacterial activity by contact against both gram-positive and gram-negative bacterial strain, proving the success of the immobilization technique. Topical application medical devices can benefit from such an active membrane material.

The **chapter II-2** investigated a two-steps strategy to bind metronidazole onto CNF-t suspensions via a chain containing a cleavable function that can react in specific conditions, as in the case of an infection site. A first step of amidation leading to the CNF-t with alkyne functions was successfully carried out, as proved by several characterization tools such as Raman spectroscopy and solid state NMR. Then, the second step took place by involving thiol-yne click chemistry reaction between such alkyne functions with the thiol function of a metronidazole prodrug. In this case, elemental analysis and, for the first time on nanocellulose, dynamic nuclear polarization enhanced NMR (DNP-NMR), helped confirming the grafting success. Moreover, in **chapter II-3**, a similar approach was used to immobilize another metronidazole prodrug that bears a maleimide function. In suspensions again, CNF-t were provided with pending furan functions, which are suitable for Diels Alder click chemistry reaction with the maleimide moieties of the prodrug. DNP-NMR was used a second time to confirm the grafting success. Whatever the chemistry used for grafting onto cellulose (thiol-yne or Dies Alder), the immobilized prodrugs all contain a cleavable function (ester), in order to be able to release the drug "on-demand" upon cleavage by enzymatic activity. This feature is of high interest for implantable medical devices that are in contact with many different enzymes, often overexpressed during wound healing or infections.

To our knowledge, these immobilization strategies of API on CNF are an innovative and original approach. In addition, they are all water-based, making them more suitable for preserving the "green" potential of CNF and facilitating the industrial up-scale. In the next chapter, these modified CNF will be used to develop materials suitable for medical devices with prolonged antibacterial activity and drug release abilities. The antibacterial properties of the latter will be discussed.

List of tables

List of figures

Bibliography

[1] Y. Habibi, L. A. Lucia, and O. J. Rojas, "Cellulose Nanocrystals: Chemistry, Self-Assembly, and Applications," *Chemical Reviews*, vol. 110, no. 6, pp. 3479–3500, Jun. 2010.

[2] BP p.l.c., "BP Statistical Review of World Energy 67th edition." 2018.

[3] F. W. Herrick, R. L. Casebier, J. K. Hamilton, and K. R. Sandberg, "Microfibrillated cellulose: morphology and accessibility," *J. Appl. Polym. Sci.: Appl. Polym. Symp.; (United States)*, vol. 37, Jan. 1982.

[4] A. F. Turbak, F. W. Snyder, and K. R. Sandberg, "Microfibrillated cellulose, a new cellulose product: properties, uses, and commercial potential," *J. Appl. Polym. Sci.: Appl. Polym. Symp.; (United States)*, vol. 37, Jan. 1982.

[5] A. Dufresne, *Nanocellulose, From Nature to High Performance Tailored Materials*. Berlin, Boston: De Gruyter, 2017.

[6] R. Bardet and J. Bras, "Cellulose Nanofibers and Their Use in Paper Industry," in *Materials and Energy*, vol. 5, WORLD SCIENTIFIC, 2014, pp. 207–232.

[7] D. Klemm *et al.*, "Nanocelluloses: A New Family of Nature-Based Materials," *Angew. Chem. Int. Ed.*, vol. 50, no. 24, pp. 5438–5466, Jun. 2011.

[8] T. Abitbol *et al.*, "Nanocellulose, a tiny fiber with huge applications," *Current Opinion in Biotechnology*, vol. 39, pp. 76–88, Jun. 2016.

[9] O. Nechyporchuk, M. N. Belgacem, and J. Bras, "Production of cellulose nanofibrils: A review of recent advances," *Industrial Crops and Products*, Apr. 2016.

[10] E. J. Foster *et al.*, "Current characterization methods for cellulose nanomaterials," *Chemical Society Reviews*, vol. 47, no. 8, pp. 2609–2679, 2018.

[11] H. Kargarzadeh *et al.*, "Advances in cellulose nanomaterials," *Cellulose*, vol. 25, no. 4, pp. 2151–2189, Feb. 2018.

[12] S. Boufi, I. González, M. Delgado-Aguilar, Q. Tarrès, M. À. Pèlach, and P. Mutjé, "Nanofibrillated cellulose as an additive in papermaking process: A review," *Carbohydrate Polymers*, vol. 154, pp. 151–166, Dec. 2016.

[13] C. Aulin, M. Gällstedt, and T. Lindström, "Oxygen and oil barrier properties of microfibrillated cellulose films and coatings," *Cellulose*, vol. 17, no. 3, pp. 559–574, Jun. 2010.

[14] A. Dufresne, S. Thomas, and L. A. Pothan, *Biopolymer Nanocomposites: Processing, Properties, and Applications*. John Wiley & Sons, 2013.

[15] Z. Shi, G. O. Phillips, and G. Yang, "Nanocellulose electroconductive composites," *Nanoscale*, vol. 5, no. 8, pp. 3194–3201, 2013.

[16] M. Wu, S. Kuga, and Y. Huang, "Quasi-One-Dimensional Arrangement of Silver Nanoparticles Templated by Cellulose Microfibrils," *Langmuir*, vol. 24, no. 18, pp. 10494–10497, Sep. 2008.

[17] P. Bober *et al.*, "Biocomposites of Nanofibrillated Cellulose, Polypyrrole, and Silver Nanoparticles with Electroconductive and Antimicrobial Properties," *Biomacromolecules*, vol. 15, no. 10, pp. 3655–3663, Oct. 2014.

[18] N. Lin and A. Dufresne, "Nanocellulose in biomedicine: Current status and future prospect," *European Polymer Journal*, vol. 59, pp. 302–325, Oct. 2014.

[19] N. Halib *et al.*, "Potential Applications of Nanocellulose-Containing Materials in the Biomedical Field," *Materials*, vol. 10, no. 8, p. 977, Aug. 2017.

[20] M. Jorfi and E. J. Foster, "Recent advances in nanocellulose for biomedical applications," *J. Appl. Polym. Sci.*, vol. 132, no. 14, p. n/a-n/a, Apr. 2015.

[21] P. Laurén, "Biomedical applications of nanofibrillar cellulose (Ph.D. thesis)," 2018.

[22] L. Alexandrescu, K. Syverud, A. Gatti, and G. Chinga-Carrasco, "Cytotoxicity tests of cellulose nanofibril-based structures," *Cellulose*, vol. 20, no. 4, pp. 1765–1775, Aug. 2013.

[23] K.-S. Hannukainen, S. Suhonen, K. Savolainen, and H. Norppa, "Genotoxicity of nanofibrillated cellulose in vitro as measured by enzyme comet assay," *Toxicology Letters*, vol. Supplement, no. 211, p. S71, 2012.

[24] R. Kolakovic, L. Peltonen, T. Laaksonen, K. Putkisto, A. Laukkanen, and J. Hirvonen, "Spray-Dried Cellulose Nanofibers as Novel Tablet Excipient," *AAPS PharmSciTech*, vol. 12, no. 4, pp. 1366–1373, Dec. 2011.
[25] R. Kolakovic, L. Peltonen, A. Laukkanen, J. Hirvonen, and T. Laaksonen, "Nanofibrillar cellulose films for controlled drug delivery," *European Journal of Pharmaceutics and Biopharmaceutics*, vol. 82, no. 2, pp. 308–315, Oct. 2012.
[26] N. Lavoine, I. Desloges, and J. Bras, "Microfibrillated cellulose coatings as new release systems for active packaging," *Carbohydrate polymers*, vol. 103, pp. 528–537, 2014.
[27] N. Lavoine, V. Guillard, I. Desloges, N. Gontard, and J. Bras, "Active bio-based food-packaging: Diffusion and release of active substances through and from cellulose nanofiber coating toward food-packaging design," *Carbohydrate Polymers*, vol. 149, pp. 40–50, Sep. 2016.
[28] N. Lavoine, C. Givord, N. Tabary, I. Desloges, B. Martel, and J. Bras, "Elaboration of a new antibacterial bio-nano-material for food-packaging by synergistic action of cyclodextrin and microfibrillated cellulose," *Innovative Food Science & Emerging Technologies*, vol. 26, pp. 330–340, 2014.
[29] S. Saini, N. Belgacem, J. Mendes, G. Elegir, and J. Bras, "Contact Antimicrobial Surface Obtained by Chemical Grafting of Microfibrillated Cellulose in Aqueous Solution Limiting Antibiotic Release," *ACS Applied Materials & Interfaces*, vol. 7, no. 32, pp. 18076–18085, Aug. 2015.
[30] S. Saini, C. B. SILLARD, M. N. Belgacem, and J. Bras, "Nisin anchored cellulose nanofiber for long term antimicrobial active food packaging," *RSC Advances*, 2016.
[31] B. A. Herbold, S. Y. Brendler-Schwaab, and H. J. Ahr, "Ciprofloxacin: in vivo genotoxicity studies," *Mutation Research/Genetic Toxicology and Environmental Mutagenesis*, vol. 498, no. 1–2, pp. 193–205, Nov. 2001.
[32] P. C. Appelbaum and P. A. Hunter, "The fluoroquinolone antibacterials: past, present and future perspectives," *International Journal of Antimicrobial Agents*, vol. 16, no. 1, pp. 5–15, Sep. 2000.
[33] S. L. A. M. Bronzwaer *et al.*, "The Relationship between Antimicrobial Use and Antimicrobial Resistance in Europe," *Emerg Infect Dis*, vol. 8, no. 3, pp. 278–282, Mar. 2002.
[34] H. A. A. Ezelarab, S. H. Abbas, H. A. Hassan, and G. E.-D. A. Abuo-Rahma, "Recent updates of fluoroquinolones as antibacterial agents," *Archiv der Pharmazie*, vol. 351, no. 9, p. 1800141, Sep. 2018.
[35] I. Turel and P. Bukovec, "Comparison of the thermal stability of ciprofloxacin and its compounds," *Thermochimica Acta*, vol. 287, no. 2, pp. 311–318, Oct. 1996.
[36] J. M. Andrews, "Determination of minimum inhibitory concentrations," *J Antimicrob Chemother*, vol. 48, no. suppl_1, pp. 5–16, Jul. 2001.
[37] U. Hubicka, J. Krzek, and M. Walczak, "Stability of ciprofloxacin and norfloxacin in the presence and absence of metal ions in acidic solution," *Pharmaceutical Development and Technology*, vol. 15, no. 5, pp. 532–544, Oct. 2010.
[38] M. L. Nelson and R. T. O'Connor, "Relation of certain infrared bands to cellulose crystallinity and crystal latticed type. Part I. Spectra of lattice types I, II, III and of amorphous cellulose," *Journal of Applied Polymer Science*, vol. 8, no. 3, pp. 1311–1324, May 1964.
[39] M. L. Nelson and R. T. O'Connor, "Relation of certain infrared bands to cellulose crystallinity and crystal lattice type. Part II. A new infrared ratio for estimation of crystallinity in celluloses I and II," *Journal of Applied Polymer Science*, vol. 8, no. 3, pp. 1325–1341, May 1964.
[40] C. Y. Liang and R. H. Marchessault, "Infrared spectra of crystalline polysaccharides. II. Native celluloses in the region from 640 to 1700 cm.−1," *Journal of Polymer Science*, vol. 39, no. 135, pp. 269–278, Sep. 1959.
[41] V. L. Dorofeev, "Infrared spectra and the structure of drugs of the fluoroquinolone group," *Pharmaceutical Chemistry Journal*, vol. 38, no. 12, pp. 693–697, Dec. 2004.
[42] T.-M. Tenhunen *et al.*, "Understanding the interactions of cellulose fibres and deep eutectic solvent of choline chloride and urea," *Cellulose*, vol. 25, no. 1, pp. 137–150, Jan. 2018.

[43] M. Jannesari, J. Varshosaz, M. Morshed, and M. Zamani, "Composite poly(vinyl alcohol)/poly(vinyl acetate) electrospun nanofibrous mats as a novel wound dressing matrix for controlled release of drugs," *Int J Nanomedicine*, vol. 6, pp. 993–1003, 2011.
[44] J.-X. Fu, H.-J. Wang, Y.-Q. Zhou, and J.-Y. Wang, "Antibacterial activity of ciprofloxacin-loaded zein microsphere films," *Materials Science and Engineering: C*, vol. 29, no. 4, pp. 1161–1166, May 2009.
[45] S. Marchesan *et al.*, "Self-assembly of ciprofloxacin and a tripeptide into an antimicrobial nanostructured hydrogel," *Biomaterials*, vol. 34, no. 14, pp. 3678–3687, May 2013.
[46] B. D. Kevadiya *et al.*, "Biodegradable gelatin–ciprofloxacin–montmorillonite composite hydrogels for controlled drug release and wound dressing application," *Colloids and Surfaces B: Biointerfaces*, vol. 122, pp. 175–183, Oct. 2014.
[47] L. B. Price, A. Vogler, T. Pearson, J. D. Busch, J. M. Schupp, and P. Keim, "In Vitro Selection and Characterization of Bacillus anthracis Mutants with High-Level Resistance to Ciprofloxacin," *Antimicrobial Agents and Chemotherapy*, vol. 47, no. 7, pp. 2362–2365, Jul. 2003.
[48] P. N. Markham, "Inhibition of the Emergence of Ciprofloxacin Resistance in Streptococcus pneumoniae by the Multidrug Efflux Inhibitor Reserpine," p. 2, 1999.
[49] N. Lavoine, I. Desloges, B. Manship, and J. Bras, "Antibacterial paperboard packaging using microfibrillated cellulose," *Journal of food science and technology*, vol. 52, no. 9, pp. 5590–5600, 2015.
[50] F. Hoeng, A. Denneulin, and J. Bras, "Use of nanocellulose in printed electronics: a review," *Nanoscale*, vol. 8, no. 27, pp. 13131–13154, 2016.
[51] T. Saito, Y. Nishiyama, J.-L. Putaux, M. Vignon, and A. Isogai, "Homogeneous Suspensions of Individualized Microfibrils from TEMPO-Catalyzed Oxidation of Native Cellulose," *Biomacromolecules*, vol. 7, no. 6, pp. 1687–1691, Jun. 2006.
[52] A. Isogai, T. Saito, and H. Fukuzumi, "TEMPO-oxidized cellulose nanofibers," *Nanoscale*, vol. 3, no. 1, pp. 71–85, 2011.
[53] K. Syverud, "SciFinder - Potential of cellulose nanofibrils in tissue engineering - ACS abstract," spring-2016. [Online]. Available: https://scifinder-cas-org.gaelnomade.ujf-grenoble.fr/scifinder/view/scifinder/scifinderExplore.jsf. [Accessed: 01-Dec-2016].
[54] H. R. Nordli, G. Chinga-Carrasco, A. M. Rokstad, and B. Pukstad, "Producing ultrapure wood cellulose nanofibrils and evaluating the cytotoxicity using human skin cells," *Carbohydrate Polymers*, vol. 150, pp. 65–73, Oct. 2016.
[55] K. Syverud, S. R. Pettersen, K. Draget, and G. Chinga-Carrasco, "Controlling the elastic modulus of cellulose nanofibril hydrogels—scaffolds with potential in tissue engineering," *Cellulose*, vol. 22, no. 1, pp. 473–481, Feb. 2015.
[56] D. Celebi, R. H. Guy, K. J. Edler, and J. L. Scott, "Ibuprofen delivery into and through the skin from novel oxidized cellulose-based gels and conventional topical formulations," *International Journal of Pharmaceutics*, vol. 514, no. 1, pp. 238–243, Nov. 2016.
[57] H. Valo *et al.*, "Drug release from nanoparticles embedded in four different nanofibrillar cellulose aerogels," *European Journal of Pharmaceutical Sciences*, vol. 50, no. 1, pp. 69–77, Sep. 2013.
[58] "Metronidazole: MedlinePlus Drug Information." [Online]. Available: https://medlineplus.gov/druginfo/meds/a689011.html. [Accessed: 30-Aug-2018].
[59] Pubchem, "Metronidazole." [Online]. Available: https://pubchem.ncbi.nlm.nih.gov/compound/4173. [Accessed: 30-Aug-2018].
[60] M. E. Campos-Aldrete and L. Villafuerte-Robles, "Influence of the viscosity grade and the particle size of HPMC on metronidazole release from matrix tablets," *European Journal of Pharmaceutics and Biopharmaceutics*, vol. 43, no. 2, pp. 173–178, Apr. 1997.
[61] O. A. Itiola and N. Pilpel, "Tableting characteristics of metronidazole formulations," *International Journal of Pharmaceutics*, vol. 31, no. 1, pp. 99–105, Jul. 1986.
[62] K. A. Gates, H. Grad, P. Birek, and P. I. Lee, "A New Bioerodible Polymer Insert for the Controlled Release of Metronidazole," *Pharm Res*, vol. 11, no. 11, pp. 1605–1609, Nov. 1994.

[63] Y. Dong, H. Paukkonen, W. Fang, E. Kontturi, T. Laaksonen, and P. Laaksonen, "Entangled and colloidally stable microcrystalline cellulose matrices in controlled drug release," *International Journal of Pharmaceutics*, vol. 548, no. 1, pp. 113–119, Sep. 2018.
[64] H. Paukkonen *et al.*, "Nanofibrillar cellulose hydrogels and reconstructed hydrogels as matrices for controlled drug release," *International Journal of Pharmaceutics*, vol. 532, no. 1, pp. 269–280, Oct. 2017.
[65] J. M. Schakenraad, M. J. Hardonk, J. Feijen, I. Molenaar, and P. Nieuwenhuis, "Enzymatic activity toward poly(L-lactic acid) implants," *Journal of Biomedical Materials Research*, vol. 24, no. 5, pp. 529–545, May 1990.
[66] Y. Habibi, "Key advances in the chemical modification of nanocelluloses," *Chem. Soc. Rev.*, vol. 43, no. 5, pp. 1519–1542, 2014.
[67] K. Missoum, M. N. Belgacem, and J. Bras, "Nanofibrillated Cellulose Surface Modification: A Review," *Materials*, vol. 6, no. 5, pp. 1745–1766, May 2013.
[68] F. Rol, M. N. Belgacem, A. Gandini, and J. Bras, "Recent advances in surface-modified cellulose nanofibrils," *Progress in Polymer Science*, Sep. 2018.
[69] H. C. Kolb, M. G. Finn, and K. B. Sharpless, "Click Chemistry: Diverse Chemical Function from a Few Good Reactions," *Angewandte Chemie International Edition*, vol. 40, no. 11, pp. 2004–2021, Jun. 2001.
[70] J. R. G. Navarro *et al.*, "Multicolor Fluorescent Labeling of Cellulose Nanofibrils by Click Chemistry," *Biomacromolecules*, vol. 16, no. 4, pp. 1293–1300, Apr. 2015.
[71] N. Pahimanolis *et al.*, "Surface functionalization of nanofibrillated cellulose using click-chemistry approach in aqueous media," *Cellulose*, vol. 18, no. 5, pp. 1201–1212, Oct. 2011.
[72] K. S. Sharma *et al.*, "Glucose-Based Amphiphilic Telomers Designed to Keep Membrane Proteins Soluble in Aqueous Solutions: Synthesis and Physicochemical Characterization," *Langmuir*, vol. 24, no. 23, pp. 13581–13590, Dec. 2008.
[73] D. da Silva Perez, S. Montanari, and M. R. Vignon, "TEMPO-Mediated Oxidation of Cellulose III," *Biomacromolecules*, vol. 4, no. 5, pp. 1417–1425, Sep. 2003.
[74] F. Hoeng, A. Denneulin, C. Neuman, and J. Bras, "Charge density modification of carboxylated cellulose nanocrystals for stable silver nanoparticles suspension preparation," *Journal of Nanoparticle Research*, vol. 17, no. 6, Jun. 2015.
[75] A. Lesage, M. Bardet, and L. Emsley, "Through-Bond Carbon−Carbon Connectivities in Disordered Solids by NMR," *J. Am. Chem. Soc.*, vol. 121, no. 47, pp. 10987–10993, Dec. 1999.
[76] E. Johan Foster *et al.*, "Current characterization methods for cellulose nanomaterials," *Chemical Society Reviews*, vol. 47, no. 8, pp. 2609–2679, 2018.
[77] N. Lavoine, J. Bras, T. Saito, and A. Isogai, "Optimization of preparation of thermally stable cellulose nanofibrils via heat-induced conversion of ionic bonds to amide bonds," *Journal of Polymer Science Part A: Polymer Chemistry*, vol. 55, no. 10, pp. 1750–1756, May 2017.
[78] G. Mangiante *et al.*, "Green Nondegrading Approach to Alkyne-Functionalized Cellulose Fibers and Biohybrids Thereof: Synthesis and Mapping of the Derivatization," *Biomacromolecules*, vol. 14, no. 1, pp. 254–263, Jan. 2013.
[79] U. P. Agarwal, "Raman Spectroscopy of CNC-and CNF-Based Nanocomposites," *Handbook of Nanocellulose and Cellulose Nanocomposites*, pp. 609–625, 2017.
[80] R. H. Atalla and D. L. VanderHart, "The role of solid state 13C NMR spectroscopy in studies of the nature of native celluloses," *Solid State Nuclear Magnetic Resonance*, vol. 15, no. 1, pp. 1–19, Oct. 1999.
[81] S. Montanari, M. Roumani, L. Heux, and M. R. Vignon, "Topochemistry of Carboxylated Cellulose Nanocrystals Resulting from TEMPO-Mediated Oxidation," *Macromolecules*, vol. 38, no. 5, pp. 1665–1671, Mar. 2005.
[82] A. J. Rossini, A. Zagdoun, M. Lelli, A. Lesage, C. Copéret, and L. Emsley, "Dynamic Nuclear Polarization Surface Enhanced NMR Spectroscopy," *Accounts of Chemical Research*, vol. 46, no. 9, pp. 1942–1951, Sep. 2013.

[83] D. Klemm, B. Heublein, H.-P. Fink, and A. Bohn, "Cellulose: Fascinating Biopolymer and Sustainable Raw Material," *Angewandte Chemie International Edition*, vol. 44, no. 22, pp. 3358–3393, 2005.
[84] M. Jorfi and E. J. Foster, "Recent advances in nanocellulose for biomedical applications," *J. Appl. Polym. Sci.*, vol. 132, no. 14, p. n/a-n/a, 2014.
[85] T. Saito, Y. Nishiyama, J.-L. Putaux, M. Vignon, and A. Isogai, "Homogeneous Suspensions of Individualized Microfibrils from TEMPO-Catalyzed Oxidation of Native Cellulose," *Biomacromolecules*, vol. 7, no. 6, pp. 1687–1691, Jun. 2006.
[86] K. Hua *et al.*, "Translational study between structure and biological response of nanocellulose from wood and green algae," *RSC Advances*, vol. 4, no. 6, pp. 2892–2903, 2014.
[87] K. Missoum, "Modification chimique de surface de NanoFibrilles de Cellulose (NFC)," phdthesis, Université Grenoble Alpes, 2012.
[88] H. C. Kolb, M. G. Finn, and K. B. Sharpless, "Click Chemistry: Diverse Chemical Function from a Few Good Reactions," *Angewandte Chemie International Edition*, vol. 40, no. 11, pp. 2004–2021, Jun. 2001.
[89] C. R. Becer, R. Hoogenboom, and U. S. Schubert, "Click Chemistry beyond Metal-Catalyzed Cycloaddition," *Angewandte Chemie International Edition*, vol. 48, no. 27, pp. 4900–4908, Jun. 2009.
[90] A. Gandini, A. J. F. Carvalho, E. Trovatti, R. K. Kramer, and T. M. Lacerda, "Macromolecular materials based on the application of the Diels–Alder reaction to natural polymers and plant oils," *European Journal of Lipid Science and Technology*, vol. 120, no. 1, p. 1700091, 2018.
[91] E. Trovatti, A. G. Cunha, A. J. F. Carvalho, and A. Gandini, "Furan-modified natural rubber: A substrate for its reversible crosslinking and for clicking it onto nanocellulose," *International Journal of Biological Macromolecules*, vol. 95, pp. 762–768, Feb. 2017.
[92] D. Bliman, M. Demeunynck, P. Leblond, S. Meignan, I. Baussane, and S. Fort, "Enzymatically Activated Glyco-Prodrugs of Doxorubicin Synthesized by a Catalysis-Free Diels–Alder Reaction," *Bioconjugate Chem.*, vol. 29, no. 7, pp. 2370–2381, Jul. 2018.
[93] N. M. Mahfouz and M. A. Hassan, "Synthesis, chemical and enzymatic hydrolysis, and bioavailability evaluation in rabbits of metronidazole amino acid ester prodrugs with enhanced water solubility," *Journal of Pharmacy and Pharmacology*, vol. 53, no. 6, pp. 841–848, Jun. 2001.
[94] C. Mura *et al.*, "Metronidazole prodrugs: Synthesis, physicochemical properties, stability, and ex vivo release studies," *European Journal of Medicinal Chemistry*, vol. 46, no. 9, pp. 4142–4150, Sep. 2011.
[95] M. Johansen, B. Møllgaard, P. K. Wotton, C. Larsen, and A. Hoelgaard, "In vitro evaluation of dermal prodrug delivery — transport and bioconversion of a series of aliphatic esters of metronidazole," *International Journal of Pharmaceutics*, vol. 32, no. 2, pp. 199–206, Oct. 1986.
[96] J. Han *et al.*, "Design, Synthesis, and Biological Activity of Novel Dicoumarol Glucagon-like Peptide 1 Conjugates," *J. Med. Chem.*, vol. 56, no. 24, pp. 9955–9968, Dec. 2013.
[97] Q. A. Bui, T. H. H. Vu, V. K. T. Ngo, I. R. Kennedy, N. A. Lee, and R. Allan, "Development of an ELISA to detect clenbuterol in swine products using a new approach for hapten design," *Anal Bioanal Chem*, vol. 408, no. 22, pp. 6045–6052, Sep. 2016.
[98] M. Rosay *et al.*, "Solid-state dynamic nuclear polarization at 263 GHz: spectrometer design and experimental results," *Phys Chem Chem Phys*, vol. 12, no. 22, pp. 5850–5860, Jun. 2010.
[99] E. O. Stejskal, J. Schaefer, and J. S. Waugh, "Magic-angle spinning and polarization transfer in proton-enhanced NMR," *Journal of Magnetic Resonance (1969)*, vol. 28, no. 1, pp. 105–112, Oct. 1977.
[100] G. Metz, X. L. Wu, and S. O. Smith, "Ramped-Amplitude Cross Polarization in Magic-Angle-Spinning NMR," *Journal of Magnetic Resonance, Series A*, vol. 110, no. 2, pp. 219–227, Oct. 1994.
[101] A. Pines, M. G. Gibby, and J. S. Waugh, "Proton-enhanced NMR of dilute spins in solids," *J. Chem. Phys.*, vol. 59, no. 2, pp. 569–590, Jul. 1973.
[102] D. L. Van Hyning and C. F. Zukoski, "Formation Mechanisms and Aggregation Behavior of Borohydride Reduced Silver Particles," *Langmuir*, vol. 14, no. 24, pp. 7034–7046, Nov. 1998.

[103] A. Callegari, D. Tonti, and M. Chergui, “Photochemically Grown Silver Nanoparticles with Wavelength-Controlled Size and Shape,” *Nano Lett.*, vol. 3, no. 11, pp. 1565–1568, Nov. 2003.
[104] M. R. El-Ghobashy and N. F. Abo-Talib, “Spectrophotometric methods for the simultaneous determination of binary mixture of metronidazole and diloxanide furoate without prior separation,” *Journal of Advanced Research*, vol. 1, no. 4, pp. 323–329, Oct. 2010.
[105] H. M. Hafez, A. A. Elshanawany, L. M. Abdelaziz, and M. S. Mohram, “Design of Experiment Utilization to Develop a Simple and Robust RP - UPLC Technique for Stability Indicating Method of Ciprofloxacin Hydrochloride and Metronidazole in Tablets,” *Eurasian J Anal Chem*, p. 23, 2015.
[106] A. Gandini, D. Coelho, and A. J. D. Silvestre, “Reversible click chemistry at the service of macromolecular materials. Part 1: Kinetics of the Diels–Alder reaction applied to furan–maleimide model compounds and linear polymerizations,” *European Polymer Journal*, vol. 44, no. 12, pp. 4029–4036, Dec. 2008.

Chapter III

Development of cellulose nanofibrils materials for medical devices

Table of Content

III. Development of cellulose nanofibrils materials for medical devices

Introduction to Chapter III

The chapter II was focused on the use of cellulose nanofibrils (CNF) as a platform to covalently immobilize active principle ingredients (API) such as ciprofloxacin and metronidazole. This chapter illustrates the activity of such grafted cellulose nanofibrils and presents a comparison with cellulose nanofibrils networks used as a tool to encapsulate APIs, through the exploitation of adsorption phenomena. Two kinds of substrates are prepared, (i) 100% CNF membranes design for potential topical applications and (ii) collagen-CNF composite intended for soft tissue repair application. The latter includes either (a) API modified CNF or (b) CNF with adsorbed APIs. These substrates are designed to prepare model medical devices and thus need to be characterized on several aspects that are related to the application: their ability to absorb wound exudate (water uptake), to release the immobilized drug and to be able to limit bacterial activity, and finally to undergo sterilization treatment without degradation. This last point is assessed by investigating the influence of sterilization through gamma radiation on drug chemical structure and activity, on substrates morphology and water immersion behavior.

Thus, the first part of this chapter deals with 100% CNF membrane for topical application. Production process influence on water uptake and release profiles will be assessed for CNF membranes containing encapsulated/adsorbed ciprofloxacin. The comparison with ciprofloxacin grafted CNF membranes will be carried out with antibacterial activity testing. Secondly, this chapter describes the production of composites combining metronidazole-modified CNF and collagen. The concept of "on-demand" release of metronidazole from the modified-CNF under enzymatic activity is investigated. The antibacterial activity of these collagen-CNF composite is also assessed. Finally, the last part of this chapter focuses on the influence of gamma radiation, CNF type and CNF proportion on the water uptake and release profiles of dig CHX loaded collagen-CNF composites. The Figure III.1 summarizes the chapter III structure.

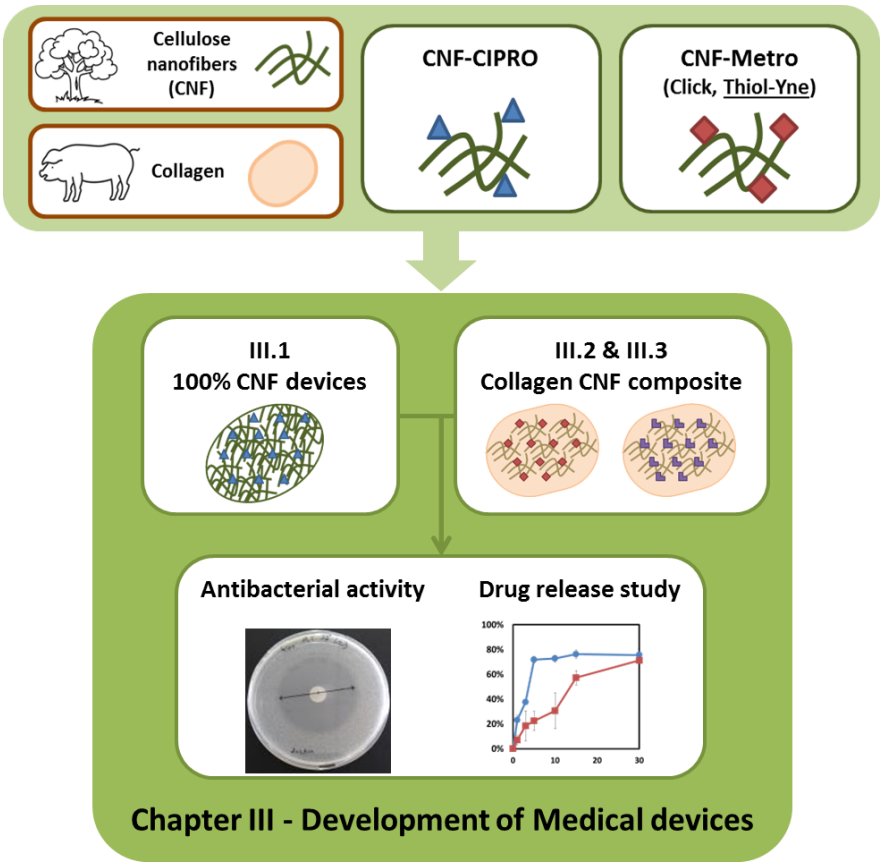

Figure III.1: Graphical representation of *chapter III* structure

1. Pure cellulose nanofibrils membranes loaded with ciprofloxacin: development and focus on drug release and antibacterial activity

This section is adapted from "H. Durand, P. Jaouen, E. Faure, C. Sillard, E. Zeno, N. Belgacem, J. Bras – Pure cellulose nanofibrils membranes loaded with ciprofloxacin: development and focus on drug release and antibacterial activity", submitted to Cellulose in November 2018

Abstract

The biocompatibility and very high specific area of enzyme pre-treated cellulose nanofibrils (CNF-e) are properties of high interest for the development of active substrates for new medical device development. CNF-e can be self-organized into nanostructured membranes that are suitable for active principle ingredients (API) encapsulation through adsorption phenomena. In addition, tunable surface chemistry of CNF-e, allow for covalent immobilization of API. In this work, ciprofloxacin is integrated to CNF-e membranes according to two different strategies. The first one relies only on adsorption mechanisms; ciprofloxacin is encapsulated in the bulk before the membrane formation by solvent casting. The influence of the membrane properties and preparation parameters such as grammage, thickness and drying technique, are assessed with water uptake measurements and API release experiments. The second strategy deals with the covalent immobilization of ciprofloxacin directly onto CNF-e membrane. The two kinds of membranes are then compared in terms of antibacterial activity, in both static and dynamic conditions. Thick CNF-e membranes loaded with adsorbed ciprofloxacin that were overdried (2h, 150°C) prove to be more resistant in liquid medium and present a more membranes with adsorbed ciprofloxacin lost rapidly their activity, while CNF-e membranes with covalently immobilized ciprofloxacin remain contact active for several days. These 100% CNF-e active nanostructured membranes can be used as new wound dressing for topical application.

1.1 Introduction

The interest for cellulose nanofibrils (CNF) has exponentially increased over the last ten years with the development of new production routes (pre-treatments, improved mechanical fibrillation [1], [2]) and announcements of its industrialization. The number of scientific paper has been multiplied by 5 between 2007 and 2017 and several books [3], [4] or reviews [5]–[7] are now available on this topic. Such nanofibrillated cellulose can be used in several applications like paper [8], [9], nanocomposites [10], cosmetic or printed electronics [11], [12]. Most of the time, barrier, mechanical and rheological properties are the main reason behind the use of CNF, in addition to its renewable character and biodegradability. More recently, the biocompatibility and large specific surface area of CNF have motivated researchers to extend its use in the biomedical field for the development of new drug delivery and tissue engineering systems [13]–[15].

If we focus on drug delivery, CNF films and membrane have been designed as entrapping systems for hydrophobic drug in 2012 for the first time by Kolakovic et al [16]. Since that time, very interesting interactions between some active molecules and cellulose nanofibrils were investigated. A comparison between caffeine and chlorhexidine digluconate has been performed by Lavoine et al . in terms of release profile [17]–[19]. The main outcomes indicated a prolonged controlled release of API thanks to the nanoporous network of CNF coatings. Cage-like molecules, i.e. cyclodextrins, were also used to complement the anchoring strategies of active molecules on CNF substrates. It resulted in multi-encapsulation systems [20]. To the best of our knowledge, there is no study on the interaction of ciprofloxacin with CNF. This new second generation fluoroquinolone is very promising since it has a broad spectrum of activity against both gram positive and gram negative bacterial strains [21]. The fluoroquinolones inhibits the enzymes involved in the DNA replication process, leading to bacteriostasis and eventually cell death [22].

In the meantime, the design of contact and long-term active structures was possible by covalently binding molecules on CNF. For instance, penicillin, nisin or amino-silane have been grafted on CNF networks [23]–[25].

In the previous chapter, the successful grafting of ciprofloxacin molecule onto enzyme pre-treated CNF (CNF-e) membranes through water based and thermally triggered method was demonstrated. The objective of this chapter is then to compare CNF-e membranes with surface covalently bound ciprofloxacin to CNF-e membranes that have bulk adsorbed ciprofloxacin. The idea is to develop membranes with active properties for topical application. First, CNF-e membranes of different thicknesses, produced with different drying techniques, are compared in term of water uptake measurements and drug release experiments. Antimicrobial testing will be finally performed to

describe the activity of CNF-e membranes with bulk adsorbed ciprofloxacin versus CNF-e membranes with covalently immobilized ciprofloxacin on its surface.

This is the first work that tries to tackle such a numerous preparation parameters and release study conditions for the design of 100% CNF-e membranes that comprise ciprofloxacin active molecule. It is believed to provide more insights on CNF-e membranes nanostructure effects on drug release.

1.2 Experimental section

1.2.1. Materials

The main material used is a cellulose nanofibrils suspension that was provided by the CTP (Centre Technique du Papier, Grenoble, FR). It was isolated from a bleached birch pulp strongly refined (up to 80°SR), before an enzymatic pre-treatment and a final homogenization: 3 passes at 1500 bars in an Ariete homogenizer from GEA (Italy). The resulting 3 wt% suspension will be referred as CNF-e. Ciprofloxacin (≥98% CAS: 85721-33-1) and hydrogen chloride (HCl, CAS: 7647-01-0) were purchased from Sigma Aldrich. Agarose was purchased from ACROS ORGANICS (CAS: 9012-36-6). Nutrient Agar for microbiology testing was obtained from Humeau and was composed of 3.0 g of beef extract, 5.0 g of peptone and 15.0 g of agar. Standard Nutrient broth I was purchased from Carl ROTH and was composed of 15 g/l peptone, 3 g/l of beef extract, and 6 g/l of sodium chloride and 1 g/l of glucose. Sodium chloride for isotonic solution preparation was also purchased from Carl ROTH. Commercial gauze was obtained from adhesive bandage produced by EUROSIREL (Italy). Deionized water was used in all experiments and had a pH of 5.50 and a conductivity of 5.9 µS/cm.

1.2.2. Methods

1.2.2.a. Covalent immobilization of ciprofloxacin on CNF-e membranes (CNF-cip-g)

The procedure is already described in Chapter II-1, a brief reminder is detailed here. CNF-e suspension concentration was adjusted to 1 wt% and dispersed with high shear Ultra-Turrax mixer (IKA, USA). The suspension was cast in petri dishes of 90 mm in diameter and dry for at least 5 days in a condition controlled room (23°C, 50%RH), resulting in 200 mg CNF-e membranes (about 30g/m²). An aqueous solution of ciprofloxacin was prepared in 0.1 M HCl and CNF-e membranes were immersed for 15 minutes. The membranes were carefully recovered and excess ciprofloxacin solution was absorbed with blotting paper. A thermal treatment was applied for 24 hours at 50°C in a büchi oven (under vacuum) to trigger the esterification reaction. Membranes were then subjected to purification step using soxhlet extraction with high purity acetone and deionized water to remove contaminants, potential degradation products and the unbound ciprofloxacin respectively. These membranes grafted with ciprofloxacin will be designated as CNF-cip-g.

1.2.2.b. Preparation of CNF-e membranes with adsorbed ciprofloxacin (CNF-cip-ads)

A second type of CNF-e membrane was prepared by adding ciprofloxacin to a CNF-e suspension in order to allow its encapsulation through adsorption onto the nanofibrils surface. The CNF-e suspension was dispersed at 1 wt% concentration into deionized water using high shear IKA Ultra-Turrax device at 10000 rpm for 15 seconds. Ciprofloxacin was dissolved in deionized water at a concentration of 2 g/L. The pH was decreased at 2.5 in order to favor the dissolution mechanism. A

specific volume of this solution was then added to the 1 wt% CNF-e suspension so that the mass of ciprofloxacin accounts for 1 % of the total mass of the membrane. The suspension was then magnetically stirred for at least 15 minutes and sonicated 30 seconds with a SONOREX Ultrasonic batch (Bandelin) to remove air bubbles. The suspension was then cast into 90 mm diameter petri dishes and drying was done with two different techniques. Room temperature drying was done in conditioned room at 23°C and 50 % relative humidity for at least 5 days (designated with "RT" for room temperature). Overdrying procedure was done on some of the RT dried samples in order to further decrease the water content. The thermal treatment was performed in the oven at 150°C for 2 hours (designated as "overdried") based on previous study [26]. Membranes of different thickness were prepared by varying the quantity of CNF-e suspension cast in the petri dish. Theoretical values of 200 mg and 400 mg of dry material were targeted, corresponding to 20 ml and 40 ml of 1 wt% CNF-e suspension. These CNF-e membranes loaded with adsorbed ciprofloxacin will be designated as CNF-cip-ads.

1.2.2.c. Physical characterization of CNF-e

CNF-e suspensions were analyzed with optical microscopy at x20 magnification on an Axio Imager A2 device equipped with an AxioCam MRm camera (Carl Zeiss, Germany). Dark field observation mode was used to obtain contrasted images. Atomic force microscopy (AFM) images were recorded on a Dimension icon® (Bruker, USA). CNF-e films were deposited on adhesive tape before stabilizing overnight at room temperature. The acquisition was performed in tapping mode using a silica coated cantilever (OTESPA® 300 kHz – 42 N/m, Bruker, USA). Zones of 1*1 µm² were analyzed and the most representative height sensor images were chosen for analysis.

CNF-e membranes characteristics such as thickness and grammage (basis weight in gram per square meter) were evaluated. Membranes were precisely weighted on analytical scale (Mettler Toledo, Switzerland). Grammage was then calculated by dividing the weight of the CNF-e membrane by its surface. Thickness of the samples were measured by two complementary techniques; a M120 micrometer (Adamel Lhomargy, France) and scanning electron microscopy (SEM, Quanta200®) imaging of CNF-e membranes cross sections were used. Carbon tape was used to immobilize samples on supports for SEM imaging, and they were then coated with a thin layer of pure carbon thanks to an EMITECH® K450X carbon coater. The working distance was 10mm with a 10kV voltage and a magnitude of x1500.

Then, the theoretical density ρ was calculated by dividing the weight of the films by the product of membranes surface and thickness. The porosity *Por* of the CNF-e membranes were calculated by considering a value of 1.5 g/cm^3 for the CNF-e material mass volume ρ_{cell} with the equation (III-1)

$$Por = 1 - \frac{\rho}{\rho_{cell}} \quad \text{(III-1)}$$

1.2.2.d. Water uptake

The water uptake of the samples was assessed with two different methods. The first one was based on the total immersion in deionized water of 16 mm diameter discs of the CNF-e membranes which were weighted (m_{before}). The water uptake was measured at predetermined time intervals, from 1 minute up to 48 hours. After immersion the excess water was removed with blotting paper and the sample was weighted again (m_{after}). The water uptake by immersion, W_i, was calculated according to equation (III-2):

$$W = \frac{m_t - m_i}{m_i} \times 100 \quad \text{(III-2)}$$

The second method involved an agar gel on which the 16 mm diameter samples were deposited. The sample is expected to suck up the water in the agar gel from one side only. This is why this method better mimics the wound behavior. Equation (III-2) was also used to assess the water uptake from agar plate absorption W_a. Triplicate measurements were performed for each analysis.

1.2.2.e. Release study methods

Release study of ciprofloxacin was performed with three different methods for CNF-e membranes. The first one simply exposes the samples to the release medium with a full immersion, the second one involves a specific device composed of two chambers separated by the sample and the last one uses agarose gel in order to better mimic wound environment solid phase. The two first tests are continuous release system where the release medium remains the same throughout the whole experiment, while in the last test the release medium is renewed regularly. For release study, only CNF-e membranes with adsorbed ciprofloxacin (CNF-cip-ads) were characterized. Indeed, these tests are really time-consuming and devoted to detect free unbound molecules, which are supposed to be removed with the soxhlet extractions performed on ciprofloxacin grafted membranes (CNF-cip-g). However, upon the antibacterial assays detailed later in this section, a comparison between the two types of membranes will be carried out since different modes of action are expected.

Continuous release systems – immersion release

Immersion release study was performed in a 500 ml volume of deionized water in order to achieve sink conditions (a sufficient dilution state so that the released drug do not influence the release mechanism). Experiments were done in triplicates with three different ciprofloxacin loaded CNF-e membranes (90 mm in diameter, around 200 mg) and an orbital shaker was used to maintain a slow agitation (75 rpm) while the whole system was kept at 37°C in an incubator as illustrated in Figure III.1. The CNF-e membranes were placed on a lifted mesh with big pore size inside the container in

order to ensure an equivalent release from both sides of the membranes and limit CNF-e membrane deterioration. At predetermined time intervals an aliquot of 3ml was withdrawn from the release medium and ciprofloxacin quantity was measured with UV spectroscopy at a wavelength of 271nm (UV1800 Shimadzu), using the previously mentioned calibration curve.

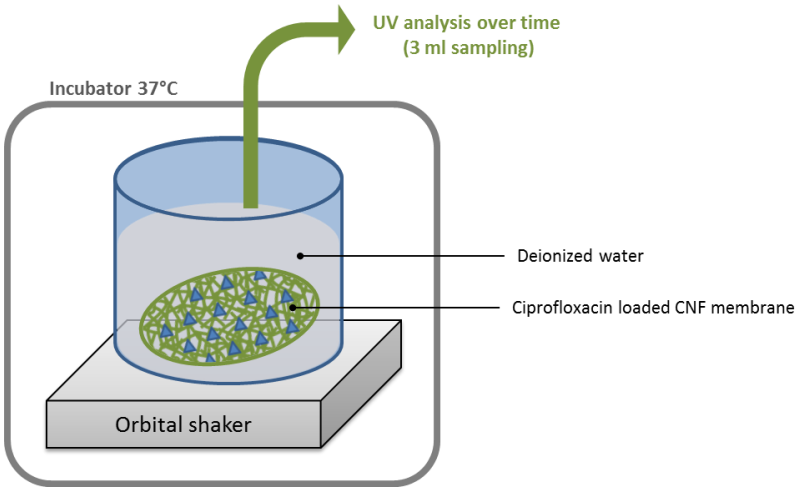

Figure III.2: Graphical description of the continuous release experimental set up

Continuous release systems – release chamber

An experimental device was also developed in the laboratory (LGP2) to be able to expose the two faces of CNF-e membranes to two different media such as liquid/liquid or liquid/air. Figure III.3 shows a graphic description of the device.

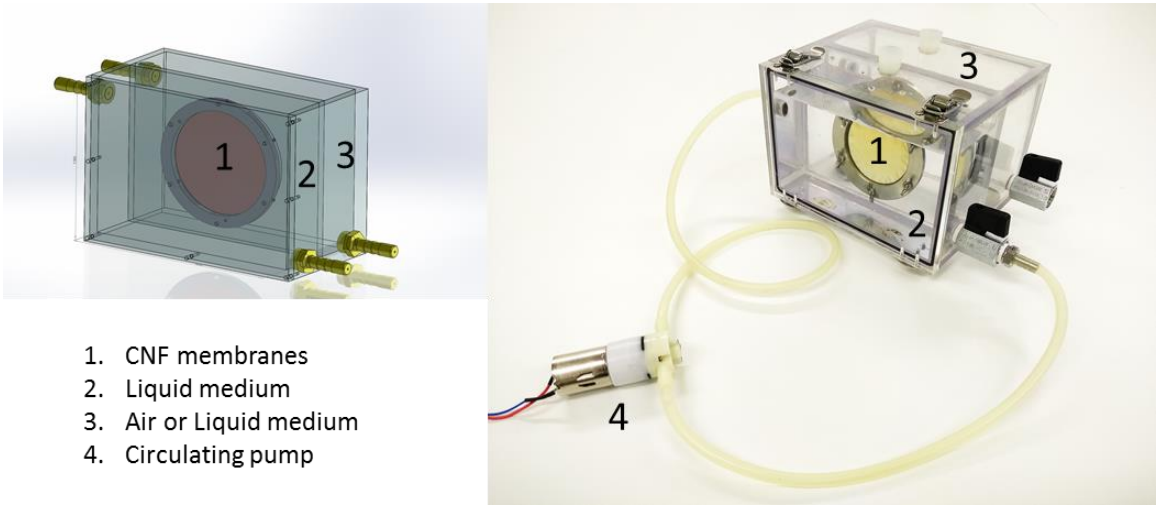

1. CNF membranes
2. Liquid medium
3. Air or Liquid medium
4. Circulating pump

Figure III.3: Graphical description and picture of the release chamber device

This system controls the flow rate of liquid which comes into contact with the sample surface in a closed loop re-circulation. It is thus possible to flow liquid in recirculation only on one side of the sample in order to stimulate the release mechanism while the other side remains in contact with air,

mimicking topical applications. Aliquots of 3 ml were collected at pre-determined time intervals from the flowed medium and ciprofloxacin concentration was measured with UV spectroscopy at 271nm. At least duplicates were performed for each sample.

Intermittent release system

A third system was designed to further mimic the environment of a low exuding wound. Agarose based hydrogels were prepared and used as solid release media in 45 mm diameter petri dishes. Circular disks of 10 mm in diameter were cut from ciprofloxacin loaded CNF-e membranes and were deposited on the surface of the agarose hydrogel to allow the drug to leach out of the sample from only one side as illustrated on Figure III.4.

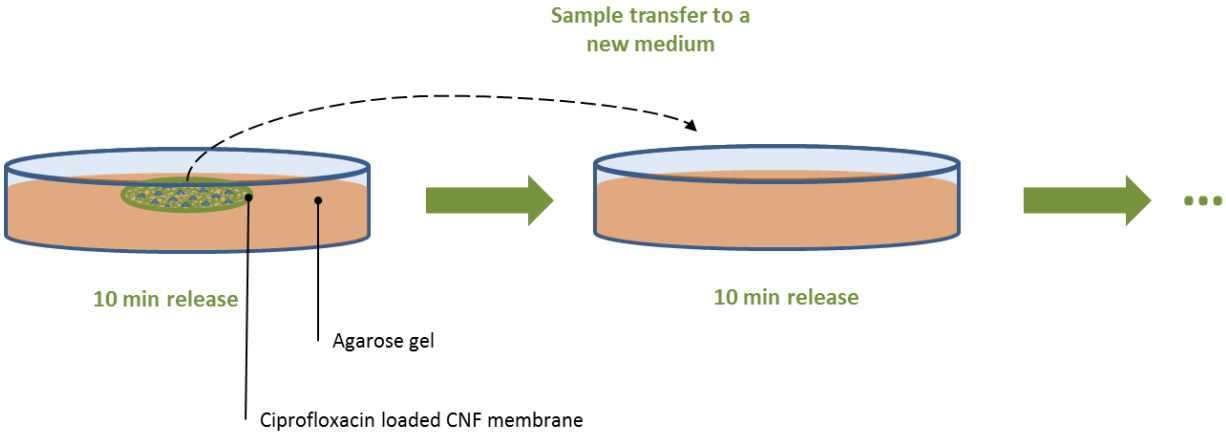

Figure III.4: Graphical description of intermittent release experimental set up

Every ten minutes, the disk sample was recovered from the agarose hydrogel and transferred to a fresh agarose medium. This technique is used to renew the release medium and mimic the renewal of body fluids in the solid low exuding wound environment. This will be referred as a "wash" step in the graphic results. After sample transfer, the agarose hydrogel was turned to liquid state with the use of micro-wave heating for at least 60 seconds and UV spectroscopy was used to measure the concentration of ciprofloxacin that was released from the membrane inside the agarose. Ciprofloxacin resistance to micro-wave treatment has been previously checked. Triplicate measurements were done for each sample.

1.2.2.f. Antimicrobial activity

Zone of Inhibition (ZOI) testing

Antimicrobial activity of the ciprofloxacin loaded CNF-e membranes was assessed through the zone of inhibition test which is inspired from the AFNOR standard NF EN 1104 test. Disks of the CNF-e membranes (10 mm in diameter) were first dry sterilized by an overnight thermal treatment in an

oven at 50°C. Nutrient agar was inoculated with one bacterial strain (*B. subtilis*, *E. coli* or *S. aureus*) and 10 ml of the solution was poured into 90 mm petri dishes. Once the agar solution turned into a gel state, disk samples were deposited on the agar surface. After incubation during 3 days (72 h) at 37°C, inhibition zones were detected or not onto the samples, indicating whether the ciprofloxacin has leached out of the membranes or not. The diameter or the radius (from the center of the CNF disk) of the circular inhibition zone was measured in order to quantitatively assess the antibacterial activity. A reference material was used to compare CNF-e membranes with a commercial product. A classic gauze membrane soaked into ciprofloxacin solution was chosen.

Successive ZOI were also performed. After the first 72 h of incubation, samples were transferred to another petri dish that also contained bacteria inoculated agar. Another incubation of 24h was applied and zone of inhibition sizes were assessed. This operation was repeated every day. This complementary test evaluated the antibacterial activity of the samples over the whole week following the first 72h incubation in order to simulate successive release like in the previous intermittent system. At least triplicates were performed for this test.

Dynamic Shake Flask

Dynamic Shake Flask testing puts in contact the CNF-e membranes with a liquid medium that contains bacteria as illustrated on Figure III.5. Isotonic (8.5 g/l NaCl) and nutrient broth solution were prepared in deionized water. Inocula were prepared by diluting bacteria suspensions in 1/500 nutrient broth (1 ml of nutrient broth in 500 ml of isotonic solution) to reach a $5x10^5$ CFU/ml concentration (CFU stands for colony forming units). Previously dry sterilized (16 h at 50°C) and weighted (about 50 mg) CNF-e membranes were cut in small pieces of ca. 0.5x0.5 cm^2 and placed inside Erlenmeyer flasks in which 10 ml of inoculum was added. The flasks were then incubated for 24 hours at 37°C and under orbital shaking at 100 rpm.

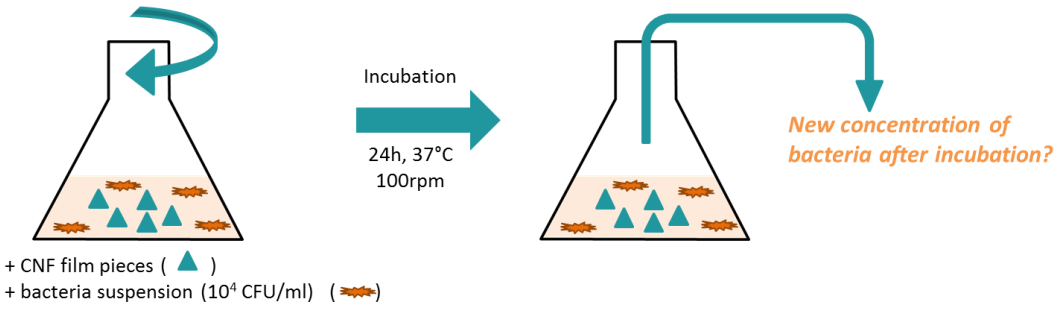

Figure III.5: Graphical description of Dynamic Shake Flask test

After the incubation, the new bacterial concentration was measured through successive dilutions of the liquid medium in 1.5 ml eppendorfs. A volume of 100 µl was taken out of each Eppendorf and

was added in petri dishes before addition of liquid agar (around 10 ml). When agar cooled down and turned to gel-like state, petri dishes were incubated overnight at 37°C. Bacterial concentration of incubated filtrates was calculated with the following equation (III-3):

$$Bacterial\ Concentration = \frac{Number\ of\ bacteria\ counted\ in\ petri\ dish\ n°X}{0.1 \times\ dilution\ factor\ of\ petri\ dish\ n°X} \quad \textbf{(III-3)}$$

The 0.1 value refers to the 100 µl added in each Eppendorf during successive dilutions. At least duplicates were performed for this assay.

Leaching assay

In contrast to Dynamic Shake Flask, Leaching Assay test does not put directly in contact the samples and the bacteria. Previously dry sterilized (16 h at 50°C) ciprofloxacin loaded CNF-e and reference CNF-e membranes pieces (about 50 mg) were first incubated for 24 hours at 37°C and 100 rpm in a volume of 10 ml of 1/500 nutrient broth (1 ml of nutrient broth in 500 ml of isotonic solution). The liquid were then collected and filtrated with 0.45 µm pore size syringe filter in order to remove the CNF-e materials. Bacteria suspensions were prepared according to supplier information and were added to the recovered filtrates at a 10^4 CFU/ml concentration as described on Figure III.6. This allowed figuring out if ciprofloxacin molecules were released during the incubation step and would inhibits the bacterial growth. After incubation for 24 h at 37°C and 100 rpm, bacterial concentrations were measured through the same method than for Dynamic Shake Flask and equation (III-3).

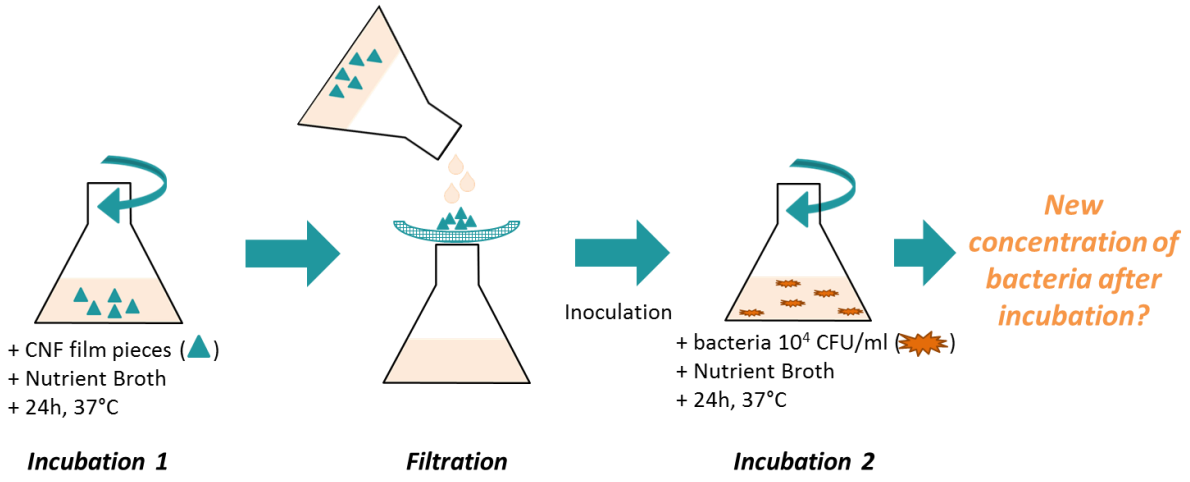

Figure III.6: Graphical description of Leaching Assay test

The test is used to determine quantitatively the effect of potential release of ciprofloxacin from the samples. If the filtrates from reference CNF-e membranes (CNF-ref) and the filtrates from ciprofloxacin loaded CNF-e membranes present the same bacterial concentration, it means that no

Ciprofloxacin was released. Duplicates were performed to further confirm the results. Both CNF-cip-ads and CNF-cip-g samples were compared with these antimicrobial test set ups.

1.3 Results and discussions

1.3.1. Physical characterization of CNF-e membranes

The CNF-e suspension was homogeneously dispersed as shown in Figure III.7a. The CNF-e membranes were transparent and proved to be composed of nanosized fibrils as confirmed by picture and height sensor AFM image of Figure III.7b and Figure III.7c. Moreover, AFM images were obtained before and after the release experiments and no differences were observed.

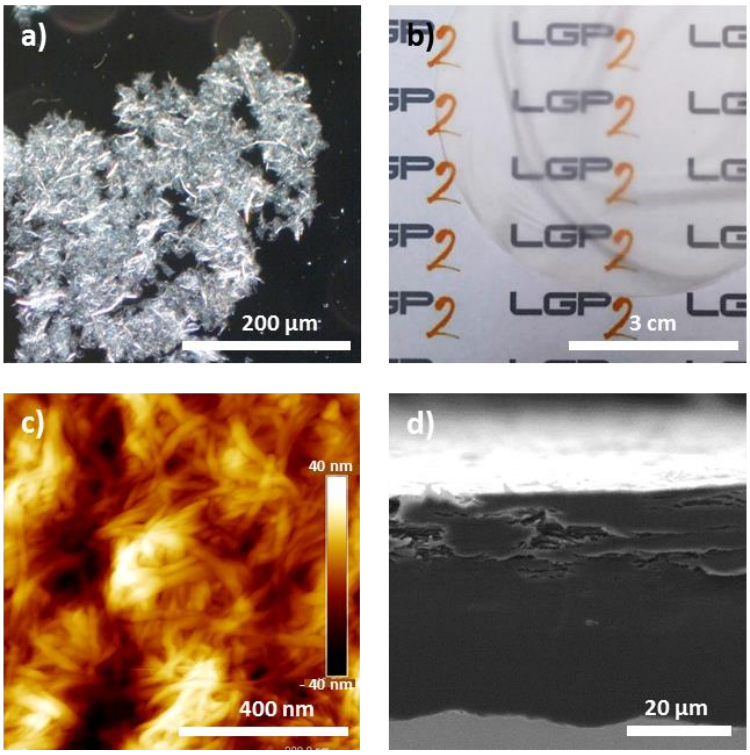

Figure III.7: Morphology of CNF-e suspension and membrane, a) optical microscopy (x20) in dark field mode of 0.1 wt% CNF-e suspension, b) picture (85mm in diameter), c) AFM height sensor and d) cross-section of the CNF-e membrane

Different qualities of CNF membranes were prepared in order to check the influence of thickness and drying on release profiles. Indeed, a recent study has shown that such thermal treatment (150°C for 2 h) of CNF-e membranes modify their Young's modulus in aqueous medium. The thinner the membrane, the higher the increase of "in-liquid" mechanical properties after overdrying [26]. This study proves that thermal treatment influences the structure of CNF-e membrane and so the release mechanisms. The difference in thickness between prepared samples will also influence the distance and specific surface area available for adsorption-desorption mechanisms that molecules undergo when leaching out of the membranes. Considering a specific surface area of 150 m^2/g for the CNF-e,

the surface of exchange will be of 30 m² and 60 m² for membrane of 200 mg and 400 mg respectively.

The Table III.1 summarizes the characterization of CNF-e membranes in terms of grammage and thickness. Membranes produced with a 200 mg dry mass target have a grammage of 29 g/m^2 and 400 mg dry mass membranes, 58 g/m^2. The thicknesses were measured with a micrometer. The grammage and thickness values are similar, 29 g/m^2 membranes have thickness of 29 µm and 58 g/m^2 membranes have a thickness of 58 µm, which confirms the high density of the membranes as shown by the values of Table III.1. CNF-e membranes were also characterized with SEM and similar thicknesses were observed (see Figure III.7d for 400 mg membranes). Also, the porosity was roughly the same for both films and in accordance with data found in the literature [27].

Table III.1: Physical characterization of CNF-e membranes

Targeted weight of CNF-e membranes	Grammage		Thickness		Theoretical Density		Theoretical porosity
mg	g/m²		µm		g/cm^3		
200	29	*±1*	28	*±2*	1.04	*±0.08*	31%
400	58	*±2*	58	*±4*	1.00	*±0.08*	33%

1.3.2. Water uptake of CNF-e membranes

One of the key properties of wound-dressing for an appropriate healing is their ability to absorb exudate. Indeed, a high water uptake will allow the wound-dressing to be used on lightly and heavily exuding wound by removing the exudate from the wound and thus preventing maceration (which make the skin more prone to damage). Maceration with the exudate is known to prolong the inflammatory phase and is detrimental to healing.

Water uptake of immersed CNF-e membranes (without ciprofloxacin) was recorded over 48h however, the absorption was very fast and data recorded in the first 10 minutes are presented on Figure III.8a. Membranes with lower grammage show a water uptake of 500 % while membranes with higher grammage reveal a water uptake of 300 %. CNF-e membranes with lower grammage were more fragile and excess water at the surface of the membranes could not be removed properly without tearing the membranes apart. Higher grammage membranes have better mechanical properties and were not affected by the removal of excess water. The maximum water uptake is quickly reached in about one minute for both types of CNF-e membranes. Even if thin membranes absorb more water in proportion, the absolute quantity of absorbed water is higher for thicker membranes as depicted in Figure III.8b. At least 2 hours are required to clearly see a strong and stable difference. Moreover, this result also indicates that when the CNF-e quantity is doubled from

200 mg to 400 mg membranes, the absorbed water quantity is really far from being doubled even after a 48 h immersion.

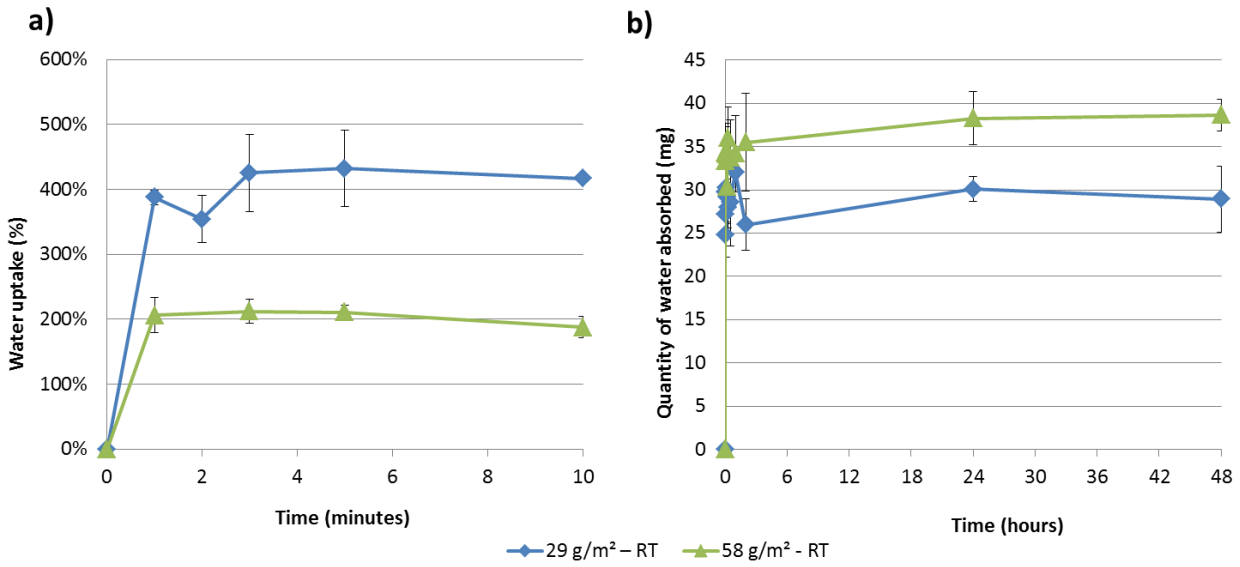

Figure III.8: Water uptake of CNF-e membranes of two different grammage, a) water uptake over the first 10 minutes and b) absolute quantity of water absorbed over the whole 48 h of experiment

Overdrying of CNF-e membranes was proven to improve the mechanical properties when immersed in liquid [26]. Water uptake capacity was also assessed for overdried CNF-e membranes in order to overcome the limitation of weak samples. After 48 h of immersion of CNF-e membranes, a similar water uptake for all the samples regardless of their grammage was revealed.

Complementary experiments were carried out with another water uptake test. Agar gel medium was used in order to better mimic the behavior associated with liquid absorption on a topical wound solid phase. A commercial wound dressing gauze was also tested and compared to the CNF-e membranes in terms of water uptake. Figure III.9 shows the water uptake of low grammage CNF-e membranes and wound dressing gauze over 48h and a zoom in the first 60 minutes. The maximum water uptake of CNF-e membranes is two times greater than that of the gauze according to Figure III.9a, reaching 300% of the initial mass. This result is much lower than the 500% reached by the low grammage CNF-e membranes samples with the previous test where full immersion in liquid was used. Here, samples were easier to recover because no excess water was to be removed.

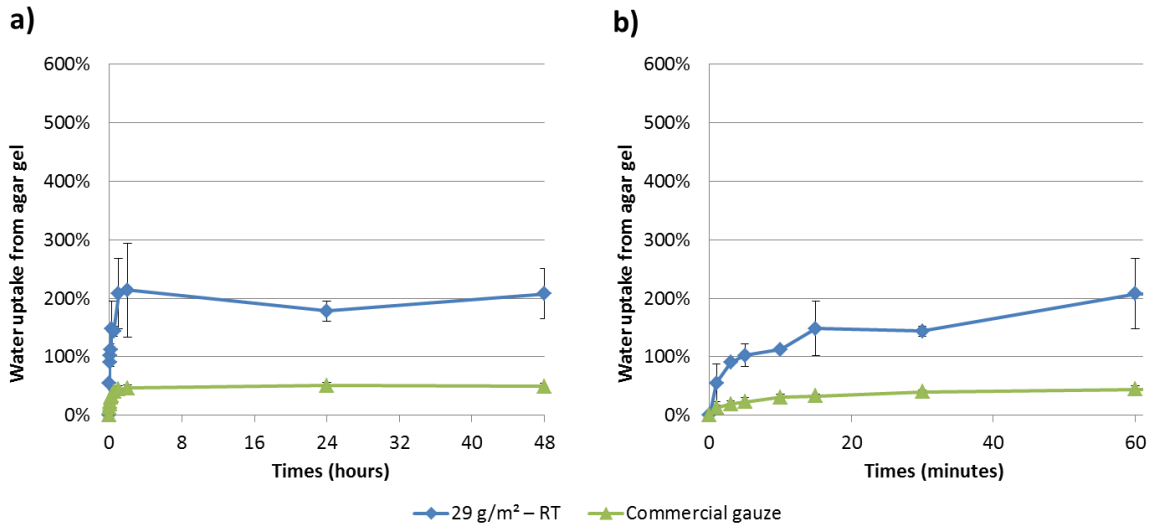

Figure III.9: Water uptake of CNF-e membranes and commercial gauze deposited on agar gel over 2a) 48h and 2b) zoomed in the first 10 min

These results suggest a high water uptake capacity for CNF-e membranes, emphasizing the interest of CNF for medical device development. The hydrophilicity of cellulose, together with the nanostructured network of CNF-e membranes, explain the observed water absorption behavior. A higher capillary absorption with such CNF membrane was expected and already reported by previous research on hemostatic application [28], [29]. Dimensional swelling that is associated with the water-uptake of CNF-e membranes justifies the high values, but it was difficult to measure because of the low thickness of the membranes and their poor mechanical properties in wet environment.

Innovative medical devices need to present active properties. Ability to release active principle ingredients (API) to better favor healing procedure and prevent infection thus appear as a promising opportunity for CNF-e based medical devices.

1.3.3. Release study

Based on recent literature, CNF-e membrane nanostructured networks seem to be good candidates for API encapsulation and subsequent release. The release profiles of ciprofloxacin from CNF-e membranes were then investigated for the first time. The influences of the CNF-e membranes production method as well as the type of CNF were studied. The medium chosen for release experiment is deionized water. Actually, other medium such as phosphate buffer saline (PBS) are available and often use in release study experiments since they mimic the human body fluids [30]. However, some preliminary experiments of release of ciprofloxacin in PBS medium showed strong interaction of the drug with the ions in the buffer. With deionized water as the release medium, the influence of the above mention parameters on the release profiles is expected to be revealed, without any interfering phenomena due to the presence of ions.

The effect of CNF-e membranes drying procedures was first investigated with 29 g/m^2 and 58 g/m² membranes that were dried (i) at room temperature over several days or (ii) at room temperature over several days followed by an overdrying treatment at 150°C for two hours. The release of ciprofloxacin was then measured with immersion protocol over at least 48 hours in triplicates for each membrane. The release profiles of four different samples, dried according to the two afore mentioned drying procedures, are shown on Figure III.10. Regardless the drying technique, the four samples reached the same maximum release rate around 70% of the theoretical quantity of ciprofloxacin, as depicted on Figure III.10a. This first result indicates that the overdrying (150°C for 2 hours) do not trigger any chemical immobilization (i.e. esterification) of ciprofloxacin onto the CNF-e membranes. It also confirms the stability of ciprofloxacin molecules inside CNF-e membranes, when exposed to this thermal treatment. This is in accordance with the study of ciprofloxacin stability in solution against thermal treatment that was performed in chapter II-1. A zoom into the first 30 minutes of the release expose on Figure III.10b, proves that for 29 g/m² membranes, overdried samples kinetic of release is similar than that of room temperature dried ones. Only 3 minute is necessary for both samples to reach 70% of drug released.

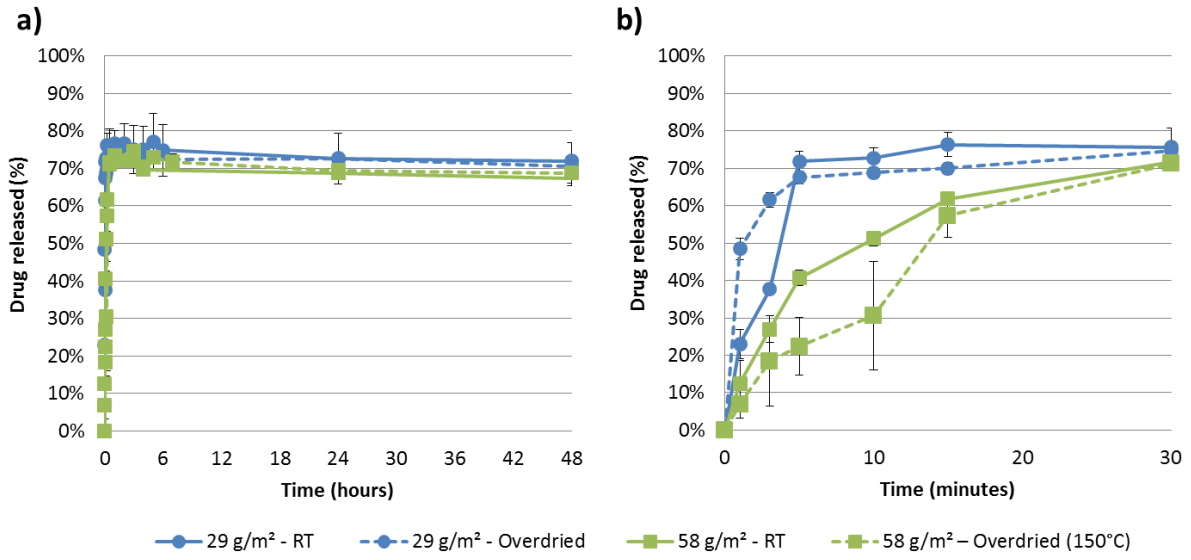

Figure III.10: Influence of drying procedures and CNF-e quantity on drug release profile of 29g/m² and 58 g/m² ciprofloxacin loaded CNF-e membranes over a) 48 hours and b) zoomed in the first 30 minutes of continuous release immersion experiment

However, for thicker membranes of 58 g/m², the tendency is not the same and overdried samples seem to behave slightly different even if we consider the high deviation obtained for the data point at 10 min in Figure III.10b. The overdrying is limiting the burst effect and creates a more prolonged release. This result suggests that a more prolonged release of drug can be achieved by increasing the thickness of CNF-e membranes.

More precisely, only 5 minutes are required for 29g/m^2 membranes to reach the maximum release rate of 70% while in 5 minutes, 58 g/m^2 membranes are barely at 40% for the room temperature dried membranes and 20% for overdried membranes. Thicker membranes will also need at least 30 minutes to reach the maximum release rate, which is six time longer. The analysis of additional quantity of drug released in between two measurement points also helps the discussion: between 5 and 10 minutes, the thinner membranes release 1 to 2 % of ciprofloxacin (1 to 2 mg) whereas thick membranes will still release about 10% of ciprofloxacin (40 mg). The same result can be extracted from additional quantity between 10 and 15 minutes or 15 and 30 minutes. In thicker CNF-e membranes, the time required to swell the nanofibrils network across the section is higher. So the drug diffusion is longer, which explains the shift observed on Figure III.10b.

Another release device has been designed to expose one side of the CNF-e membrane to a liquid release medium in continuous re-circulation while the other side is in contact with the air. This better mimic the external application for heavily exuding wounds. As mentioned before and confirmed with above described experiments, overdried samples exhibit a higher resistance to liquid medium exposition and prolonged release abilities. They were thus chosen to carry on the study with the

release chamber device. Figure III.11 shows that the closed loop re-circulation of liquid medium in the device provided an extended release for 29 g/cm² membrane. Indeed, about 90 % of the theoretical amount of ciprofloxacin was released in 24 hours in these dynamic conditions while only 70 % was released with the mild agitation in the immersion protocol used in the previous studies. This tendency is not observed for the thicker membrane and suggests that the ciprofloxacin entrapped in the membrane side that is exposed to the air is more complicated to retrieve with the re-circulating liquid medium. This could also be a reservoir layer for longer time release.

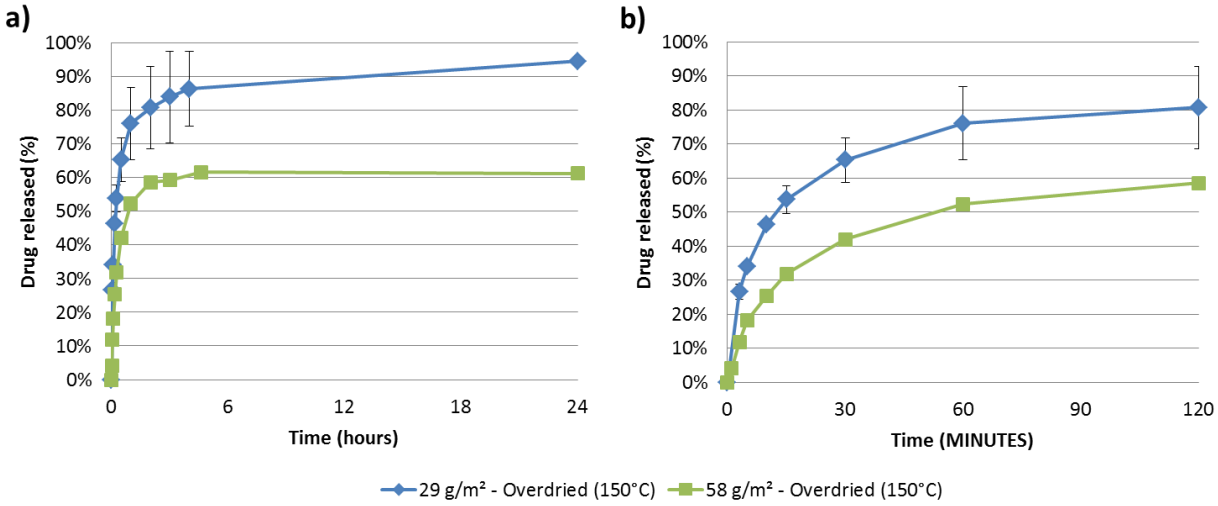

Figure III.11: Release study for overdried ciprofloxacin loaded membranes in the release chamber with closed loop liquid medium recirculation

A third set up of experiment was used to further characterize the overdried samples. This one was designed to mimic low exuding wound environment. Samples were in contact with agarose gel that was renewed every 10 min (the "wash" step). Figure III.12 shows the comparison of the drug concentration evolution in agarose media for 29 g/m² and 58 g/m² overdried membranes, over the number of washing steps. Similar evolutions are observed with a strong decrease from the first washes toward stabilization after about 10 washes. The lowest minimum inhibitory concentrations of ciprofloxacin for bacteria commonly found on wound infection sites (*Staphylococcus aureus, Pseudomonas aeruginosa* or *Streptococcus pneumoniae*) is 0.5 µg/ml [31]–[33]. The thin membranes can be considered as non-active since the drug concentration that was detected rapidly goes under this value. On the contrary, after 30 washes, thick membranes still release significant amount of ciprofloxacin.

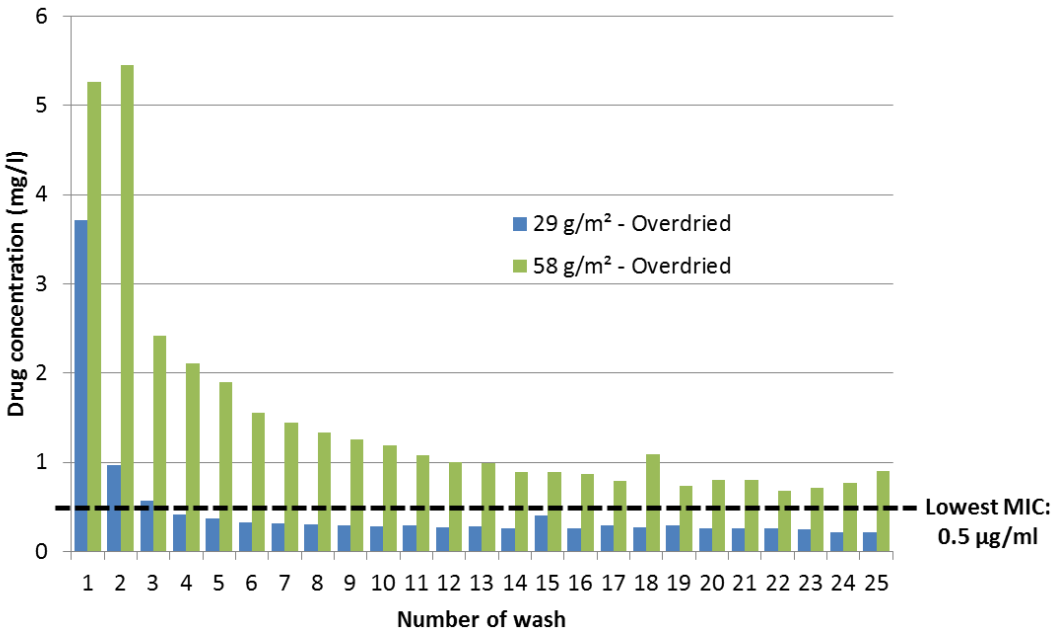

Figure III.12: In solid release study, agarose gel was used to release ciprofloxacin from 58g/m2 overdried membrane

CNF-e membranes with increased thickness (and associated grammage) that are overdried are recommended for the development of active medical devices for topical applications since they exhibit better resistance when exposed to liquid medium and revealed a more controlled release in immersion conditions together with active behavior in agarose release system. These samples will be used in priority for the antimicrobial testing and referred as CNF-cip-ads.

1.3.4. Antimicrobial activity

Antibacterial activity testing was carried out in order to evaluate the capacity of ciprofloxacin loaded CNF-e membranes (CNF-cip-ads, *overdried* and CNF-cip-g) to be active against bacterial strain. In parallel, reference CNF-e membranes of 29 g/m² without ciprofloxacin are also characterized and referred to as CNF-ref. Widely used *B. subtilis* strain was chosen to perform zone of inhibition (ZOI) testing as depicted on Figure III.13 where a clear ZOI is observed on CNF-cip-ads (C) and CNF-cip-g (D) samples while CNF-ref disks do not exhibit any activity (B). Both samples proved to be strongly active against *B. subtilis* since ZOI radius of 2.4 and 2.6 cm were measured confirming the antibacterial activity of such CNF-e membranes.

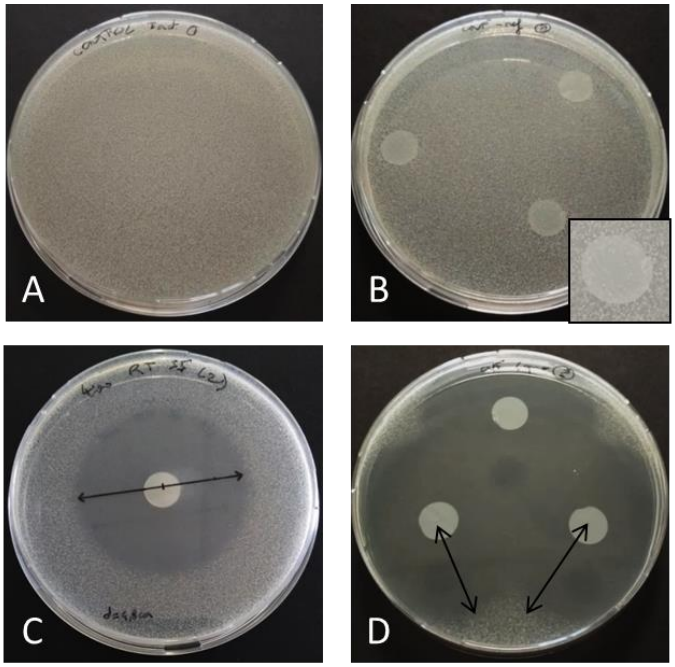

		ZOI radius (cm)	
B	CNF-ref	0	-
C	CNF-cip-ads	2.4	±0.2
D	CNF-cip-g	2.6	±0.3

Figure III.13: Zone of Inhibition testing of CNF-cip-ads (*overdried*) and CNF-cip-g against *B. subtilis* strains and values of ZOI radius. Picture A proves the correct growth of the bacterial strain. Pictures B, C and D refer to CNF-ref, CNF-cip-ads and CNF-cip-g respectively

All the samples were then exposed to a new inoculated medium during 24h of incubation for 3 more cycles. Figure III.14 shows the evolution of ZOI radius over this prolonged incubation. CNF-cip-ads samples were tested against *B. subtilis* only (Figure III.14a) while CNF-cip-g samples were tested against *E. coli* and *S. epidermidis* (Figure III.14b, *results obtained in chapter II-1*). In both cases, CNF-ref membranes do not show any antibacterial activity. Both thin and thick membranes of CNF-cip-ads are compared on Figure III.14a. The activity described by the ZOIs radius is strongly decreasing with the number of cycle from 2.3 and 2.4 cm ZOI radius until it reaches zero. Thin membranes are detected to be inactive within only 3 cycles while one more is required for thick membranes, confirming again their more potent activity and prolonged release. On Figure III.14b, CNF-cip-g membranes show a smaller ZOI radius of 1.0 and 1.2 cm but a different phenomenon occurs after cycle 1. The detected ZOI are limited to the edge of the sample disk indicating a contact active antibacterial behavior. This suggests that the covalently bound ciprofloxacin acts locally at the surface of the CNF-cip-g membrane, which confirms a prolonged activity against both gram positive and gram negative bacterial strain.

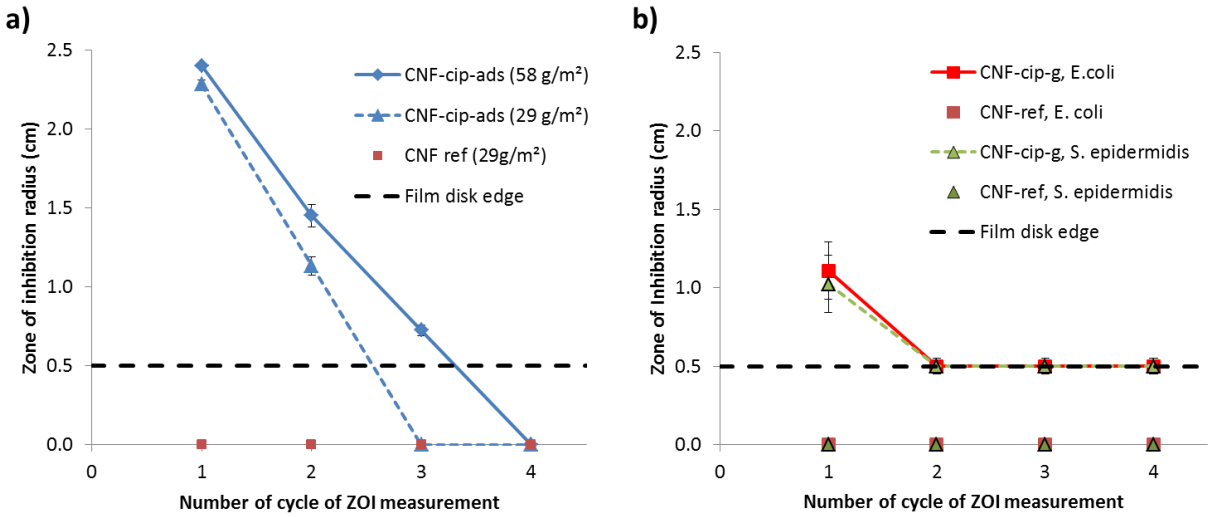

Figure III.14: Successive ZOI experiments results, the radius of ZOIs is plotted against the number of cycle of exposition, a) CNF-cip-ads samples (29 and 58 g/m², *overdried*) against *B. subtilis* and b) CNF-cip-g samples against E. coli and S. epidermidis, only 29 g/m² membranes

The test of ZOI detection is only qualitative and performed under static conditions. However, most of the release experiments that were discussed in the previous section were performed under dynamic conditions, especially those which were set up to mimic heavily exuding wounds (continuous release in immersion with orbital shaking or in the release chamber with closed loop recirculation). Complementary antibacterial testing is necessary to assess the activity of the ciprofloxacin loaded CNF-e membranes in similar conditions.

In the dynamic shake flask protocol, samples are put in contact with liquid medium that contains bacterial strains for several hours. The quantitative evolution of the logarithm of bacterial concentration over incubation time reveals the activity of the CNF-e substrates, as displayed on Figure III.15. CNF-ref samples give a very similar result when compared to the positive control ("No sample"). From time 0 to 3 and 24 hours of incubation, a growth of bacteria is suggested by the increase in bacterial concentration observed for both strains from 5.5 log to more than 7.5 log. On the contrary, ciprofloxacin loaded CNF-e membranes present strong decreases in bacterial concentration. Within only 3 hours, the CNF-cip-g samples reduce the bacterial concentration to zero while the CNF-cip-ads membranes only give a 2 log and 1 log reduction for *E. coli* and *S. aureus* respectively. After 24h of incubation of the samples in the bacteria containing liquid medium, both ciprofloxacin loaded CNF-e membranes reduce the bacterial concentrations to zero. The CNF-cip-g antibacterial activity is stronger than CNF-cip-ads samples in Dynamic Shake Flask test conditions. The 24 hours release applied prior to the test must have depleted the ciprofloxacin quantity of CNF-cip-ads whereas the covalently bound ciprofloxacin in CNF-cip-g samples was not affected.

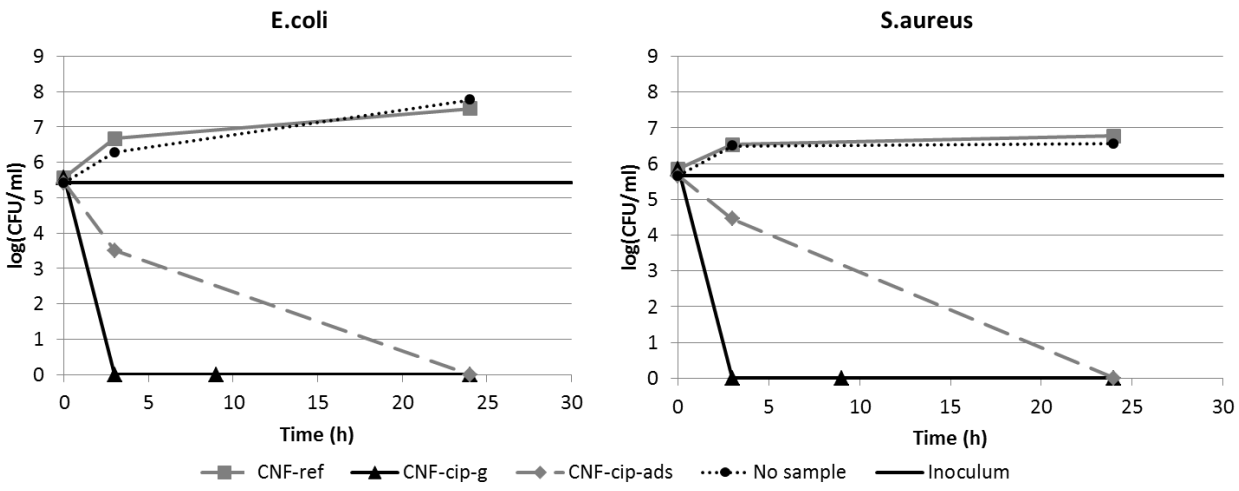

Figure III.15: Dynamic shake flask test applied on CNF ref, CNF-cip-ads and CNF-cip-g samples against two bacterial strains, *E. coli* and *S. aureus (note that the legend is common to both graphs)*

In Dynamic Shake Flask test, samples are in direct contact with the bacteria. The bacterial growth inhibition can thus be explained both by the release of active molecule and contact active inhibition phenomena. In order to be able to draw precise conclusions, a last complementary test was used. As for the Dynamic Shake Flask, it measures quantitatively the evolution of bacterial concentration of an inoculated medium, but this liquid does not contain the sample itself. The sample was exposed to the liquid and then removed before the test, eliminating the possibility of contact active inhibition phenomena. In the Leaching Assay, samples are put in contact with a liquid medium that does not contain bacteria, in immersed conditions for 24 hours (incubation 1). After this, the solid samples are recovered and then the liquid is inoculated with bacteria and incubated for 24 hours (incubation 2). If some active substances leached out from the samples during the incubation 1, the bacterial growth during incubation 2 will be affected. If the sample did not release any active substances, bacteria concentration is supposed to remain stable or to slowly increase with bacterial growth.

The logarithms of bacterial concentrations after the incubation 2 are compared in Figure III.16 for each sample, including a positive control that was not put in contact with any CNF-e substrates. The positive control shows a bacterial growth up to 6.1 and 6.6 log for *S. aureus* and *E. coli* respectively, compared to the initial bacterial concentration of 4.1 log. CNF-ref samples have a very similar response since bacterial growth is confirmed for both strains. For *E. coli* the bacterial growth is significantly higher than the positive control, suggesting that the CNF-e promote the bacterial growth. This has been already observed and indicates good nutrient conditions for bacterial growth [23]. The CNF-cip-ads sample obviously released ciprofloxacin molecules during the immersion since these conditions are exactly the same than for immersion release experiments discussed previously. After 24 hours of incubation with bacteria, the liquid medium does not exhibit any remaining

bacterial activity. The CNF-cip-g sample shows a bacteriostatic effect since a log variation inferior to 1 compared to the initial concentration is detected. This result confirms again that ciprofloxacin is actually covalently bound to the CNF-e surface and did not leach out from the membrane during the incubation 1. Moreover, the initial concentration for Leaching Assay is 1 log inferior to that of Dynamic Shale Flask. A ten times less concentrated medium is much more sensitive to the presence of active compounds, which also confirms the insignificant effect of CNF-cip-g in these conditions.

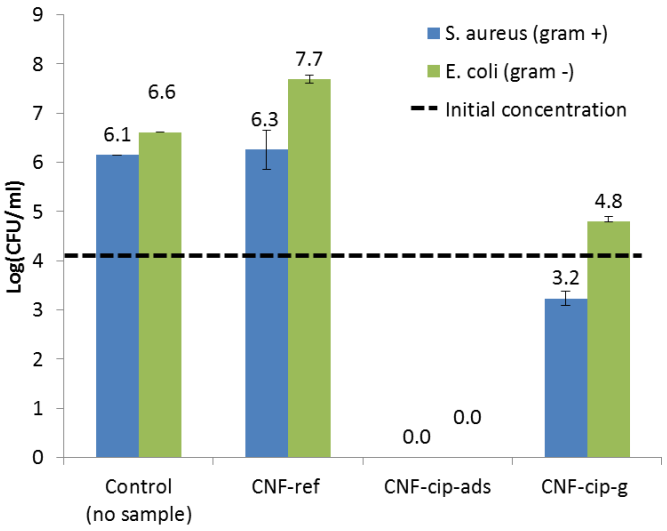

Figure III.16: Leaching assay that assess the release of active substances from the samples, CNF-ref, CNF-cip-ads and CNF-cip-g. All samples were subjected to a 24h release in immersed conditions before the test

This last result closes the comparison between CNF-cip-ads and CNF-cip-g in terms of antibacterial activity. Both samples demonstrated strong antibacterial activity against gram positive (*B. subtilis, S. aureus, S. epidermidis*) and gram negative strains (*E. coli*), CNF-cip-ads by release mechanisms and CNF-cip-g by contact active phenomena. CNF-cip-g is then preferable when a quick ad persistent long term activity as shown on Figure III.14 and Figure III.15.

1.4 Conclusion

The physical properties of CNF-e membranes were characterized as well as their water uptake properties. Influence of thickness and overdrying (150°C, 2h) of the samples on the water uptake was investigated. Overdried thick CNF-e membranes proved to absorb more water and better resist the exposure to the liquid medium. The multiple release study experiments allowed the ciprofloxacin loaded CNF-e membranes to be exposed to different conditions that mimicked both heavily and low exuding wounds environment. Thick overdried membranes demonstrated the most prolonged release in immersion and release chamber protocols. Compared to thin overdried membranes, they were also more active in the intermittent release protocol with above-MIC ciprofloxacin concentrations.

The antibacterial experiments were used to compare CNF-e membranes with bulk adsorbed ciprofloxacin (CNF-cip-ads) versus CNF-e membranes with surface grafted ciprofloxacin (CNF-cip-g). Both samples offered a similar response to classic ZOI testing, in static conditions. However, upon successive ZOI measurements, CNF-cip-ads rapidly lost its activity while CNF-cip-g proved to have a stable contact activity thanks to the covalently bound ciprofloxacin. The Dynamic Shake Flask test was used to put samples in contact with bacteria in a dynamic environment and allowed to retrieve quantitative values. Both samples demonstrated antibacterial activity but the CNF-cip-g revealed a more potent response. Finally the Leaching Assay test confirmed that CNF-cip-ads obviously released ciprofloxacin that hindered the bacterial growth, whereas CNF-cip-g offered a contact-active potency towards bacterial strains.

Both CNF-e membranes are then good candidate for the development of medical device for topical applications but CNF-cip-g membranes seems to present better long term persistent contact antibacterial activity. Medical device intended to be used for a treatment up to 24 hours can include CNF-cip-ads membranes. However, for longer treatment time, CNF-cip-g membranes are more adapted.

Covalent binding of molecule to CNF-e substrates appears like a promising strategy for the development of innovative topical application medical device with active functionalities like drug release. The use of such strategies for the development of internal application medical devices will be investigated in the next chapter.

2. Composites of collagen and metronidazole-modified CNF as materials for "on-demand" drug release and antibacterial activity

Abstract

Cellulose nanofibrils (CNF) were modified with ametronidazole based prodrug through a two-step immobilization, using first amidation and then thiol-yne click chemistry in water suspension. The ability of these modified CNFs to release metronidazole upon enzymatic action of human carboxylesterase was confirmed by high performance liquid chromatography (HPLC). Some re-arranged metronidazole product was also detected and attributed to photo-sensibility. Prodrug modified CNF were then successfully embedded in a collagen matrix in order to develop a medical devices for internal soft tissue repair application. Collagen CNF nanocomposites antibacterial activity against anaerobic bacteria was assessed by zone of inhibition (ZOI) testing. Moreover, a prolonged antibacterial activity was obtained for non-irradiated samples when exposed to successive ZOI testing. Nevertheless, gamma radiation inhibited the antibacterial activity of collagen-CNF-metro nanocomposites. Meanwhile, NMR analysis confirmed that gamma radiation do not affect metronidazole prodrug structure. These samples are promising for the development of active soft tissue repair medical devices.

2.1 Introduction

Soft tissue repair (STR) is one of the major business activities of the medical device industry. It mainly comprises ventral and inguinal hernia repair devices. The worldwide market associated with these devices currently exceeds 3 billion euros and has an 8% of mean annual growth rate (Medtronic internal source). In this area, infections and post-operative pain remain the main recurrence problem encountered by surgeons and healthcare authorities [34]. They involve a high medico-social cost since re-do surgeries and heavy treatments are often required to be able to finally heal patients. Post-operative quality of life and life expectancy directly relies on the capacity of healthcare systems to develop more efficient medical devices. Recently, the treatments for soft tissue repair evolved from suture closure to using 2D materials often designated as mesh repair [35]. Biologic mesh that involve animal derived material, such as collagen, show less infections, adhesion (unwanted bridging of organs to the medical device causing secondary complications) and erosion complications than synthetic implants [36]–[38]. Nowadays, collagen is successfully used for internal application such as soft-tissue repair with patented technologies like the Symbotex® hernia repair medical device [39].

Meanwhile, the use of cellulosic material such as nanocellulose for biomedical research is constantly increasing as proved by recent reviews [13], [14]. The tremendous interest of the scientific community towards nanocellulose is explained by its biocompatibility, renewability, biodegradation properties and its easily tunable surface chemistry combined with high specific area [6].

The idea of combining the regenerative properties of collagen together with bioactive cellulose can bring new innovative functionalities to medical devices. A few scientific papers investigated this topic using various forms of cellulose. For instance, nanocomposites of bacterial cellulose and type I collagen were designed for in-vitro bone regeneration. Cross-linking was achieved by modifying bacterial cellulose with glycine esterification and subsequent cross-linking to collagen with 1-ethyl-3-(3-dimethylaminopropyl)-carbodiimide. Osteoblastic phenotype cell were able to develop onto the biomaterial *in-vitro* indicating its suitable use for bone tissue engineering [40]. Similar systems were produced as thin membranes for the mimicking of soft-tissues and stem-cell growth studies. Results indicated that mesenchymal stem cells put in contact with collagen-cellulose composites membranes had a higher proliferation index [41]. More recently, wood derived nanocellulose was also crosslinked with collagen matrices to build up artificial ligament or tendons. Coupling agents were glutaraldehyde [42] or genepin [43]. However, none of these strategies tried to include active principle ingredients (APIs) in the collagen-cellulose network in spite of very promising and recent studies dealing with using CNF for prolonged release of drugs [19], [44], [45]. Up to our knowledge, only one study related to nano-scaled cellulose of bacterial origin investigated this solution. Indeed,

very recently, bacterial nanocellulose was used in combination with fish scale collagen to produce microneedles that comprises lidocaine, for an alternative to transdermal drug delivery [46]. But for wood-derived nanocellulose based collagen composite as drug carrier, no study has been published yet.

Chapter II showed how APIs modified cellulose nanofibrils can be obtained. These CNF nanomaterials were modified in suspension in chapters II-2 and II-3, resulting in water based systems suitable for the design of collagen-CNF composites as model mesh repair. This approach could not be followed with ciprofloxacin grafting presented on chapter III-1 since the chemistry involved relied on an esterification reaction that cannot take place in water. In our study, cellulose nanofibers were modified in aqueous suspension with a prodrug containing metronidazole molecule. This API is of particular interest for STR medical devices since it is mainly active against anaerobic microbial strains and only rare resistance were observed [47], [48].

In this chapter, the novelty is to introduce these prodrug modified CNF into collagen composites that could release drug in presence of esterase enzyme in the hernia defect area. So, for the first time, composites were produced with collagen and metronidazole modified cellulose nanofibrils to build up model medical devices intended for internal soft-tissue repair applications.

2.2 Experimental section

2.2.1. Materials

Oxidized cellulose nanofibers suspensions were provided by the Centre Technique du Papier (CTP, Grenoble, France). The TEMPO mediated oxidation was performed on a pre-refined (40°SR) bleached softwood bisulfite pulp provided by TEMBEC (Tartas, France) following classical procedure developed by A. Isogai's team in 2006 [49], [50]. Briefly, the cellulose fiber pulp concentration was adjusted at 1.5 wt% and the reaction was performed at pH 10 for 2h in presence of NaBr, NaClO and the TEMPO reagent. High pressure homogenizer (Panda GEA, Niro Soavi) was then used to produce the CNF suspension from the oxidized pulp, later referred as CNF-t.

Propargyl-amine (CAS: 2450-71-7), N-(3-Dimethylaminopropyl)-N'-ethylcarbodiimide Hydrochloride (EDC, CAS: 25952-53-8), N-Hydroxysuccinimide (NHS, CAS: 6066-82-6), Sodium Hydroxide (NaOH, CAS: 1310-73-2), hydrogen chloride (HCl, CAS: 7647-01-0) and carboxylesterase 2 human (expressed in baculovirus infected BTI insect cells) were purchased from Sigma Aldrich and used as received. Tris(hydroxymethyl) aminomethane (TRIS, >99.8% CAS: 77-86-1) was purchased from Euromedex. Tris(2-carboxyethyl)phosphine hydrochloride (TCEP, >98%, CAS: 51805-45-9) was purchased from ThermoFisher Scientific. Biocompatible photoinitiator Lithium Phenyl(2,4,6-trimethylbenzoyl)phosphinate (LAP, >98%, CAS: 85073-19-4) was purchased from Tokyo Chemical Industry. Bacterial strains of *Bacteriodes vulgatus*, *Bacteriodes fragilis* and *Clostridium difficile* were obtained from the biological resource center of the Regional University Hospital Center (CHRU, Besançon, France).

Oxidized collagen solution of porcine origin was provided by Medtronic (Trévoux, France). The modified metronidazole molecule was synthetized by the Département de Pharmacochimie Moléculaire (DPM, France) as described in the chapter II-2, and will be referred as prodrug. The collagen was extracted from porcine dermis through chemical oxidative treatment. A 4 wt% collagen solution was obtained. Polyethylene glycol 4000 (PEG, CAS: 25322-68-3) and glycerol (Gly, CAS: 56-81-5) were obtained from MERCK Millipore. Sterile deionized water was used in all the following experiments.

2.2.2. Methods

2.2.2.a. Production of CNF-metronidazole

Chapter II-2 was focused on the preparation of CNF-metronidazole through two steps chemical surface modification of CNF-t. A brief reminder of the procedure will be presented. The first step of the covalent immobilization is to provide the CNF-t substrate surface with pending alkyne functions.

This was achieved through amidation reaction between the carboxylic acid groups of CNF-t and the amine group of propargylamine in aqueous medium with the aid of coupling agents EDC/NHS. Purification was done by several cycles of centrifugation/redispersion in acidic water to remove excess unbound reactants and coupling agents, followed by 5 days dialysis against neutral water. Obtained modified CNF are referred as CNF-yne. Meanwhile, metronidazole molecule was chemically enhanced to design a new binding strategy with CNF-yne. Terminal thiol function was introduced on metronidazole through esterification reaction. Thiol group was then available for the second step of drug immobilization on CNF substrates, the thiol-yne click chemistry. The resulting modified CNF are referred as CNF-metro.

2.2.2.b. Preparation of CNF, CNF-yne and CNF-metro loaded collagen nanocomposites

A solution of 10 wt% PEG and 6 wt% glycerol was prepared in sterile deionized water (PEG/Gly solution). After complete dissolution under magnetic stirring, the solution was further purified by filtration on 0.200 µm pore size filters. CNF suspensions concentrations were adjusted to 0.1 wt% with sterile deionized water and dispersed with Ultra-Turrax high shear mixer at 10 000 rpm for one minute. Collagen stock solutions are stored at -80°C after their production procedure and they show a solid gel-like structure at room temperature, which is not suitable for composite production. It was then placed in a water bath at 40°C to obtain a liquid collagen solution. PEG/Gly solution, CNF-metro suspensions were also placed in the 40°C water bath to favor the following mixing steps. The temperature is one key parameter to control when working with collagen since it turns quickly to a gel-like structure when cooled down.

Collagen and PEG/Gly solutions were first mixed together in a beaker on a hot plate heater with magnetic stirring. A temperature of 40°C was maintained during all experiment in order to prevent the collagen to turn back to gel-like state. The pH was adjusted to 8.9 – 9.1 with NaOH 0.1 M or 0.5 M solutions. The pH adjustment is required for the subsequent cross-linking of the collagen strands upon drying. The CNF suspensions were then added slowly under magnetic stirring. 5 wt% proportion of CNF in the final dry composite was targeted. The pH was controlled and adjusted again if necessary, the final dilution level was reached by the addition of deionized sterile water previously heated at 40°C. The whole mixture was then stirred for 15 min to favor the dispersion of the CNF in the collagen solution and ensure a homogeneous temperature.

The casting of the formulation was performed on inert surface (PVDC sheets) equipped with silicone molds of rectangular shape. The surface weight (grammage) objective was 64 g/m². Once cast under a laminar flow hood, after 15 min cooling down, the solutions had a gel-like state. The drying was

then performed overnight at 20°C and 40 % of relative humidity in a controlled oven. Pure collagen-PEG/Gly membranes were also prepared as reference materials. The composite membranes were recovered and stored in individual sealed pouches. Half of the samples were sterilized with gamma radiation at 30-35 kGy doses. Table III.2 describes the prepared composites. As PEG/Gly solution is present in every samples, it is not mentioned in the denomination used (i.e. Coll-CNF stands for collagen-PEG/Gly-CNF composites).

Table III.2: Designation and composition of Coll-CNF composites prepared with CNF-t, CNF-yne and CNF-metro

Designation	Collagen-PEG/Gly matrix	CNF type		
		CNF-t	CNF-yne	CNF-metro
Coll	■			
Coll-CNF-t-5%	■	■		
Coll-CNF-yne-5%	■		■	
Coll-CNF-metro-5%	■			■

2.2.2.c. Release of Metro from CNF-metro

The release of metronidazole was assessed from suspension of CNF-metro. It was induced by the addition of a human carboxylesterase 2 (hCE2). This enzyme favors the cleavage of the ester bond that binds metronidazole to the CNF-metro and prodrug arm. CNF-metro suspension was centrifuged at 20 000 g for 10 min and re-dispersed in TRIS buffer (pH 7.4, 50 mM). This operation was repeated 2 times. A volume of 10 ml of CNF-metro suspension was poured into a balloon and heated at 37°C. The commercial enzyme solution was diluted to 1 mg/ml with TRIS buffer and 2 ml of this solution was introduced in the CNF-metro suspension. The mixture was maintained under magnetic stirring and at 37°C for 48 hours. In parallel, a 10 ml CNF-metro suspension without the enzyme (also re-dispersed in TRIS buffer) was exposed to the same condition, acting as a reference. Aliquots were collected from both balloons in order to assess the influence of the enzyme addition on the release of the metronidazole. 500 µl aliquots were collected at predetermined time intervals and centrifuged at 14 000g for 10 min and filtrated with syringe filter (0.45 µm, polyamide/nylon, CHROMAFIL AO-45/3 MACHEREY NAGEL) before characterization. Reverse-phase high performance liquid chromatography (HPLC) was performed with a micro-bondapak-C18 analytical column (Waters Associates) to track the presence of metronidazole in the aliquot. A Waters chromatographic system was used, with two M-510 pumps and photodiode array detector Waters 996 using Millenium 32 software. A linear gradient from 10 to 100 % methanol in H_2O pH 2.5 (phosphoric acid), 1 ml/min flow rate, was used.

After 48 hours of reaction, the CNF-metro suspension was diluted with 40 ml of dichloromethane in order to retrieve the metronidazole that could have been trapped onto the CNF by strong adsorption phenomena and not visible in the HPLC analysis. The mixture was maintained under stirring for 72 hours. Upon phase separation, the organic phase that may contain metronidazole is separated from the aqueous phase and liquid ^{1}H NMR analysis was performed to investigate its composition.

2.2.2.d. Antibacterial testing

Nanocomposites antibacterial activity was assessed through zone of inhibition (ZOI) experiments against anaerobic bacteria strains *Bacteriodes vulgatus*, *Bacteriodes fragilis* and *Clostridium difficile*. Bacterial strains were grown overnight in an anaerobic incubator at 37°C in blood sheep stained agar filled petri dishes. On the next day, bacterial suspensions were prepared and adjusted at a 10^{8} CFU/ml concentration. Fresh blood sheep stained agar petri dishes were prepared and bacterial suspensions were spread on the surface to achieve the inoculation of the medium. A positive control composed of a 10 mm disk of blotting paper in which 16 µg of metronidazole was deposited on the agar surface in each petri dish. 10 mm disk were cut off from each samples and deposited in the inoculated petri dishes. Anaerobic incubation was performed for 24h at 37°C. In parallel, bacteria strains were grown again as previously described to prepare successive cycles of ZOI experiments. After incubation, petri dishes were observed to detect inhibition zones.

Two distinct experiments were then realized: (i) standard ZOI experiments against *Bacteriodes vulgatus*, *Bacteriodes fragilis* and *Clostridium difficile*, and (ii) successive ZOI experiments against *Bacteriodes fragilis,* where the sample from cycle 1 are collected and exposed to freshly prepared inoculated petri dishes in order to assess the evolution of the antibacterial activity over time. In total, four cycles of successive ZOI experiments were performed on Coll-CNF-t and Coll-CNF-metro-5% against *Bacteriodes fragilis.*

2.3 Results and discussion

2.3.1. Release of metronidazole from CNF-metro suspensions with enzymatic stimuli

The concept of "on demand" release of metronidazole under enzymatic stimuli was analyzed. Indeed infection sites have important enzymatic activity suitable for ester bond cleavage. Two suspensions of CNF-metro were maintained at 37°C for 48 hours under magnetic stirring. Human carboxylesterase 2 was added in one of the two suspensions for releasing the metronidazole grafted on CNF substrate, through the cleavage of the ester function. Aliquots of the suspensions were analyzed over time. After 1 hour of agitation, a clear signal appears at 3.726 minutes of elution on chromatograms of the suspension that contains the enzyme, as illustrated on Figure III.17a. By comparison with chromatograms of metronidazole solution (results not shown), this signal can be

attributed to the release of the metronidazole. In UV spectra, the peak at 283.9 nm also demonstrates the presence of metronidazole. The CNF-metro suspension that was reacted in the absence of the enzyme was also analyzed with HPLC. However, even after 4 hours, no trace of the metronidazole is detected as confirmed by both the chromatogram and UV spectrum of Figure III.18b. This very positive result validates the concept of "on-demand" release of metronidazole under enzymatic activity.

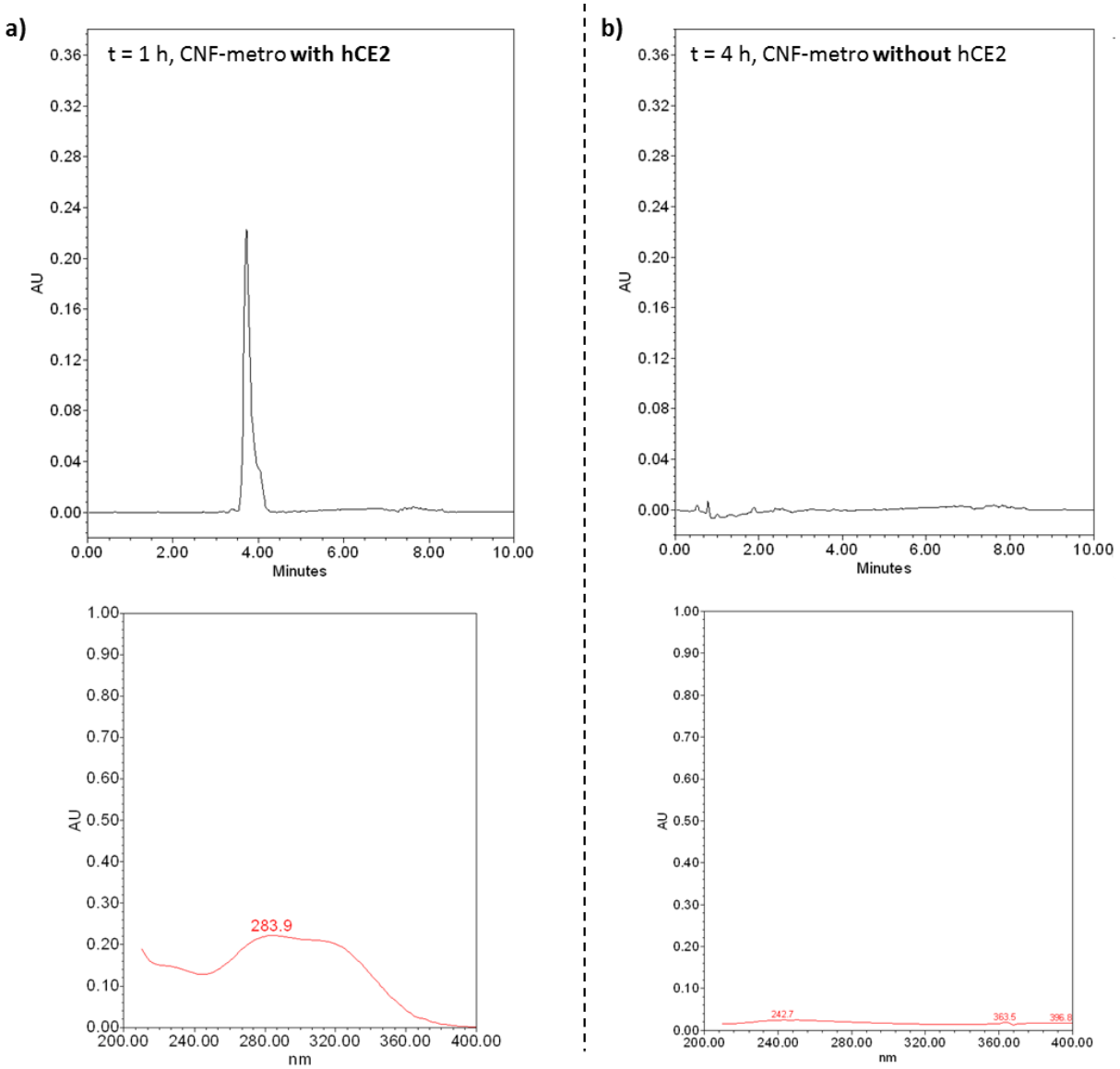

Figure III.17: HPLC chromatograms (top) and associated UV spectra (bottom) of CNF-metro suspensions reacted with (a) and without (b) the presence of carboxylesterase human 2 (hCE2)

After the reaction, both CNF-metro suspensions were extracted with dichloromethane so that entrapped metronidazole related compounds that were not detected before could be transferred easily from the aqueous to the organic phase. Liquid ^{1}H NMR was then conducted but surprisingly, no significant trace of metronidazole was detected although sugar moieties seemed to be present.

Even if further investigation is required, especially on longer time release, the main outcome of this study is that CNF-metro suspension, when exposed to hCE2 enzyme, is able to release metronidazole molecule in one hour. This very positive result validate the concept of "on demand" release by prodrug modified CNF.

2.3.2. Antibacterial activity in anaerobic conditions

Further in-vitro characterization was conducted with antibacterial activity testing in order to discuss the presence of non-covalently bound metronidazole. Collagen-CNF composites were tested with ZOI experiments in order to assess their antibacterial activity against anaerobic bacteria *Bacillus fragilis*, *Bacteriodes vulgatus*, and *Clostridium difficile*. The different samples that were characterized included CNF from the different stage of the chemical modification: CNF-t, CNF-yne and CNF-metro. An example of the results obtained is shown on Figure III.18. The positive control (sample disk 0, impregnated with metronidazole) shows a wide zone of inhibition that confirms the activity of the metronidazole against the three strains that were used. ZOI radiuses of 2.3 to 3.2 cm are detected according to the table in Figure III.18. Sample disks 1 and 4 do not exhibit any zone of inhibition indicating that oxidized (Coll-CNF-t-5%) and alkyne function bearing CNF (Coll-CNF-yne-5%) do not show antibacterial activity when embedded in collagen matrices. However, metronidazole modified CNF based collagen nanocomposites (Coll-CNF-metro-5%) present a significant zone of inhibition (sample disk 2) and radiuses of 1.6 to 2.3 cm are detected for the three bacterial strains. This result confirms the possibility of using such materials as active soft tissue repair devices. Some of the Coll-CNF-metro-5% samples were subjected to gamma radiation sterilization as in the current industrial practice. Unfortunately, it does not show any zone of inhibition. This result suggests that gamma radiation causes the composite to lose its antibacterial activity. Several hypotheses can be formulated to explain the loss of activity.

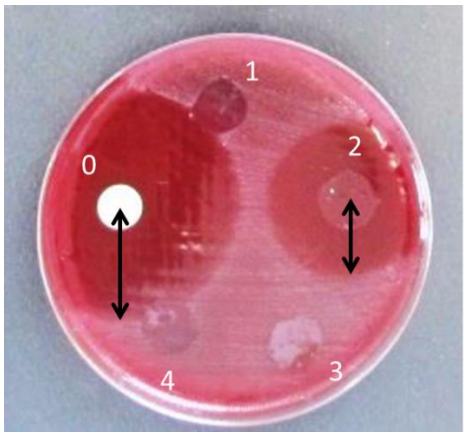

Sample reference		ZOI radius (cm)		
		Bacillus fragilis	*Bacteriodes vulgatus*	*Clostridium difficile*
0	Positive control	2.6	2.3	3.2
1	Coll-CNF-t-5%	0	0	0
2	Coll-CNF-metro-5%	1.8	1.6	2.3
3	Coll-CNF-metro-5% (gamma)	0	0	0
4	Coll-CNF-yne-5%	0	0	0

Figure III.18: ZOI experiment on Collagen-CNF nanocomposites. On the left, a picture of the agar medium inoculated with *Clostridium difficile*. Very similar inhibition zones were observed with *B. fragilis* and *Bacteriodes vulgatus*. On the right, the table shows ZOI radius

The gamma radiation could chemically affect the molecular structure of the metronidazole resulting in a non-active compound. In a parallel project, xyloglucans molecules were chemically modified with metronidazole prodrug and the influence of gamma radiation on such compounds was assessed through ^{1}H liquid NMR. The spectra showed no change related to metronidazole peaks before and after gamma radiation, as illustrated on Figure III.19. The irradiation effect could be different on solid collagen-CNF composites compared to solubilized modified xyloglucans, but this result still leaves space for another hypothesis to explain the loss of activity.

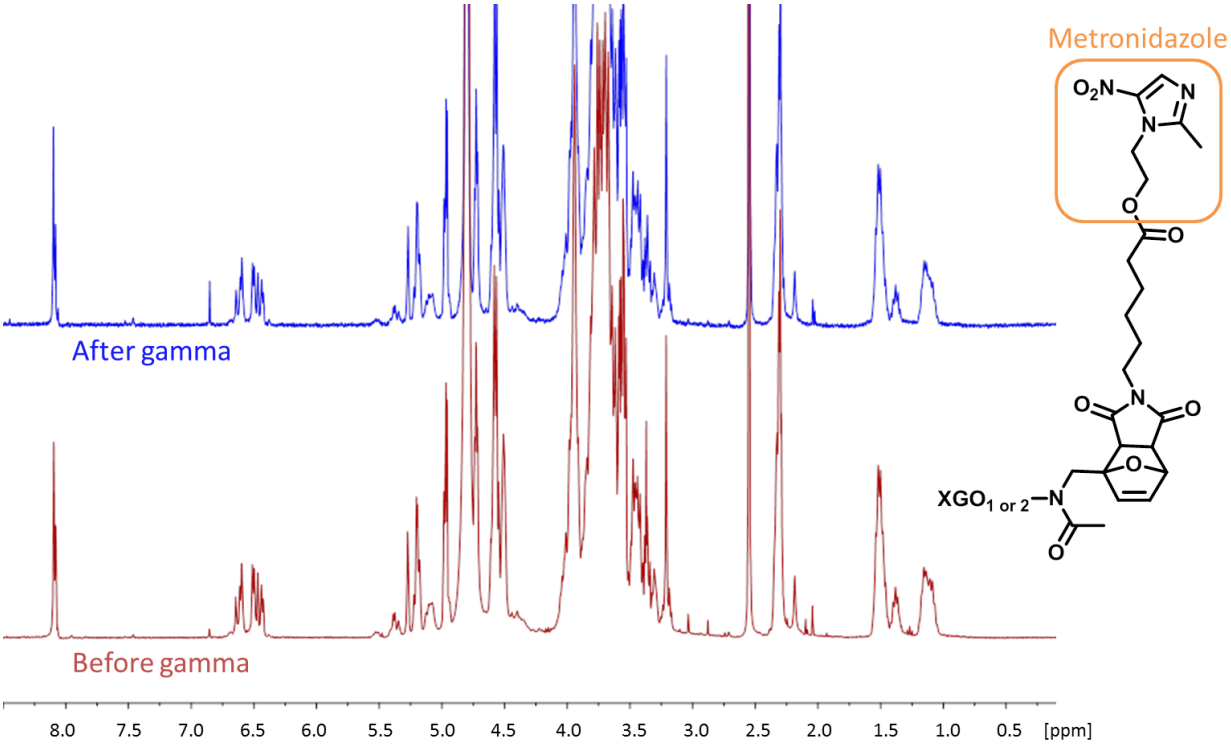

Figure III.19: Liquid ^{1}H NMR spectra of compound that include metronidazole, before (red) and after (blue) gamma radiation treatment (35-50 kGy)

The second hypothesis deals with the collagen matrix structure. The gamma radiation creates many radicals in the exposed materials and triggers many chemical reactions that can be beneficial or detrimental to the collagen structure. For instance, gelatin hydrogels were crosslinked with gamma radiation and significant increase of mechanical properties were obtained [51]. Likewise, type I collagen scaffolds were reinforced with dextran polysaccharide before gamma radiation. This resulted in an enhanced gel yield after gamma radiation [52]. Consequently, one can assume that the metronidazole is not degraded but only trapped into a denser crosslinked collagen/CNF structure provoked by gamma radiation treatment. The influence of such heavy treatment on collagen/CNF nanocomposites will be further investigated in the next chapter. The rest of the discussion will now focus only on non-irradiated collagen/CNF samples.

Successive ZOI experiments were conducted to assess the antibacterial activity of collagen/CNF-metro and collagen/CNF-t samples over time. At each cycle of ZOI, after collection of ZOI dimensions, disk samples were transferred to a fresh bacteria-inoculated agar medium. On cycle 1, similarly to first experiment, significant ZOI is detected for Coll-CNF-metro-5% while Coll-CNF-t-5% did not exhibited any antibacterial properties as depicted on Figure 19. Upon cycle 2, the activity of Coll-CNF-metro-5% decreases and ZOI is limited to the edge of the disk sample. The two last cycles led to the same results, proving the contact active properties of Coll-CNF-metro-5% samples as shown on the evolution of ZOI radiuses on. As expected, Coll-CNF-t-5% does not show any antibacterial activity on cycles 1, 2, 3 and 4.

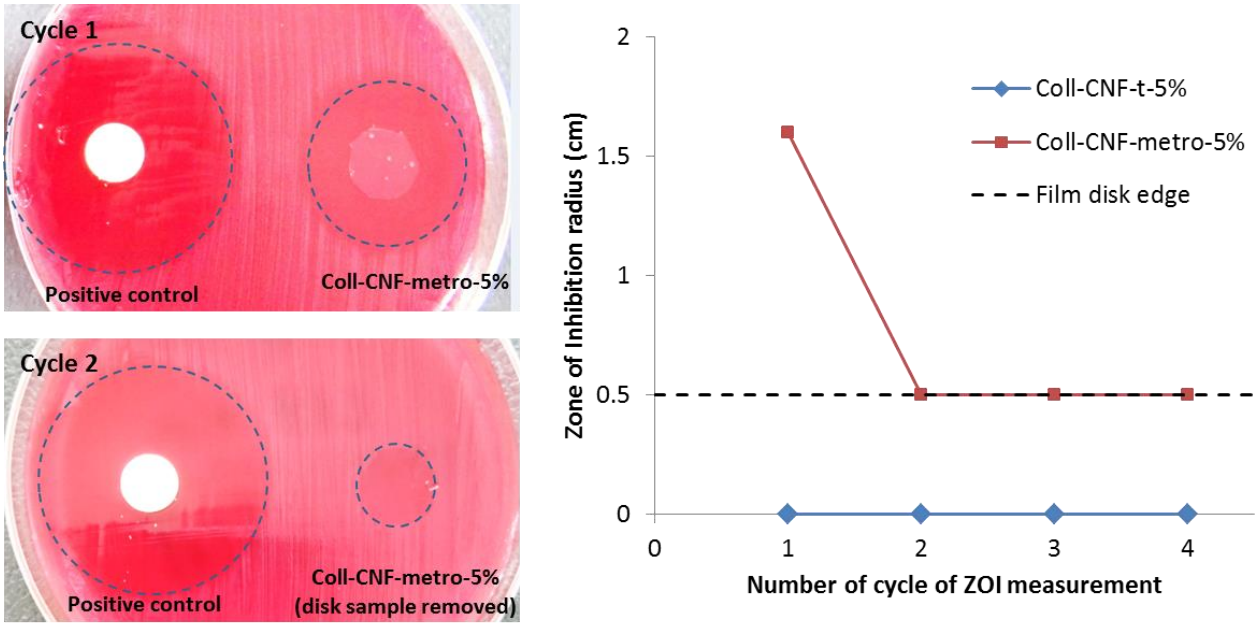

Figure III.20: Successive ZOI experiments, picture of the agar medium for Cycle 1 and 2 showing ZOIs (left) and evolution of the ZOI radiuses over the number of cycles of experiments (right)

The prolonged contact-active behavior indirectly confirms the covalent immobilization of metronidazole molecule to the CNF that were included in the collagen matrix. This sample proved to have significant antibacterial properties against anaerobic bacteria, which makes it suitable for soft tissue repair application.

2.4 Conclusion

Highly innovative two-step chemical modification was applied to graft a prodrug that included metronidazole and ester function. Enzymatically triggered cleavage of this ester function was performed and confirmed by addition of human carboxyl esterase 2. “On demand” release strategy of metronidazole has been successfully proved for CNF-metro suspension. The production of model soft tissue repair devices composed of collagen and metronidazole-modified CNF was achieved through complex preparation that involves temperature and pH control. Nanocomposites exhibited an antibacterial activity against both gram-positive and gram-negative anaerobic bacteria in static conditions, as proven by ZOI experiments. A prolonged activity against *Bacteriodes fragilis* was detected upon successive ZOI tests, which indirectly confirmed the covalent immobilization of metronidazole on CNF substrates thanks to the prodrug anchoring strategy that was implemented. The gamma radiation treatment of the samples resulted in the loss of antibacterial activity suggesting the degradation of the metronidazole molecule, or the intense densification of the collagen/CNF structure. Preliminary NMR analyses of metronidazole-containing compound suggested that no chemical modification occurred upon gamma radiation treatment. Such result calls for further investigations but the study clearly shows that collagen-CNF-metro samples are promising 2D structures for the design of active soft tissue repair model medical devices.

***NB**: Authors would like to acknowledge Alexandre Meunier and Xavier Bertrand from the Regional University Hospital Center (CHRU, Besançon, France) for the antibacterial testing against anaerobic bacterial strains.*

3. Composites of collagen and cellulose nanofibrils with prolonged release of chlorhexidine for antibacterial substrates

This section is based on the results obtained in collaboration with N. Esseghir, Y. Karrout and J. Siepmann at INSERM U1008, located in Lille, France, in the context of the CELLICAL project.

Abstract

Active composites of collagen and cellulose nanofibrils (CNF) that include chlorhexidine digluconate (digCHX), a broad range antiseptic, were prepared. The quantity of CNF and the gamma radiation influence were studied in terms of water-uptake, antibacterial activity against gram-positive and gram-negative bacterial strains, and drug release experiments. Increased quantity of CNF and gamma radiation limit the water uptake of the composites. The antibacterial activity was confirmed only for drug loaded samples, with or without gamma radiation. Firstly, it indicates that collagen and CNF alone do not present bactericidal or bacteriostatic effect. Meanwhile significant bactericide effect is demonstrated when the API is included in the composite for both irradiated and non-irradiated samples suggesting that radiation does not hinder the activity of the digCHX. Finally, drug release experiments benefited from increasing quantity of CNF since they strongly interact with the API and thus provide sustained release. Gamma radiation also presents similar effect to a lesser extent. Overall, these composites appear to be promising material for the design of soft tissue repair medical devices.

3.1 Introduction

Cellulose is the most abundant natural polymer on earth. In the 20th century, cellulosic products have been used under various forms for medical application, *i.e.* as membrane for hemodialysis in blood purification or as excipient for the tablet production (micro-crystalline cellulose) in the pharmacology industry [53], [54]. In the 1980's, a new type of cellulose has been unveiled by Herrick, Turbak and co-workers: cellulose nanofibrils [55], [56]. This new cellulosic material can be isolated by mechanical treatment after chemical or biological pretreatment of biomass (wood, annual plants), resulting in flexible cellulose nanofibrils of 1-2 µm in length and 5-30 nm in diameter [1], [2]. In parallel to numerous potential application in the paper and packaging industry [8], [57], nanocomposites [10] or printed electronics [12], such nanocellulose is also investigated as a new substrate for medical applications, as indicated by several recent reviews [5], [13], [14]. New nanocellulose-based medical devices address topics such as wound healing and drug delivery. The biocompatibility and high specific surface area of such nanomaterials, together with their tunable surface chemistry are considered as the main features pointed out by the above mentioned reviews.

This work deals with the use of nanocellulose for soft tissue repair (STR), which is one of the major business activities of the medical device industry. In hernia repair, implants can be used to re-build soft tissues and regenerate wounded skin layers. Post-operative pains and infections upon implants surgery remain the most reported complications. Collagen based systems are proved to avoid infections and also prevent adhesions phenomena that bind the medical implant and the organs, which is detrimental for correct healing [37], [38]. In the previous study, collagen was successfully used as a matrix that included metronidazole-modified cellulose nanofibrils to design active medical devices. The gamma radiation treatment applied to the samples led to a loss of antibacterial activity and its influence on the properties of collagen/CNF systems needs to be more specifically addressed, especially when drugs are embedded in the nanocomposite. Gamma radiation is mainly used for sterilization purposes but it is also known to strongly affect polymers such as collagen. While 20th century scientific papers describe a degradation of collagen molecular structure upon gamma radiation sterilization at 10-750 kGy doses [58], [59], some beneficial effects were recently detected with lower radiation dose. For instance, collagen derived gelatin was reinforced with polyvinyl alcohol (PVA) up to 15% and mild gamma treatments were applied (from 0,5 to 5 kGy) to trigger the crosslinking. Tensile strength was increased until 1 kGy gamma radiation, before decreasing under the values of non-irradiated samples for higher gamma doses [60]. All these work confirm the densification of collagen structures upon gamma radiation.

In parallel, CNF have been used as a reinforcing agent of several matrices like thermoplastics or water soluble polymers (starch, proteins, chitosan) [61]. Similarly, the addition of high ratio of CNF to collagen based structures was proven to be beneficial for both mechanical properties and stability in moist conditions when crosslinked with glutaraldehyde or combination of genepin and gamma radiation treatment. Tensile strength of 132-186 MPa and elastic modulus of 5-14 MPa were obtained, which is significantly higher than pure collagen matrices (2 to 3 times more for tensile strength and to 4 times more for modulus). Moreover, reduced liquid uptake of PBS was observed upon CNF addition and crosslinking confirming the stability of such nanocomposites. Finally, cytocompatibility and biocompatibility was assessed and results confirmed good cell adhesion and growth making these structures suitable for bone and ligaments implantable scaffolds [42], [43]. Other works report the preparation of bacterial cellulose-collagen composites aerogels and chemically crosslinked membranes that also exhibit mechanical improvements and better cytocompatibility than reference materials [40], [62].

Among the available literature, only one attempt of combining CNF and collagen (gelatin) with encapsulated API was found. The targeted application was enhanced bone regeneration. The scaffold presented sustained release of osteoinductive molecule, *i.e.* the simvastatin, after a burst release, thanks to the cellulose nanofibrils [63]. However, no mention of the influence of sterilization process such as gamma radiation was done. In this work, the combination of CNF, collagen and active molecule will be used to design prototypes of soft tissue repair medical devices. The influence of gamma radiation and quantity of CNF will be investigated in terms of water-uptake, antibacterial activity and drug release experiments.

3.2 Experimental section

3.2.1. Materials

The cellulose nanofibers suspensions were provided by the Centre Technique du Papier (CTP, Grenoble, France). A first suspension referred as CNF-e was produced by a 2h enzymatic pre-treatment of a pre-refined (40°SR) bleached birch pulp followed by homogenization: 3 passes at 1500 bars in an Ariete homogenizer from GEA. The second suspension, which is referred as CNF-t, was also produced the Centre Technique du Papier (CTP, Grenoble, France). The 2,2,6,6-tetramethylpiperidine-1-oxyl (TEMPO) mediated oxidation was performed on a pre-refined (40°SR) bleached softwood bisulfite pulp provided by TEMBEC following classical procedure developed by A. Isogai's team [49], [50]. Briefly, the pulp was reacted 2 hours with TEMPO and sodium bromide at pH 10, which was controlled with sodium hypochloride. Collagen solution was provided by Medtronic (Trévoux, France). The collagen was extracted from porcine dermis through chemical oxidative treatment. A 4 wt% of oxidized collagen solution was obtained. For clarity purposes, o*xidized collagen* will be referred as *collagen* in the samples description.

Chlorhexidine di-gluconate 20 wt% solution in water was purchased from SIGMA-Aldrich (digCHX, CAS: 18472-51-0, Figure III.21) and diluted for composite formulation. Sodium hydroxide and hydrogen chloride were also purchased from SIGMA Aldrich, 1 M stock solution were prepared. Poly ethylene glycol 4000 (PEG, CAS: 25322-68-3) and glycerol (CAS: 56-81-5) were obtained from MERCK Millipore. Sterile deionized water was used in all the following experiments. Phosphate buffer saline (PBS) at pH 7.4 was used for release experiments.

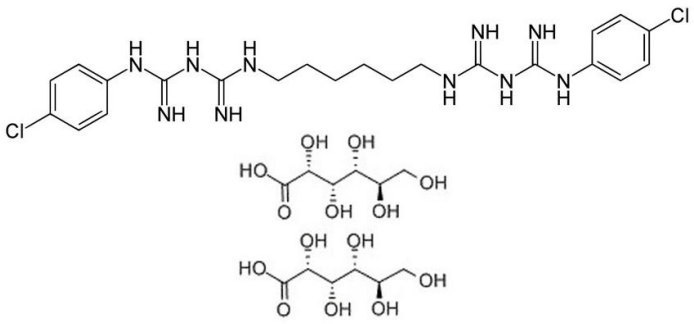

Figure III.21: Chlorhexidine digluconate molecular structure

3.2.2. Methods

3.2.2.a. Physical characterization of CNF and collagen-CNF composites

CNF-t and CNF-e 0.1 wt% suspensions were analyzed with optical microscopy at x20 magnification on an Axio Imager A2 device equipped with an AxioCam MRm camera (Carl Zeiss, Germany). Dark field observation mode was used to obtain contrasted images. Atomic force microscopy (AFM) images

were recorded on a Dimension icon® (Bruker, USA). The suspension concentration was adjusted at $7.5x10^{-4}$ wt% by several dilution of the gel using high shear mixer Ultra-Turrax (IKA). A drop of this suspension was deposited on freshly cleaved mica plate before drying overnight under fumehood at room temperature. The acquisition was performed in tapping mode using a silica coated cantilever (OTESPA® 300 kHz – 42 N/m, Bruker, USA). Zones of 3,3*3,3 µm² were analyzed. Environmental scanning electron microscopy (SEM) was performed on a HITACHI TM1000 to obtain images of the collagen-CNF composites. A working distance of 2 cm and a magnification of x1000 were used.

3.2.2.b. Liquid nuclear magnetic resonance (NMR)

Liquid ^{13}C nuclear magnetic resonance (^{13}C NMR) was performed on digCHX solutions at the « Institute for Nanoscience and Cryogenics (INAC) » in the «French Alternative Energies and Atomic Energy Commission (CEA) » at Grenoble, on a Bruker AVANCE400 spectrometer. Acquisition and data treatment was done using the LINUX TopSpin 3.2 software. 20 wt% digCHX solutions were diluted in D_2O and Chromium (III) acetylacetonate relaxant agent was added in 10 mg/ml final concentration. The experiments were conducted with 1.3 s acquisition time, 5 s relaxation delay and a 30° pulse using a 250 ppm spectral width (relaxant agent in the mixture). Proton broad band decoupling was applied only during acquisition time. 64 k data points were used for data acquisition. Prior to Fourier transformation, zero-filling at 128 K was applied, followed by apodization with a 2 Hz exponential. Chemical shifts are given relative to TMS (tetramethylsilane, $\delta = 0$ ppm). The positions of the peaks were referred to the residual solvent signal

3.2.2.c. Production of digCHX loaded Collagen-CNF composites

A solution of 10 wt% PEG and 6 wt% glycerol was prepared in sterile deionized water (PEG/Gly solution). After complete dissolution under magnetic stirring, the solution was further sterilized by filtration on 0.200 µm pore size filters. Commercial digCHX solution was diluted to 1 wt%. CNF-e and CNF-t suspensions concentrations were adjusted at 1 wt% and 0.4 wt% respectively and dispersed with Ultra-Turrax high shear mixer (IKA, USA) for at least one minute at 10 000 rpm. The pH of the suspensions was adjusted to 9 with 0.1 M and 0.5 M NaOH solutions. All these solutions were pre-heated at 40°C in a hot water bath. Oxidized collagen solutions are stored at -80°C after their production procedure and they show a gel like structure at room temperature, which is not suitable for composite production. Oxidized collagen solutions were then placed in the hot-water bath at 40°C in order to obtain liquid collagen solutions. The temperature is one of the key parameters to control when working with collagen based systems since it shows a gel like structure when cooled down.

The next step is the most challenging one, where PEG/Gly solution, CNF suspensions, oxidized collagen and digCHX solutions are mixed together. Numerous attempts were necessary to find the best protocol that ensures a good dispersion of CNF and digCHX in the collagen matrix while avoiding the introduction of air bubbles that are detrimental to the stability of the composite.

The best procedure selected was as follows: oxidized collagen and PEG/Gly solutions were first mixed together in a beaker on a hot plate heater with magnetic stirring to maintain the solution temperature at 40°C during all experiment in order to prevent the collagen turning back to gel state. The pH was adjusted to 8.9 – 9.1 with NaOH 0.1 M or 0.5 M solutions. The pH adjustment is required for the subsequent cross-linking of the collagen strands upon drying.

A final quantity of 2 wt% of digCHX in the composite was targeted and the corresponding volume of the 1 wt% digCHX solution was added to the collagen-PEG/Gly mixture drop by drop. Pre-heated CNF suspensions were then slowly introduced in the mixture. Amounts of 5, 10 and 20 wt% of CNF were targeted for the composite. The pH was controlled and adjusted again if necessary. The final solid content (*i.e.* 1.5 wt%) was reached by the addition of hot deionized sterile water (40°C). The whole mixture was then stirred for 15 min to favor the dispersion of the CNF in the oxidized collagen solution and ensure a homogeneous temperature.

The casting of the formulation was performed on inert surface (PVDC sheets) equipped with silicone molds of rectangular shape. The basis weight (grammage) objective was 64g/m². Once cast under a hood that ensures laminar air flow, after 15 min cooling down, the solutions turned to gel state. The drying was then performed overnight at 20°C and 40 % of relative humidity in a controlled oven. The composite membranes were recovered and stored in individual Tyvek™ pouches that were sealed. Half of the samples were sterilized with gamma-irradiation at 35-50 kGy doses. The Table III.3 summarizes all the samples prepared according to afore mentioned protocol. The following abbreviation will be used in the discussion: Coll-CNF-t-5%-CHX refers to collagen-PEG/Gly-CNF composites comprising 5% of CNF-t with digCHX. Coll-CHX refers to Collagen-PEG/Gly membranes only loaded with digCHX.

Table III.3: Composition of composites prepared with oxidized collagen, CNF-t or CNF-e and chlorhexidine digluconate (digCHX)

Designation (x = t or e)	Collagen-PEG/Gly matrix	CNF loading				2 wt% digCHX	
		0%	5%	10%	20%	yes	no
Coll	■	■					■
Coll-CHX	■	■				■	
Coll-CNF-x-5%	■		■				■
Coll-CNF-x-5%-CHX	■		■			■	
Coll-CNF-x-10%	■			■			■
Coll-CNF-x-10%-CHX	■			■		■	
Coll-CNF-x-20%	■				■		■
Coll-CNF-x-20%-CHX	■				■	■	

3.2.2.d. Water uptake

Disks of 15 mm diameter were cut out from every sample and immersed in 20 ml deionized water before incubation at 37°C. At 2, 7, 24 and 96 hours, the weight of discs was measured after removal of excess water. The samples were then immersed again in the same medium. The water uptake W (%) was then calculated according equation (III-4).

$$W = \frac{m_t - m_i}{m_i} \times 100 \qquad \textbf{(III-4)}$$

Where m_t is the weight of the disc at time t and m_i is the initial weight of the disc before immersion. Measurements were done in triplicates to assess standard deviation of the results. Water uptake measurements give indication on the internal crosslinking of the composite and the influence of CNF and digCHX addition.

3.2.2.e. Antibacterial activity

The antibacterial activity of the Coll-CNF composites was assessed through zone of inhibition (ZOI) testing against *Staphylococcus aureus* and *Escherichia coli.* The bacterial suspensions were spread on Muller-Hinton agar and 15 mm diameter disks of samples were deposited onto the surface. After 24 hours incubation, ZOI were detected or not, indicating whether the sample present antibacterial activity or not. When ZOI were observed, dimensions were collected. Each sample was characterized in triplicates.

3.2.2.f. Release study experiments

Drug loaded Coll-CNF composites samples were used for release study experiments. Two techniques were used, with partial or full release medium renewal. In the first one, 30 cm² samples were

immersed in 50 ml of phosphate buffer saline (PBS, pH 7.4) in opaque flasks under orbital sharing (80 rpm) and maintained at 37°C in an incubator. Sink conditions were respected. Aliquots of 3 ml were taken at pre-determined time intervals and replaced with the same amount of fresh PBS (Figure III.22a). Results will be presented as the cumulative release of digCHX over time. The second technique involves the same equipment but the entire release medium was renewed at the same pre-determined time intervals by transferring the sample to a new flask with fresh PBS. An aliquot of 3 ml was collected to trace the presence of digCHX (Figure III.22b).

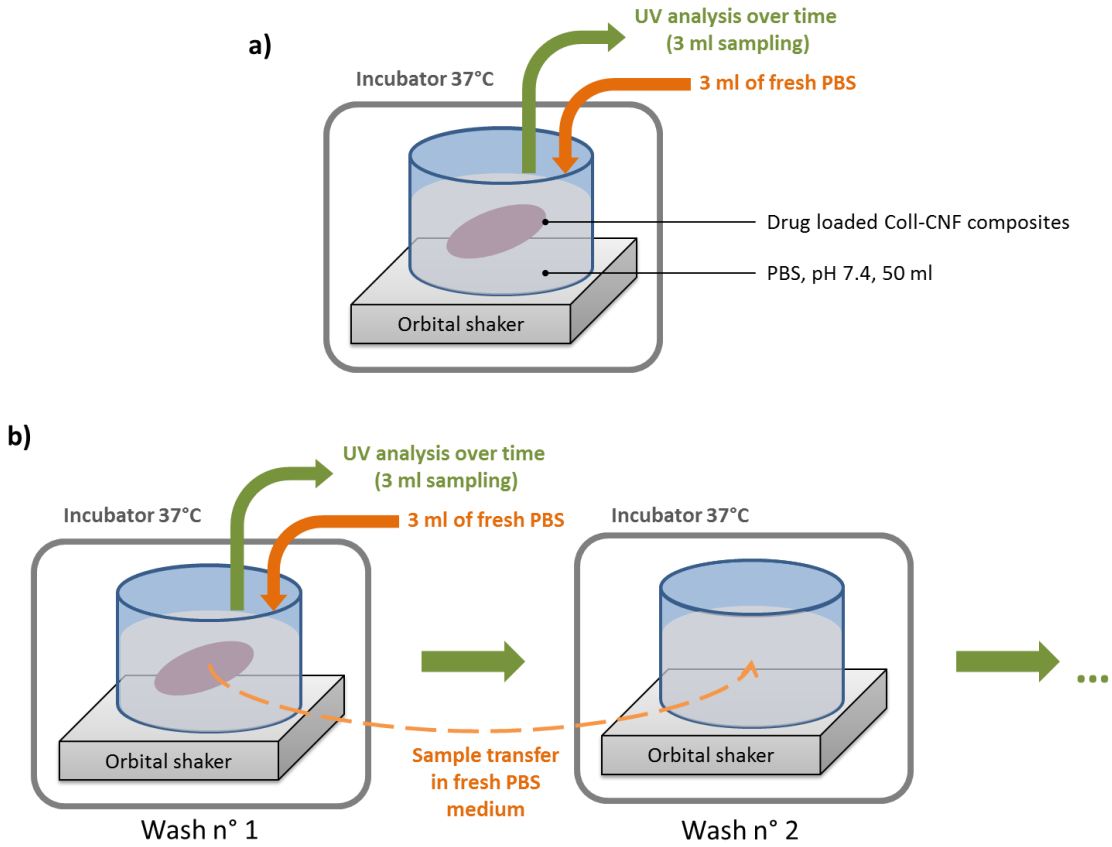

Figure III.22: Graphical description of release study techniques with a) partial renewal of the release medium: 3 ml aliquots were taken and replaced with 3 ml of fresh PBS, and b) full renewal of the 50 ml release medium, 3ml aliquots are also use for analysis

Here, results will be presented as the cumulative release of digCHX over the number of release medium renewal (*i.e.* washing number). Inverse phase high performance liquid chromatography (HPLC) was used to determine the concentration of digCHX over time. Mobile phase was composed of NaH_2PO_4 0.08 M (65 volumes), acetonitrile (35 volumes) and tri-ethylamine 0.5%. The pH was adjusted at 3 with glacial acetic acid. Flow rate was 1 ml/min and a wavelength of 270 nm was used for the UV analysis. Injections of 20 µl were sent in the stationary phase composed of a Gemini C18 column of 100 mm. Pre-established chromatograms of known-concentrations digCHX solutions were used to produce a calibration curve and be able to calculate the concentration of digCHX in the

aliquots. Every release analysis was done in triplicates. All these release studies have been performed during the master thesis of Nourhene Esseghir at Institut National de la Santé et de la Recherche Médical (INSERM, U1008) in Lille, France.

3.3 Results and discussion

3.3.1. CNF and collagen-CNF composite physical characterization

Various qualities of CNF-e and CNF-t are described in the literature. In this study, highly homogeneous suspensions of CNF-e and CNF-t were obtained. A quick characterization of these CNF suspensions is provided on Figure III.23. Optical microscopy shows microfibrils and nanofibrils aggregates for CNF-e while the CNF-t are not visible since they are much more individualized. AFM height sensor images confirm the nanoscale dimensions of CNF-t and CNF-e.

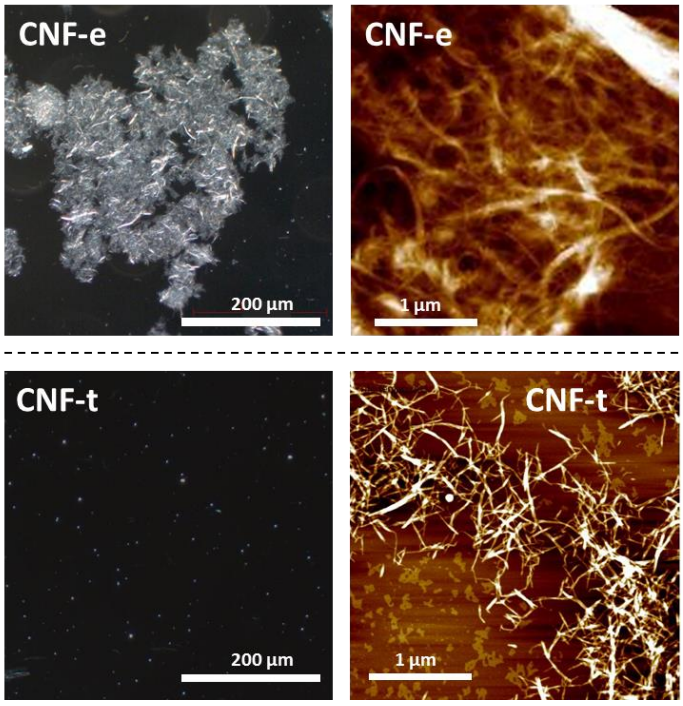

Figure III.23: Morphology of CNF-e and CNF-t: left, optical microscopy (suspensions 0.1 wt%, x20) and right, AFM height sensor images of CNF-e and CNF-t suspension

Preparation of collagen-CNF composite has been continuously optimized to avoid any air bubbles and ensure good dispersion of CNF-e, CNF-t and digCHX in collagen matrix. Such homogeneity has been confirmed visually and also with SEM for CNF-t loaded composites, as exposed by Figure III.24. The collagen-CNF composites with the highest content of CNF-t (*i.e.* 20 wt%) are transparent and homogeneous. However, the transparency of CNF-e loaded composite was slightly lower than CNF-t loaded ones.

It can be explained by the presence of microfibrils aggregates in CNF-e suspension, as observed with optical microscopy, that are complicated to further disperse. Meanwhile, for lower proportion of both CNF-e and CNF-t (5 wt% and 10 wt%), good dispersion was achieved.

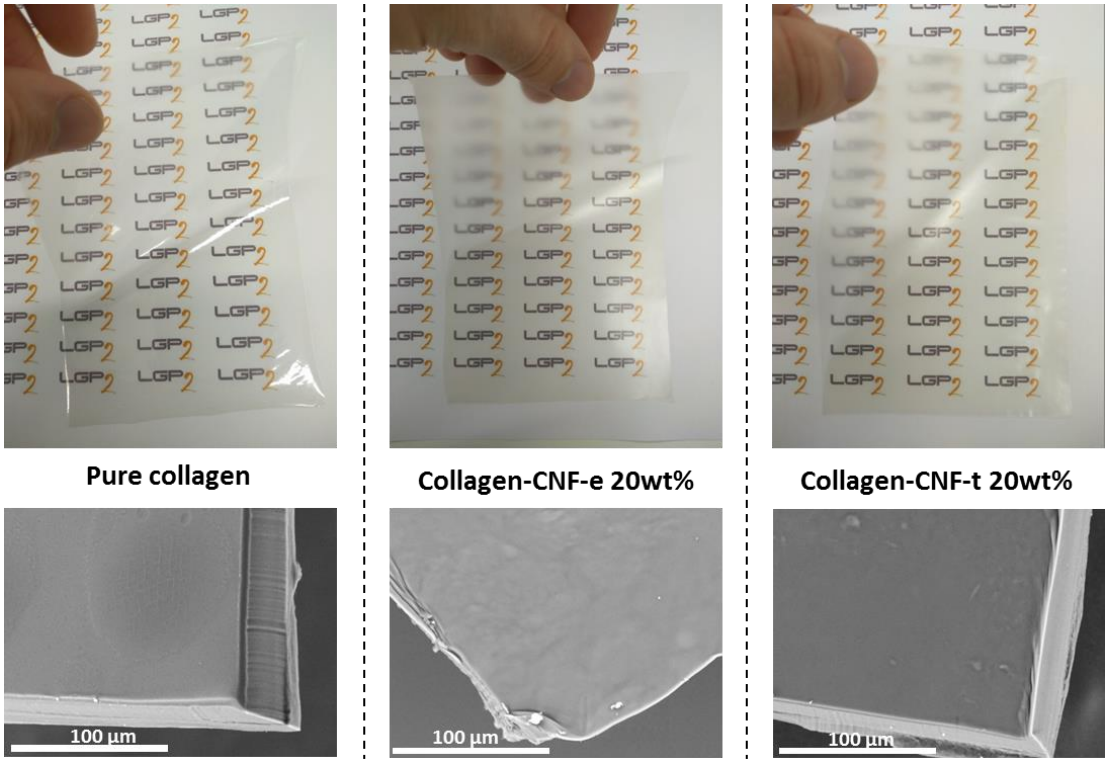

Figure III.24: Morphology of collagen-CNF composites, pictures of composite films showing transparency and SEM pictures proving the dispersion of CNF

3.3.2. Influence of gamma irradiation on STR

The influence of gamma irradiation that is usually applied on commercial medical devices was assessed for the collagen-CNF composites in terms of swelling behavior. Water uptake experiments were performed on Coll-CNF samples. Figure III.25 exposes typical effects of CNF-e or CNF-t addition and gamma irradiation on water uptake of collagen composite membranes. For non-irradiated samples, the effect of CNF addition in oxidized collagen gives a reduced water uptake from more than 1000 % without CNF to 650 % for CNF-t loaded and 450 % for CNF-e loaded membranes, after 24h of immersion. Presence of CNF prevents the collagen membranes to swell indicating good interactions between oxidized collagen strands and cellulose nanofibrils that stabilizes the internal structure. The decrease in water uptake is lower for CNF-t because of its more hydrophilic character,

which increases the Coll-CNF-t composite water affinity. For gamma irradiated samples, the same tendency is observed even if it is of moderate extent for CNF-t loaded membranes.

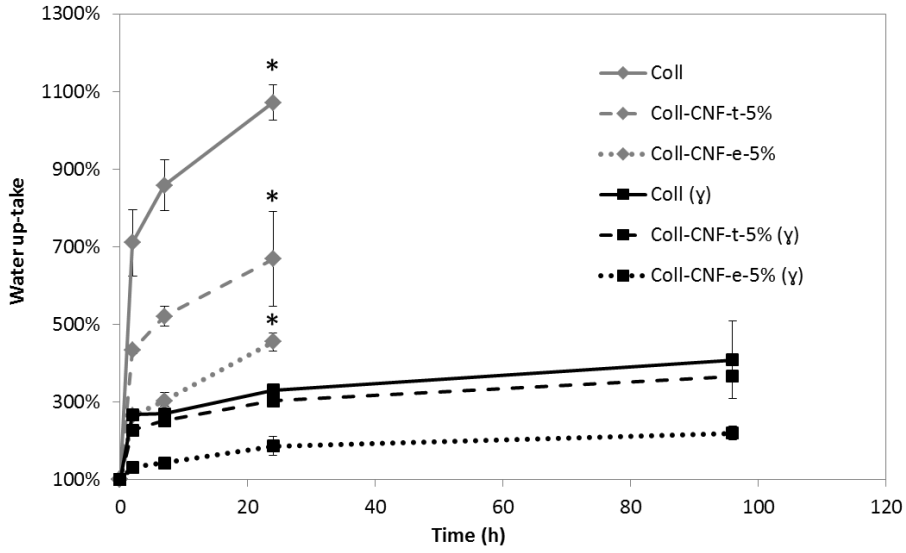

Figure III.25: Evolution of water uptake with time for Coll, Coll-CNF-t-5% Coll-CNF-e-5% composites and influence of gamma irradiation. The stars * indicate the degradation of the sample

After 24 h of immersion, samples that were not irradiated with gamma treatment were dispersed in the swelling medium and no water uptake values were possible to measure. Meanwhile, irradiated samples were still structured enough to undergo water uptake measurement at 96 h of immersion in water. Very narrow standard deviation can also be observed for irradiated samples confirming a more homogeneous and stable internal structure. The overall effect of gamma irradiation is a strong decrease in the water uptake. When non-irradiated samples swells until degradation (indicated by *) after 24h, gamma treated composites are able to undergo rapid swelling that stabilizes around 350% for Coll and Coll-CNF-t-5% and 220% for Coll-CNF-e-5%. This confirms the beneficial influence of gamma irradiation on the internal crosslinking of this oxidized collagen strands with each other but also together with CNF.

The effect of CNF-t addition and gamma irradiation is also confirmed when plotting the evolution of water uptake of Coll-CNF-t composites over time, against the amount of CNF-t in the composite. From 0 to 10 wt% of added CNF-t, water uptake is decreasing for both non-irradiated and irradiated samples from 700-1000 % to below 500 % and from 250-350 % to below 150 % respectively, after 24 h of immersion (Figure III.26). This confirms the afore-mentioned stabilization effect of CNF addition on Coll-CNF membranes. Again, irradiated samples values show narrower standard deviations that

also prove that every CNF-t loadings allow for the production of stable composites. Similar tendencies were observed with CNF-e loaded composites (results not shown).

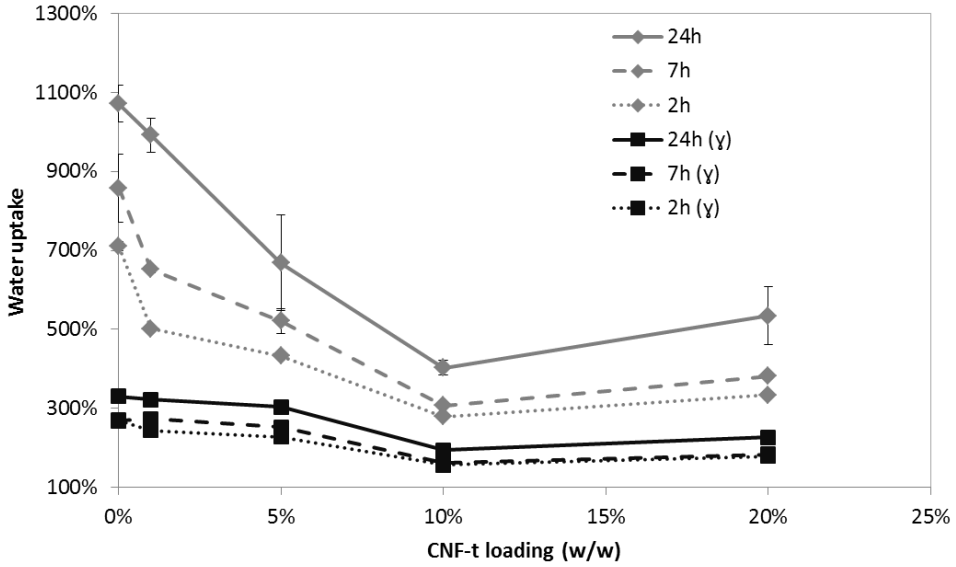

Figure III.26: Evolution of water uptake with CNF-t loading of Coll-CNF composites and influence of gamma irradiation over time (up to 24h swelling)

These results indicate how gamma radiation treatment and CNF addition limit the capacity of collagen-CNF composites to absorb water and eventually be dispersed in liquid media. Hydrogen bonding governs most of these two polymers structures, which suggests that hydrogen bonding between cellulose and collagen strengthen the composites. Moreover, gamma radiation treatment must induce chemical cross linking in between oxidized collagen strands and also between CNF and oxidized collagen strands, improving again the binding between the two materials.

3.3.3. Antibacterial activity of collagen-CNF composites

Zone of inhibition (ZOI) testing was used to characterize the antibacterial activity of all collagen-CNF composites (with or without digCHX, with or without gamma radiation treatment), against both *S. aureus* and *E. coli* in static conditions. The ones without digCHX do not exhibit any zone of inhibition after incubation, confirming that neither pure oxidized collagen nor collagen-CNF composites present antibacterial activity. However, as soon as digCHX was included in the composite preparation, significant zones of inhibition are detected for every sample. This is in accordance with literature when CNF structures where loaded with digCHX [18]. The most representative are shown on Figure III.27, where only irradiated samples are plotted. Overall, slightly larger zones of inhibition are obtained against *S. aureus*. It is a gram-positive bacterial strain that is known to be affected more easily by digCHX than gram-negative strains, such as *E. coli*. Regarding *S. aureus* results, the size of the inhibition zones is roughly the same, no matter the presence, type or quantity of added CNF.

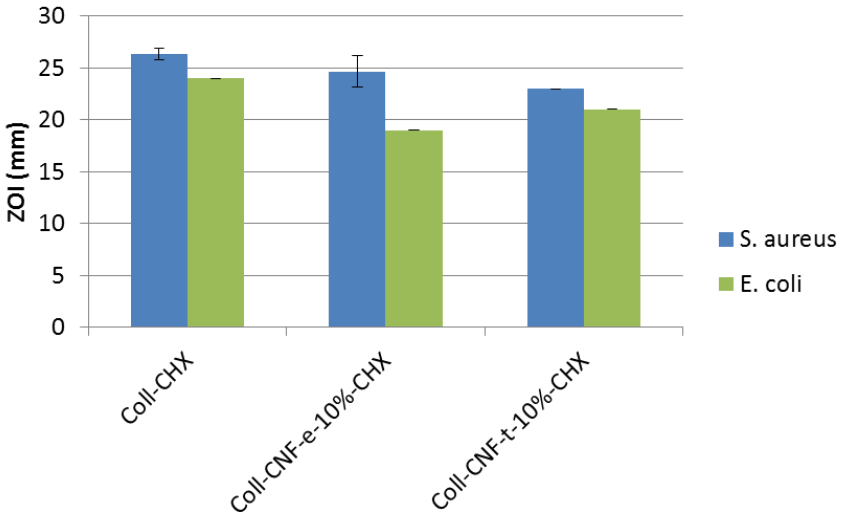

Figure III.27: Zone of inhibition testing against *S. aureus* and *E. coli* of collagen-CNF (10% CNF-e or CNF-t) composites loaded with 2 wt% chlorhexidine digluconate (digCHX) after gamma radiation

Concerning the gram-negative bacterial strains *E. coli*, smaller zones of inhibition are observed. The outer layer of gram negative bacteria is often composed of a lipo-polysaccharide barrier that is more difficult to penetrate for chlorhexidine. All the samples containing digCHX demonstrated significant zone of inhibitions against both gram-positive and gram-negative bacterial strains. The overall influence of gamma radiation is very low, which confirms that gamma radiation did not affect the digCHX molecules nor prevented their diffusion through the collagen-CNF composite structure, contrary to the previous study with metronidazole. This confirms that metronidazole is more sensitive to the radicals arising from the gamma radiation.

3.3.4. Drug release experiment

Chlorhexidine digluconate release experiments were also performed on every sample to assess the release profiles in dynamic conditions. In the absence of digCHX, release experiments confirmed that neither oxidized collagen nor CNF presented overlapping signals with chlorhexidine, when comparing to data collected for the calibration curve. It is worth noting that a release of 100% of the digCHX introduced is never achieved contrary to what was expected and observed in the literature for release in water [64]. Such difference is mainly due to digCHX interaction with PBS buffer ions. Indeed, it seems clear that positively charged chlorhexidine interacts with negatively charged phosphate ions. Some mixing tests of digCHX in PBS have confirmed this result when precipitate was observed. Moreover, the influence of gamma radiation on digCHX solution was investigated through liquid ^{13}C NMR. Surprisingly, this technique did not reveal any chemical change upon gamma radiation, as depicted on Figure III.28, confirming that the missing digCHX in drug release results cannot be attributed to potential degradation caused by radiation. Similarly, strong interaction of

digCHX with CNF might also explain that 100% of the drug is not released. Adsorption of digCHX onto CNF surface certainly prevents part of the drug to leach out the composite. Nevertheless, despite this analytical issue, the following drug release results can still be used for comparative analysis.

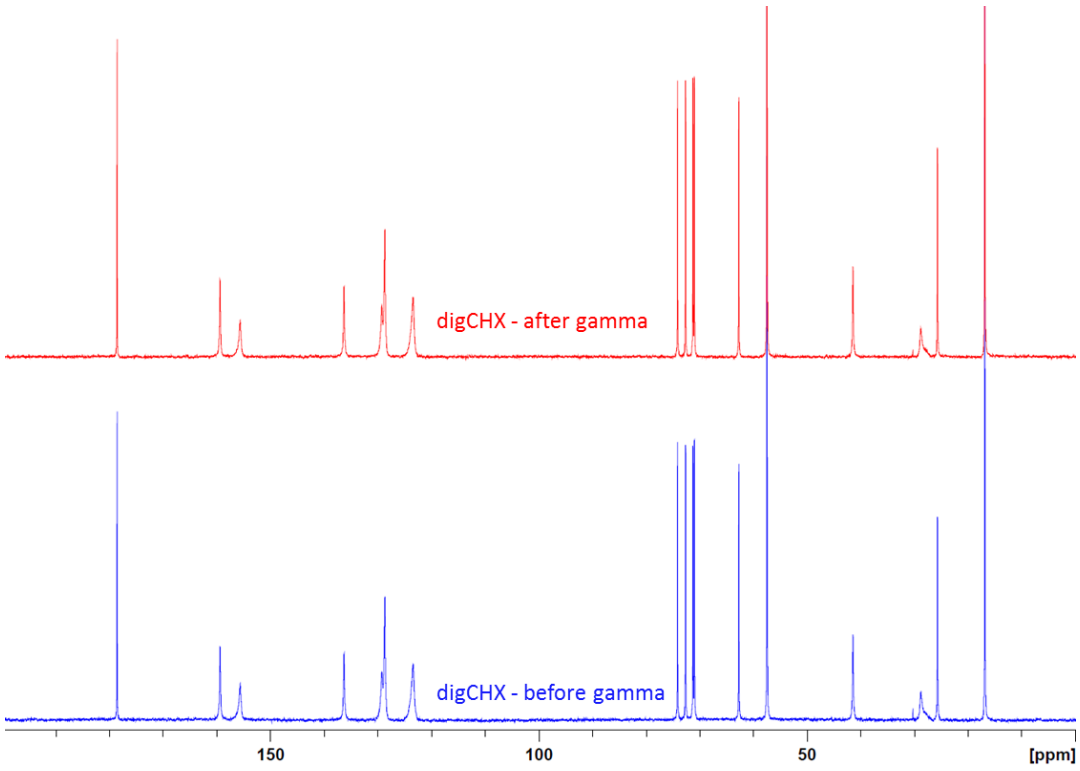

Figure III.28: Liquid ^{13}C NMR analysis of 20 wt% chlorhexidine digluconate solution, before and after gamma radiation treatment

The influence of CNF type was strong in terms of maximum amount of digCHX released, no matter the release technique. When partial renewal technique was used, for CNF-e loaded samples, 60% of the theoretical quantity of digCHX is released while CNF-t provide only 25% (Figure III.29a). The full renewal technique however, clearly increase the maximum release achieved: 75% is reached for CNF-e loaded samples and almost 50% for CNF-t (Figure III.29b). Also, the tendency of CNF-t to offer a sustained release after 80 hours with the partial renewal technique is confirmed with the full renewal technique. Indeed, during the composite preparation the pH was adjusted to 9, converting every carboxylic acid groups on CNF-t to anionic carboxylate groups. The positively charged digCHX molecule thus strongly interacts with CNF-t, which explain the prolonged release tendency despite the low amount of CNF-t.

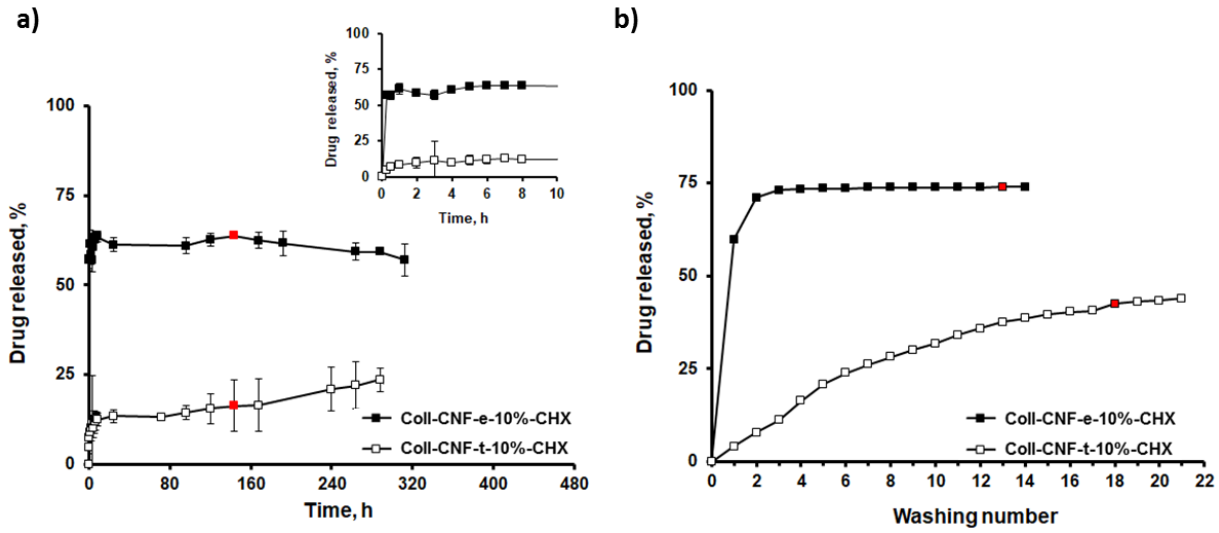

Figure III.29: Cumulative digCHX release experiments in PBS for Coll-CNF-e-10%-CHX and Coll-CNF-t-10%-CHX (no gamma radiation applied) with a) partial renewal of the medium (3 ml aliquots replaced by 3 ml of fresh PBS) and b) full renewal of the release medium

The red marks on the graphs indicate the disintegration of the composite inside the release medium. While it happens after the same duration of experiment for partial renewal technique (150 h), the full renewal technique gives a different result: CNF-t loaded composites are able to maintain their structure for a much longer time than CNF-e loaded ones. This might be explained by the absence of aggregates in CNF-t suspension compared to CNF-e, as observed with optical microscopy. The TEMPO-mediated oxidation of cellulose fibers allows for a better isolation of cellulose nanofibrils upon mechanical treatment. Moreover, the presence of high amount of carboxylic acid function on CNF-t might induce more interaction with oxidized collagen strands and limit the degradation. On the contrary, remaining microfibrils aggregates in CNF-e suspension could lead to defects in collagen-CNF-e composites, which are weak points resulting in structures that are more sensible to swelling during immersion, and leading to subsequent degradation.

The cumulative release of digCHX is presented in percentage of the theoretical quantity introduced during the composite preparation (*i.e.* 2 wt%). For release experiments, each samples had at least 3.8 mg of digCHX (30 cm^2 at 64 g/m^2). This quantity of active compound already proved to provide the composite with antibacterial activity through ZOI testing. In order to further confirm the activity of such materials, the above mentioned released digCHX quantities can be compared to minimal inhibitory concentration (MIC), the lowest concentration of a drug that inhibits the visible growth of an organism [65]. For digCHX, values ranging from 2 to 16 mg/l are commonly reported against *S. aureus* and *E. coli* [66], [67]. Both release techniques used 50 ml of PBS. For partial renewal technique, digCHX concentrations of 45 mg/l and 20 mg/l are reached with CNF-e and CNF-t loaded composites, respectively. These values are above the MICs proving the activity of the prepared

collagen-CNF-CHX composites in partial renewal drug release conditions. In the second technique, full renewal of the release medium is done. Thus, over the successive washing steps, the digCHX that was released from the composite is progressively removed. On Figure III.29b, the release profile obtained for Coll-CNF-e-10%-CHX reaches a plateau at almost 75% after 3 washing steps, indicating that the following steps do not retrieve more digCHX from the sample. Each volume of 50 ml that is put into contact with the sample after the third washing step does not contain any trace of digCHX. This confirms the loss of activity of the collagen-CNF-e sample after 3 washing steps since no more digCHX is released. However, in between each washing steps of the Coll-CNF-t-10%-CHX sample, the cumulative amount of digCHX increases by 1 to 3%. These small proportions of digCHX that are released at each washing step in the 50 ml PBS medium represent a concentration of 0.76 to 2.28 mg/l, which is in the range of the above mentioned MICs. This level of release is maintained until washing step n°15, after which the digCHX concentration is inferior to MICs values. It demonstrates the sustained antibacterial activity of Coll-CNF-t-10%-CHX samples.

The other CNF-e and CNF-t loadings offer very similar behavior. Although the different CNF-e loadings do not seem to significantly impact the release profiles of full renewal experiments, the tendency of CNF-t to provide sustained release is even improved with 20% CNF-t loaded samples (Figure III.30 a & b).

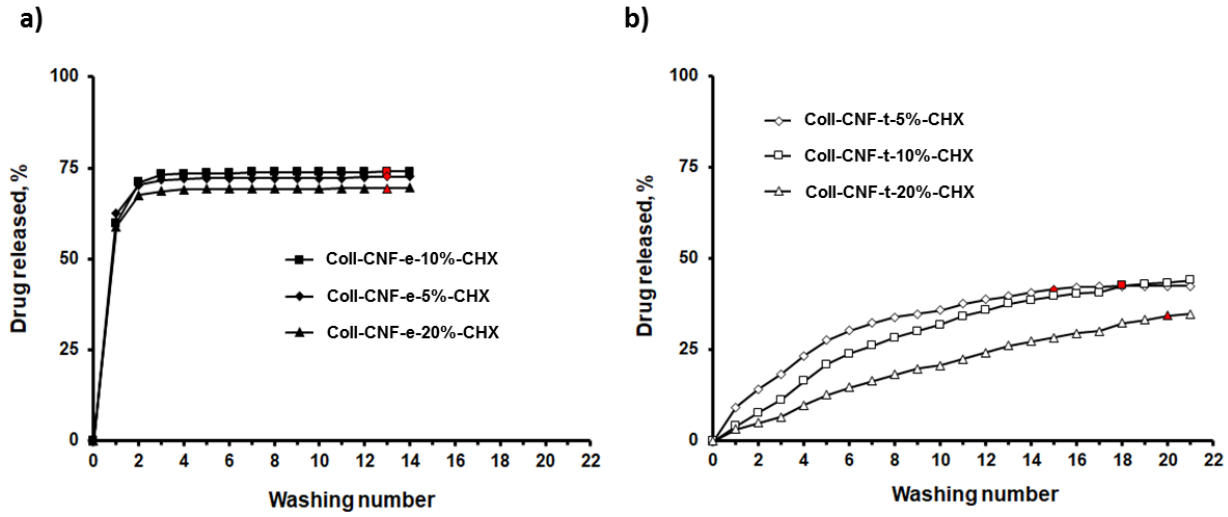

Figure III.30: Cumulative digCHX release experiments in PBS with full renewal of the release medium for non-irradiated samples, a) with CNF-e loading and b) CNF-t loading

While CNF-e loaded samples all reach almost 75% of maximum release within the same duration, CNF-t loaded samples present a slower release. Moreover, the more CNF-t, the more sustained the release profile appears to be, shifting from logarithmic to almost linear curve for 20% CNF-t loaded composites. Regarding the degradation of the sample, CNF-e loaded composite degrade after the

same duration, but with increasing CNF-t quantity the degradation of the sample is significantly delayed. This confirms again the better interaction of CNF-t with the oxidized collagen compared to CNF-e.

When gamma radiation is applied on collagen-CNF composites, the release of digCHX seems to be slightly hindered since a lower quantity is released for both types of drug release technique, with partial or full renewal of PBS medium (Figure III.31a & b). The tendency for other samples is mostly the same (not shown). Even if the difference is very low, gamma radiation could have affected the digCHX molecule, explaining the lower quantity. But antibacterial activity of the composites was proven to be unaffected by gamma radiation treatment (Figure III.27). Moreover, liquid ^{13}C NMR proved that digCHX was insignificantly affected by irradiation. Certainly, the gamma radiation favors the crosslinking of collagen based systems, as described in the introduction, and further limits the diffusion of digCHX in the oxidized collagen matrix. The late degradation of gamma irradiated Coll-CNF-t-10%-CHX sample in the partial renewal release technique confirms this hypothesis (Figure III.31a).

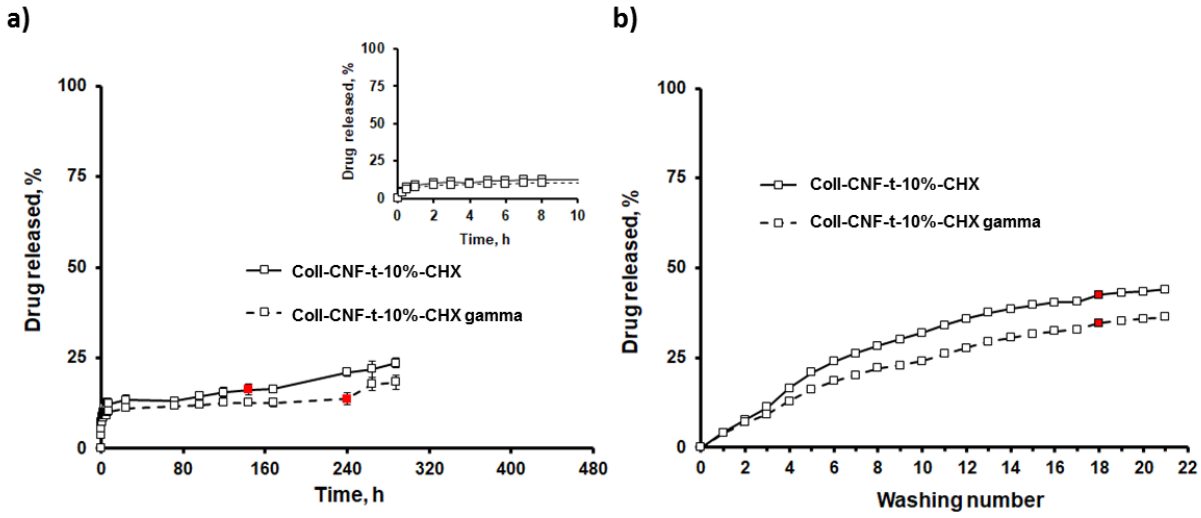

Figure III.31: Influence of gamma radiation on cumulative digCHX release from Coll-CNF-t-10%-CHX composites for a) partial renewal technique and b) full renewal technique

The lower release of digCHX can thus be explained by the concomitant action of anionic CNF-t and densification of collagen matrices upon gamma radiation. The gamma irradiated samples present a comparable sustained digCHX release profile, for both drug release techniques. Finally, similarly to the non-radiated sample, the activity of irradiated Coll-CNF-t-10%-CHX is confirmed for at least 15 washing steps thanks to the repeated release in each 50ml PBS volumes. The addition of a low amount of CNF-t strongly improves the drug release of these biocompatible collagen-CNF composites.

3.4 Conclusion

The effect of CNF addition and gamma radiation on collagen-CNF composites was described with water uptake measurements. CNF addition and irradiation tend to limit the water uptake of the composites. Gamma radiation also provides a more durable composite structure since chemical crosslinking is triggered. The concomitant action of CNF presence and gamma radiation-induced crosslinking requires complementary investigations to determine if CNF are also chemically involved in the collagen crosslinking. Still, such composite did not disperse in PBS medium even after several days (240 h). When digCHX was included in the formulation, antibacterial activity was demonstrated in static conditions (ZOI), even with gamma irradiated samples. The stability of digCHX molecule after irradiation was also confirmed by liquid ^{13}C NMR. Moreover, the release of the molecule was confirmed in dynamic conditions (*i.e.* under orbital shaking). Increased quantity of CNF led to slower sustained release that was further limited thanks to gamma radiation treatment. CNF-t is even more beneficial to extend the drug release. These composites thus appear like promising material for the design of active medical devices.

Conclusions of Chapter III

The aim of this chapter was to design CNF based substrates for medical device development, by exploiting the functionalized CNF prepared in Chapter II. Three different kinds of CNF substrates were prepared in order to obtain (i) 100% CNF membranes and (ii) & (iii) collagen-CNF composites.

In **chapter III-1**, thick and overdried CNF-e membranes with adsorbed/entrapped ciprofloxacin proved to be able to absorb more water and better resist the exposition to liquid medium. These membranes also demonstrated the most prolonged release in immersion and release chamber protocols. The antibacterial experiments were used to compare CNF-e membranes with bulk adsorbed ciprofloxacin (CNF-cip-ads) versus CNF-e membranes with surface grafted ciprofloxacin (CNF-cip-g). CNF-cip-g membranes presented better long term contact antibacterial activity. Covalent binding of molecule to CNF-e substrates appears like a promising strategy for the development of innovative topical application medical device.

The **chapter III-2** validated the "on-demand" controlled release of metronidazole from functionalized CNF suspensions upon enzymatic activity of carboxyl human esterase. These CNFs were embedded in collagen matrix to produce active composites. A prolonged activity against anaerobic *Bacteriodes fragilis* was detected upon successive zone of inhibition testing. The study clearly shows that collagen-CNF-metro composites are promising 2D structures for the design of active soft tissue repair model medical devices.

Finally, the **chapter III-3** assessed the influence of CNF type and proportion and gamma radiation of collagen-CNF composites on the release profiles of chlorhexidine. Increasing amounts of CNF-t strongly prolonged the release of the drug. The influence of sterilization upon gamma radiation was positive on water uptake of composites since it limited the degradation but its influence on the release and on the crosslinking requires further investigations. Still, these composites thus appear like promising material for the design of active medical devices.

List of tables

List of figures

Bibliography

[1] F. Rol, M. N. Belgacem, A. Gandini, and J. Bras, "Recent advances in surface-modified cellulose nanofibrils," *Progress in Polymer Science*, Sep. 2018.

[2] O. Nechyporchuk, M. N. Belgacem, and J. Bras, "Production of cellulose nanofibrils: A review of recent advances," *Industrial Crops and Products*, Apr. 2016.

[3] A. Dufresne, *Nanocellulose, From Nature to High Performance Tailored Materials*. Berlin, Boston: De Gruyter, 2017.

[4] K.-Y. Lee, *Nanocellulose and sustainability: production, properties, applications, and case studies*. 2018.

[5] D. Klemm *et al.*, "Nanocelluloses: A New Family of Nature-Based Materials," *Angew. Chem. Int. Ed.*, vol. 50, no. 24, pp. 5438–5466, Jun. 2011.

[6] H. Kargarzadeh *et al.*, "Advances in cellulose nanomaterials," *Cellulose*, vol. 25, no. 4, pp. 2151–2189, Feb. 2018.

[7] T. Abitbol *et al.*, "Nanocellulose, a tiny fiber with huge applications," *Current Opinion in Biotechnology*, vol. 39, pp. 76–88, Jun. 2016.

[8] R. Bardet and J. Bras, "Cellulose Nanofibers and Their Use in Paper Industry," in *Materials and Energy*, vol. 5, WORLD SCIENTIFIC, 2014, pp. 207–232.

[9] C. Aulin, M. Gällstedt, and T. Lindström, "Oxygen and oil barrier properties of microfibrillated cellulose films and coatings," *Cellulose*, vol. 17, no. 3, pp. 559–574, Jun. 2010.

[10] A. Dufresne, S. Thomas, and L. A. Pothan, *Biopolymer Nanocomposites: Processing, Properties, and Applications*. John Wiley & Sons, 2013.

[11] P. Bober *et al.*, "Biocomposites of Nanofibrillated Cellulose, Polypyrrole, and Silver Nanoparticles with Electroconductive and Antimicrobial Properties," *Biomacromolecules*, vol. 15, no. 10, pp. 3655–3663, Oct. 2014.

[12] F. Hoeng, A. Denneulin, and J. Bras, "Use of nanocellulose in printed electronics: a review," *Nanoscale*, vol. 8, no. 27, pp. 13131–13154, 2016.

[13] M. Jorfi and E. J. Foster, "Recent advances in nanocellulose for biomedical applications," *J. Appl. Polym. Sci.*, vol. 132, no. 14, p. n/a-n/a, 2014.

[14] N. Lin and A. Dufresne, "Nanocellulose in biomedicine: Current status and future prospect," *European Polymer Journal*, vol. 59, pp. 302–325, Oct. 2014.

[15] P. Laurén, "Biomedical applications of nanofibrillar cellulose (Ph.D. thesis)," 2018.

[16] R. Kolakovic, L. Peltonen, A. Laukkanen, J. Hirvonen, and T. Laaksonen, "Nanofibrillar cellulose films for controlled drug delivery," *European Journal of Pharmaceutics and Biopharmaceutics*, vol. 82, no. 2, pp. 308–315, Oct. 2012.

[17] N. Lavoine, I. Desloges, and J. Bras, "Microfibrillated cellulose coatings as new release systems for active packaging," *Carbohydrate polymers*, vol. 103, pp. 528–537, 2014.

[18] N. Lavoine, I. Desloges, C. Sillard, and J. Bras, "Controlled release and long-term antibacterial activity of chlorhexidine digluconate through the nanoporous network of microfibrillated cellulose," *Cellulose*, vol. 21, no. 6, pp. 4429–4442, Dec. 2014.

[19] N. Lavoine, V. Guillard, I. Desloges, N. Gontard, and J. Bras, "Active bio-based food-packaging: Diffusion and release of active substances through and from cellulose nanofiber coating toward food-packaging design," *Carbohydrate Polymers*, vol. 149, pp. 40–50, Sep. 2016.

[20] N. Lavoine, N. Tabary, I. Desloges, B. Martel, and J. Bras, "Controlled release of chlorhexidine digluconate using β-cyclodextrin and microfibrillated cellulose," *Colloids and Surfaces B: Biointerfaces*, vol. 121, pp. 196–205, 2014.

[21] P. C. Appelbaum and P. A. Hunter, "The fluoroquinolone antibacterials: past, present and future perspectives," *International Journal of Antimicrobial Agents*, vol. 16, no. 1, pp. 5–15, Sep. 2000.

[22] B. A. Herbold, S. Y. Brendler-Schwaab, and H. J. Ahr, "Ciprofloxacin: in vivo genotoxicity studies," *Mutation Research/Genetic Toxicology and Environmental Mutagenesis*, vol. 498, no. 1–2, pp. 193–205, Nov. 2001.

[23] S. Saini, N. Belgacem, J. Mendes, G. Elegir, and J. Bras, “Contact Antimicrobial Surface Obtained by Chemical Grafting of Microfibrillated Cellulose in Aqueous Solution Limiting Antibiotic Release,” *ACS Applied Materials & Interfaces*, vol. 7, no. 32, pp. 18076–18085, Aug. 2015.
[24] S. Saini, C. B. SILLARD, M. N. Belgacem, and J. Bras, “Nisin anchored cellulose nanofiber for long term antimicrobial active food packaging,” *RSC Advances*, 2016.
[25] S. Saini, M. N. Belgacem, M.-C. B. Salon, and J. Bras, “Non leaching biomimetic antimicrobial surfaces via surface functionalisation of cellulose nanofibers with aminosilane,” *Cellulose*, pp. 1–16, 2016.
[26] M. Smyth, C. Fournier, C. Driemeier, C. Picart, E. J. Foster, and J. Bras, “Tunable Structural and Mechanical Properties of Cellulose Nanofiber Substrates in Aqueous Conditions for Stem Cell Culture,” *Biomacromolecules*, vol. 18, no. 7, pp. 2034–2044, Jul. 2017.
[27] M. Henriksson, L. A. Berglund, P. Isaksson, T. Lindström, and T. Nishino, “Cellulose Nanopaper Structures of High Toughness,” *Biomacromolecules*, vol. 9, no. 6, pp. 1579–1585, Jun. 2008.
[28] A. Basu, J. Lindh, E. Ålander, M. Strømme, and N. Ferraz, “On the use of ion-crosslinked nanocellulose hydrogels for wound healing solutions: Physicochemical properties and application-oriented biocompatibility studies,” *Carbohydrate Polymers*, vol. 174, no. Supplement C, pp. 299–308, Oct. 2017.
[29] M. Sukul, R. D. Ventura, S. H. Bae, H. J. Choi, S. Y. Lee, and B. T. Lee, “Plant-derived oxidized nanofibrillar cellulose-chitosan composite as an absorbable hemostat,” *Materials Letters*, vol. 197, pp. 150–155, Jun. 2017.
[30] M. Smyth, “Nanocellulose based materials for Cell Culture,” phdthesis, Université Grenoble Alpes, 2017.
[31] P. N. Markham, “Inhibition of the Emergence of Ciprofloxacin Resistance in Streptococcus pneumoniae by the Multidrug Efflux Inhibitor Reserpine,” p. 2, 1999.
[32] D. C. Hooper and J. F. Wolfson, “Fluoroquinolone Antimicrobial Agents,” *THE NEW ENGLAND JOURNAL OF MEDICINE*, p. 11, 1991.
[33] G. Dow, A. Browne, and R. G. Sibbald, “Infection in chronic wounds: controversies in diagnosis and treatment.,” *Ostomy Wound Manage*, vol. 45, no. 8, pp. 23–7, 29–40; quiz 41–2, Aug. 1999.
[34] E. Wassenaar, E. Schoenmaeckers, J. Raymakers, J. van der Palen, and S. Rakic, “Mesh-fixation method and pain and quality of life after laparoscopic ventral or incisional hernia repair: a randomized trial of three fixation techniques,” *Surg Endosc*, vol. 24, no. 6, pp. 1296–1302, Jun. 2010.
[35] C. F. Bellows, A. Alder, and W. S. Helton, “Abdominal wall reconstruction using biological tissue grafts: present status and future opportunities,” *Expert Review of Medical Devices*, vol. 3, no. 5, pp. 657–675, Sep. 2006.
[36] N. J. Smart and S. Bloor, “Durability of Biologic Implants for Use in Hernia Repair: A Review,” *Surg Innov*, vol. 19, no. 3, pp. 221–229, Sep. 2012.
[37] F. M. Shaikh, S. K. Giri, S. Durrani, D. Waldron, and P. A. Grace, “Experience with Porcine Acellular Dermal Collagen Implant in One-stage Tension-free Reconstruction of Acute and Chronic Abdominal Wall Defects,” *World J Surg*, vol. 31, no. 10, pp. 1966–1972, Oct. 2007.
[38] P. Bhanot, K. S. King, and F. P. Albino, “Biologic mesh for abdominal wall reconstruction,” *Chronic Wound Care Management and Research*, p. 57, Nov. 2014.
[39] Y. Bayon, P. Gravagna, and J.-L. Tayot, “Method for preparing two-layer bicomposite collagen material for preventing post-operative adhesions,” US6596304B1, 22-Jul-2003.
[40] S. Saska *et al.*, “Bacterial cellulose-collagen nanocomposite for bone tissue engineering,” *Journal of Materials Chemistry*, vol. 22, no. 41, pp. 22102–22112, 2012.
[41] T. W. J. Steele *et al.*, “Collagen–cellulose composite thin films that mimic soft-tissue and allow stem-cell orientation,” *J Mater Sci: Mater Med*, vol. 24, no. 8, pp. 2013–2027, May 2013.
[42] A. P. Mathew, K. Oksman, D. Pierron, and M.-F. Harmad, “Crosslinked fibrous composites based on cellulose nanofibers and collagen with in situ pH induced fibrillation,” *Cellulose*, vol. 19, no. 1, pp. 139–150, Feb. 2012.

[43] A. P. Mathew, K. Oksman, D. Pierron, and M.-F. Harmand, "Biocompatible Fibrous Networks of Cellulose Nanofibres and Collagen Crosslinked Using Genipin: Potential as Artificial Ligament/Tendons," *Macromol. Biosci.*, vol. 13, no. 3, pp. 289–298, Mar. 2013.
[44] Y. Dong, H. Paukkonen, W. Fang, E. Kontturi, T. Laaksonen, and P. Laaksonen, "Entangled and colloidally stable microcrystalline cellulose matrices in controlled drug release," *International Journal of Pharmaceutics*, vol. 548, no. 1, pp. 113–119, Sep. 2018.
[45] H. Paukkonen *et al.*, "Nanofibrillar cellulose hydrogels and reconstructed hydrogels as matrices for controlled drug release," *International Journal of Pharmaceutics*, vol. 532, no. 1, pp. 269–280, Oct. 2017.
[46] P. Medhi *et al.*, "Lidocaine-loaded fish scale-nanocellulose biopolymer composite microneedles," *AAPS PharmSciTech*, vol. 18, no. 5, pp. 1488–1494, Jul. 2017.
[47] P. P. Poulet, D. Duffaut, and J. P. Lodter, "Metronidazole susceptibility testing of anaerobic bacteria associated with periodontal disease," *J. Clin. Periodontol.*, vol. 26, no. 4, pp. 261–263, Apr. 1999.
[48] J. Wüst, "Susceptibility of Anaerobic Bacteria to Metronidazole, Ornidazole, and Tinidazole and Routine Susceptibility Testing by Standardized Methods," *Antimicrob Agents Chemother*, vol. 11, no. 4, pp. 631–637, Apr. 1977.
[49] T. Saito, Y. Nishiyama, J.-L. Putaux, M. Vignon, and A. Isogai, "Homogeneous Suspensions of Individualized Microfibrils from TEMPO-Catalyzed Oxidation of Native Cellulose," *Biomacromolecules*, vol. 7, no. 6, pp. 1687–1691, Jun. 2006.
[50] A. Isogai, T. Saito, and H. Fukuzumi, "TEMPO-oxidized cellulose nanofibers," *Nanoscale*, vol. 3, no. 1, pp. 71–85, 2011.
[51] F. Cataldo, O. Ursini, E. Lilla, and G. Angelini, "Radiation-induced crosslinking of collagen gelatin into a stable hydrogel," *J Radioanal Nucl Chem*, vol. 275, no. 1, pp. 125–131, Jan. 2008.
[52] Y. Zhang, X. Zhang, L. Xu, S. Wei, and M. Zhai, "Radiation cross-linked collagen/dextran dermal scaffolds: effects of dextran on cross-linking and degradation," *Journal of Biomaterials Science, Polymer Edition*, vol. 26, no. 3, pp. 162–180, Feb. 2015.
[53] N. A. Hoenich, "Cellulose for Medical Applications: Past, Present, and Future," *BioResources*, vol. 1, no. 2, pp. 270–280, Aug. 2007.
[54] T. Shibata, "Chapter 3:Cellulose and Its Derivatives in Medical Use," in *Renewable Resources for Functional Polymers and Biomaterials*, 2011, pp. 48–87.
[55] A. F. Turbak, F. W. Snyder, and K. R. Sandberg, "Microfibrillated cellulose, a new cellulose product: properties, uses, and commercial potential," *J. Appl. Polym. Sci.: Appl. Polym. Symp.; (United States)*, vol. 37, Jan. 1982.
[56] F. W. Herrick, R. L. Casebier, J. K. Hamilton, and K. R. Sandberg, "Microfibrillated cellulose: morphology and accessibility," *J. Appl. Polym. Sci.: Appl. Polym. Symp.; (United States)*, vol. 37, Jan. 1982.
[57] S. Boufi, I. González, M. Delgado-Aguilar, Q. Tarrès, M. À. Pèlach, and P. Mutjé, "Nanofibrillated cellulose as an additive in papermaking process: A review," *Carbohydrate Polymers*, vol. 154, pp. 151–166, Dec. 2016.
[58] D. T. Cheung, N. Perelman, D. Tong, and M. E. Nimni, "The effect of γ-irradiation on collagen molecules, isolated α-chains, and crosslinked native fibers," *Journal of Biomedical Materials Research*, vol. 24, no. 5, pp. 581–589, May 1990.
[59] J. H. Bowes and J. A. Moss, "The Effect of Gamma Radiation on Collagen," *Radiation Research*, vol. 16, no. 3, p. 211, Mar. 1962.
[60] M. A. Khan, N. Rahman, and M. Rahman, "Preparation and Characterization of Gamma Radiation Cured Gelatin-PVA Bio-Blend," *Advanced Materials Research*, vol. 123–125, pp. 347–350, Aug. 2010.
[61] H. Kargarzadeh *et al.*, "Recent developments in nanocellulose-based biodegradable polymers, thermoplastic polymers, and porous nanocomposites," *Progress in Polymer Science*, vol. 87, pp. 197–227, Dec. 2018.

[62] C. Zhijiang and Y. Guang, “Bacterial cellulose/collagen composite: Characterization and first evaluation of cytocompatibility,” *Journal of Applied Polymer Science*, vol. 120, no. 5, pp. 2938–2944, Jun. 2011.
[63] M. Sukul, Y.-K. Min, S.-Y. Lee, and B.-T. Lee, “Osteogenic potential of simvastatin loaded gelatin-nanofibrillar cellulose-β tricalcium phosphate hydrogel scaffold in critical-sized rat calvarial defect,” *European Polymer Journal*, vol. 73, pp. 308–323, Dec. 2015.
[64] N. Lavoine, N. Tabary, I. Desloges, B. Martel, and J. Bras, “Controlled release of chlorhexidine digluconate using β-cyclodextrin and microfibrillated cellulose,” *Colloids and Surfaces B: Biointerfaces*, vol. 121, pp. 196–205, Sep. 2014.
[65] J. M. Andrews, “Determination of minimum inhibitory concentrations,” *J Antimicrob Chemother*, vol. 48, no. suppl_1, pp. 5–16, Jul. 2001.
[66] T. J. Karpanen, T. Worthington, E. R. Hendry, B. R. Conway, and P. A. Lambert, “Antimicrobial efficacy of chlorhexidine digluconate alone and in combination with eucalyptus oil, tea tree oil and thymol against planktonic and biofilm cultures of Staphylococcus epidermidis,” *J Antimicrob Chemother*, vol. 62, no. 5, pp. 1031–1036, Nov. 2008.
[67] T. Koburger, N.-O. Hübner, M. Braun, J. Siebert, and A. Kramer, “Standardized comparison of antiseptic efficacy of triclosan, PVP–iodine, octenidine dihydrochloride, polyhexanide and chlorhexidine digluconate,” *J Antimicrob Chemother*, vol. 65, no. 8, pp. 1712–1719, Aug. 2010.

General conclusions

&

Perspectives

General conclusions & perspectives

This Ph.D. work investigated the functionalization of cellulose nanofibrils (CNF) with active molecules in order to develop innovative model medical devices. Bio-active structures of 100% CNF films and collagen-CNF composites were designed to address remaining clinical needs such as wound bed infections after accidents or surgery.

Indeed, **chapter I** described how biobased polymers, like cellulose or collagen, can be used as biomaterials. They have inherent biocompatibility and can assemble in structures that mimic the natural extra-cellular matrix. Particularly, cellulose nanofibrils have a strong potential for medical application since they present widespread availability, numerous 2D and 3D organized structures with high specific surface area and enhanced tunability. Actually, CNF can be modified to further improve their functionalities. The review of functionalization techniques evidenced the high versatility of such material and the possibility to modify it for conferring a bio-activity, by using water based methods and thus avoiding environmental concerns. So, the literature review confirmed the large window for CNF applications in the biomedical field. To support this conclusion, it can be worth mentioning that over the Ph.D. project timeline, the emerging literature associated with the use of CNF for medical application has largely increased as illustrated on Table 1.

Table 1: Literature evolution over the Ph.D. projet

Topic	Beginning - January 2016		End - January 2019	
	Publications	*Patents*	*Publications*	*Patents*
CNF	2700	326	4100 *(x1.5)*	520 *(x1.6)*
CNF + medical	32	22	65 *(x2)*	37 *(x1.7)*
CNF + functionalization	214	16	420 *(x2)*	22 *(x1.4)*

Thus, the immobilization of drugs was investigated in **chapter II**. The single step water based esterification procedure applied to CNF films resulted in a device with prolonged antibacterial effect. For modifying CNF aqueous suspensions with prodrugs, more complex procedures were required. In these cases, first, CNF were provided with a reactive function to enable a new efficient chemistry (instead of –OH or –COOH reactions) for grafting the drug. Then, modified CNF were made to react with a prodrug. The latter is a drug modified for adding a cleavable function that allows triggering the “on-demand”

release in a specific medium (namely an ester to release the molecule at an infection site, where human esterase concentration increases). Within this approach, pending alkyne and furan functions were attached to CNF surface through amidation for subsequent binding with prodrugs by click chemistry reactions, respectively thiol-yne and Diels Alder.

Such strategies are rarely reported in the literature and, to our knowledge, were successfully used for the first time to bind active principle ingredients to CNF. This positive result was confirmed by the possibility to access a high technology DNP-NMR technique, which allowed detecting very low amounts of substances. Actually, in some cases, classical characterization tools (FTIR, standard NMR,…) did not reveal the presence of the immobilized molecules, in agreement with the low quantities added for technical-economic reasons (and therapeutic needs) and with the generally low yield for reactions in heterogeneous medium (dissolved molecules were added to CNF suspensions). Thus, even if in some cases it is still difficult to conclude on the nature of the drug-CNF linkage, the presence of the drug onto CNF was definitively proved.

Finally, these modified CNF were used to develop model active devices in **chapter III**. First, 100% CNF substrates containing ciprofloxacin were prepared: a first series with unreacted ciprofloxacin and a second one where ciprofloxacin was made to react with CNF. With the first approach, sustained release was achieved, especially with thick and overdried films. However, when analyzing the ciprofloxacin grafted CNF films, a better antibacterial activity with a prolonged contact active effect was detected, confirming the interest of the covalent immobilization strategy. This material has potential for being used in topical applications. Secondly, composites of collagen and CNF-metronidazole were successfully produced. Modified CNF suspensions were embedded in collagen matrix and proved to be active against anaerobic bacteria, confirming their potential use in soft-tissue repair application, where collagen based materials are already used but without an anti-infectious function. Neat CNF suspensions were also mixed with collagen solution and chlorhexidine digluconate to produce composites and further study the influence of CNF type and quantity on drug release. Addition of CNF-t resulted in prolonged release compared to CNF-e. These collagen-CNF composites can be used for external application on complex wound environments.

During the work performed, another aspect, not clearly identified at the beginning of the thesis, was pointed-out. Actually, in many cases, once prepared, medical devices undergo a sterilization procedure, more and more often through gamma radiation. In the case of collagen, the gamma-rays also play an active role on the structure, by inducing a chemical crosslinking that leads to a better dimensional

stability and a reduction of the water up-take. The addition of CNF further decreased the water uptake suggesting the densification of the inner structure of the composite. Unfortunately, with metronidazole, gamma irradiation negatively affected the antibacterial activity, but this was not the case with the chlorhexidine. With this latter active principle ingredient, CNF even helped to control and extend the release in physiological medium. The main results of this Ph.D. work are summarized in Table 2.

Table 2: Main results of this Ph.D. work

Scientific challenges			Key results
Immobilization of drug	on CNF-e films	→	Ciprofloxacin is immobilzed on CNF films through esterification
	on CNF-t suspensions, *step 1*	→	Efficient **amidation** was confirmed on CNF-t suspensions and provides: > alkyne functions > furan functions
	on CNF-t suspensions, *step 2*	→	Successful **click chemistry** was confirmed on modified CNF suspensions with: > thiol-metronidazole prodrug (thiol-yne) > maleimide-metronidazole prodrug (Diels Alder)
Antibacterial activity	CN-e films	→	Ciprofloxacin modified CNF-e films show prolonged antibacterial activity
	collagen-CNF composites	→	Composites with metronidazole modified CNF are active against anaerobic bacteria (gram+/gram-)
		→	Composites with chlorhexidine show activity with and without gamma radiation treatment
Drug release experiments	From CNF films	→	Overdried thick CNF films demonstrate better prolonged release of ciprofloxacin
	From modified CNF suspension	→	**"On-demand" enzyme triggered release** of metronidazole is achieved for prodrug modified CNF suspension
	From collagen-CNF composites	→	Increased amounts of CNF-t allow for more prolonged release than CNF-e

Nevertheless, further work would be required to further study these scientific challenges. Regarding immobilization strategies, the investigation of alternative coupling agents for the first step amidation reactions could help to further improve the conversion of carboxylic groups to amide, and the final amount of available API after the click chemistry reactions. The organic triazine 4-(4,6-dimethoxy-1,3,5-triazin-2-yl)-4-methyl-morpholinium chloride (DMTMM) is able to activate carboxylic groups in one step while EDC and NHS needs two. The second and third scientific challenges cover the characterization of

the antibacterial activity and drug release of the prepared samples. Within these topics, the development of CNF films with API that are grafted, adsorbed and complexed (*i.e.* in cyclodextrins for instance) at the same time, could bring a multi-profile drug release, combined with long term antibacterial activity. Complementary perspectives are described in Table 3.

Table 3: Main perspectives of this Ph.D. work

Scientific challenges			Perspectives
Immobilization of drug	on CNF-e films	→	Immobilize other types of API with the same chemical route
	on CNF-t suspensions, *step 1*	→	Keep optimizing coupling agents use and compare with DMTMM (1 molecule vs 2 with EDC/NHS)
	on CNF-t suspensions, *step 2*	→	Further study the influence of the solvent for the prodrug, the reaction time, UV exposure and temperature on click chemistries
Antibacterial activity	CNF-e films	→	Measure the antibacterial activity of CNF films with adsorbed, grafted and complexed APIs (cyclodextrins) at the same time
	collagen-CNF composites	→	Characterize industrial demonstrator of soft-tissue repair (STR) or patch devices *in-vivo*, Control the interaction of CNF with polyester textile that are currently used with collagen in STR
Drug release experiments	from CNF films	→	Measure the release profiles of CNF films with adsorbed, grafted and complexed APIs (cyclodextrins) at the same time Investigate the possible synergy of different APIs included in the same CNF film
	from modified CNF suspension	→	Improve release conditions with esterase and launch *in-vivo* testing with modified CNF suspension first
	From collagen-CNF composites	→	Further investigate the interaction of digCHX with CNF-t that resulted in prolonged release

Apart from these scientific challenges, further knowledge is required on the topic of the biodegradation of CNF *in-vivo*. When CNF are embedded in a medical device intended for internal application, an investigation of the elimination or degradation processes of the CNF inside the human body must be carried out to avoid complications, which would negate CNF beneficial effects.

To conclude, results obtained show that it is possible to prepare CNF based efficient bio-active materials through “green” water based reactions. Different strategies and active principles are proposed, enabling a selection according to the final application and the industrial implementation.

This Ph.D. work is believed to improve the field of cellulose nanofibrils functionalization by investigating water based innovative binding techniques. Also, this work gives insights on the potential use of such enhanced CNF systems for medical application, paving the way for better treatments.

Extended French Abstract

Résumé Français

Résumé Français

Au travers de perpétuelles innovations dans le domaine de la santé, l'espérance de vie a globalement augmenté au cours de ce dernier siècle. Cependant, alors que les plus graves maladies du passé sont aujourd'hui traitées avec succès, ce sont les infections et effets secondaires liés aux traitements actuels qui posent parfois problèmes. Ces complications peuvent entraîner de nouvelles interventions chirurgicales et représentent un coût médico-social conséquent. Ainsi, le développement de dispositifs médicaux bioactifs capables de pallier à ces problèmes promet d'améliorer le confort et la convalescence des patients. Afin d'atteindre un tel objectif, il paraît nécessaire de disposer de biomatériaux innovants offrant de nouvelles fonctionnalités, notamment antibactériennes ou anti-inflammatoires.

Les biomatériaux regroupent les céramiques, les métaux et les polymères qui sont destinés à être mis en contact avec des tissus vivants, des organismes et des micro-organismes [1]. Les céramiques et les métaux ont été traditionnellement utilisés pour la réparation dentaire ou osseuse, puisqu'ils présentent un bonne biocompatibilité et des formes lisses [2]. Néanmoins, ils sont de plus en plus remplacés par des polymères issus de ressources fossiles. En effet, ces matières offrent une meilleur flexibilité et des températures de mise en forme plus faibles, qui donnent accès au design de structures complexes [3]. Cependant, la présence de produits contaminants comme des résidus de plastifiants, peut mener à une réponse inflammatoire potentiellement indésirable. Une alternative possible consiste à s'orienter vers l'utilisation de polymères naturels issus de la biomasse, qui présentent souvent une biocompatibilité intrinsèque, et qui ont l'avantage supplémentaire de remplacer des matériaux pétro-sourcés, dans le contexte de raréfaction des ressources fossiles. Ainsi, la chitine, la cellulose ou encore le collagène connaissent un fort engouement dans le domaine des biomatériaux, comme l'indiquent plusieurs revues récentes sur le sujet [4]–[6].

Dans ce contexte, les nanocelluloses représentent une excellente alternative en tant que biomatériau. Ce terme désigne des particules de cellulose qui présentent une dimension inférieure à 100 nanomètres. Deux types de nanocellulose sont généralement utilisés : les nanofibrilles de cellulose (CNF) et les nanocrystaux de cellulose (CNC). Les nanocelluloses sont aujourd'hui extraites principalement du bois, à l'échelle pilote et industrielle (Figure 1). D'autres sources sont possibles comme les plantes annuelles, certaines espèces animales et les micro-organismes, mais l'industrialisation de ces procédés est encore très limitée.

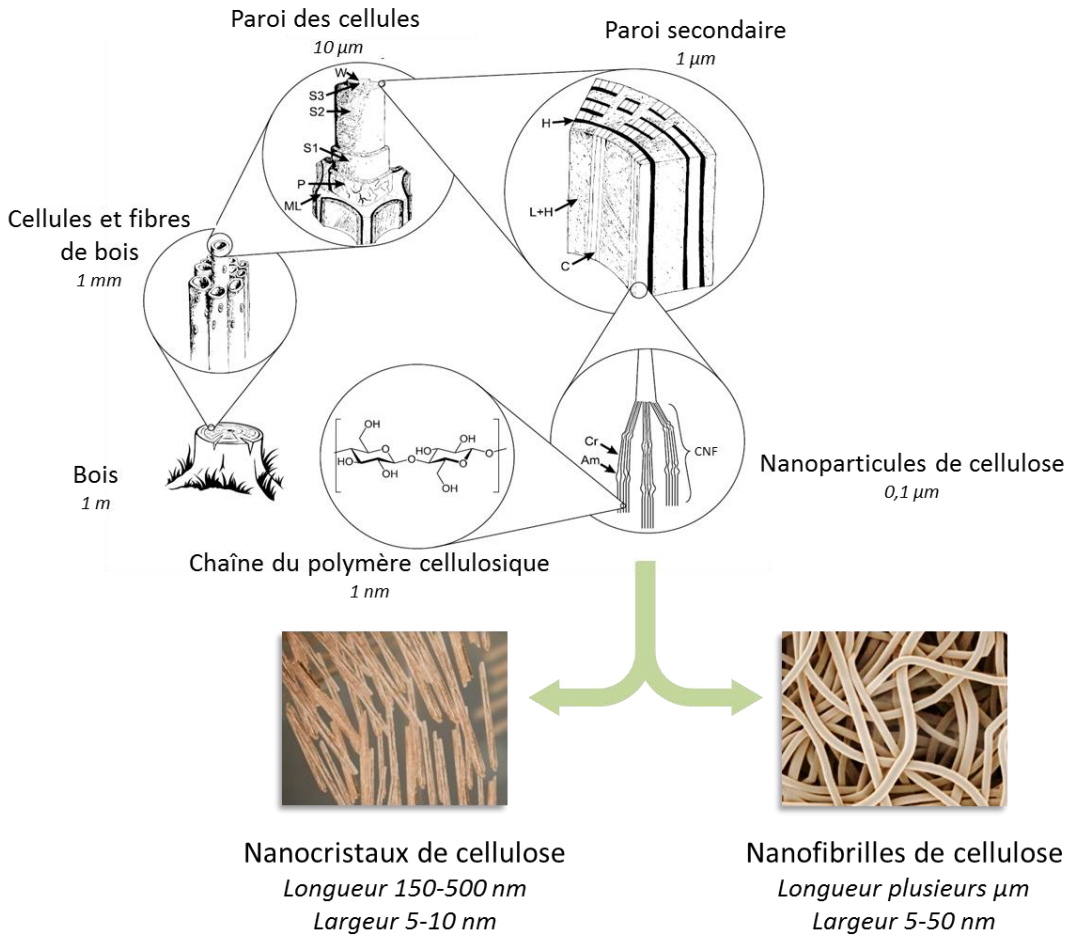

Figure 1: Du bois aux nanocellulose

Une combinaison de propriétés inédites (caractère renouvelable, biodégradabilité, grande disponibilité géographique, faible densité et excellente propriétés mécaniques) confère aux nanocellulose, depuis quelques décennies maintenant, un engouement puissant au sein de la communauté scientifique. En effet, une augmentation exponentielle du nombre de publications scientifique sur le sujet est constatée depuis le début des années 2000. Quand alors seulement quelques dizaines de publication paraissaient chaque année, c'est aujourd'hui 2 à 3 publications par jour. Cet engouement ne se cantonne pas seulement à la recherche académique puisqu'une tendance similaire est constatée pour le rythme de dépôt de brevet, qui atteint à présent un brevet par jour. Ceci démontre le fort intérêt des industriels pour ce nouveau matériau et confirme son futur développement dans des applications aussi variées que le papier et l'emballage, le bâtiment, l'environnement, les matériaux composites et plus récemment, le biomédical.

Depuis les premiers travaux relatant la découverte des nanofibrilles de cellulose (CNF) dans les années 1980 [7], [8], les procédés de production ont été améliorés et optimisés. Les prétraitements tels que l'oxydation TEMPO ou le recours aux enzymes ont permis de réduire la consommation énergétique nécessaire à la production des CNF et ont ouvert la voie à une industrialisation plus rapide que pour les CNC. De plus, de nombreux travaux de recherche ont prouvés la biocompatibilité des CNF. Par exemple, la prolifération des cellules ainsi que leur migration au contact des CNF ont été démontrées [9], [10]. Par ailleurs, leurs modifications chimiques de surface combinées à leur très grande surface spécifique offrent de nombreuses possibilités de fonctionnalisation. Des CNF bioactives peuvent être obtenues par adsorption ou immobilisation covalente de molécules d'intérêt. Par exemple, la pénicilline a déjà été immobilisée de manière covalente sur les CNF pour former un film antibactérien par contact [11]. De plus, les CNF peuvent être organisées en différentes structures 2D ou 3D par des méthodes de filtrations, de casting ou de lyophilisation. Ceci offre un large éventail de possibilités pour des applications biomédicales que plusieurs revues ont synthétisées [12]–[14].

Par conséquent, un consortium de plusieurs partenaires issus du monde de la recherche académique et industrielle a été formé afin d'étudier et de développer l'utilisation des CNF dans le domaine du biomédical. Cette collaboration est née au sein du projet CELLICAL qui est financé par l'Agence Nationale de la Recherche (ANR-15-CE08-0033) et qui a débuté en Janvier 2016. Le travail de thèse a été effectué dans le cadre du projet CELLICAL et s'attache à étudier les aspects suivants :

i. La fonctionnalisation de surface des nanofibrilles de cellulose (CNF) avec des molécules actives
ii. La préparation de structures 100% CNF ainsi que de composite avec les CNF
iii. L'étude des propriétés de relargage et de l'activité antibactérienne des structures à base de CNF

Ainsi, ce travail de thèse a été mené dans un contexte très dynamique. De nombreuses interactions ont eu lieu avec les experts de la production et fonctionnalisation des nanocelluloses (LGP2, CTP, TEMBEC Rayonier group et la start-up InoFib), avec les experts des glyco-conjugués (CERMAV), ceux du design des drogues et prodrogues (DPM) ainsi que ceux de l'étude et de la modélisation du relargage (INSERM). Le leader mondial des dispositifs médicaux (Medtronic) a également apporté son savoir-faire et son expérience tout au long du projet. Des expériences et caractérisations ont été réalisées dans les laboratoires de chacun des partenaires, confirmant la richesse pluridisciplinaire de ces travaux, dont l'organisation est présentée sur la Figure 2. Le **premier chapitre** décrit l'état de l'art qui concerne les matériaux bio-sourcés pour application biomédical en détaillant les éléments déjà mentionnés au début de ce résumé.

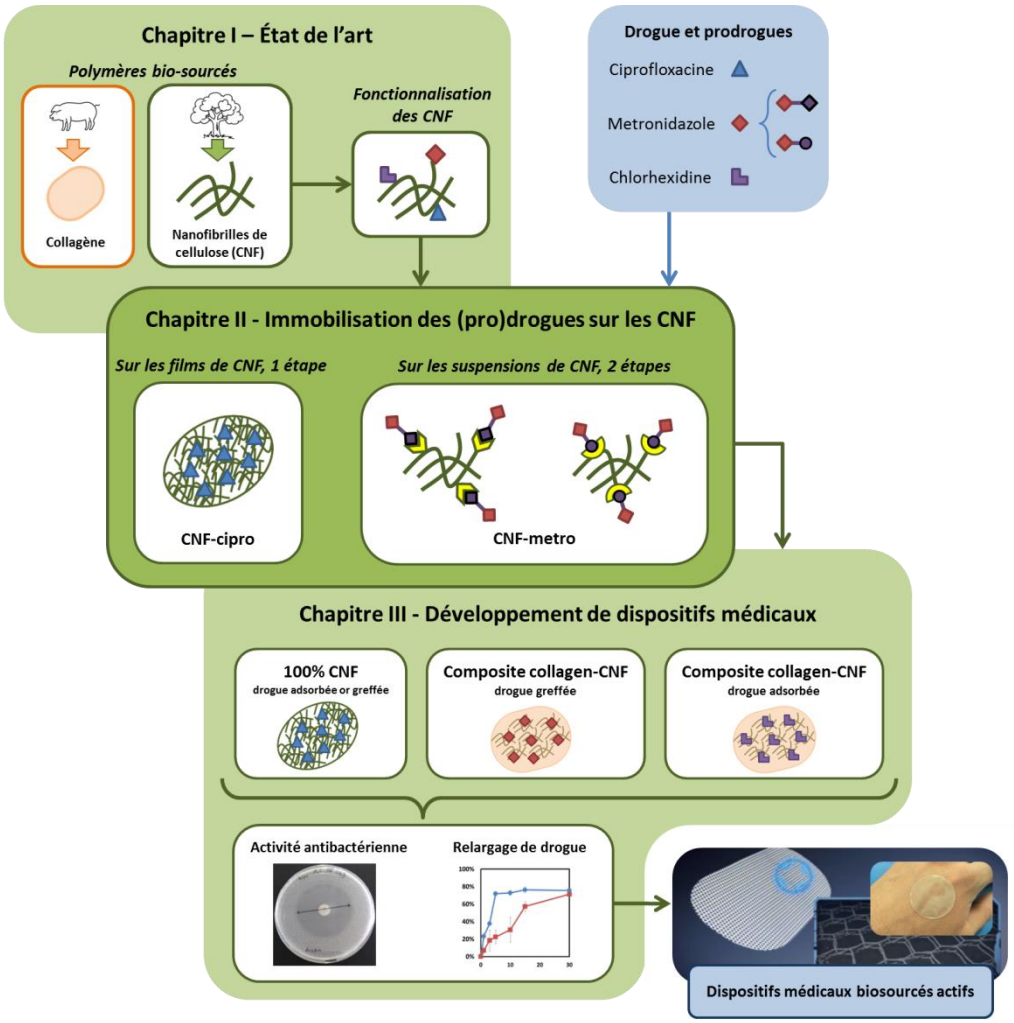

Figure 2: Représentation graphique de l'organisation du projet

Dans le **second chapitre**, les stratégies de fonctionnalisation des CNF sont exposées. La première partie décrit la modification de surface de films de CNF produites par prétraitement enzymatique (CNF-e). La ciprofloxacine, un antibiotique à large spectre, est immobilisée de manière covalente par estérification après une mise en contact en phase aqueuse. Le succès du greffage est confirmé par l'analyse élémentaire ainsi que des tests d'activité antibactérienne. Il est également démontré que ce film modifié présente une activité antimicrobienne prolongée, confirmant sa potentielle utilisation pour le développement d'un patch pour application externe (*publication scientifique n°1*, cf. Figure 3a).

La seconde partie décrit l'utilisation d'une procédure de modification de suspension de CNF produites grâce au prétraitement par oxydation TEMPO (CNF-t). Cette seconde stratégie est plus complexe puisqu'elle se déroule en deux étapes. La première consiste à modifier la surface des CNF-t avec des fonctions alcynes par amidation à l'aide des agents de couplage EDC/NHS, toujours en phase aqueuse.

Cette étape est confirmée, entre autre, par spectroscopie Raman et résonance magnétique nucléaire (RMN) du solide. Ensuite, ces fonctions alcynes sont exploitées en chimie click (thiol-yne) par réaction avec un principe actif thiolé, la prodrogue, contenant aussi une fonction ester. (Figure 3b). Le principe actif utilisé est la métronidazole, un antibactérien actif contre les micro-organismes anaérobies. Une nouvelle technique de caractérisation très puissante, la RMN dopée par Polarisation Nucléaire Dynamique (RMN-DNP), est utilisée pour la première fois sur les nanocelluloses et permet de confirmer le succès de la procédure (*publication scientifique n°2*). Enfin, la dernière partie de ce chapitre II présente une stratégie similaire à la précédente. Dans un premier temps, ce sont des fonctions furane qui sont alors immobilisées sur les CNF-t, pour ensuite réagir avec la prodrogue de métronidazole, cette fois-ci modifié avec une fonction maléimide (Figure 3b). La réaction chimique de Diels Alder est ainsi activée entre les deux composés et les mêmes outils de caractérisation démontrent le succès de cette troisième procédure (*publication scientifique n°3*). Ces prodrogues sont censées pouvoir libérer la métronidazole des CNF sur demande grâce au clivage de la fonction ester qu'ils contiennent par activité enzymatique, en principe plus importante en proximité d'un site d'infection.

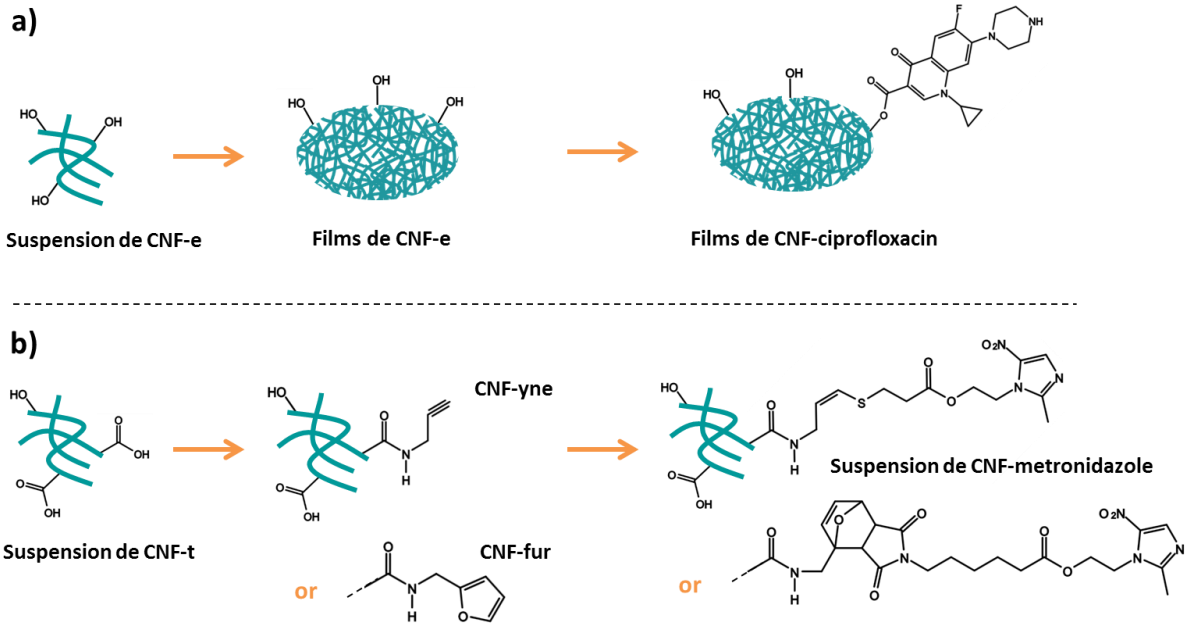

Figure 3: Procédures d'immobilisation de principes actifs sur les CNF sous forme de films (a) ou suspensions (b)

Différents grades de CNF bioactives ont donc pu être obtenus. La dernière partie de ce travail de thèse s'attache à utiliser ces différents grades pour développer des dispositifs médicaux modèles et évaluer leurs activités antibactériennes et leurs propriétés de relargage de principe actif.

Ainsi, le **troisième chapitre** présente dans un premier temps l'utilisation de films 100% CNF incluant de la ciprofloxacine greffée (CNF-cip-g), comme dans le chapitre II, ou simplement pre-adsorbée (CNF-cip-ads). Les propriétés de relargage des échantillons de CNF-cip-ads sont étudiées avec plusieurs protocoles expérimentaux qui confirment l'intérêt que les films plus épais (400 µm) ayant subi un traitement thermique poussé (150°C, 2 h) offre un meilleur contrôle du relargage de la ciprofloxacine. Ensuite, ces films sont comparés aux échantillons CNF-cip-g en termes d'activité antibactérienne. Les films contenants la ciprofloxacine greffée montrent une activité prolongée, contrairement aux échantillons contenant la ciprofloxacine seulement adsorbée. La seconde partie de ce chapitre est consacrée à l'utilisation des CNF greffée en suspension avec le métronidazole. Tout d'abord, le concept du relargage sur demande du métronidazole depuis la suspension de CNF modifiées est validé grâce à un test de clivage enzymatique *in-vitro*, avec suivi en chromatographie liquide. Puis, les composite de collagène et CNF modifiées sont mis en forme. Leur activité antibactérienne est confirmée par des tests de zone d'inhibition sur des souches anaérobie. Ces composites présentent donc un intérêt tout particulier pour le développement d'implants bioactifs. Enfin, des composites similaires sont préparés en incluant un principe actif modèle, la chlorhexidine, avec le collagène et des CNF-e et CNF-t non-modifiées. L'influence du type et de la quantité de CNF sur la capacité d'absorption d'eau et le relargage de chlorhexidine est étudiée. De plus, compte tenu que la plus part de dispositifs médicaux subissent industriellement une stérilisation, souvent par rayonnement gamma, l'influence de ce traitement est également évaluée. Les résultats montrent que l'utilisation de CNF tend à limiter la capacité d'absorption d'eau des composites, en limitant leur dégradation. Par ailleurs, l'ajout de CNF, et particulièrement de CNF-t, permet d'obtenir un relargage contrôlé de la chlorhexidine, avec une activité prolongée. Le traitement gamma n'affecte pas l'activité antibactérienne des composites, et donc de la chlorhexidine. En revanche, il réduit très légèrement le relargage du principe actif puisqu'il a pour effet de densifier la matrice collagène en activant le cross-linking entre les différents composants.

En conclusion, ce travail de thèse montre la possibilité d'utiliser avantageusement des nanofibrilles de cellulose pour développer des matériaux innovants, en vue de leur utilisation dans des dispositifs médicaux. De plus, il contribue au développement de procédures de fonctionnalisation en phase aqueuse et de caractérisation poussée des CNF, qui peuvent être appliquées aussi dans d'autres domaines.

Références

[1] H. Pun, "Terminology for biorelated polymers and applications (IUPAC Recommendations 2012," Jul. 2018.

[2] B. J. Love, *Biomaterials : A Systems Approach to Engineering Concepts*. Elsevier Science, 2017.

[3] T. Srichana and A. J. Domb, "Polymeric Biomaterials," in *Biomedical Materials*, Springer, Boston, MA, 2009, pp. 83–119.

[4] R. P. Babu, K. O'connor, and R. Seeram, "Current progress on bio-based polymers and their future trends," *Progress in Biomaterials*, vol. 2, no. 1, p. 8, 2013.

[5] L. S. Nair and C. T. Laurencin, "Biodegradable polymers as biomaterials," *Progress in Polymer Science*, vol. 32, no. 8–9, pp. 762–798, Aug. 2007.

[6] L. Bedian, A. M. Villalba-Rodríguez, G. Hernández-Vargas, R. Parra-Saldivar, and H. M. N. Iqbal, "Bio-based materials with novel characteristics for tissue engineering applications – A review," *International Journal of Biological Macromolecules*, vol. 98, pp. 837–846, May 2017.

[7] A. F. Turbak, F. W. Snyder, and K. R. Sandberg, "Microfibrillated cellulose, a new cellulose product: properties, uses, and commercial potential," *J. Appl. Polym. Sci.: Appl. Polym. Symp.; (United States)*, vol. 37, Jan. 1982.

[8] F. W. Herrick, R. L. Casebier, J. K. Hamilton, and K. R. Sandberg, "Microfibrillated cellulose: morphology and accessibility," *J. Appl. Polym. Sci.: Appl. Polym. Symp.; (United States)*, vol. 37, Jan. 1982.

[9] C. Endes *et al.*, "A critical review of the current knowledge regarding the biological impact of nanocellulose," *Journal of Nanobiotechnology*, vol. 14, no. 1, p. 78, Dec. 2016.

[10] A. Rashad, K. Mustafa, E. B. Heggset, and K. Syverud, "Cytocompatibility of Wood-Derived Cellulose Nanofibril Hydrogels with Different Surface Chemistry," *Biomacromolecules*, vol. 18, no. 4, pp. 1238–1248, Apr. 2017.

[11] S. Saini, N. Belgacem, J. Mendes, G. Elegir, and J. Bras, "Contact Antimicrobial Surface Obtained by Chemical Grafting of Microfibrillated Cellulose in Aqueous Solution Limiting Antibiotic Release," *ACS Applied Materials & Interfaces*, vol. 7, no. 32, pp. 18076–18085, Aug. 2015.

[12] M. Jorfi and E. J. Foster, "Recent advances in nanocellulose for biomedical applications," *J. Appl. Polym. Sci.*, vol. 132, no. 14, p. n/a-n/a, 2014.

[13] N. Lin and A. Dufresne, "Nanocellulose in biomedicine: Current status and future prospect," *European Polymer Journal*, vol. 59, pp. 302–325, Oct. 2014.

[14] N. Halib *et al.*, "Potential Applications of Nanocellulose-Containing Materials in the Biomedical Field," *Materials*, vol. 10, no. 8, p. 977, Aug. 2017.

Appendix – Posters

Cellulose nanofibrils as a new substrate for beta-cyclodextrin immobilization in medical device

Hippolyte Durand[1], Seema Saini[1], Deborah Quinot[1], Elisa Zeno[2], Naceur Belgacem[1], Julien Bras[1]

[1] Univ. Grenoble Alpes, LGP2, F-38000 Grenoble, France
[2] Centre Technique du Papier, Domaine Universitaire, BP. 251, 38044, Grenoble CEDEX 9, France

Abstract

The use of **Beta Cyclodextrin (β-CD)** as encapsulating agent for medical application is well known. It allows higher solubility and better efficiency for many different drugs thanks to the inclusion complex formation.

Cellulose Nanofibrils (CNF) are more and more considered for their outstanding properties (**high specific area, low density, excellent mechanical properties,…**) besides their character of **renewable bio-resource**. In addition, such fibrils of **5-20nm in width and 1-5µm long** are able to form highly entangled networks, resulting in films with high mechanical and barrier properties that make them interesting candidates for a number of applications. The possibility to further expand the CNF use by tailoring their surface properties and functions has also been intensively explored in the last decade.

The project intends to **combine the properties of beta-cylodextrin and CNF** for the design of **biobased medical devices** able to release active molecules. So far, oxidized CNF obtained by TEMPO mediated oxidation were used. The latter allows introducing carboxylic groups on the surface of CNF that can be available for esterification with hydroxyl groups of β-CD. First results showed carvacrol molecule adsorption in CNF- β-CD membranes that were evaluated in terms of **molecule release and antimicrobial activities**.

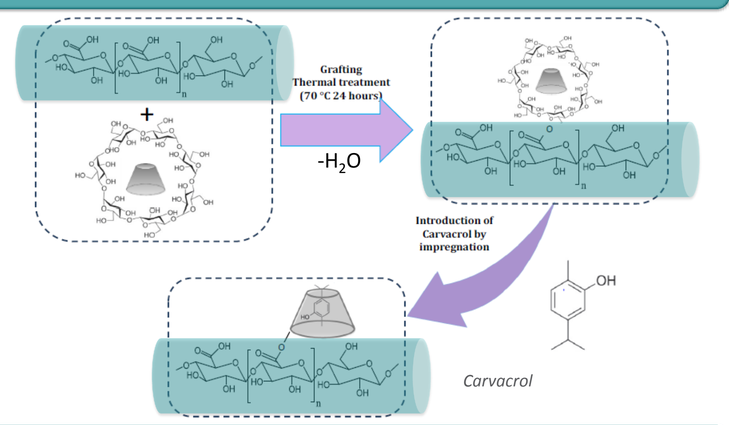

Current work

Introduction

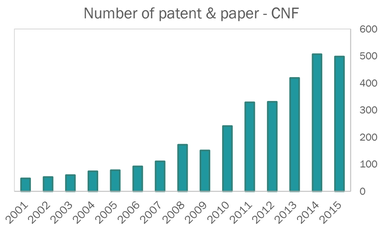

(Extracted from Scifinder, Februay 2016)

Our consumption of petro-based raw materials is changing and we are slowly shifting towards more sustainable resources. Cellulose Nanofibrils is of high interest and it has been intensively studied in the last two decades for many different applications. Its very high specific area (~100 m²/g) is a relevant property for this work.

On the other hand, cyclodextrins are well known for their ability to form inclusion complex with guest molecules. They are produced on large scale from starch since the 1980's and find application in food, pharmaceutics & cosmetics industries.

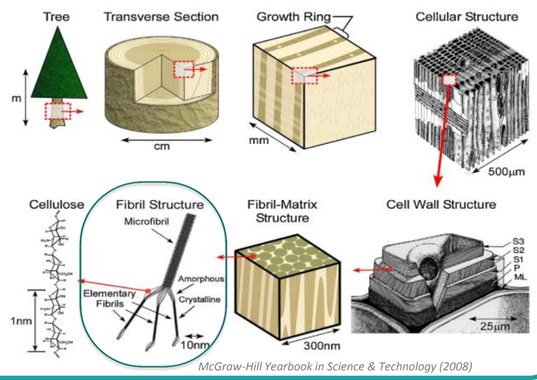

McGraw-Hill Yearbook in Science & Technology (2008)

Results & discussions

Grafting beta-cyclodextrin on oxidized CNF & Carvacrol incorporation

Sample	Carboxylate content (µmol/g)	Carboxylate grafting %	Absorbed Carvacrol Quantity (mg/g)
TM gel	1313 ± 52	-	-
TM film	812 ± 20	-	18,6 ± 1,7
TM_CD_f	556 ± 69	31,5	41,1 ± 0,4
TM_CD_s	406 ± 45	50	47,9 ± 2,4

Carboxylate content and grafting efficiency determined by conductimetric titration and quantification of the total amount of carvacrol introduced in CNF samples

- Better grafting efficiency on suspension in comparison to grafting on film

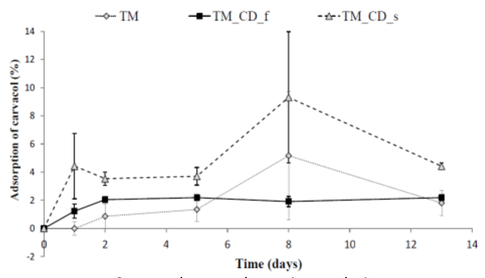

Carvacrol vapor absorption evolution

- Confirmation with higher Carvacrol adsorption

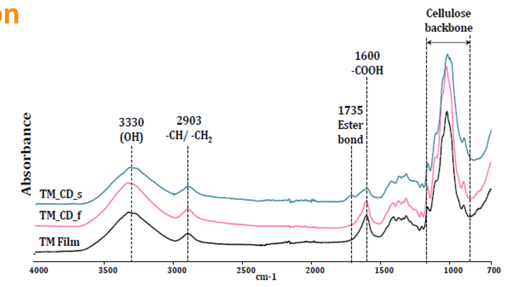

ATR-FTIR spectra of neat and beta-cyclodextrin graftde cellulose nanofibrils films

- Cellulose characteristic peaks
- Presence of carboxyl groups (1660cm^{-1})
- Ester bond detection for oxidized CNF grafted on suspension (1735cm^{-1})

Carvacrol Relase Study in acqueous medium

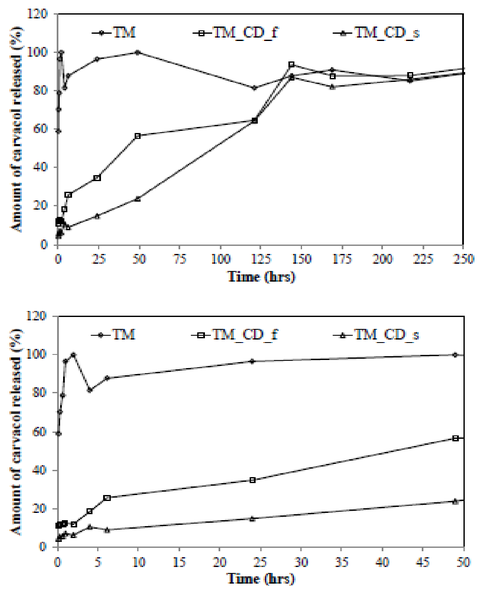

Impact of beta-cyclodextrin and CNF on the release of carvacrol from neat and CD grafted samples. 250h (left) and zoom on 50h (right)

Sample	Time to reach plateau
TM	2h
TM_CD_f	~140h
TM_CD_s	~140h

- 250h (up): impact of beta-CD grafting on CNF
- 50h (down): grafting on suspension (TM_CD_s) leads to a slower release than grafting on film (TM_CD_f)

- ✓ **more beta-CD immobilized on TM_CD_s**
- ✓ **enhanced (+138h) controlled release of active molecule**

Antimicrobial activity assesment

- **24h** antimicrobial activity?

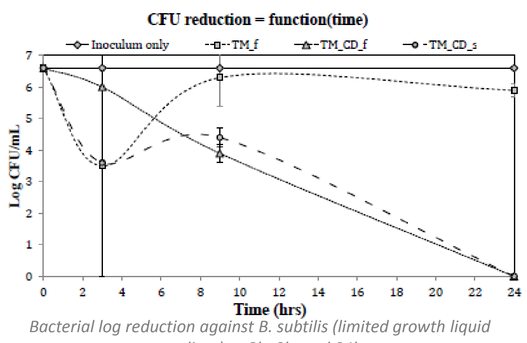

Bacterial log reduction against B. subtilis (limited growth liquid medium) at 3h, 9h, and 24h

- **TM_f** showed early inhibition until all carvacrol is consumed
- **TM_CD_film** slowly killed all bacteria in 24h
- **TM_CD_suspension** showed early inhibition AND complete killing after 24h

Successive wash: replaced inoculated media with fresh media every 24h

- **Prolonged** antimicrobial activity?

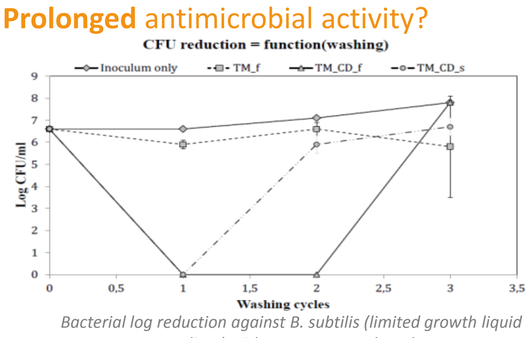

Bacterial log reduction against B. subtilis (limited growth liquid medium) with respect to wash cycle

- **TM_f**: no more antibacterial effect after 24h
- **TM_CD_film**: lost antibacterial activity after **48h**
- **TM_CD_suspension**: lost antibacterial activity after **72h**

Materials & Methods

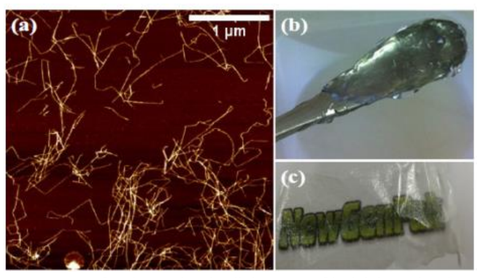

AFM images for the oxidized cellulose nanofibrils(a), oxidized CNF suspension (1wt.%) and transparent film prepared by solvent casting method (c)

Oxidised Cellulose Nanofibrils (CNF)

Oxidized CNF suspension (1,6 wt.%) was produced and supplied by Betulium Oy (Finland). Conductimetric titration were used to assess the carboxyl content of the oxidized CNF suspension introduced by TEMPO mediated (TM) oxidation.

Grafting beta-cyclodextrin on oxidized CNF

β-cylodextrin (CAS no. 7585-39-9) was supplied from Sigma Aldrich and was grafted either on oxidized CNF film or suspensions through an esterification reaction between hydroxyl groups of β-CD and carboxyl groups of oxidized CNF.

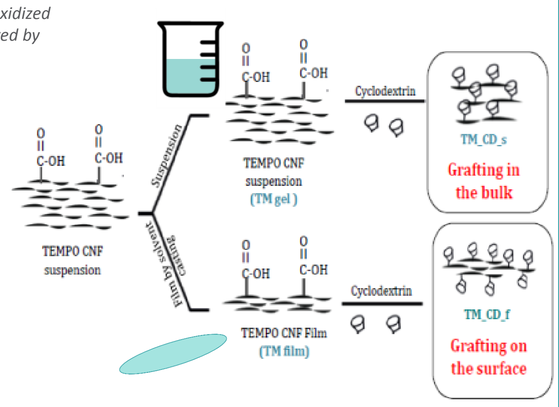

Sample	Description
TM(_f)	Tempo Modified CNF (film)
TM_CD_f	Tempo modified CNF, grafting on film
TM_CD_s	Tempo modified CNF, grafting on suspension

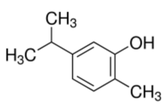

Carvacrol (CAS 499-75-2)

Relase Study in aqueous medium

β-cyclodextrin grafted samples were impregnated in Carvacrol/ethanol solution. The release study was carried out at 23°C and under sink conditions.
UV spectroscopy was used to follow the Carvacrol release (absorbance at 273nm) in water.

Antimicrobial activity assesment

Standard **Dynamic Shake Flask Method**: initial number of bacteria of 10^5 CFU/ml (CFU = Colony Forming Units) in a growth limiting liquid medium (diluted nutrient broth).
Quantitative bacterial reduction was tested at different time (3h, 9h & 24h).
The **antibacterial activity**, i.e. bacteria log reduction at the time t, of the samples was calculated as follows:

Bacterial log reduction = log CFU (t) [control sample] - log CFU (t) [CNF samples]

Conclusions & Perspectives

- **Cyclodextrin was succesfully grafted** on Tempo modified CNF without using crosslinkers, confirmed by FTIR & Carvacrol absorption
- As expected, CD grafted CNF samples **released Carvacrol more progressively** (up to 150h to reach a plateau)
- Cyclodextrin also **enhanced the antibacterial effect** of grafted samples up to 48h & 2 washing cycles
- Further study is needed in order to **increase CD grafting efficiency**
- **Inclusion complex** formed by active molecules & CD is to be more precisely understood

Acknowledgements

This research was supported by New Generation Packaging (NEWGENPACK) project of the seven framework program of European research (under Grant agreement No 290098) and CELLICAL (ANR project, ANR-15-CE08-0033).

References

Lavoine & al, Colloids Surf. B Biointerfaces. 2014 Sep 1;121:196-205
Lavoine & al, J. APPL. POLYM. SCI. 2014, DOI: 10.1002/APP.40106
Saini & al, Journal of materials science, in press.
D.O. Castro, B. Martel & al, Mat. Sc. and Engineering C 69 (2016) 1018–1025

LGP2, 461 rue de la papeterie, CS10065, 38402 Saint-Martin-d'Hères
http://pagora.grenoble-inp.fr/recherche/

hippolyte.durand@lgp2.grenoble-inp.fr
julien.bras@lgp2.grenoble-inp.fr

Cellulose nanofiber surface functionalization for functional medical membrane applications

Hippolyte Durand[1], Heloïse LeDrezen[1,2], Elisa Zeno[2], Isabelle Baussanne[3], Naceur Belgacem[1], Julien Bras[1]

[1] Univ. Grenoble Alpes, LGP2, F-38000 Grenoble, France
[2] Centre Technique du Papier, Domaine Universitaire, BP. 251, 38044, Grenoble CEDEX 9, France
[3] Univ. Grenoble Alpes, DPM, F-38000 Grenoble, France

Abstract

Cellulose Nanofibers (CNF) appears like the next generation of biorefinery high value added product. During the last decade, the interest towards these new bio-based materials exponentially increased due to their outstanding properties and the announced industrialization in 2011.

In this **CELLICAL project**, we intend to use this CNF to develop a novel class of biomaterial substrate device with controlled release of active molecules for improving soft tissue repair. It will offer clear and expected solutions for addressing remaining clinical needs, such as infection, pain and recurrence.

The main idea of this project is **to start from biomass to biomedical applications** through the use of surface functionalization and characterization of the CNF based substrate.

Both antiseptics or drugs with different modes of action will be chosen and grafted **onto the nanofibrillated cellulose** treated medical device. First, high-quality grade of CNF will be grafted with several components like yne or thiol molecule. In the meantime, active bioconjugates will be synthesized with innovative chemical ligation with active molecules. Subsequently, medical devices will be prepared following different possibilities. The efficiency of the final materials and drug release studies will help confirming the promising effect.

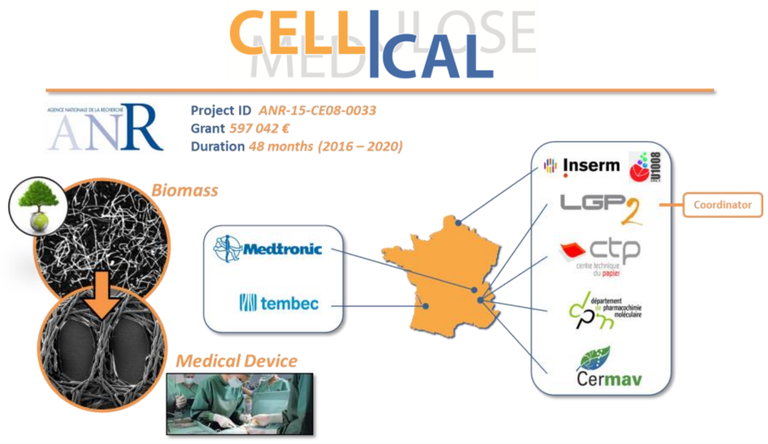

Current work

Introduction

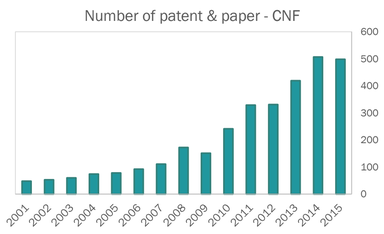

(Extracted from Scifinder, Februay 2016)

Our consumption of petro-based raw materials is changing and we are slowly shifting towards more sustainable resources. Cellulose Nanofibrils is of high interest and it has been intensively studied in the last two decades for many different applications. Its very high specific area (~100 m²/g) is a relevant property for this work.

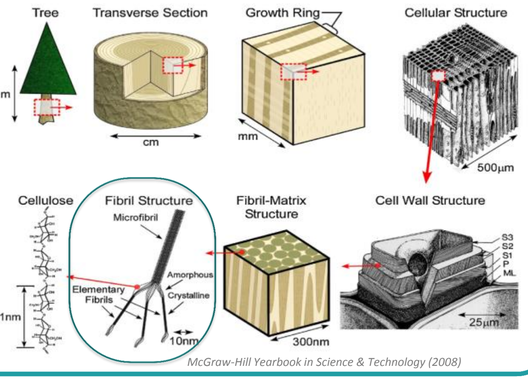

McGraw-Hill Yearbook in Science & Technology (2008)

On the other hand, drug release or antimicrobial medical device are well known for their ability to form inclusion complex with guest molecules. They are produced on large scale from textile and polysacchcharides films like collagen since the 1990's and find application in soft tissue repair or hernia mesh

Materials & Methods

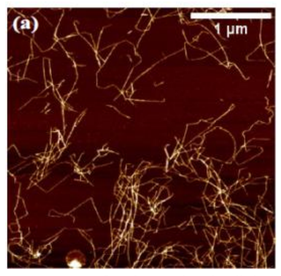

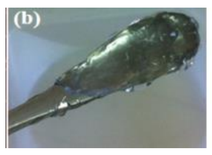

AFM images for the oxidized cellulose nanofibrils(a), oxidized CNF suspension (1wt.%)(b)

Oxidised Cellulose Nanofibrils (CNF)

Oxidized CNF suspension (1,6 wt.%) was produced or supplied by Betulium Oy (Finland). Conductimetric titration were used to assess the carboxyl content of the oxidized CNF suspension introduced by TEMPO mediated oxidation.

Grafting Alcyne on oxidized CNF

Alkyne groups will be firstly introduced on CNF surface, and subsequently linked through thiol-yne click chemistry to thiol modified Pro-drug. Alkyne modified CNF will also be used for direct grafting of drugs

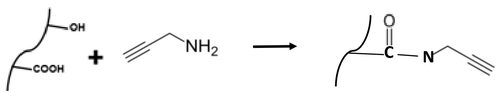

Grafting of thiol group on oxidized CNF

Amidation was used to graft Cystamine on oxidized CNF through EDC/NHS activation. Many parameters, (such as temperature and pH) have been investigated in order to optimize this grafting strategy

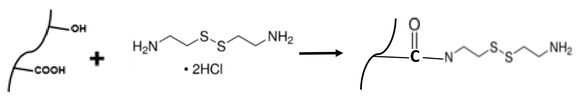

Grafting of pro-drug

A maleimide modified Ibuprofen molecule has been synthetized in order to use click chemistry with the thiol modified cellulose nanofibers. A thiolated drug will be designed for the thiol-yne click chemistry with alkyne modified cellulose nanofibers.

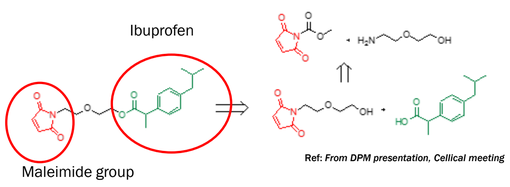

Grafting characterization

FTIR and Raman spectrometry were performed on washed samples to confirm grafting with peak visualization. Elemental analyses provide more detail on quantitative grafting of thiol moleculles , as well conductive measurement gives indication of % of COOH neutralized during the different peptidic grafting strategies

Results & discussions

Grafting of thiol group on oxidized CNF

The percentage of neutralized COOH groups by the grafting procedure is shown here with the influence of different parameters. The values are obtained after the conductometric titration of the remaining COOH.

- pH

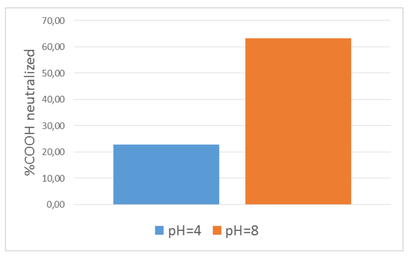

- Temperature and µ-wave treatment

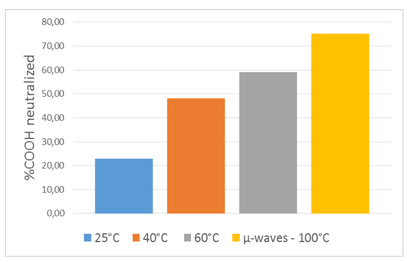

- Time of reaction and µ-wave treatment

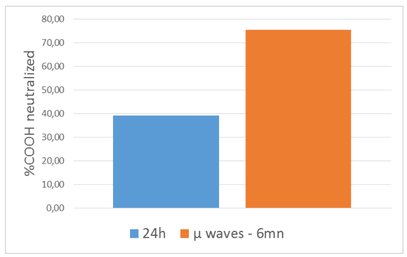

Elemental analysis was used to confirm the grafting. Sulfur content drastically increased in washed samples. Lower but significate increase were detected on other samples.

Sample	%C raw	%H raw	%N raw	%S raw	%O raw	DS
TEMPO reference	36,90	5,70	0,10	0,11	53,70	
Tempo CNF-Cystamine	36,20	6,01	0,45	**2,08**	49,12	0,055

Grafting of alkyne group on oxidized CNF,

Alkyne groups were successfully grafted on CNF according to the Raman spectroscopy, conductimetric titration of remaining COO^- groups and Elemental analysis results.

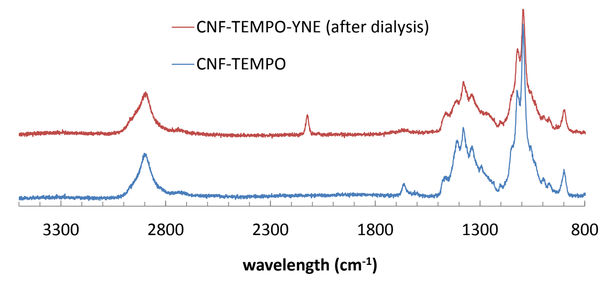

Raman spectroscopy on neat and modified CNF

=> Characteristic peak of alkyne group at 2150 cm^{-1} is clearly observed on CNF tempo grafted materials after soxhlet extraction proving

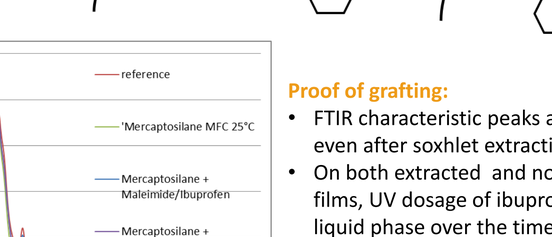

$$\%_{COOH\ grafted} = 68,5\ \%$$

=> Conductimetric titration proves the decreasing of carboxylic content and allows calculating the percentage of grafting equivalent to the number of COOH neutralized during amidation.

Sample	%C raw	%H raw	%N raw	%S raw
CNF-T	38,05	5,74	< 0,10	< 0,10
CNF-T-YNE	40,59	5,69	**1,15**	< 0,10

=> Elemental analysis of soxhlet extracted materials confirmed the presence of alkyne group with the presence of Nitrogen assessing the amide bond formation.

Grafting prodrug onto CNF

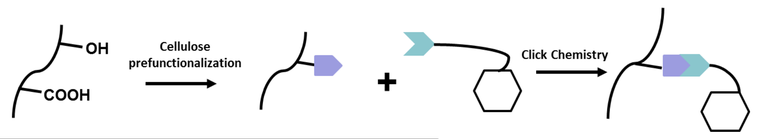

Click conditions:
- Two hours
- Room temperature
- Ene/SH ratio : 5
- Under UV lamp

- Metal free system

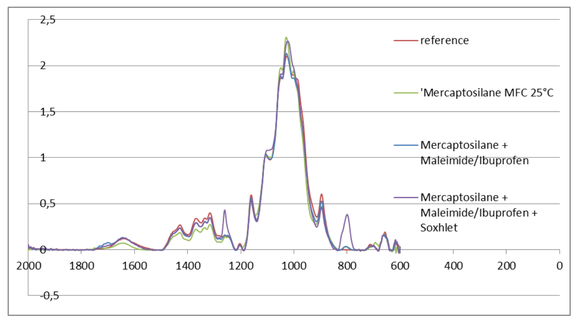

Proof of grafting:
- FTIR characteristic peaks are present even after soxhlet extraction of sample
- On both extracted and not extracted films, UV dosage of ibuprofene in the liquid phase over the time shows that no release occurred

→ No release ibuprofen confirms covalent grafting

Conclusions & Perspectives

- Two steps **prodrug grafting strategy** by click chemistry have been achieved **with success** with using only green approach in water onto oxidized CNF
- Two pre-functionnalized CNF have been obtained and their grafting confirmed by elemental analysis, FTIR or even Raman spectroscopy
- The **microwave activated** grafting will be optimized with different peptidic grafting strategies
- The thiol **quantity measurement** thanks to a fluorescent maleimide probe will be proposed to know which minimum quantity is needed for prodrug activity
- Prodrug **release study with using esterase** enzyme will be tested to characterized the prolonged release of drugs in body fluids

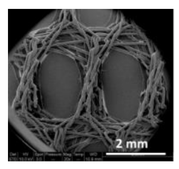

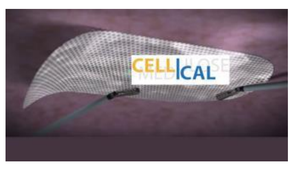

Acknowledgements

This research was supported by CELLICAL (ANR project, ANR-15-CE08-0033). This work has been partially supported by the PolyNat Carnot Institute (Grant agreement ANR-11-CARN-007-01). We would like to thank Martine Demeunynck (DPM – UGA) for their expertise in providing maleimide prodrug and Sébastien Fort (CERMAV) for µ-wave treatments.

References

- Missoum K., Belgacem M. N. and Bras J. (2013), Nanofibrillated cellulose surface modification: a review, Materials, 6, 1745-1766.
- Lin, N. and A. Dufresne (2014). Nanocellulose in Biomedicine: current status and future prospect. European Polymer Journal 59: 302-325.

LGP2, 461 rue de la papeterie, CS10065, 38402 Saint-Martin-d'Hères
http://pagora.grenoble-inp.fr/recherche/

hippolyte.durand@lgp2.grenoble-inp.fr
julien.bras@grenoble-inp.fr

English abstract — Résumé Anglais

In line with the ever-increasing academic and industrial interest for wood derived nanocellulose, the present work investigates the chemical surface modification of cellulose nanofibrils (CNFs) for biomedical application. Drugs and prodrugs of active principle ingredients (APIs) were covalently immobilized or adsorbed onto CNFs films or suspensions. For covalent immobilization, the first strategy selected calls for water-based and single step esterification of CNF films. The resulting materials demonstrated antibacterial activity against both gram-positive and gram-negative bacterial strains, with a prolonged contact-active effect. In the second strategy, CNFs suspensions were modified through a multistep reaction, involving amidation and click chemistry, still water-based. Highly innovative characterization tools, such as dynamic nuclear polarization (DNP) enhanced nuclear magnetic resonance (NMR), complemented well-established techniques to confirm the success of grafting. In parallel to covalent immobilization, an adsorption strategy was also adopted, on both CNFs films and suspensions. Then, the CNF films with grafted or adsorbed APIs were used for preparing 100% CNF membrane for potential topical applications. Another component of this work used CNF suspensions with grafted or adsorbed APIs that were embedded in collagen matrices to prepare composites for designing soft tissue repair implants. Antibacterial activity against both aerobic and anaerobic bacteria, together with controlled release properties were assessed confirming that such composites present the expected active properties, and can be used for the design of innovative medical devices.

Key words: *nanocellulose, cellulose nanofibrils, functionalization, medical devices, antibacterial activity, drug release*

Résumé Français — French abstract

Au niveau académique et industriel, les nanocelluloses connaissent un engouement toujours grandissant. Ce projet de thèse explore la modification chimique des nanofibrilles de cellulose (CNF) pour des applications médicales. Des drogues et prodrogues de principes actifs (PA) ont été liées de manière covalente ou adsorbées sur des films ou des suspensions de CNF. Pour l'immobilisation covalente, une première stratégie d'estérification en milieu aqueux a été utilisée sur des films de CNF. Les propriétés antibactériennes contre des bactéries à gram positif et à gram négatif, ainsi que l'activité par contact prolongée de ces films, ont été confirmées. La seconde stratégie a porté sur la modification des suspensions de CNF au travers d'une procédure multi-étape (amidation puis chimie click), à nouveau en phase aqueuse. Des outils de caractérisation innovants comme la résonance magnétique nucléaire (RMN) dopée par polarisation dynamique nucléaire (PDN), ont permis de compléter les techniques classiques afin de prouver le succès du greffage chimique. L'adsorption de PA sur les films et suspensions de CNF a été menée en parallèle de l'immobilisation covalente. Ensuite, les films de CNF avec des PA greffés ou adsorbés ont été utilisés pour former des membranes pour application externe. Quant aux suspensions de CNF avec PA greffé ou adsorbé, elles ont été intégrées à des matrices de collagène pour créer de nouveaux composites pour la réparation tissulaire. Leur activité antibactérienne et leurs propriétés de relargage contrôlé confirment l'intérêt de ces composites pour le design de dispositifs médicaux innovants.

Mots-clés: *nanocellulose, nanofibrilles de cellulose, fonctionnalisation, dispositif médical, activité antibactérienne, relargage contrôlé*